

Masonry

Brian E. Trimble and Joseph H. Brisch
Editors

STP 1496



STP 1496

Masonry

*Brian Trimble and Joseph Brisch,
editors*

ASTM Stock Number: STP1496



ASTM
100 Barr Harbor Drive
PO Box C700
West Conshohocken, PA 19428-2959

Printed in the U.S.A.

Library of Congress Cataloging-in-Publication Data

Masonry / Brian Trimble and Joseph Brisch, editors

p. cm.

ISBN: 978-0-8031-3492-8

1. Masonry--Materials--Congresses. 2. Masonry--Testing--Congresses.

3. Masonry--Congresses. I. Trimble, Brian, 1963- II. Title. Brisch, J. H. (Joseph H.), 1947-

TA425.M372 2008

693'.1--dc22

2008008238

Copyright © 2008 AMERICAN SOCIETY FOR TESTING AND MATERIALS INTERNATIONAL, West Conshohocken, PA. All rights reserved. This material may not be reproduced or copied, in whole or in part, in any printed, mechanical, electronic, film, or other distribution and storage media, without the written consent of the publisher.

Photocopy Rights

Authorization to photocopy items for internal, personal, or educational classroom use, or the internal, personal, or educational classroom use of specific clients, is granted by the American Society for Testing and Materials International (ASTM) provided that the appropriate fee is paid to the Copyright Clearance Center, 222 Rosewood Drive, Danvers, MA 01923; Tel: 978-750-8400; online: <http://www.copyright.com/>.

Peer Review Policy

Each paper published in this volume was evaluated by two peer reviewers and at least one editor. The authors addressed all of the reviewers' comments to the satisfaction of both the technical editor(s) and the ASTM International Committee on Publications.

The quality of the papers in this publication reflects not only the obvious efforts of the authors and the technical editor(s), but also the work of the peer reviewers. In keeping with long-standing publication practices, ASTM International maintains the anonymity of the peer reviewers. The ASTM International Committee on Publications acknowledges with appreciation their dedication and contribution of time and effort on behalf of ASTM International.

Printed in Mayfield, PA
May, 2008

Foreword

The Eleventh Symposium on Masonry was held in Toronto, Ontario, Canada on June 13, 2006. This symposium was sponsored by ASTM Committee C12 Mortars and Grouts for Unit Masonry, Committee C15 Manufactured Masonry Units, C1 Cement, and C7 Lime. The symposium co-chairmen of this publication were Brian E. Trimble and Joseph H. Brisch.

Contents

Overview	vii
Investigation and Repair of Glazed Brick Cladding: A Case Study —TODD A. GORRELL AND IAN R. CHIN	1
A Discussion of the Benefits and Problems of ASTM C 1324 for Analyzing Hardened Masonry Mortars —LAURA POWERS, ANN COLEMAN AND SUSANNE PAPAS	11
Laboratory Study of Time-of-Tooling Effects on Mortar Joint Color —BERNARD ERLIN AND TIM CONWAY	20
The Selection and Use of Natural and Manufactured Stone Adhered Veneer — RICHARD J. GODBEY AND MARGARET L. THOMSON	32
Deflection Criteria for Masonry Beams —RICHARD M. BENNETT, WILLIAM M. MCGINLEY, AND JIM BRYJA	39
Variations in the Activity of Dry-Powder Water-Repellent Mortar Admixtures with Different Mortar Formulae —HERB NORDMEYER AND PAM HALL	49
Evaluation of ASTM Methods to Determine Splitting Tensile Strength in Concrete, Masonry, and Autoclaved Aerated Concrete —CODY K. PARKER, JENNIFER E. TANNER, AND JORGE L. VARELA	62
Type S Portland Cement-Lime Mortar as a Low-Lift Grout —DAVID T. BIGGS, AND MARGARET L. THOMSON	74
The Effect of Void Area on Brick Masonry Performance —JOHN P. SANDERS AND DENIS A. BROSNAN	84
Evaluation of the Effectiveness of Clear Water Repellent Coatings on Partially Grouted Single-Wythe Concrete Masonry Walls —JEFFREY H. GREENWALD AND THOMAS C. YOUNG	98
Seismic Evaluation of Low-Rise Reinforced Masonry Buildings with Flexible Diaphragms —GREGORY L. COHEN, RICHARD E. KLINGNER, JOHN R. HAYES, JR., AND STEVEN C. SWEENEY	109
Greening of Mortars with Pozzolans —KEITH BARGAHEISER AND D. HERBERT NORDMEYER	147
Replacement of the Final Time of Setting Maximum with an Initial Time of Setting Maximum as Measured with the Gillmore Needles in ASTM C 91, C 1328, and C 1329 —JOHN T. CONWAY	156

Overview

These Proceedings are the eleventh in a series of ASTM symposia on masonry that began in 1974. Sponsored jointly by ASTM Committee C1 on Cement, C7 on Lime, C12 on Mortars for Unit Masonry, and C15 on Manufactured Masonry Units, the symposia provide a forum for the exchange of ideas, information, and practical experience in multiple areas related to masonry. This resulting STP includes papers presented orally at the June 13, 2006 symposium held in Toronto, Ontario, Canada.

This “2006 ASTM Masonry Symposium” was dedicated to Committee C12 on Mortars and Grouts for Unit Masonry on its 75th Anniversary of developing ASTM standards. It was the committee’s desire to elicit papers on the importance of standards that were developed through the ASTM consensus process. Current research, new ideas, and new products all assist with the development of good ASTM standards.

The papers contained in this symposium volume represent the work of 33 authors and co-authors; they were peer reviewed by approximately 70 members of ASTM Committees C1, C7, C12, and C15. The Joint Symposium Committee was made up of members of the four sponsoring committees, with C12 acting as the lead committee for the 2006 Symposium and STP.

Committee members were Brian Trimble and Joseph Brisch co-chairs and representatives of Committee C12; Denis Brosnan and Richard Klingner representing C15; Mike Tate and Margaret Thomson representing C7; and Bill Behie representing C1.

Finally, many ASTM staff members aided the Joint Committee in conducting the Symposium and preparing this STP. We thank the authors, reviewers, symposium attendees, sponsoring committee members, and ASTM staff for their work to enhance the success of this symposium and corresponding STP.

Brian E. Trimble
Brick Industry Association
Symposium Co-chairman and STP editor

Joseph H. Brisch
Rockwell Lime Company
Symposium Co-chairman and STP editor

Todd A. Gorrell¹ and Ian R. Chin¹

Investigation and Repair of Glazed Brick Cladding: A Case Study

ABSTRACT: The design and repair of exterior glazed brick walls differ from that of unglazed (normal) brick walls. Water that penetrates a typical brick wall usually enters through mortar joints, through failed sealant joints, and by absorption of the brick and mortar. Much of this water escapes the wall by evaporation from the face of the wall. However, the impervious face of ceramic glazed brick significantly reduces the amount and rate of evaporation of water that enters a wall, thereby exposing the glazed brick cladding to spalling caused by the freezing of moisture trapped in the brick units. In addition, since the glaze will trap efflorescence in the brick, the buildup of this cryptoflorescence behind the glaze can result in spalling of the glazed surface of the brick. Therefore, the prevention of water penetration into the masonry wall and the rapid removal of water that has entered the wall are critical to the successful performance and durability of glazed brick clad walls. This paper discusses the common failure modes of glazed brick walls and the current industry recommendations for the design and detailing of glazed brick walls. A case study of a project that includes the investigation of a wall with spalled glazed brick and the design and installation of new glazed brick on the wall is presented. This paper discusses the specification of glazed brick materials; the difficulties in color matching new glazed brick to existing glazed brick; the design and detailing of a new glazed brick wall; and other repair methods to prevent water infiltration and increase the durability of glazed brick walls.

KEYWORDS: glazed brick, flashing, weep holes, venting, expansion joints

Introduction

Glazed brick has been used as an exterior cladding material on buildings in the United States since the early 20th century [1] due to its unique appearance compared to typical unglazed brick and the availability of a wide variety of colors and finishes, from matte to high-gloss. The glazed finish also provides an impervious surface that is durable, stain resistant, and easily cleaned and maintained. Glazed brick has performed successfully in all types of climates [2]. However, glazed brick is potentially more susceptible to damage and deterioration due to the effects of water infiltration than typical unglazed brick. Therefore, the design, detailing, and repair of glazed brick cladding differ from that of normal brick cladding.

This paper discusses the common failure modes of glazed brick walls and the current industry recommendations for the design and detailing of glazed brick walls. A case study of a project that includes the investigation of a wall with spalled glazed brick, the design and installation of new glazed brick, and the successful performance of the wall is presented. This paper discusses the specification of glazed brick materials; the difficulties in color matching new glazed brick to match existing glazed brick; the design and detailing of a new glazed brick wall; and other repair methods to prevent water infiltration and increase the durability of glazed brick walls.

Failure Modes of Glazed Brick

Brick masonry walls are subjected to water infiltration from wind driven rain and snow through mortar joints, failed sealant joints, faulty flashing and coping details, cracks in the wall, and through absorption of the mortar and brick. Typical unglazed brick walls allow much of this water to escape by evaporation through the face of the brick. However, evaporation of water in a glazed brick wall through the glazed

Manuscript received January 17, 2006; accepted for publication November 10, 2006; published online January 2007. Presented at ASTM Symposium on Masonry on 13 June 2006 in Toronto, Canada; B. Trimble and J. Brisch, Guest Editors.

¹ Senior Associate, Vice President and Principal, respectively, Wiss, Janney, Elstner Associates, Inc., 120 North LaSalle Street, Suite 2000, Chicago, IL 60602.

Copyright © 2007 by ASTM International, 100 Barr Harbor Drive, PO Box C700, West Conshohocken, PA 19428-2959.



FIG. 1—Spalling of the faces of glazed brick caused by freeze/thaw action.

surface cannot occur because the glazed surface, which is typically comprised of mineral oxides sprayed onto the face of a clay brick and fired in an oven [3], forms an impervious glass surface [2].

Water that is trapped in a glazed brick wall can saturate the brick and can potentially cause damage to the brick by freeze/thaw action, as shown in Fig. 1. Water that penetrates a glazed brick may also cause efflorescence. Dissolved efflorescence salts that migrate toward the face of the brick are trapped behind the impervious surface glaze resulting in a buildup of efflorescence salts behind the face of the brick, which is known as cryptoflorescence. The buildup of cryptoflorescence behind the glazed surface subjects the face of the brick to high stresses, which can cause spalling of the face of the brick.

Case Study Project

In 1996, our firm performed an investigation and prepared a repair design for a deteriorated glazed brick wall on a two-story tall base structure of a 1960s high-rise building in Chicago, IL that is located along the shore of Lake Michigan. The two-story base structure is approximately 540 ft by 220 ft in plan and approximately 35 ft tall. The majority of the roof level of the base structure consists of a landscaped park. The base structure is clad with a glazed brick cavity wall and had a brick parapet wall with a poured-in-place concrete coping enclosing the park area. The gloss-finished, glazed brick is green in color with small brown and black raised spots that provide variation in the color and texture of the glazed surface.

Investigation Findings

The existing parapet wall and portions of the top of the wall below the parapet were exhibiting significant spalling and cracking of the faces of the brick, as shown in Figs. 2 and 3. There was efflorescence present on the face of the brick at mortar joints and cracks, as shown in Fig. 4, as well as cryptoflorescence behind the spalling faces of the brick, as shown in Fig. 5.

A cross section of the original parapet wall is shown in Fig. 6. The typical parapet wall was 2-ft, 6-in. thick and consisted of a 8-in. thick masonry wall at the exterior side of the parapet and a 10-in. thick masonry wall at the interior side of the parapet with a 12-in. wide cavity between each wall. Each wall was comprised of an interior wythe of either 4 or 6-in. thick concrete masonry backup and an exterior 4-in.



FIG. 2—Existing parapet wall and portions of the top of the wall below the parapet exhibiting significant spalling and cracking of the faces of the glazed brick.

thick wythe of glazed brick with no air cavity between the concrete masonry backup wall and the glazed brick veneer. At some locations, there was a cast-in-place concrete backup wall instead of the 6-in. thick concrete masonry backup wall, with a specified 1-in. wide space between the glazed brick and the concrete backup wall. The top of the parapet wall was capped with a poured-in-place, exposed-aggregate concrete coping with no overhang to provide a drip edge. Through-wall “plastic” flashing was specified below the coping. The base of the parapet wall was specified to have plastic flashing with weep holes spaced at 36 in. on centers to drain water that had infiltrated the wall. No vents were specified for the glazed brick veneer.

Our investigation revealed that portions of the parapet wall brick had previously been replaced with a different green glazed brick in the 1980s. Although similar in color, this brick did not match the original brick spots or texture. It was also observed that a large amount of the deterioration and spalling present during our investigation had occurred in the 1980s replacement brick, as well as in the original brick.

Existing vertical expansion joints in the brick veneer were not straight, but were stepped to follow the running-bond pattern of the mortar joints. These joints were 3/8-in. wide and were spaced at approximately 36 ft apart. No vertical expansion joints were specified near the building corners. Expansion of the brick veneer at some of the expansion joints was typically greater than could be accommodated by the sealant



FIG. 3—Existing parapet wall exhibiting significant spalling and cracking of the faces of the glazed brick.



FIG. 4—Efflorescence present on the face of the glazed brick at mortar joints and cracks.



FIG. 5—Cryptofluorescence behind the spalling faces of the glazed brick.

material and caused failure of these sealant joints. Also, many of these joints were discovered to be partially filled with mortar, making them ineffective in accommodating brick expansion. The unaccommodated movement of the brick veneer resulted in cracking of brick and mortar joints.

The mortar joints in the wall were typically eroded and in some locations were cracked. The condition of the mortar joints at the parapet wall was typically worse than the wall below the parapet.

The concrete coping was severely cracked and many of these cracks had been covered with multiple layers of sealant over the years. The specified through-wall flashing was not present below the coping; consequently, water that penetrated the coping through cracks or through absorption of the concrete was able to enter the brick wall below. Figure 7 shows the original coping.

The 1-in. wide space behind the glazed brick at the concrete backup wall was typically filled with

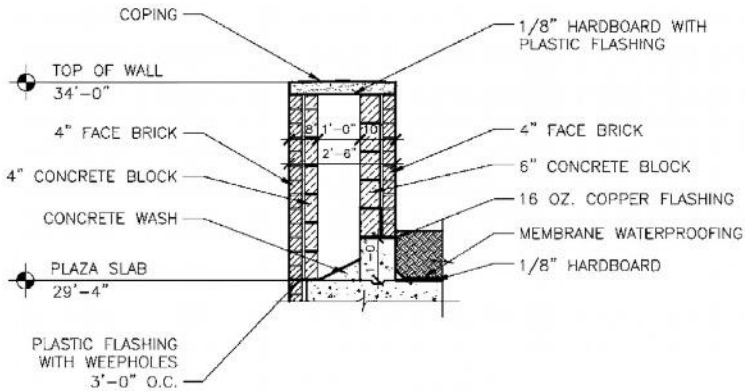


FIG. 6—A cross section of the original parapet wall.



FIG. 7—Original concrete coping with surface cracks. No through-wall flashing was found below the coping.

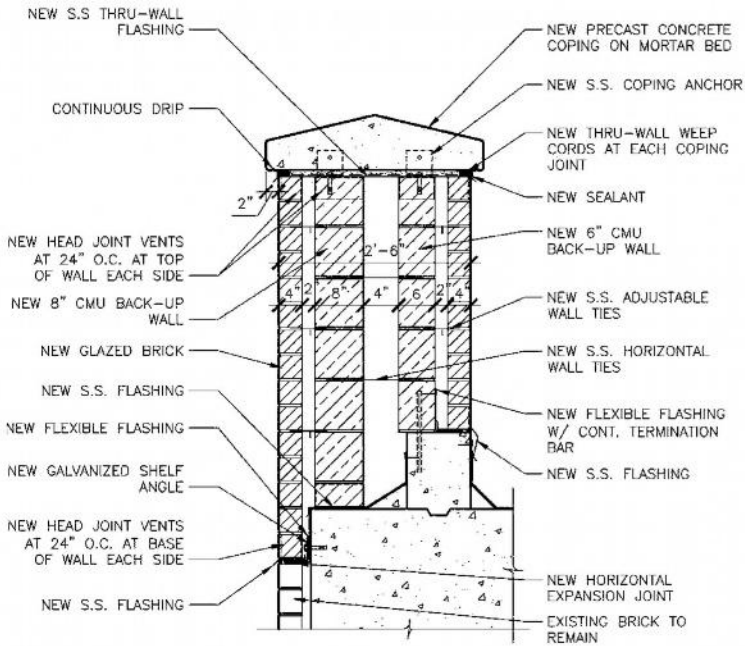


FIG. 8—A cross section of the new parapet wall design.

mortar droppings that prevented the free flow of water down to the flashing level at the base of the parapet wall. Also, the plastic flashing at the base of the parapet wall was brittle and cracked, and did not typically extend to the exterior face of the wall. There was no ventilation provided for the wall cavities. We also discovered that the thin-gage corrugated metal ties used to tie the glazed brick to the backup wall were severely corroded and in some locations corroded completely through.

During our investigation, we observed that the irrigation system for the park level had sprinkler heads that sprayed water directly onto the interior face and onto the top of the parapet wall.

Our investigation determined that water was able to enter the wall through the deteriorated concrete coping, through cracked and deteriorated mortar joints, and through failed sealant joints. The irrigation system increased the amount of water entering the wall. Water that infiltrated the wall was not quickly removed due to the lack of effective drainage cavities, ineffective wall flashings, and a lack of ventilation, thereby allowing the brick to remain wet and saturated. The subsequent development of cryptoflorescence behind the glazed surface coupled with freeze/thaw action resulted in cracking and spalling of the glazed brick faces.

Repair and Rebuilding of the Brick Walls

Based on the results of the investigation, the decision was made to entirely remove the existing parapet wall and reconstruct it with new details to prevent water infiltration into the wall, to quickly remove water that might infiltrate the wall, and to ventilate the drainage cavity to allow evaporation of infiltrated water. This repair method also included the removal of the previous 1980s replacement brick that did not match the appearance of the original brick and which was of questionable durability. A cross section of the new parapet wall design is shown in Fig. 8, and includes the following items.

- New precast concrete copings to match the appearance of the original concrete coping. The width of the coping was increased to provide an overhang and drip edge at each face of the wall.



FIG. 9—The new parapet wall with through-wall flashing below the coping and 2-in. wide drainage and ventilation cavities.

- New stainless steel through-wall flashing below the coping to prevent water from entering the top of the brick wall.
- Relocation of the concrete masonry backup to allow for a 2-in. wide drainage and ventilation cavity between the glazed brick veneer and the concrete masonry backup wall. The specifications required that the contractor take special precautions during construction to maintain the cavity space free of mortar droppings.
- Two-part stainless steel and flexible membrane flashings with weep holes at the base of the wall to collect and drain water from inside the wall.
- Regularly spaced head joint vents at the base and near the top of the parapet wall to ventilate the cavity.
- New 1/2-in. wide linear vertical expansion joints near the building corners and along the length of the wall spaced at 18 ft apart rather than the original 3/8-in. wide stepped joints spaced at 36 ft apart.

Figure 9 is a view of the new parapet wall during construction.

The existing wall below the parapet was deemed to be salvageable; therefore, the following repairs were specified:

- Rebuilding of deteriorated portions of the wall.
- Installation of stainless steel retrofit lateral wall ties to replace the corroded corrugated wall ties.
- Surface grouting of the mortar joints to provide improved resistance to water infiltration through the mortar joints. This repair method is described in more detail below.
- Rebuilding of ineffective or closed vertical expansion joints to remove mortar droppings while maintaining the original stepped appearance, as shown in Fig. 10.

Specifying Glazed Brick

At the time the repair design of the parapet wall was performed, ASTM C 1405 “Standard Specification for Glazed Brick (Single Fired, Brick Units)” had not been published. Therefore, a combination of specifications was used: ASTM C 126 “Standard Specification for Ceramic Glazed Structural Clay Facing Tile, Facing Brick, and Solid Masonry Units” was used for the properties of the ceramic glaze finish; and ASTM C 216 “Standard Specification for Facing Brick (Solid Masonry Units Made from Clay or Shale)” was used for the physical requirements of the body of the brick. The project specifications required that the glazed brick manufacturer be made aware by the contractor that their product was intended for exterior use in the given climate. It was also required that the manufacturer provides a letter of certification acknowledging that the project brick was appropriate for the project conditions.

Currently, ASTM C 1405 is the standard for specifying single-fired glazed brick, which includes brick where the glaze is applied to the unfired body and then both are fired together. ASTM C 1405 establishes minimum requirements for both the glaze and the brick body. Glazed brick intended for exterior use should be specified as “Class Exterior.” The grade, type and division of the brick should also be specified: the brick “grade” specifies the permissible variation in face dimension (“S” for standard and “SS” for select sized); the brick “type” indicates single-glazed face or double-glazed face (Types I and II, respectively); and the “division” specifies the amount and placement of the hollow void spaces of the brick (“solid” with



FIG. 10—*Ineffective portions of the stepped expansion joints were rebuilt. The vertical expansion joints in the parapet wall above are straight instead of stopped.*

less than 20 % voids, “H40V” between 25 % and 40 % voids, and “H60V” between 40 % and 60 % voids) [4].

Currently, there is no ASTM standard for double-fired bricks, which includes bricks that have a glaze added after the initial firing of the brick body and then are fired a second time. In such a case, the method described above combining ASTM C 126 and ASTM C 216 may be used [2], but the brick manufacturer must certify that the brick is appropriate for exterior use in the intended climate.

Design and Detailing of Glazed Brick Walls

The reconstructed parapet wall of the case study project was detailed as recommended in the Brick Industry Association (BIA) Technical Note 13 “Ceramic Glazed Brick Exterior Walls,” which is an excellent resource for the design of glazed brick veneers.

Exterior glazed brick veneer walls should be designed as a vented drainage cavity wall. A minimum 2-in. wide air cavity behind the brick is recommended [2]. The project specifications should include the requirement to keep the cavity free of mortar droppings and other materials which prevent the vertical flow of water in the cavity towards the flashing and the vertical flow of air between vents at the top and bottom of the wall.

Flashings, with end dams at discontinuous ends, should be installed at all horizontal interruptions of the air cavity, such as copings, window and door lintels and sills, shelf angles, and at the base of the wall, in order to collect water and drain it to the exterior [2]. Weep holes spaced at a maximum of 24 in. on centers should be provided at all flashing levels.

The cavity should be vented to allow for evaporation of moisture out of the wall. Wall vents spaced at approximately 4 ft [2] on center should be installed above and approximately two courses below interruptions in the air cavity, such as the flashing level at shelf angles, the base of the wall, and the top of the wall. Vents may be formed by leaving head joints open or by installing prefabricated head joint vents that prevent insect access.

Similar to typical brick veneers, glazed brick walls should be detailed to accommodate vertical and horizontal expansion of the brick due to changes in temperature and moisture content and horizontal and vertical elastic movement of the structural building frame. Vertical expansion joints should be specified near corners and wall offsets and regularly spaced along the length of the wall [2] typically spaced 20 to

25 ft apart. Vertical expansion joints in parapet walls should be more closely spaced, typically 15 to 18 ft apart. Horizontal expansion joints should be regularly spaced and should normally be placed below shelf angle supports. The width and spacing of the expansion joints should be determined based upon the calculated anticipated movement of the brick and the structural building frame, as well as the movement capability of the chosen joint sealant. Refer to BIA Technical Note 18A for additional information regarding the design of movement joints [5]. Compressible foam joint fillers should be used in constructing the expansion joints to maintain the joints free of mortar and debris that would render the joint ineffective.

Glaze and Color Matching

When performing a repair of an existing building where only a portion of the existing glazed brick is to be replaced, it is necessary to match the color, texture, and finish of the original glazed brick as closely as possible. The difficulty level of this task varies depending on the complexity of the original color(s) and the condition of the existing finish. For example, a glazed brick that was originally manufactured with a high gloss may have weathered to an extent where the glaze no longer retains the original gloss level. Aesthetically, the new brick should be manufactured to match the existing finish appearance. Also, some glaze colors are more difficult to match than others. This is often due to the fact that materials used in the manufacture of the original brick may no longer be allowed in the manufacturing process due to environmental concerns.

For example: the case study project has a dark green glaze color with brown and black textured spots. As noted above, the 1980s replacement brick did not closely match either the color or the texture of the original brick. During the repair project, the glazed brick manufacturer prepared more than 50 color samples over the course of several months in an attempt to match the original brick. Although the texture and appearance of the black and brown spots of the new brick matched the original brick closely, the background green color remained slightly different than the original brick. This was primarily due to the unavailability of materials used in the original glaze materials, such as heavy metals.

Therefore, it is advisable to begin the color matching process early in the repair project. Color matching of glazed brick can take many months for the brick manufacturer to develop initial samples, the project team to review the samples and provide feedback, and then repeat this process until an acceptable glaze color and texture is reached.

It is also recommended that replacement of original brick with new brick be performed in areas with defined edges so that the color difference from one area to another is less noticeable. If spot replacement of individual brick units is required, consider the salvage and reuse of intact original brick from an area designated for full replacement. This is contingent upon the suitability of the original brick for reuse.

Repointing versus Grouting of Mortar Joints

Typical mortar joint repair consists of repointing, which includes grinding of the mortar joints with a power grinder. However, this method can cause damage to the glazed surface. A trial repair of power grinding was performed on the case study project, which resulted in chipping of the glaze adjacent to the edges of the brick. If possible, hand tool removal of the mortar should be considered.

Although not as effective to reduce water permeability as 3/4-in. deep repointing of mortar joints, grouting of mortar joints improves the water resistance of the joints without the related potential glaze damage caused by power grinding. This method, sometimes referred to as the “bag and grout method,” consists of preparing a grout mixture (1 part portland cement, 1/3 part hydrated lime, and 1-1/3 part fine sand) to a fluid consistency thinner than pointing mortar [6]. The grout mixture is applied to the cleaned and moistened mortar joints with a stiff fiber brush. The grout should be vigorously worked into the joints to completely fill all voids and cracks and to ensure good physical bond with the existing mortar. Excess grout should be removed from the glazed brick faces with clean cloths using circular motions, which is easy to do with the smooth glazed surfaces that prevent bonding of the grout to the brick face. Unglazed brick would require masking of the surfaces to prevent grout bonding to the face of the brick units. After a one-day cure, a second application of the grout should be applied. Tooling of the joints may also be performed. Figures 11 and 12 show an example of mortar joint grouting from the case study project.



FIG. 11—*Removal of excess grout from the glazed brick after grouting of the mortar joints.*

Epilogue

The construction of the specified repair design of the case study project was completed in 1998. Since that time, the repaired walls have performed successfully and there has been no spalling, crazing, or cracking of the glazed brick veneer.

Conclusions

Glazed brick is an attractive alternative to typical unglazed brick that can provide a durable, easily maintained exterior wall finish and is available in numerous colors and finishes. However, proper specification of glazed brick material and detailing of the wall assembly is critical to the successful performance of an exterior glazed brick wall, which should include the following:

- Glazed brick material should be specified to comply with ASTM C 1405 and be rated “Class Exterior.”
- Detailing of a glazed brick wall should be as recommended in the BIA Technical Note 13 “Ceramic Glazed Brick Exterior Walls.”
- The wall should be designed as a vented drainage cavity wall with a minimum 2-in. wide unobstructed air cavity behind the brick and the project specifications should include the requirement to keep the cavity free of mortar droppings and other obstructing materials.

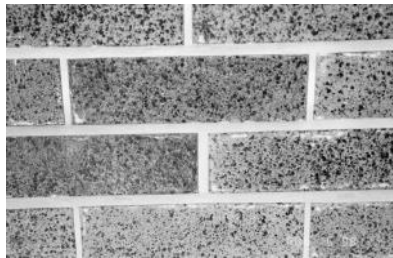


FIG. 12—*Grouted mortar joints prior to final cleaning.*

- Flashings, with end dams at discontinuous ends, should be installed at all horizontal interruptions of the air cavity and weep holes spaced at a maximum of 24 in. on centers should be provided at all flashing levels.
- The cavity should be vented to allow for evaporation of moisture out of the wall. Wall vents should be located above and below interruptions in the air cavity and should be spaced at approximately 4 ft on centers.
- Glazed brick veneer should be detailed to accommodate vertical and horizontal expansion of the brick due to changes in temperature and moisture content and horizontal and vertical elastic movement of the structural building frame. The width and spacing of the expansion joints should be determined based upon the calculated anticipated movement of the brick, as described in BIA Technical Note 18A, and the movement of the structural building frame, as well as the movement capability of the chosen joint sealant. Compressible foam joint fillers should be used in constructing the expansion joints to maintain the joints free of mortar and debris that would render the joint ineffective.
- The glazed brick wall should not be exposed to additional water from irrigation and sprinkler systems.

The following items should be considered during a repair project of an existing glazed brick wall:

- The color matching of the new glaze to the existing glaze should be started early in the repair project due to the potential lengthy duration of this process.
- Replacement of original brick with new brick should be performed where possible in areas with defined edges so that the color difference from one area to another is less noticeable.
- Consider the salvage and reuse of intact original brick for spot replacement if the original brick is suitable for reuse.
- Consider surface grouting of existing mortar joints to prevent possible chipping and damage to the existing glazed finish often caused by power tool grinding of mortar joints during typical repointing.

References

- [1] Gonser, K., “The History of Glazed Brick (GN) and Structural Glazed Facing Tile (SGFT),” Technical Tips, Elgin-Butler Brick Company, 1999.
- [2] “Technical Notes 13—Ceramic Glazed Brick Exterior Walls, December 2005,” *Technical Notes on Brick Construction*, Brick Industry Association, <http://www.bia.org/BIA/technotes/TN13.pdf>, pp. 1–6.
- [3] Gonser, K., “Ceramic Glazes: What Are They? Where Do They Come From?,” Technical Tips, Elgin-Butler Brick Company, 1999.
- [4] ASTM, Standard C 1405, “Standard Specification for Glazed Brick (Single Fired, Brick Units),” *Annual Book of ASTM Standards*, Vol. 4(5), ASTM International, West Conshohocken, PA, 2002, p. 916.
- [5] “Technical Notes 18A—Design and Detailing of Movement Joints, Part 2, Reissued September 2001,” *Technical Notes on Brick Construction*, Brick Industry Association, <http://www.bia.org/BIA/technotes/t18a.pdf>, pp. 1–14.
- [6] “Technical Notes 7F—Moisture Resistance of Brick Masonry—Maintenance, Reissued Oct. 1998,” *Technical Notes on Brick Construction*, Brick Industry Association, <http://www.bia.org/BIA/technotes/t7f.htm>, pp. 1–11.

Laura Powers,¹ Ann Coleman,² and Susanne Papas³

A Discussion of the Benefits and Problems of ASTM C 1324 for Analyzing Hardened Masonry Mortars

ABSTRACT: Laboratory testing of mortars by chemical analysis and petrography is generally appropriate to determine mortar composition, and to provide a basis for the formulation of compatible repair or replacement mortars. In cases of masonry distress and failures, analysis by C 1324 alone is often less useful unless the laboratory work is guided by knowledge obtained in the field. In addition to requiring the technical skills of experienced chemists and petrographers, the application of C 1324 requires knowledge of the specifications for mortar for unit masonry and benefits from the knowledge of how mortars are prepared and installed. The quality of the sampling for laboratory tests, the physical condition of the samples obtained, and the mortar constituents can all influence the reliability of the results obtained by the chemical analysis and the petrographic examination. We review the development of the standard, discuss related standards, and present our experience with modern mortars prepared in the field and tested in the laboratory in accordance with ASTM C 1324 to provide insight into the results and limitations of such analysis.

KEYWORDS: mortar, analysis, chemical tests, petrography

Introduction

The analysis, restoration, and repair of existing materials and structures requires technical expertise, practical knowledge, and experience to understand the cause of existing conditions and to provide effective solutions. In the case of hardened masonry mortar and cement-based stucco and plaster, ASTM Standard C 1324, "Standard Test Method for Examination and Analysis of Hardened Masonry Mortar," [1] which was first introduced in 1996 provides invaluable information. Like most test methodologies, C 1324 has evolved as new technology has become more readily available, and its application has expanded beyond its original scope. The current methodology is the culmination of the efforts of many chemists and petrographers; notable among them are William Hime of Wiss, Janney, Elstner and Bernie Erlin of The Erlin Company. Hime and Erlin's paper "Methods for Analyzing Mortar" was presented in 1985 at The Masonry Society's Third North American Masonry Conference, [2] providing the basis for C 1324.

This test method is generally appropriate to determine the composition of modern mortar and portland cement plaster, often as a basis for determining whether the proportions of materials comply with project specifications or the proportion requirements of ASTM Standard C 270 "Specification for Mortar for Unit Masonry," [3]. It can be used to provide a basis for the formulation of compatible repair or replacement mortars. Combined with knowledge obtained in the field, C 1324 can be useful to determine the cause of distress and premature failures.

As the test method warns, some historic mortars may contain nonresolvable constituents that may skew test results; however, our experience has shown that significant information may be obtained by the petrographic examination outlined in this test method. There are current developments for a separate standard to address historic mortars. Until such standards exist, petrographers with extensive experience in historic mortars can provide useful information to the architect/engineer involved with preservation and restoration projects.

The quality of the sampling for laboratory tests, the physical condition of the samples obtained, and the mortar constituents themselves can all influence the reliability of the results obtained by the chemical

Manuscript received January 6, 2006; accepted for publication January 18, 2007; published online March 2007. Presented at ASTM Symposium on Masonry on 13 June 2006 in Toronto, Canada; B. Trimble and J. Brisch, Guest Editors.

¹ Consultant, Wiss, Janney, Elstner Associates, Inc., 330 Pflingsten Road, Northbrook, IL 60062.

² Consultant, Wiss, Janney, Elstner Associates, Inc., 245 First Street, Suite 1200, Cambridge, MA 02142.

³ Associate III, Wiss, Janney, Elstner Associates, Inc., 330 Pflingsten Road, Northbrook, IL 60062.

analysis and the petrographic examination. The collaborative effort of the petrographer, chemist, and architect/engineer is critical for the successful analysis of mortar, stucco, and plaster.

Experience, Knowledge and Collaboration

ASTM C 1324 consists of two distinct activities: petrographic examination and chemical analyses. The effective and intended application of this method requires that the chemist and the petrographer be knowledgeable of the methodology and the requirements of ASTM C 270, "Standard Specification for Mortar for Unit Masonry." The architect/engineer must have a basic understanding of the technical aspects of both activities to be able to communicate with the petrographer and the chemist. The examination, analysis, and application of the test results require all team members to have an understanding of specifications for these materials, and how they are prepared and installed.

Knowledge of Specifications of Masonry Mortar

Since the 1951 introduction of ASTM C 270, it has become the industry standard for masonry mortar. ASTM C 270 provides guidance for selecting the appropriate mortars for various applications. For example, ASTM C 270 recommends a Type O mortar for exterior above grade walls where the masonry is unlikely to be frozen when saturated or unlikely to be subjected to high winds or other significant lateral loads. Type N or S mortar should be used in other cases. The Portland Cement Association (PCA) also quotes ASTM C 270 in its recommendations for mortar use. [4] The Brick Institute of America (BIA) recommends Type N or Type S mortar for veneer or non-loadbearing walls in exterior above grade applications. Type N or S mortar is also recommended by BIA for masonry with an average initial rate of absorption of between 10 and 30 g per 30 in.² (194 cm²) [5].

Few specifiers recognize that C 270 addresses three classifications of mortar (cement-hydrated lime, mortar cement, and masonry cement) with eight kinds of cementitious materials divided into 24 different types of cements and hydrated lime. Too often the project specifications simply reference C 270 without specifying a particular mortar type that conforms to either the proportion specification requirements or property specification requirements of C 270.

Knowledge of How Mortars are Prepared in the Field

As the architect/engineer should understand how mortar is prepared and installed, the chemist and petrographer should be aware of how mortars are prepared and placed. Skill levels and regional practices of masons vary from one part of the United States to the other. Highly skilled workers, often mix mortar, lay masonry or apply plaster, and pride themselves on being able to "do it by eye." Unskilled labor may have little to no knowledge of the appropriate mortar for various applications. In both instances, additives, and admixtures are sometimes used indiscriminately, affecting mortar performance. These additives and admixtures are not detected by C 1324 chemical analysis. In addition, acid-washing rather than a neat finishing job can affect both performance and appearance. Intrusion of acids into the mortar is also not detected by C 1324 chemical analysis, but damage caused by acids may be seen by the petrographer.

In most regions of the country, mortar that is supplied by premix plants has good quality control of measuring and materials. The composition of this mortar would be expected to be uniform. In the past, some premix plants often supplied contaminated mortar mixes that may have affected the performance and characteristics of the mortar. Large projects that do not utilize premix mortar materials often measure mortar by bags of cement, lime, and sand in mechanical batch mixers. The composition of this mortar might also be expected to be fairly uniform. Other projects may measure materials by volume and mix the mortar in small batches by hand in mortar boats resulting in considerable batch to batch variation in composition.

Size and Condition of Mortar Samples

Field observations obtained by the architect/engineer are critical to determine whether sampling is representative of the existing conditions. When examining a localized failure, samples should be extracted from both distressed and non-distressed locations.

When the purpose of mortar testing is to determine the cause of distress or failure, sampling needs (sample size and location) may be different. ASTM Standard C 823, "Practice for Examination and Sampling of Hardened Concrete in Constructions," [6] provides guidance for examining and sampling concrete constructions, and is referenced by C 1324. ASTM Standard C 1532, "Practice for Selection, Removal, and Shipment of Masonry Assemblage Specimens from Existing Construction," [7] is not referenced in ASTM C 1324, but provides guidance for conducting a visual assessment of existing masonry construction, and for selecting, removing, and shipping masonry specimens.

The number of samples and the size of samples removed for analysis are determined in large part by the needs of the petrographer and chemist for the analysis. The preferred sample is a prism consisting of masonry units bonded with mortar. Such a sample provides ample amounts of mortar for both the chemical analysis and the petrographic examination. ASTM C 1324 recommends a 10 g sample for each composite petrographic and chemical analysis. We have found that a minimum sample size equivalent to a 3 in. by 3 in. piece of a bed joint, which is closer to 30 g of mortar, is ideal when prism samples are unavailable. Smaller sample sizes reduce the efficiency of performing the analysis. Samples that are too small and samples that are in poor condition are likely to be unreliable. Sample conditions that may adversely influence the analysis include friability (crumbling) and alteration caused by leaching, environmental degradation, or chemical attack.

Mortar samples need to be representative of the materials used in the structure. Many times, particularly in older structures, several successive layers of repointing mortars may exist in the joints. In all cases, it is useful to have a complete representation of all the mortar present within a given joint. This gives the chemist and petrographer a large enough sample to determine the joint stratigraphy and select an appropriate sample for analysis. It is critical that a mortar analysis be done from a solid sample, rather than rubble or "dust" to achieve correct paste to aggregate ratios. Depending on the size of a structure, multiple mortar samples would usually be preferred to better characterize the mortar composition. Areas where there are changes in materials, such as cornices or caps, should be considered separately from the body mortar of the structure. For smaller projects, consideration should be given to taking cores at T-joints where head, bed and masonry unit are captured for examination. Mortar samples alone will only provide information about the mortar rather than the masonry/mortar system.

Distress of in-place mortar refers to the failure or the perceived failure of the mortar to function as intended. This distress may include crumbling, cracking, efflorescence, debonding and discoloration. A sample of mortar taken from distressed joints may fit the sample size requirements of ASTM C 1324 (intact pieces with a mass of about 10 g), but may be inadequate to address the cause of the distress. Problems such as leakage, efflorescence, cracking, and separation along bond lines often warrant removing a larger sample of the masonry assembly (a prism or wallette) so that the petrographer can study the contact between the masonry units and the mortar. Observation of the in-place mortar can also provide information regarding the mortar as-placed. These observations not only provide useful information about the observed failure or distress, but also can provide information about adjustments that may be needed to the mix design of the repair or replacement mortar.

Information About Materials Used

The more information the architect/engineer can provide to the materials scientists the more likely they will be able to determine whether a mortar meets industry standards or specified requirements. Therefore, the architect/engineer should gather as much information possible about the actual materials used or specified. Such information should include project specifications, submittal data, and when possible, physical samples of mortar components. When the materials scientists understand what was specified they can compare it to physical samples. In the case of mortar cements, this information is extremely critical as chemical analysis may or may not give the correct composition.

Physical samples of materials are very useful when analyzing mortars. The constituent components including cement, hydrated lime, and sand can be analyzed along with the hardened mortar. The component samples will provide a more accurate proportioning of the hardened mortar than that which can be achieved by using the assumed compositions of silica and calcium in ASTM C 1324. Pigments, and other additives, particularly organic additives, are useful to compare to the hardened mortar sample.

Material data sheets or product data sheets, or both, can provide useful information; however, many are too generic to provide specific information for a given mortar mix. Many MSDS and product data

sheets are prepared to generically provide information for a broad group of mortar mixes or products, and thus may not give useful information in terms of the composition of an actual mortar. In addition, most mortars consist of multiple components from multiple sources, further rendering data sheets useless.

Another critical issue is for all team members to understand what is being tested. Are samples representative of original construction or repointing mortar? As stated previously, large masonry construction projects often use premixed or full bag materials that are proportioned based on the weight of material. Smaller repointing projects often utilize mortar that is mixed in smaller batches by volume. We have demonstrated in the field and in the laboratory that a Type N mortar proportioned by weight will not be a Type N proportioned by volume. The resulting conclusions of ASTM C 1324 testing may state that the mortar appears to be “over sanded” from the specified mix; however, the act of measuring the cement by volume reduces the amount of cement in relationship to the sand resulting in an “under-cemented” mortar.

To successfully analyze and apply test results, communication is essential. Information gathered in the field during sample removal should be communicated to the petrographer and the chemist. During analysis, the petrographer provides critical information to the chemist for the analysis of data and can provide initial observations to the architect/engineer. If each party develops his or her own contradictory opinions and conclusions based on individual observations without communicating with other members of the team, the result is a disjointed report of analysis or worse. The application of the test results is more effective if more information is provided to, reviewed by, and discussed among all parties.

Successful Laboratory Analysis

Petrographic Examination

The petrographic examination is the first step in the analysis of the mortar sample. Generally, the amount of detail required depends on the purpose of the analysis and the nature of the mortar. The petrographer examines the condition and general characteristics of the mortar sample. A detailed study of the aggregate and paste is completed. The information from these detailed studies is important as the components of the aggregate and paste can influence or adversely affect the chemical analysis.

ASTM Standard C 856, “Standard Practice for Examination of Hardened Concrete,” [8] outlines the methods for the examination of the mortar sample. A visual and stereomicroscopic examination allows the petrographer to characterize and describe the sample including; exposed surfaces and tooled surfaces, fracture characteristics, aggregate characteristics, estimation of the air content and the characteristics of the air-void system. Surfaces in contact with masonry units are examined for evidence of bond with adjacent masonry units, and evidence of moisture infiltration along the bond line. Deposits on surfaces and secondary deposits in interior voids are described and identified. If the mortar shows evidence of deterioration, chemical analysis may be problematic. A thin section examination using a petrographic microscope can be used to evaluate the characteristics of the paste and the aggregate.

The petrographer generally studies the aggregate component of the mortar in great detail because the chemist needs to know whether the aggregates (sand) contain materials that may adversely affect or bias the chemical analysis. Aggregates typically comprise at least 60% of the mortar. Even small amounts of soluble or partly soluble natural minerals or man-made phases can greatly influence the chemical analysis. The petrographer may crush a small portion of the mortar, dissolve the paste, and isolate the aggregates in order to evaluate the gradation of the sand and to better establish the proportions of rock and mineral constituents. This method can be very useful for color analysis. One drawback to using this method to determine sand gradation is that some aggregates tend to fracture in the crushing process. The fractured grains may report to the smaller sieve sizes.

The petrographer also studies the paste system in detail to determine the cementitious components of the mortar, and to evaluate the effects of leaching and alteration as these may influence the chemical analysis. Cementitious components that are normally observed in modern mortars may include portland cement, hydrated lime, and masonry cement (portland cement and finely ground limestone). Some mortars may contain other cementitious materials such as ground granulated blast-furnace slag, volcanic ash, siliceous diatoms, fly ash, silica fume, metakaolin, and non-portland cement. The presence of these materials often precludes chemical analysis. Petrographers who examine older mortars should recognize the

characteristics of natural cement, hydraulic lime, and other materials used in historic construction. In some cases, analysis of residual natural cement grains using scanning electron microscopy with EDS has provided information useful to the chemist.

For modern mortars, the petrographer should not attempt to identify the type of mortar (N, S, etc.) or make recommendation for replacement mortar based only on samples provided for examination/testing. The observations of the petrographer can be useful for the architect/engineer for preliminary reporting, but conclusions about the type of mortar should be saved until the completion of the ASTM C 1324 chemical analysis.

Some materials in the mortar (paste or aggregate) may be difficult to identify, perhaps because the material is too small (fine-grained) or because it is unusual (possibly due to the complex history of the mortar). X-ray diffraction analysis and scanning electron microscopy are frequently used to gather more information about specific components of the mortar. ASTM C 1324 does not yet instruct the petrographer in procedures that might be used to distinguish whether an organic admixture other than air-entraining admixture is present in the mortar. Many petrographers do study the absorption characteristics of tooled and fracture surfaces and the response of the mortar to heating as evidence of an organic modifier in the paste system. Since many modern mortars may contain organic admixtures, the lack of a methodology to detect these could be viewed as a drawback. These admixtures are not usually present in amounts that would be expected to have an impact on the accuracy of the chemical analysis.

Chemical Analysis

Using the information provided by the architect/engineer and the petrographic examination of the mortar, chemical analysis using ASTM C 1324 is undertaken. The chemist chooses the appropriate analytical procedures based on the information obtained from the petrographer. Chemical analysis usually begins with analyzing a representative portion of ground mortar by X-ray diffraction. After the X-ray diffraction analysis is completed and reviewed in conjunction with the petrographic analysis, the remaining portions of the chemical analysis can be completed. Provided that the petrographic examination and the X-ray diffraction studies do not suggest interferences or bias, information on the components of the mortar can then be calculated as discussed below.

X-ray diffraction determines the crystalline components present in a mortar. Typical components detected are quartz, calcite, portlandite, brucite, dolomite, feldspars, and ettringite. Quartz, feldspars, and dolomite are components of the aggregate system. Portlandite, brucite, and ettringite are components of the paste system. Calcite can be present as a component of the aggregate (limestone), as a component of the paste (carbonated calcium hydroxide), or as finely ground limestone in masonry cement. Review of the petrographic examination data can provide guidance in the interpretation of where the crystalline components detected by X-ray diffraction fit into the mortar system. X-ray diffraction can also provide information as to possible failure modes that have occurred within the mortar system. The presence of a substantial amount of gypsum, for example, in an exterior mortar application would suggest that the mortar used was inappropriate for an exterior environment, as gypsum will soften when exposed to moisture. Gypsum could also cause destructive expansion of the mortar when it interacts with portland cement present in the mortar mix.

Review of the X-ray diffraction data and the petrographic examination also gives information as to possible interferences or bias that may occur during the chemical analysis of the mortar. Feldspar present in the aggregate can cause a slight to moderate bias of the silica analysis as, depending on the degree of weathering of the feldspar, some silica from the feldspar may be extracted during the soluble silica sub-procedure of ASTM C 1324. Fly ash present in the mortar will cause a significant bias to the silica procedure and, in the case of Class C fly ash, cause a bias in the calcium procedure. Therefore, the presence of fly ash as detected during the petrographic examination would render chemical analysis of the mortar using the silica sub-procedure useless. These interferences would cause an over-estimation of the portland cement portion of the mortar.

Problems can also occur during the analysis of the mortar using the calcium subprocedure. Analysis of a mortar that contains a calcitic hydrated lime (one composed of only calcium hydroxide) and a calcitic limestone as the aggregate would be of no value as there would be no way to determine how much of the calcium present is due to the hydrated lime and how much is due to the aggregate. Again, the information obtained during the petrographic examination and the X-ray diffraction study provides essential informa-

tion to guide the chemist during his analysis. The petrographer may perform modal analysis on a thin section of the mortar in order to determine the proportion of limestone in the aggregate. The chemist can use this information to assign calcium to the hydrated lime and to the aggregate. Currently, ASTM C 1324 does not include these procedures.

The chemical analysis outlined in ASTM C 1324 consists of the determination of soluble silica, calcium oxide, magnesium oxide, magnesium hydroxide, insoluble residue, and losses on ignition. The soluble silica, calculated as percent SiO_2 , is usually used to calculate the amount of portland cement present in the mortar. Portland cement can either be present as a mortar component itself or as a portion of the binding material present in either masonry or mortar cement.

The calcium oxide (CaO) content is used to calculate the amount of hydrated lime present in the mortar after correction for the calcium present in the portland cement in portland cement-hydrated lime mortars. The amount of hydrated lime present can be overestimated based on the presence of calcitic limestone in the aggregate. It can also be underestimated based on the degree of leaching of calcium from the system due to moisture migrating through the masonry system. The calcium oxide content can also, after correction for the calcium in the portland cement, be combined with the portland cement content to better estimate the amount of masonry cement in a mortar, providing that hydrated lime was not detected by petrography or X-ray diffraction.

The magnesium oxide (MgO) content can consist of magnesium oxide from the portland cement, magnesium hydroxide from dolomitic hydrated lime, magnesium carbonate from dolomitic limestone, or as a magnesium component of other aggregates. It is primarily used to calculate the total composition of the mortar; however, a high magnesium oxide content (greater than one percent) could also suggest that magnesium hydroxide is present in the hydrated lime. Magnesium hydroxide contents less than 1 to 2 1/2% may not be detected by X-ray diffraction or petrographic examination.

Magnesium hydroxide (Mg(OH)_2) is determined by differential thermal analysis (DTA) or thermal gravimetric analysis (TGA). The magnesium hydroxide content can be used to calculate the amount of hydrated dolomitic lime present directly or can be combined with the excess calcium present after the correction for portland cement to determine the hydrated lime content.

The insoluble residue determines the amount of aggregate present in a mortar that contains only siliceous and other insoluble aggregates. For mortars that contain a combination of siliceous and calcareous aggregates, the sand content will be significantly underestimated if insoluble residue alone is used.

The losses on ignition, determined as the loss from room temperature to 110°C , from 110°C to 550°C , and from 550°C to 950°C , give additional information on mortar composition. The loss from room temperature to 110°C determines free water, present as H_2O . The loss from 110°C to 550°C determines the combined water in the form of hydroxide (OH), present from either noncarbonated portland cement or hydrated lime. The final loss, from 550°C to 950°C , determines the amount of carbonate (CO_2) present, either from carbonated cementitious components or carbonate aggregates.

After completing chemical analysis of a mortar, the chemist should first total the amounts of soluble silica, calcium oxide, magnesium oxide, insoluble residue, and losses on ignition for the mortar. This total should be near 100%, plus or minus about 5%. If the total is greater than this, the chemist should review the chemical and petrographic data with the petrographer to determine the possible source of interference or bias.

Calculating the Mortar Composition from the Data

Calculating mortar composition using ASTM C1324 of a portland cement-hydrated lime mortar with a siliceous aggregate is a relatively simple process. The mortar "type" is based on comparison of the analytical results with the proportions given in Table 1 in ASTM C 270. As mentioned, the soluble silica content is used to determine the portland cement content, the calcium oxide, corrected for the calcium in the portland cement is used to calculate the hydrated lime, and the insoluble residue accounts for the sand. Using the mass to volume conversions provided in ASTM C1324 will produce mix proportions that can then be compared to either Table 1 of ASTM C270 or to the specifications provided on the specific project. The proportions of the mortar cement may not match the proportions given in Table 1, but may instead match the property requirements of Table 2 which are outside the scope of ASTM C 1324.

Calculating masonry cement or mortar cement-to-sand ratios using ASTM C 1324 is more problematic. ASTM C 270 allows either masonry or mortar cements to contain portland cement, hydrated lime or

finely ground limestone, or both. Therefore, it may not be possible to determine chemically whether a mortar contains a masonry cement or a mortar cement if a sample of the original unhydrated material is not available for chemical analysis at the same time as the mortar analysis. Often the distinction between masonry cement and mortar cement is made on the basis of the entrained air content observed by the petrographer. A reasonably accurate estimation of the total binder content to sand ratio often can be made by chemical analysis. This ratio can be useful in determining potential problems with the mortar due to over sanding (under cementing), which seems to be a common problem in modern mortars.

ASTM C 1324 Applications and Limitations

General Application of ASTM C 1324 Examination and Analysis

ASTM C 1324 procedures are intended for testing mortars that comply with the proportion specification requirements in ASTM C 270 Table 1. These mortar types may contain portland cement, masonry cement, or hydrated lime. The procedures cannot determine whether a mortar sample meets the property specification requirements of ASTM C 270 Table 2. ASTM C 1324 is not intended for analyzing mortars made with specialty cements or proprietary mixtures of cementitious materials. In our experience, important information can often be obtained from analyzing such mortars, especially if a sample of the specialty cement or proprietary mixture can be obtained for comparative analysis.

Historic mortars, those made before about 1930, can be analyzed using ASTM C 1324 provided that the petrographer and chemist have a good knowledge of the materials and methods pertaining to the era and are mindful of the chemical interferences or biases that may be associated with some of the components.

The test results will typically consist of a general description of the sample that was analyzed, the proportions of the mortar components as determined by chemical analysis, and a petrographic description of the mortar components. The amount of detail will usually be dictated by the purpose of the study. In some situations the chemical analysis cannot be performed, for example where the sample size is too small or when certain materials or combinations of materials interfere or generate a bias in the analysis. Detailed petrographic studies must sometimes suffice to describe the mortar.

Post Construction

ASTM C 1324 can be useful in determining compliance with some mortar specifications. Limitations are encountered when mortar cements are used, as no material properties are specified in ASTM C Standard 1329, "Specification for Mortar Cement," [9] for these types of mortar due to the inclusion of other materials. However, C 1324 can still be used as a guide, particularly if a sample of the mortar cement (product) specified is available for comparison.

Determination of appropriate repair or replacement mortar

ASTM C 1324 can be a useful tool in the determination of an appropriate repair or replacement mortar. The information generated by both the petrographic exam and chemical analysis can give useful information about the composition of the mortar; however, architect/engineers should not recommend repair mortar based solely on results of an ASTM C 1324 analysis of a mortar sample. While it is one effective tool, other contributing factors may affect the recommendations for repair mortar. Consider situations where masonry has been damaged due to sand blasting. Consider implications of original mortar not being suitable for the quality of brick. Consider the performance and construction of the existing mortar joints.

More useful in the determination of the repair or replacement mortar is the use of ASTM C 1324 in conjunction with masonry prism analyses where the mortar and masonry are observed as a system. No matter how good a mortar is, if it is not placed properly or matched properly with the adjacent masonry, it can be of little use. There is no one-size-fits-all mortar. Each system is unique and success of the masonry system depends on not only the mortar specified but also the interaction of the mortar with the masonry or stone interface.

Looking at the characteristics of the masonry itself can also prove useful. Adjustments to the mix design to compensate for the absorptive nature of the bricks can be critical to good performance of the

system. In addition to laboratory studies, detailed observations, photographs, and information gathered at the site are critical to the success of a repair or replacement mortar. It takes the cooperation of the architect/engineer, chemist, and petrographer to produce a successful repair.

When used as the basis for formulating repair or replacement mortars, the proportions of mortar components determined by ASTM C 1324 should be considered in conjunction with the information contained in the appendices of ASTM C 270. This information is considered “nonmandatory” and is often overlooked or under appreciated by the practitioners and users of ASTM C 1324. These appendices include: X1 Selection and Use of Mortar for Unit Masonry; Appendix X2 Efflorescence; X3 Tuck Pointing Mortar; and X4 Examples of Material Proportioning for Test Batches of Mortar.

Distress and Failure Analysis

Most of the problems related to masonry construction can be traced back to the mortar joint. The quality of the mortar joint relies on appropriateness of mortar materials, mortar preparation, and workmanship in laying the masonry. Sometimes distress or failure of masonry and mortar joints can be the result of poor design or specifications. Many premature failures and distress are the result of a combination of design and construction errors. ASTM C 1324 can be utilized as a starting point to determine whether the existing hardened mortar meets the intended project specifications. Too often, mortar analysis in isolation can and will often lead to a less than successful result. As with failure and distress of masonry and mortar, masonry prism analysis is crucial, when combined with the field observations and history of the structure.

Problems and Limitations

ASTM C 1324 does not currently have a precision and bias statement, and this lack has been perceived by some as limiting the acceptability of the method. In our experience, specific procedures used by the chemists and petrographers vary both within and between laboratories. An interlaboratory testing program comparing the results and procedures is needed and has been planned by C12 Task Group C.12.02.02.

Some opponents of ASTM C 1324 complain that for cement-based stucco and plaster, the weight of sand used to calculate the material proportions from the data does not always represent the weight of sand used in construction. In the case of hardened mortar and plaster, our laboratory studies have shown that 80 lb/ft³ (1281 kg/m³) is an appropriate assumption for the mass of the sand. Whether the sand was damp and loose or dry and compact during proportioning is irrelevant once the mortar or plaster has hardened. The petrographic examination will provide observations about the gradation and quality of the sand used and ASTM C 1324 can determine whether the mix is sand rich or not.

Other complaints commonly arise in the case of analyzing historic mortars. Besides the cautionary remarks in the test method about nonresolvable constituents of historic mortars ASTM C 1324 also acknowledges that not all mortars can be accurately quantified by oxide analysis and proportional analysis cannot definitively be made. However, a skilled petrographer can usually identify the cementitious components of historic mortars and can provide other useful information about the characteristics of the mortar.

Other Applications

Since the adoption of ASTM Standard C 780, “Standard Test Method for Preconstruction and Construction Evaluation of Mortars for Plain and Reinforced Unit Masonry” [10] in 1974, specifiers have relied on preconstruction and construction testing to test the plastic and hardened properties of mortar to establish a standard of quality for construction and to verify mortar quality and consistency during construction. This type of testing is most beneficial for large scale new masonry construction, but is less often used for small scale projects. Projects that utilize ASTM C 780 attempt to ensure mortar quality during construction by comparing the results of various construction tests with the project baseline values. The performance characteristics of the specified mortar are verified in pre-construction tests. ASTM C 1324 mortar analysis can be performed as part of the preconstruction testing program to determine the composition of the mortar. Subsequent mortar analysis during the construction period can then be used as a quality assurance tool to evaluate the consistency of the mortar composition. Such information can be useful in addressing claims in disputes in cases of premature deterioration or failure.

ASTM C 780 is not suitable for accurately determining the composition of mortar. A relationship between the proportions established by analysis using ASTM C 1324 and the results obtained using the mortar aggregate ratio test method in Annex A4 of ASTM C 780, can provide a quick way to monitor the mortar composition during the construction phase. Once an acceptable range of mortar to aggregate ratios is established, this quick test can be used to monitor the ongoing quality of the site mixed mortar batches.

Conclusion

ASTM C 1324 is not without its supporters and opponents. Most complaints about ASTM C 1324 arise from a misunderstanding of the test method or misinterpretation of the results. The responsibility of architect/engineers who prescribe and materials scientists who perform ASTM C 1324 is to educate their clients on the types of test methods available and the information that will be gathered from the various test methods. Through this education process, misunderstandings and misinterpretations of test results should be minimized.

The expanded and continued use of ASTM C 1324 to analyze hardened masonry mortars and cement-based stucco and plaster will allow the test method to develop further. As new technologies are discovered and applications are explored, this test method will become a valuable and widely used tool in the analysis, restoration, or repair of existing materials and structures.

References

- [1] ASTM Standard C 1324, "Test Method for Examination and Analysis of Hardened Masonry Mortar," *Annual Book of ASTM Standards*, Vol. 4.05, ASTM International, West Conshohocken, PA, 2004.
- [2] Hime, W. G., and Erlin, B., "Methods for Analyzing Mortar," *Proceedings of the 3rd North American Masonry Conference*, Masonry Society, West Conshohocken, PA, 1985.
- [3] ASTM Standard C 270, "Specification for Mortar for Unit Masonry," *Annual Book of ASTM Standards*, Vol. 4.05, ASTM International, West Conshohocken, PA, 2004.
- [4] Panarese, W. C., Kosmatka, S. H., and Randall, Jr., F. A., *Concrete Masonry Handbook for Architects, Engineers, Builders*, Portland Cement Assn., West Conshohocken, PA, 1991.
- [5] "Technical Notes 8B-Mortars for Brick Masonry—Selection and Quality Assurance," Revised June 2000, Brick Industry Association Technical Notes on Brick Construction, available online at: www.bia.org/BIA/technotes/t8b.htm
- [6] ASTM Standard C 823 "Practice for Examination and Sampling of Hardened Concrete in Constructions," *Annual Book of ASTM Standards*, Vol. 4.02, ASTM International, West Conshohocken, PA, 2004.
- [7] ASTM Standard C 1532, "Practice for Selection, Removal, and Shipment of Masonry Assemblage Specimens from Existing Construction," *Annual Book of ASTM Standards*, Vol. 4.05, ASTM International, West Conshohocken, PA, 2004.
- [8] ASTM Standard C 856, "Practice for Petrographic Examination of Hardened Concrete," *Annual Book of ASTM Standards*, Vol. 4.02, ASTM International, West Conshohocken, PA, 2004.
- [9] ASTM Standard C 1329, "Specification for Mortar Cement," *Annual Book of ASTM Standards*, Vol. 4.01, ASTM International, West Conshohocken, PA, 2004.
- [10] ASTM Standard C 780, "Test Method for Preconstruction and Construction Evaluation of Mortars for Plain and Reinforced Unit Masonry," *Annual Book of ASTM Standards*, Vol. 4.05, ASTM International, West Conshohocken, PA, 2004.

Bernard Erlin¹ and Tim Conway²

Laboratory Study of Time-of-Tooling Effects on Mortar Joint Color

ABSTRACT: Early tooling results in laitance at tooled surfaces. The laitance consists of smooth, soft, and optically continuous high water-cementitious materials ratio (w/cm) paste that contains fines that bled to the surface from the cementitious materials and aggregate. The cement is extensively hydrated. Late tooling results in discontinuous, fine, chatter-marked surfaces. These discontinuities create surface shadows. Portland cement hydration is very poor due to a low w/cm. Normal tooling results in surface textures between those from early and late tooling along with cement hydration close to that associated with late tooling. In normal- and late-tooled joints, the portland cement evidences restricted hydration due to water "squeezed" from the relatively stiff surfaces, which creates a low w/cm. Significant color differences from light to dark result when joints are, respectively, struck and tooled early, normal, and late. Overall lower w/cm results because masonry units absorb some of the mix water. Wetted bricks extend curing. Affecting the time of mortar stiffening, which controls the time of tooling, is loss of water from joint surfaces and water absorbed by masonry units. The rate of water loss from joint surfaces is a function of the water retention properties of the mortar and ambient atmospheric conditions. Pigment properties of the mortar-making materials, and particularly the portland cement, plus surface textures, establish the color and color tone of joints. A primary contributor to darker surfaces is the degree of cement hydration: the poorer the hydration, the darker the color and color tone. Affecting the degree of cement hydration is the w/cm and the curing period: higher w/cm and longer curing increases hydration and lightens color. A secondary contributor to color tone is surface texture: the greater the number of surface discontinuities the darker the color tone. Cementitious materials components that generally contribute to lighter color tones include hydrated lime and the inert material in masonry cements.

Introduction

Masonry mortars are often selected on the basis of color to achieve a desired appearance. If the color of masonry mortar joints is different from the selected color or exhibits variations within a masonry structure (Fig. 1), questions arise about the cause of the color changes.

Major contributors to the color of tooled masonry mortar joints are: (a) portland cement pigment properties, (b) degree of cement hydration, (c) hydrated lime, (s) masonry cement filler materials (usually limestone or marble much finer than the portland cement), (e) aggregate fines, and (f) time of tooling.

Natural joint colors result from six main influences: (1) color of the ferrite phase and, to a lesser extent, the dicalcium silicate phase of portland cement; (2) degree of cement hydration; (3) mixing water content (water-cementitious materials ratio w/cm); (4) hydrated lime; (5) fines contributed by the aggregate; and (6) "stiffness" of the mortar at the time of striking and tooling. Items 1, 2, 4, and 5 act as "pigments." Items 2 and 3 change "pigment" properties of the portland cement by affecting the degree of cement hydration. Item 6 reduces w/cm at tooled surfaces, which is accompanied by less cement hydration and, hence, enhances the pigment properties of portland cement.

Portland cement is very finely ground and, in addition to its function as a binder, also acts as a pigment. The primary component of the portland cement that influences pigment properties is the ferrite phase, commonly referred to as tetracalcium aluminoferrite (brownmillerite), which in cement parlance is abbreviated C₄AF and, to a lesser extent, its degree of hydration. The ferrite phase does not have a fixed formula and varies in composition and color (e.g., from translucent brownish red to almost opaque). A second portland cement contributor to color is its dicalcium silicate component, commonly referred to as

Manuscript received January 25, 2006; accepted for publication November 27, 2006; published online January 2007. Presented at ASTM Symposium on Masonry on 13 June 2006 in Toronto, Canada; B. Trimble and J. Brisch, Guest Editors.

¹ The Erlin Company, Materials and Construction Consultants, 5578 Route 981, Latrobe, PA 15650.

² Holcim US Inc., 6211 Ann Arbor Road, Dundee, MI 48131.



FIG. 1—*Example of varicolored joints.*

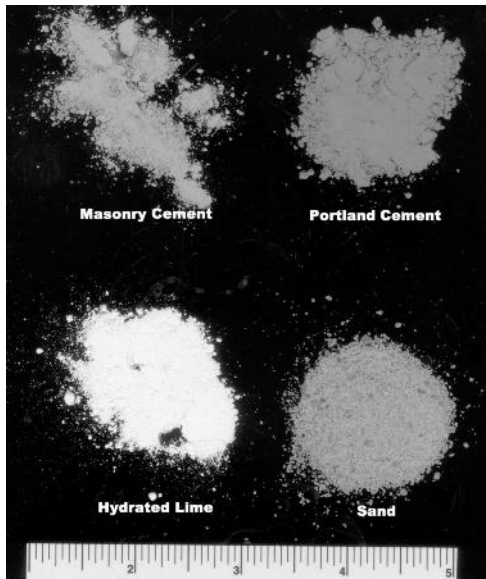


FIG. 2—*Mortar-making materials used in this study. Scale in 1-in. numerical increments.*

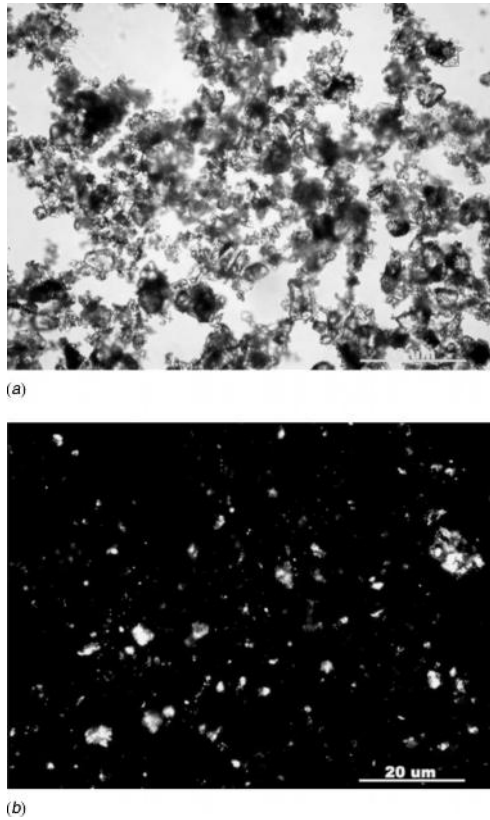


FIG. 3—Immersion preparation of portland cement viewed using a petrographic microscope. (a) Plane polarized light. The darker material is the ferrite phase. (b) Crossed polarized light. Some of the C_3S particles are light gray. The darker particles are the ferrite phase.

belite, in cement parlance abbreviated C_2S , which varies from clear to dark brown.

Proprietary pigmented masonry cements are available from a number of manufacturers, and pigments are sometimes added to field mortars. Color changes due to aggregate fines, efflorescence, leaching, and weathering of nonpigmented and pigmented mortars are not subjects of this study.

Masonry cements are typically ground much finer than portland cement to enhance water retention and workability. These cements are usually air-entraining mixtures of portland cement and limestone ground much finer than ordinary portland cement (e.g., 7000 versus 3800 Blaine). The limestone component of masonry cement can have a variety of colors, which is advantageously used in some proprietary, colored, masonry cements. Portland cement is usually a shade of gray and may have a brown overtone. Hydrated lime is white. Sand varies in color depending upon its mineralogical composition. Colors of the mortar-making materials used in this study are shown in Fig. 2. Figures 3(a), 4(a), 5(a), and 6(a) provide a comparison of their fineness and show the intrinsic colors of their components.

Portland cement, limestone, hydrated lime, and aggregate fines each play a role in the color of joints because they act as pigments. A major cause of joint color variations is the time when joints are struck and tooled. For a given mortar mixture, variations of water contents and time of tooling are the largest contributors to color variations.

Variable shades of joint color tones invariably occur at jobsites (Fig. 1) even where the same formulated mortars are used. The usual cause of these variations is changes in mixing water contents, absorption of bricks or other masonry units, and time of tooling. Usually these changes of color are sufficiently subtle

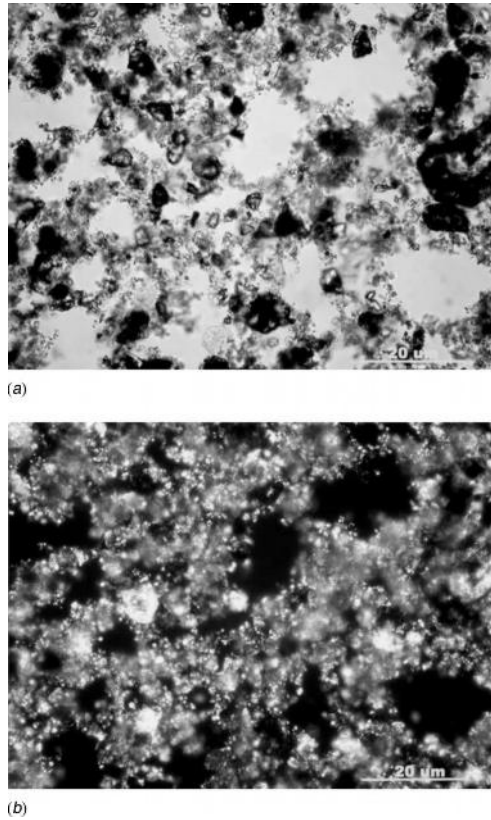


FIG. 4—Immersion preparation of masonry cement viewed using a petrographic microscope. (a) Plane polarized light. The darker material is mainly the ferrite phase of the portland cement (b). Crossed polars. Crossed polarized light. The bright particles are ground limestone.

and are overlooked. With time, as joints weather and pastes carbonate, they become even subtler until there is an apparent even match of joint color throughout the construction.

This study provides results of petrographic examinations of laboratory-prepared brick masonry prisms designed to provide variations of color and color tone due to the time when concave mortar joints are struck and tooled. Two different sets of masonry prisms were made: (a) masonry cement-sand mixtures and (b) portland cement-hydrated lime-sand mixtures. Joints were struck and tooled early, normal, and late for providing color and color tone differences to the joints. Bricks used in the normal and late-tooled specimens were oven-dried. Bricks used in the early-tooled surfaces were wetted.

Laboratory Study

Mortars

The two mortar mixes evaluated were: (a) mix HS made using Type S masonry cement and natural sand and (b) mix CL made using portland cement, hydrated lime, and natural sand. The masonry cement is air entraining and contains portland cement and limestone ground much finer than the portland cement. The brick has a 12.8-g/min initial rate of absorption.

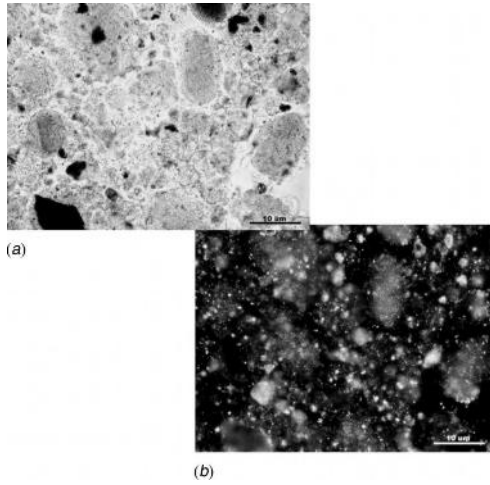


FIG. 5—Immersion preparation of hydrated lime viewed using a petrographic microscope. (a) Plane polarized light. The darker particles are impurities. (b) Crossed polarized light. The brighter particles are impurities.

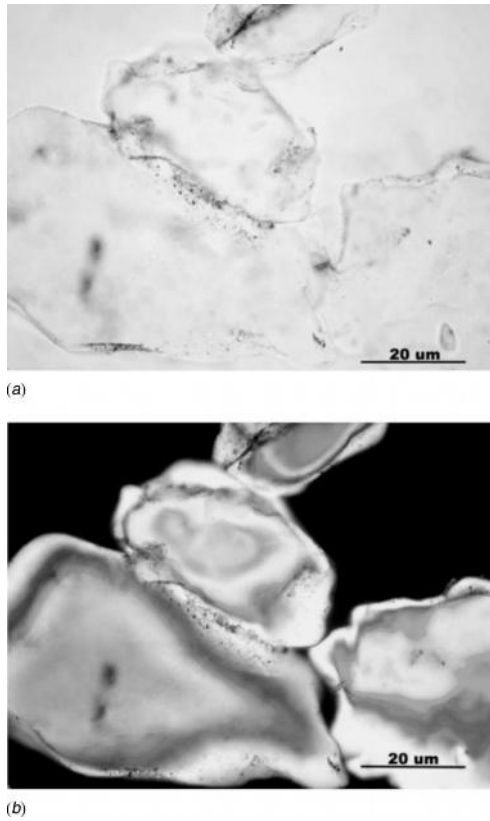


FIG. 6—Immersion preparation of natural sand particles viewed using a petrographic microscope and plane polarized light (a) and crossed polarized light (b). The sand particles are quartz.

TABLE 1—Proportions for mixtures used for the study and time of tooling. The brick has a 12.8-gs/min initial rate of absorption. Bricks for the early tooling were wetted. Bricks for the normal and late tooling were oven-dried.

Mortar mixture	Masonry or portland cement, lb	Hydrated lime, lb	Sand, lb	Water, lb	w/cm	Conditional time of tooling
Masonry cement-sand (HS)	15	...	48	6.34	0.42	(1) Tooled early (wet) (2) Tooled normal (3) Tooled late (dry)
Portland cement-hydrated lime-sand (CL)	12.5	2.6	48	8.52	0.56	(1) Tooled early (wet) (2) Tooled normal (3) Tooled late (dry)

Joints prepared for each mixture were struck and tooled early (wet), normal, and after the mortar had attained greater rigidity than normal (dry). Thus, there are six configurations of mortars and concave tooled joints. A summary of the mortar proportions is given in Table 1.

Petrographic Examinations

Immersion preparations of the masonry-making materials and pastes picked from surfaces of joints were examined using a petrographic microscope at magnifications up to 600 times. Joint surfaces were examined using a stereomicroscope at magnifications up to 45 times.

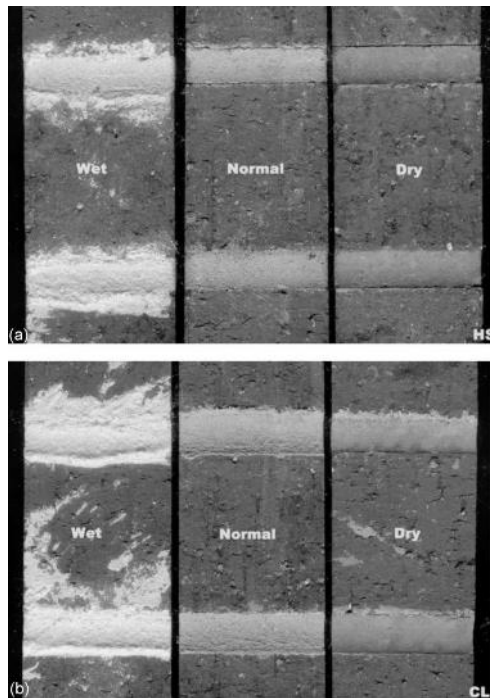


FIG. 7—Color differences resulting from different materials and tooling times. (a) Joint surfaces of the masonry cement-sand mortars tooled at different times. (b) Joint surfaces of the portland cement-hydrated lime-sand mortars tooled at different times.

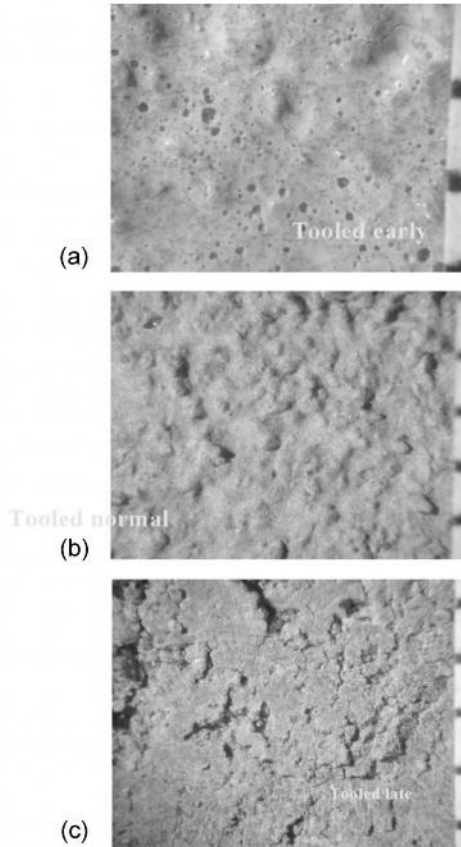


FIG. 8—Surface textures of the masonry cement-sand mortars that vary from smooth (due to laitance) to chatter marks (due to surface drag). (a) Early-finished smooth surface due to laitance. The surface is intersected by entrained air voids. Scale in 1/16-in. increments. (b) Normal-finished surface. Scale in 1/16-in. increments. (c) Chatter-marked late-finished surface due to mortar dragging during finishing. Scale in 1/16-in. increments.

Tooled Joint Color

Overall Color Changes—Color tone of joints becomes progressively darker from very light gray to medium gray to darker medium gray as the time of striking and tooling is delayed. The color change is similar for the mortars made using masonry cement (Fig. 7(a)), or the portland cement-hydrated lime mixtures (Fig. 7(b)).

Effects of Surface Texture—Also contributing to the color change is the texture of joint surfaces, which results in increased shadowing as textures progressively change from smooth (Figs. 8(a) and 9(a)) to chatter-marked (Figs. 8(c) and 9(c)). In addition to being smooth, the early-tooled mortars have laitance-like surfaces (Figs. 8(a) and 9(a)) resulting from bleeding that causes portland cement and aggregate fines to migrate to surfaces after the surfaces are struck and tooled.

Typically accompanying the laitance is the crystallization of coarse, platy calcium hydroxide ($\text{Ca}(\text{OH})_2$) crystals, which changes, due to carbonation, to microcrystalline calcium carbonate (CaCO_3)

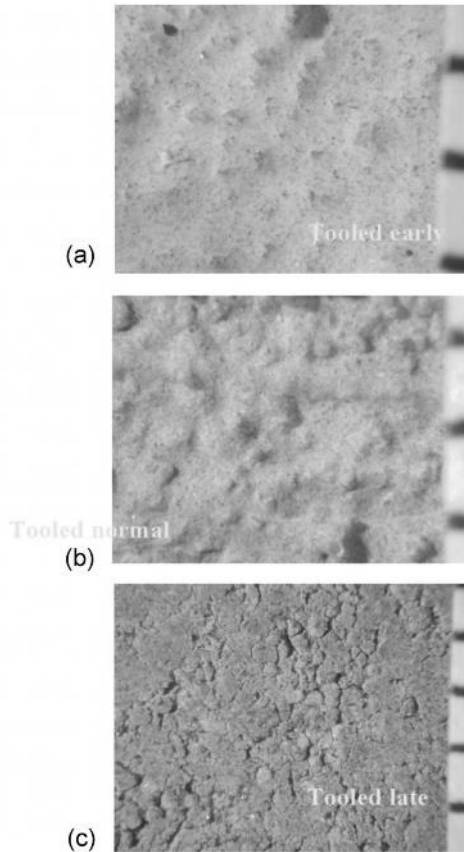


FIG. 9—Surface textures of the portland cement-hydrated lime-sand mortars that vary from smooth (due to laitance) to chatter marks (due to surface drag). (a) Early-finished smooth surface due to laitance. Scale in $1/16$ -in. increments. (b) Normal-finished surface. Scale in $1/16$ -in. increments. (c) Chatter-marked late-finished surface due to mortar dragging during finishing. Scale in $1/16$ -in. increments.

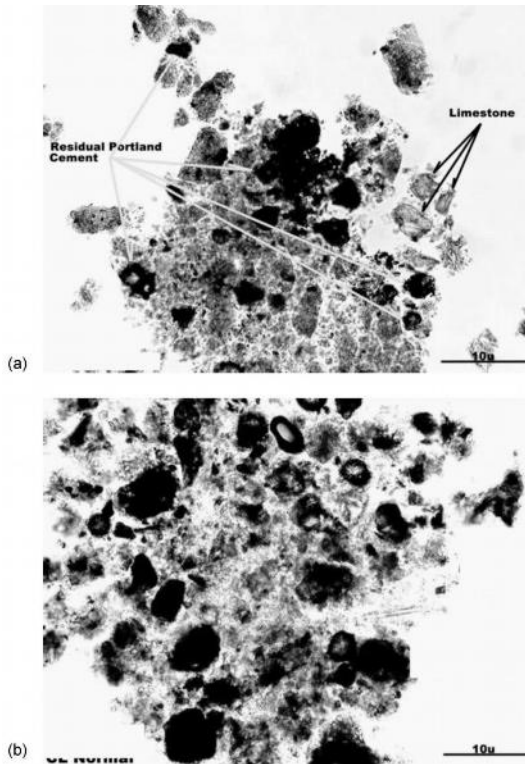


FIG. 10—Photomicrograph examples of paste picked from tooled surfaces of the mortars. Taken using a petrographic microscope and plane polarized light. (a) Paste picked from the early-finished joint surface of the masonry cement mortar. (b) Paste picked from the normal-finished joint surface of the portland cement-hydrated lime mortar.

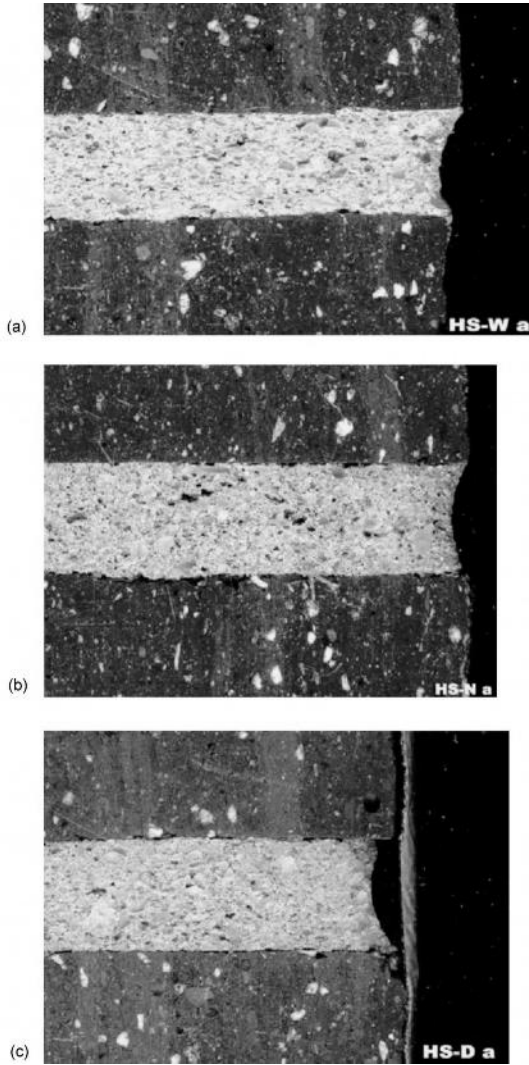


FIG. 11—Cross sections of the masonry cement mortar joints. (a) Tooled early. (b) Tooled normal. (c) Tooled late.

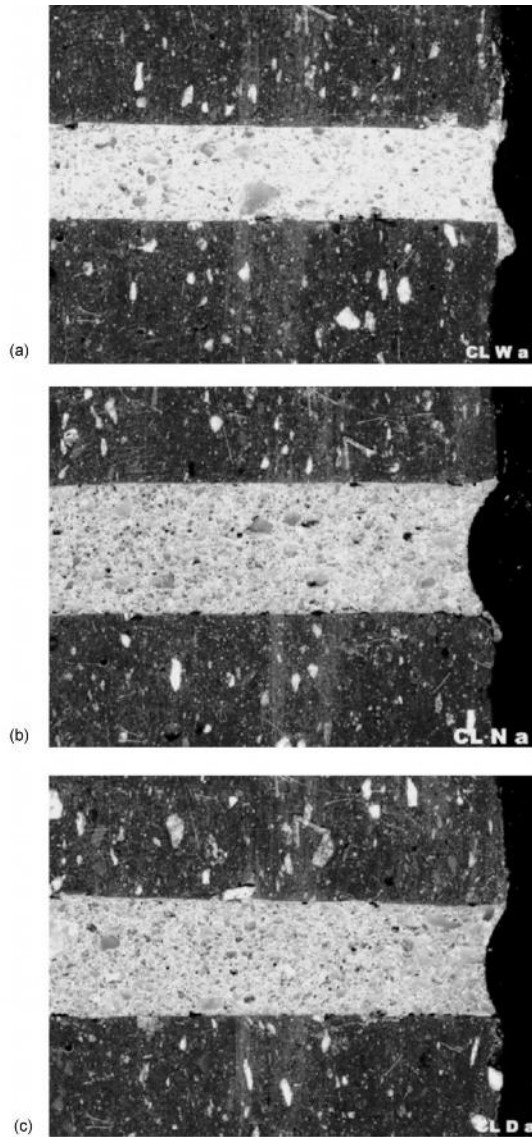


FIG. 12—Cross sections of the portland cement-hydrated lime mortar joints. (a) Tooled early. (b) Tooled normal. (c) Tooled late.

contiguous within the former calcium hydroxide crystals.

Effects of Cement Hydration and Hydrated Lime—The degree of portland cement hydration in the surface region decreases as the delay in striking and tooling increases (Fig. 10), which gives the surfaces a pepper-like appearance when the joints are viewed at high magnification. Each of these factors results in darker surfaces.

Because hydrated lime is white, it would be expected to impart a lighter color to joint surfaces than the masonry cement. However, the color of the limestone in the masonry cement used in this study imparts a

similar white color to early-struck joints so color differences are not pronounced (Figs. 7(a) and 7(b)).

Mortar of the early-finished joints are lighter than companion joints, a phenomenon judged due to extended curing resulting because of the use of wetted rather than oven-dried bricks (Figs. 11 and 12).

Comments

Based upon this laboratory study where mixing water content was constant, there is a relationship of color changes of tooled concave mortar joints and stiffness of the mortar when striking and tooling occurs. Color and color tone variations should be expected because of variable jobsite conditions, differences in assessing the exact time of mortar stiffening, and jobsite variations of mortar proportions and changes of mortar-making materials.

Richard J. Godbey¹ and Margaret L. Thomson²

The Selection and Use of Natural and Manufactured Stone Adhered Veneer

ABSTRACT: Adhered natural and manufactured stone veneer is increasing in popularity as an architectural element in both commercial and residential construction. The paper provides a brief overview of building code requirements, mortar specifications, back-up substrates, veneer application, and tips to avoid material failures. Building code requirements are based on typical references in the Uniform Building Code, International Building Code and Building Code Requirements for Masonry Structures. Mortar specifications are based on references as stated in the building codes, ASTM Standard Specification for Mortar for Unit Masonry (C 270), and typical manufacturer's specifications. Back-up substrates are discussed in regards to building code requirements and ASTM standards for weather-resistive barriers, metal lath or mesh and corrosion resistant fasteners. Veneer application and finishing guidelines as based on building codes and typical manufacturer specifications. Discussions of tips to avoid failure are based on good workmanship and material selection.

KEYWORDS: adhered veneer, adhered veneer application, manufactured stone, natural stone

Introduction

Adhered veneer is increasing in popularity as an architectural element in all types of commercial and residential construction (Fig. 1). The system attests to the continuing popularity of masonry design elements in both traditional, and contemporary architecture. The masonry units can vary from thin clay-brick to concrete masonry to natural stone. Colors and styles of units are available to match and complement nearly any style of architecture. Adhered veneer is typically defined as a nonstructural masonry material "...secured to and supported by the backing through adhesion" [1], or "veneer secured and supported through adhesion to an approved bonding material applied over an approved backing" [2].



FIG. 1—Adhered veneer on concrete block retaining walls. (Red Rock Country Club; Las Vegas, Nevada. Photo by R.J.Godbey.)

Manuscript received November 3, 2005; revised June 12, 2006; accepted for publication November 20, 2006; published online January 2007. Presented at ASTM Symposium on Masonry on 13 June 2006 in Toronto, Canada; B. Trimble and J. Brisch, Guest Editors.

¹ Chemist, Chemical Lime Company, Henderson, Nevada, E-mail: richard.godbey@chemicallime.com

² Technical Manager, Chemical Lime Company, Henderson, Nevada, E-mail: margaret.thomson@chemicallime.com

Building Code Requirements

The most common building code requirements for adhered veneer include the distribution of loads through the veneer to the backing, mortar requirements, unit size limitations, wall area limitations, shear strength of adhesion, back-up material requirements, and method of application. As a type of masonry system, special attention must be given to adhered veneer in terms of controlling expansion and contraction, the effects of out of plane loading potential, and management of moisture infiltration and masonry to backing bond strength.

The three main building codes considered are the Uniform Building Code (UBC 1997) [3], International Building Code (IBC) [2], and Building Code Requirements for Masonry Structures (ACI 530-05/ASCE 5-05/TMS 402-05) [1]. Supporting specifications for masonry structures as related to most building codes is based on Specification for Masonry Structures (ACI 530.1-05/ASCE 6-05/TMS 602-05) [4]. These codes and specification were chosen because many building regulation jurisdictions in the United States use, or incorporate by adoption, masonry construction requirements as outlined in one or more of these three building codes.

UBC 1997 and IBC state that the maximum density of for all exterior adhered veneer is 73.2 kg/m^2 (15 lb/ft^2). In addition, veneer units cannot exceed 914 mm (36 in.) in length on one side nor may the overall face area of the stone be greater than 0.46 m^2 (720 in.^2). UBC 1997 states, "Veneer units weighing less than 14.6 kg/m^2 (3 lb/ft^2) shall not be limited in dimension or area. Additionally, UBC 1997 states "Exterior veneer shall not be attached to wood-frame construction a point more than 9144 mm (30 ft) in height above the noncombustible foundation, except...when special construction is designed to provide for differential movement and when approved by the building official." IBC states: "The backing of...adhered veneer shall be of concrete, masonry, steel framing or wood framing." Additionally, IBC states that the minimum thickness of adhered masonry veneer will be 6.35 mm ($1/4 \text{ in.}$) and the weight of interior adhered masonry veneer cannot exceed 97.6 kg/m^2 (20 lbs/ft^2). Another stipulation in IBC is: "Where the interior veneer is supported by wood construction, the supporting members shall be designed to limit deflection to $1/600$ of the span of the supporting members." According to ACI 530-05/ASCE 5-05/TMS 402-05, the maximum thickness of adhered veneer units can be 66.7 mm ($25/8 \text{ in.}$) and the face area of the stone may not be greater than 0.46 m^2 (720 in.^2); maximum weight according to this code is also 73.2 kg/m^2 (15 lb/ft^2). In some seismic zones, such as Los Angeles, CA, adhered veneer units cannot weigh more than 48.8 kg/m^2 (10 lb/ft^2) [5]. It is also interesting to note that in some parts of seismically active California, "Units of tile, masonry, stone or terra cotta which exceed 16 mm ($5/8 \text{ in.}$) in thickness shall be applied as for anchored veneer where used over exit ways or more than 6096 mm (20 ft) in height above adjacent ground elevations." [6]. It is important to remember that local building code jurisdictions will have different requirements for adhered veneer and that installations must comply with local building officials' requirements.

Mortar and Shear Strength Specifications

Many manufacturers of adhered veneer products specify one or more mortar materials for the specific installation of their product. The most common types manufacturer recommended mortar materials are Type N and Types S masonry mortars as specified in ASTM Standard Specification for Mortar for Unit Masonry (C 270). In rare cases, Type M mortar is specified for both back-up plaster scratch and masonry unit-bedding coats. Individual manufacturers may also specify modified mortars containing admixtures (e.g., bonding agents). General guidelines for mortar selection can also be found in UBC 1997 and ACI 530-05/ASCE 5-05/TMS 402-05. Both of these codes recommend brushing a paste of neat Portland cement on the back-up and veneer unit and then applying Type S mortar to both the back-up and veneer unit prior to setting. The resulting adhesion of the cured system is specified in ACI 530-05/ASCE 5-05/TMS 402-05 and must have a shear strength of at least 0.34 MPa (50 psi) when tested in accordance with ASTM Test Method for Bond Strength of Ceramic Tile to Portland Cement (C 482); or be applied using neat cement followed by bedding in Type S mortar in compliance with requirements outlined in ACI 530.1-05/ASCE 6-05/TMS 602-05.

What is the best mortar to use for adhered veneer applications? According to the Rocky Mountain Masonry Institute (RMMI) [7], "Type N is a good all around mortar choice for most applications." and "In hot weather applications, it performs better and overall it is easier to use." "Type S has a stronger bond, but

with this increased bond strength comes an increase in possible shrinkage and cracking.” “Type S may be required by some building codes, especially in seismic areas.” RMMI also states that bonding agents “...are normally not required if correct application procedures are followed.” but “a bonding agent...may be advantageous...in...soffits or other overhead uses” or “when placing non-absorptive, high density stones (such as granite or marble) with smooth cut surfaces.”

On interior installations not exposed to moisture, some manufacturers of adhered veneer allow the application to be made using mortar or epoxy adhesives. Adhesives are applied using tile trade techniques in which a thin bedding of adhesive is applied to the back-up wall using a notched trowel.

Back-up Substrates

ACI 530-05/ASCE 5-05/TMS 402-05 states “Backing shall provide a continuous, moisture-resistant surface to receive the adhered veneer. Backing is permitted to be concrete block, concrete, or metal lath and Portland cement plaster applied to masonry, concrete, steel framing, or wood framing.”

Steel and wood stud systems with sheathing (e.g., exterior grade plywood, green treated plywood, rigid composite board and flush metal siding) in exterior uses must provide a weather barrier to protect the interior of the structure. UBC 1997 and ACI 530-05/ASCE 5-05/TMS 402-05 both outline the requirements for weather-resistive barriers for steel and wood stud framing systems. ASTM Specification for Asphalt-Saturated Organic Felt Used in Roofing and Waterproofing (D 226) and ASTM Specification for Metal Lath (C 847) provide excellent guidance in specifying materials that will provide good weather-resistive barriers on steel and wood stud framing systems. Guidance for installation of metal lath is provided in ASTM Specification for Installation of Lathing and Furring to Receive Interior and Exterior Portland Cement-Based Plaster. In general, all lath and lath fasteners must be corrosion resistant, as may be specified to meet ASTM Specification for Zinc Coating (Hot-Dip) on Iron and Steel Hardware (A 153), or other standards.

New concrete block or poured concrete walls normally do not require any special preparation except to insure that any form release agents (e.g., oil) are cleaned and etched with a suitable agent (e.g., muriatic acid followed by rinsing with water and wire brushing). Existing concrete block or poured concrete walls must be strong and sound and may need sandblasting to remove any paint or sealers that could interfere with adhesion. Insulated concrete form walls should have a vapor barrier applied and then be covered in expanded metal lath with corrosion resistant fasteners that penetrate through the insulation into the concrete core. Framed interior walls must be faced to meet local building codes (e.g., sheetrock, green sheetrock, concrete board or plywood) and covered with metal lath using corrosion resistant fasteners (except concrete board where allowed).

Veneer Application and Finishing Guidelines

General

The overall goal of an exterior installation should be to provide an attractive and durable wall facing that protects the interior of the structure from the weather. Interior installations must consider the type of location (e.g., wet or dry) and the type of back up (e.g., wood or concrete). The manufacturer’s installation guidelines should be understood and followed. Installations of adhered veneer should follow the guidelines of local building departments as outlined in the specific requirements of that jurisdiction. Proper material selection and good workmanship is critical to the success of the installation. Prior to large-scale application, sample panels of the work should be constructed and approved by both the building owner and his/her architect.

Structural Loads

The first step to a quality adhered veneer installation is the recognition that structural loads are carried entirely by the backing. Each back-up substrate material has unique characteristics that must be considered before the installation process begins. For example, wood and steel framing systems are fairly flexible, whereas masonry materials are relatively stiff and inflexible. Wood is more likely to move, as it shrinks

and swells, depending on weather conditions, and therefore, is a more challenging back-up substrate than concrete, which is well matched to the character of the adhered masonry units. Application to metal panels is similar to that of wood or steel framing.

As the structure adjusts to loads, temperature differences, creep, deflection, changes in humidity and foundation settlements, the back-up substrate will move. Flexible members may more easily absorb this movement, in contrast with stiff masonry members, where cracks can develop. Slight cracks are not harmful and will not compromise the integrity of the veneer if the cracks are pointed with new mortar to keep water out of the wall. Movement joints should be incorporated into the system, particularly near building corners, window and door openings, where veneer meets other materials (e.g., veneer meets stucco) and for large walls without openings exceeding 9144 to 10 668 mm (30 to 35 ft). Individual movement joints should be at least 9.5 to 12.7 mm ($\frac{3}{8}$ in. to $\frac{1}{2}$ in.) wide and filled with a suitable backer rod and compatible sealant [8]. The architect, designer or structural engineer must specify movement joints installed to limit the effect of cracking, deflection and delamination, with help as needed or recommended, by the veneer manufacturer.

Moisture Penetration

The second step to a quality installation is recognition that masonry veneers are not waterproof. There are three conditions needed to cause water penetration into masonry systems: (1) there is water on the wall, (2) there is a path of entry for water, and (3) there are forces present to drive the water through the wall (e.g., wind driven rain, differential atmospheric pressures) [9]. Because of the potential for water penetration, a moisture resistant barrier is needed at the face of the backing to prevent water damage to the interior of the structure. Building paper is commonly used over wood and steel stud walls in conjunction with flashing at the base of walls, around windows, doors and other openings, on sills and under any wall caps to direct or deflect any potential moisture penetration to the exterior. Concrete block and poured concrete walls are inherently water resistant and generally do not require the application of any supplemental moisture barriers.

Considering that water may find a way into the wall, it is very important that full mortar coverage exists between the back of the masonry unit and the cement plaster or backing substrate. When the mortar coverage is not 100 %, a void is present that can fill with water. Water expands about 10 % when frozen [10], and when water filled voids are present behind the veneer, freeze-thaw failure is common and may be evidenced by masonry units literally “popping” off the wall.

Many veneer manufacturers recommend the use of rain screen or weep systems to be installed on exterior wood and steel framed walls. Rain screen and weep systems allow the veneer to be separated from the backing while providing a percolation system that directs any water penetration back to the exterior. This percolation system improves ventilation and helps to prevent the growth of mold or mildew. The separation of the veneer from the framing substrate helps to control cracking due to differential movement of the materials.

General Guidelines For Application

The application procedures generally include preparing the wall surface, layout of the wall area, applying mortar to the wall and/or the unit, applying the unit, grouting and finishing. Table 1 shows general guidelines for wall surface preparation.

After the wall area has been prepared for application, the second step requires layout of the wall area to receive the units. There are many types of materials and “looks” available; from traditional running bond thin-clay brick to random patterned natural or manufactured stone. To achieve the most pleasing match of color and texture from lot to lot of material, it is recommended by most manufacturers that installation moves forward by selecting material for use from several boxes at the same time.

When laying out the wall area for coverage, the area to be covered must be calculated and if the pattern includes mortar joints, the thickness of the mortar joint should be included to calculate and mark off the number of courses required. A dry run layout on the ground to find the most pleasing unit pattern is often helpful and may speed installation. Level or other pencil mark guidelines are typically helpful to insure proper placement of coursed materials like brick and ashlar stone, or to mark off boundaries for random

TABLE 1—General Guidelines For Wall Surface Preparation.

Wall surface type	Exterior and interior preparation required
Rigid Walls Over Studs: Sheetrock Plywood and OSB Paneling Sheathing Concrete Board Polystyrene Insulation Board (over a rigid back wall)	Install a breathing-type weather resistant barrier from the bottom of the wall up, with joints lapped 4 in. Per local building code and specifications, lap and install lath or mesh using corrosion resistant fasteners 6 in. on center penetrating studs at least 1 in. Insure that all weather resistant barrier and metal lath or mesh continuously wraps a minimum of 16 in. around all inside and outside corners. Depending on the manufacturer and the type of veneer material to be installed, a scratch coat of Type S C 270 mortar is applied and allowed to cure.
Clean and New: Concrete Masonry Stucco	No special preparation is needed. Make sure that any newly poured concrete is free of form release agents (e.g., oil). If release agents are present, etch surface with muriatic or other approved acid, rinse clean with fresh water and lightly score surface with a wire brush. Generally, a scratch coat of stucco is not required and units will be bedded directly in mortar applied to the wall and/or unit itself.
Existing: Concrete, Masonry, Stucco	Sand or water blast dirty, painted, or sealed areas down to original surface. Wash surface with fresh water or if surface cannot be thoroughly cleaned, attach lath or mesh. Generally, a scratch coat of stucco is not required and units will be bedded directly in mortar applied to the wall and/or unit itself.
Metal Buildings:	See local building code and manufacturer's instructions.
Open Studs: Polystyrene Insulation Board (over open studs)	Lap and install paper-backed lath or mesh to studs using corrosion resistant fasteners penetrating a minimum of 1 in. into studs and 4 in. on center. Apply $\frac{1}{2}$ -in. to $\frac{3}{4}$ -in. cement based stucco scratch coat and allow to moist cure at least 48 h.

patterns. Mortar joint size can be adjusted as necessary to minimize horizontal cutting using a tile saw, chisel, and hammer, or hand-held grinder with a masonry approved diamond-cutting wheel.

Prior to mortar application, it is beneficial to dampen the receiving surface with water to help slow the absorption of water from the mortar. This simple step will help improve bond strength of the unit to the substrate. Surfaces should be damp but not dripping wet. Using a trowel and Type N or Type S mortar, or mortar as specified by the building code or veneer manufacturer, apply a 9.5 to 19.1 mm ($\frac{3}{8}$ to $\frac{3}{4}$ -in.) thick layer of mortar directly to the back-up substrate in an area of approximately 0.46 to 0.92 m² (5 to 10 ft²). Just prior to setting the unit, apply a 100 % coverage mortar approximately 9.5 to 19.1 mm ($\frac{3}{8}$ to $\frac{3}{4}$ -in.) thick to the back of the unit. A slight excess of mortar at the edges is helpful so that mortar will squeeze out when setting the unit (Fig. 2).

Depending on the thickness of the desired mortar joint, the amount of mortar placed on the back of the unit will vary. To minimize shrinkage cracks, mortar joints should never be larger than 12.7 mm ($\frac{1}{2}$ in.). Corners are generally set first and workers may choose to apply the field units from the top-down or the bottom-up. Some workers find that it is beneficial to work from the top-down so that mortar droppings do not hit the stones below and cause more clean-up. Some workers will slightly "wiggle" the units into place to assure 100 % bond and some will use a rubber mallet to "tap" the units into place as specified by many veneer manufacturers. At the end of the work period, mortar smears can be gently brushed off the unit. The brush should be dry to prevent staining the mortar joints and causing smears to be worked into the unit. It is never recommended to use aggressive cleaning methods that could loosen the unit (e.g., pressure washing). Chemical cleaners are generally not necessary, but the unit manufacturer may have recommendations for cleaning their particular product.



FIG. 2—Backing prepared with horizontally raked stucco scratch coat, layout completed, corner stones set, adhered veneer installation proceeding. (Summerlin Masterplanned Community; Las Vegas, Nevada. Photo by R.J. Godbey.)

As with conventional masonry unit construction, mortar joints are smoothed and compacted with a jointing tool when the mortar is thumbprint hard. Concave joints are the best choice to minimize water penetration. Grouting and filling of mortar joints may be accomplished after the initial set, generally after 24 h has elapsed. Some workers find that a grouting bag is the easiest and most efficient manner to fill any unmortared spaces between units.

Tips to Avoid Material Failure

Good design, careful workmanship and quality materials are the best insurance against premature system failure. Generally speaking, materials selected for use in interiors are governed primarily by aesthetics; however, materials selected for use on the exterior are more suitable when they have low water absorption rates, high flexural strength, and high weathering resistance [11]. The number one goal should be to ensure that the coverage between the properly prepared backing substrate and the veneer unit is filled 100 % with mortar. According to the Masonry Institute of Washington, cement-lime mortar provides a higher degree of rain resistance and “Type N mortar is recommended for exterior use above grade. It is medium strength mortar and suitable for general use in exposed masonry.” [12]. Without full mortar coverage, existing voids will collect water and in freeze-thaw environments, and units may pop off the wall. Mortar joints themselves must be full and well compacted by proper tooling. Try to avoid using raked joints that are more susceptible to water penetration than concave finished joints. Dry stack patterns are not the best choice for areas of severe freeze-thaw cycling without the installation of rain screen and weep systems or the specification of a thin, full mortar joint between units. Wide mortar joints should be avoided because of higher shrinkage rates and increased potential for water penetration. Flashing and cant strips should be properly installed and combined with gutters and downspouts to prevent excessive water from running freely down the wall. Sprinklers should never be directed against adhered veneer. Retaining walls covered with adhered veneer should be well designed and have good drainage. Chimney caps should extend at least 1 in. beyond the veneer face to provide protection against run-off. Movement joints should be designed into the system. De-icing salts should not be used in the areas of adhered veneer.

Conclusion

Adhered veneer is a popular material for the facing of commercial and residential structures. When good workmanship is combined with quality materials, installations are both aesthetically pleasing and durable. Perhaps the words of a practicing mason, Jeff Leonard, as quoted in *Masonry Magazine*, best sum up the choice to use adhered veneer: “There are so many different materials you can put on a building now that

we've got to figure out a way to compete...Masonry can be replaced by so many different materials on the skin of a building that we've got to get more cost-effective. We have to figure out better ways of keeping masonry materials on the skin of these buildings. Thin stone veneer just happens to be one of them." [13].

Acknowledgments

Thanks to the many manufacturers of natural and manufactured masonry veneer materials for providing information on the installation of their specific products. While it is not possible to name them in this paper, their help is appreciated.

References

- [1] Masonry Standards Joint Committee, *Building Code Requirements for Masonry Structures*, 2005. Chap. 1, General Design Requirements for Masonry, Section 1.6 (ACI 530–05/ASCE 5–05/TMS 402–05), American Concrete Institute, Farmington Hills, MI, Structural Engineering Institute of the American Society of Civil Engineers, Reston VA and The Masonry Society, Boulder CO, 2005.
- [2] International Code Council, *International Building Code*, Chap. 14-Exterior Walls, Country Club Hills IL, 2003.
- [3] International Conference of Building Officials, *Uniform Building Code*, 1997, Chap. 14, Exterior Wall Coverings, Whittier CA.
- [4] *Masonry Standards Joint Committee*, Specification for Masonry Structures, Chap. 1, General Design Requirements for Masonry, Section 1.6 (ACI 530.1–05/ASCE 6–05/TMS 602–05), American Concrete Institute, Farmington Hills, MI, Structural Engineering Institute of the American Society of Civil Engineers, Reston VA and The Masonry Society, Boulder CO, 2005.
- [5] City of Los Angeles, *Los Angeles Building Code*, Los Angeles, CA, 2003.
- [6] California Building Standards Commission, *California Building Standards Code*, Section 1403A.5.3 Unit Size Limitations, Sacramento, CA, 2001.
- [7] Rocky Mountain Masonry Institute, "Adhered Natural Stone Veneer Installation Guide," Denver CO, 2004, pp. 6.
- [8] Munro, C., "Troubleshooting Masonry, Part 1: Accommodating Movement in Masonry Walls," World of Concrete Seminar MO-42, Las Vegas, Nevada, Jan. 2005.
- [9] Masonry Institute of Washington, *The Northwest Masonry Guide*, Part IV-A, "Requirements for Rain Resistant Masonry Construction," Kirkland WA, 2003, p. 1.
- [10] Migliore, V., Marble Institute of America, "Adhered Exterior Stone Veneers," Westlake, OH, March 2002, pp. 1.
- [11] Gere, A., Building Stone Institute, "Recommended Practices for the Use of Natural Stone in Construction," 3rd ed., Itasca IL, 2002, p. 9.
- [12] Masonry Institute of Washington, *The Northwest Masonry Guide*, Part IV-A, "Requirements for Rain Resistant Masonry Construction," Kirkland WA, 2003 p. 3.
- [13] Leonard, J., President of Leonard Masonry Inc., St. Louis MO, Masonry Contractors of America, "Stone Veneer: Through Thick and Thin," *Masonry Magazine*, Vol. 42, 2003, pp. 25.

Richard M. Bennett, Ph.D, PE,¹ William M. McGinley, Ph.D, PE,² and Jim Bryja, M.Sc, SE³

Deflection Criteria for Masonry Beams

ABSTRACT: This paper examines issues related to deflection criteria for masonry beams. Masonry walls supported by beams and lintels act compositely with the beam. As the height of the masonry wall increases, the behavior becomes more like that of a tied arch, with the masonry in compression and the beam acting as the tension tie. Deflection limits are only needed so that sufficient stiffness is provided during construction to prevent serviceability problems, with the suggested limit being $l/600$. Several methods for determining the deflection of reinforced masonry beams are examined, and a method for the effective moment of inertia of cracked reinforced sections is recommended. Beams and lintels that exceed this deflection do not necessarily have to be increased in size, but rather shores could be used during construction. Masonry beams and lintels with $l/d \leq 8$ should not be controlled by deflections. Therefore, it is recommended that the code not require these members to be checked for deflections.

KEYWORDS: masonry, beam, lintel, deflection, stiffness, limits

Notation

- A_s = area of steel
 A_{bal} = area of steel at balanced conditions, or such that the steel yields and the masonry crushes simultaneously
 b = width of member
 d = depth from the extreme compression fiber to the centroid of the tension reinforcement
 E_m = modulus of elasticity of masonry
 f_{cr} = stress at steel level in cracked condition due to M_{cr}
 f_a = stress at steel level in cracked condition due to M_a
 f_m^c = compressive strength of masonry
 F_r = modulus of rupture
 h = height of member
 I_{cr} = moment of inertia of cracked cross-sectional area of a member
 I_{eff} = effective moment of inertia
 I_g = moment of inertia of gross cross-sectional area of a member
 I_n = moment of inertia of net cross-sectional area of a member
 l = span length
 M_a = maximum moment in member due to the applied loading for which deflection is computed
 M_{cr} = nominal cracking moment strength
 M_n = nominal moment strength
 Δ = deflection
 Δ_{cr} = deflection using I_{cr}
 Δ_n = deflection using I_n
 ϕ = curvature
 ϕ_{cr} = curvature using cracked section properties
 ϕ_n = curvature using net section (uncracked) section properties

Manuscript received October 31, 2005; accepted for publication November 20, 2006; published online January 2007. Presented at ASTM Symposium on Masonry on 13 June 2006 in Toronto, Canada; B. Trimble and J. Brisch, Guest Editors.

¹ Professor, Department of Civil and Environmental Engineering, The University of Tennessee, Knoxville, TN 37996-2010.

² Professor, Department of Architectural Engineering, North Carolina A & T State University, Greensboro, NC 27411.

³ Manager Technical Services, General Shale Products Corporation, Johnson City, TN 37601.

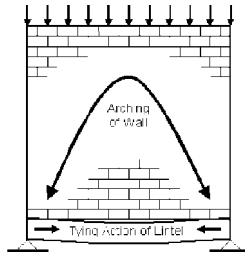


FIG. 1—Composite tied arch system.

Introduction

Currently, the Masonry Standards Joint Committee (MSJC) code [1] has few requirements limiting the deflections of masonry beams and lintels. MSJC, Section 1.10.1 requires that deflections of beams and lintels due to combined dead and live loads not exceed the lesser of $l/600$ or 0.3 in. (7.6 mm) when providing vertical support to unreinforced masonry designed using the allowable stress design provisions or to empirically designed masonry. The code commentary states that these deflection limits apply to beams of all materials that provide support to unreinforced masonry. These empirical requirements limit excessive deflections that may result in damage to the supported masonry. In reinforced masonry systems, it is assumed that crack width will be controlled by the reinforcement so that the deflection requirements are waived.

Section 6.3.5.1 of the Canadian Masonry Code [2] requires that elements supporting masonry be limited to elastic deflections under load of $l/600$ or less and long-term deflections under sustained loads of $l/480$ or less. Section 12.4.1 of this code requires that deflection of beams need to be checked only when the clear span exceeds $15d$, where d is the depth from the extreme compression fiber to the centroid of the tension reinforcement.

When the beam or lintel supporting the unreinforced masonry is a reinforced masonry member, Section 3.1.5.3 of the MSJC code [1] addresses the computation of deflection. This section requires that the deflection of reinforced masonry members be determined based on cracked section properties. Historically, an effective moment of inertia has been calculated using net and cracked cross-sectional area properties and the ratio of cracking moment strength to the applied moment resulting from unfactored loads as shown in Eq 1. The commentary states that this equation has successfully been used for estimating the post-cracking flexural stiffness of both concrete and masonry:

$$I_{\text{eff}} = I_n \left(\frac{M_{\text{cr}}}{M_a} \right)^3 + I_{\text{cr}} \left[1 - \left(\frac{M_{\text{cr}}}{M_a} \right)^3 \right] \leq I_n \leq 0.5I_g \quad (1)$$

This paper examines issues related to deflection criteria for masonry beams. Specifically, the behavior of masonry beams and lintels supporting unreinforced masonry is examined, and appropriate criteria for deflections and the loading conditions for which deflections should be checked are discussed. Several methods for determining the deflection of reinforced masonry lintels are examined, and a method for the effective moment of inertia of cracked reinforced sections is recommended. A span limit under which deflections do not need to be checked is also developed.

Behavior of Beams and Lintels Supporting Masonry

The behavior of a beam/lintel supporting unreinforced masonry is very different from that of a beam/lintel carrying the exact same load, but where the load being applied is from some other source, such as roof or floor joists. In the former, the masonry acts compositely with the lintel. For lower heights of masonry, the system acts like a deep beam. For higher heights, it acts like a tied arch, as shown in Fig. 1. The following paragraphs describe test results that illustrate this behavior.

Rosenhaupt [3] evaluated the performance of vertically loaded masonry walls on simply supported

TABLE 1—Summary of results of vertically loaded wall/beam tests by Rosenhaupt [3].

Description	Height of wall/span length	First crack load, psi (kPa)	Description of crack	Failure load, psi (kPa)	Mode of failure	Midspan deflection at load of 14.2 psi (98 kPa), in. (mm)
Concrete beam	...	8 (50)	Tension crack	20 (130)	Yielding of reinforcement	1.425 (36.2)
Ytong blocks	0.21	31 (220)	Shear crack in beam	57 (390)	Shearing and bending of beam	0.118 (3.0)
Ytong blocks	0.38	43 (290)	Tension crack in beam	57 (390)	Diagonal shear in masonry above support	0.102 (2.6)
Ytong blocks	0.54	43 (290)	Diagonal crack in extreme block above support	54 (370)	Crushing of extreme block above support	0.083 (2.1)
Ytong blocks	0.72	71 (490)	Diagonal crack in extreme block above support	71 (490)	Crushing of extreme block above support	0.047 (1.2)
Concrete blocks	0.72	71 (490)	Tension crack over whole depth of beam	127 (880)	Vertical shear above support over whole wall height	0.020 (0.5)

reinforced concrete beams, and compared this to the performance of the concrete beam alone. Two types of masonry were used; a “Ytong” block, which was a lightweight cellular concrete block manufactured with lime and sand and steam cured, and traditional concrete masonry units. A reinforced tie beam was cast atop the unreinforced masonry wall. The span of the beam was 6.07 ft (1.85 m) and the top of the wall was vertically loaded through a series of spreader beams to simulate a uniform load. Measurements using a mechanical strain gage showed the force applied to the beam by the masonry wall concentrated near the supports. Horizontal compressive stresses appeared to be distributed over the height of the wall, with the beam acting as a tension tie. Table 1 summarizes the results of these tests and, to be consistent with the original data, loads are given in terms of force per unit of applied area. Rosenhaupt [3] concluded that the masonry is acting compositely with the concrete beam, and the masonry wall-beam system is both much stiffer and stronger than the concrete beam alone. Based on the presented data, cracking and damage to the masonry did not appear to have been a problem.

Burhouse [4] reported on ten full-scale tests where simply supported beams carrying unreinforced brick walls were tested over a span of 12 ft (3.66 m). Five of the beams were reinforced concrete and five were concrete encased structural steel joists. For each specimen, the top of the walls were loaded with a series of jacks to simulate a uniform load. Table 2 summarizes the results of only the tests of masonry walls supported on the reinforced concrete beams, since they are the most applicable. The failure loads of the concrete beams alone were calculated based on material properties given by Burhouse [4], assuming a uniform distributed load, and are given in terms of total applied load to be consistent with the original data. All of the tests, except Specimen 10, used a “Fletton” brick and 1:1:6 mortar, where the brick and mortar had compressive strengths of 3000–3500 psi (20.7–24.1 MPa) and 490–850 psi (3.38–5.86 MPa),

TABLE 2—Summary of results of tests on reinforced concrete beams by Burhouse (1969).

Specimen	Height of wall/span length	Failure load, kips (kN)	Failure load of beam alone, kips (kN)
6	0.5	120.0 (533)	10.0 (44.5)
7	0.5	119.4 (531)	19.5 (86.7)
8	0.75	98.6 (438)	10.0 (44.5)
9	0.25	104.8 (466)	19.5 (86.7)
10	0.73	189.0 (840)	10.0 (44.5)

TABLE 3—Recorded deflections as reported by Stafford Smith et al. [5].

Beam Type	Deflection	Fraction of ultimate load at which deflection was recorded
Steel beam	//1143	0.77
	//497	0.98
	//1286	0.68
Concrete encased steel beam	//714	1.00
	//549	1.00
	//520	1.00

respectively. Specimen 10 had “engineer” bricks and a 1:1/4:3 mortar in the lower corners with Fletton brick elsewhere. The engineer brick and 1:1/4:3 mortar had compressive strengths of 12 240 psi (84.4 MPa) and 2450 psi (16.9 MPa), respectively.

The masonry wall/concrete beam panels behaved as tied arches, with the brick acting as the arch and the beam as the tension tie. With the exception of Specimen 9, failure was by crushing of the brickwork at the lower outer corner of the panels followed by what was identified as “failure of the beam.” Specimen 10, with the higher strength bricks and mortar in the critical lower corners, failed at a much higher load than the other specimens. In Test 9, with the height of the brickwork being only one-fourth of the span length, the failure occurred when the bricks in the flexural compression block at the top of the beam near center span crushed, as in a typical flexural failure of a reinforced concrete beam. A shear crack also developed in this test. Little information was given on the deflections other than the statement that the deflections were small. For Specimen 9, the deflection was 1/840 of the span at 80 % of the ultimate load. The deflections of other tests were said to be smaller at the same load level.

Tests by Burhouse [4] of brickwork supported by concrete encased steel joist tests showed similar behavior, with the system acting as a tied arch. Again little information was given on deflections, other than noting that deflections were small. In one test, it was reported that the deflection was 1/1123 of the span at 89 % of the ultimate load.

Stafford Smith et al. [5] used the results of Burhouse’s tests and additional wall tests at the University of Surrey on concrete encased steel joists and McGill University on steel beams to develop a method for the analysis and design of masonry walls supported on beams. Recorded deflections of the University of Surrey and the McGill University tests are given in Table 3. The deflections are quite small, even at the ultimate load. Stafford Smith et al. also describe the behavior the masonry wall/beam system as that of a tied arch. As the beam is loaded, the beam tends to deflect away from the wall in the middle of the span leaving the wall only supported in the end regions. They state that a brick height of at least 0.6 times the span length is needed for the tied arch to form.

McGinley et al. [6] reported on the results of field measurements of the deflection of a 5 by 3-1/2 by 1/4 in. (127 by 89 by 6.3 mm) steel angle lintel over a garage door opening. In this investigation, a 16-ft (4.88-m) long angle was shored in three places along the span and then 18.5 in. (467 mm) of brick was laid on top of the angle. The masonry consisted of a soldier course followed by three courses of running bond masonry with two-wire, 9-ga. (3.76-mm) joint reinforcement in each bed joint in the three running bond courses. The shores were removed after 2.5 days of curing, and the deflection of the steel angle at midspan was measured as 0.0235 in. (0.600 mm). Just considering the angle, the calculated flexural deflection would be 0.582 in. (14.8 mm). Considering the brick and steel angle acting compositely and the brick having only 40 % of its code-specified elastic modulus due to early age loading, the calculated flexural deflection is 0.061 in. (1.55 mm).

Two reshores were placed to re-support the lintel and additional brick was laid to a total height of 9 ft-4 in. (2.84 m) in approximately 1.5 h. Immediately after the additional brick was laid, the reshores were removed. The measured deflection at midspan was 0.1215 in. (3.09 mm). Just considering the angle, the calculated flexural deflection would be 3.52 in. (89.4 mm). Consider the brick and steel angle acting compositely, the calculated flexural deflection is 0.368 in. (9.35 mm). It was postulated that part of the reason the measured deflections were less than the calculated deflections was due to partial end fixity that was not accounted for in the calculations. However, this support fixity does not account for all the differences between the measured and calculated deformations and it is clear that the brick veneer is significantly adding to the stiffness of the system and carrying a good portion of its own weight. It is also

clear that, if a significant amount of masonry is present above the lintel, it no longer acts primarily as a beam, but can develop significant arching action.

Both the laboratory testing and field observations have shown that unreinforced masonry supported by a beam or lintel participates in carrying its own weight as well as any superimposed loads. Any method for computation of deflections that ignores the contribution of the masonry to the stiffness of the system is not going to give accurate results. Indeed, controlling deflections of the lintel will not eliminate cracking of the unreinforced masonry. Furthermore, if there is composite action between the masonry and the lintel, the masonry is primarily in compression and cracking is usually not a problem. Given the stiffness of masonry walls, it appears that it is not necessary to check long-term deflections of beams and lintels supporting masonry. The masonry, whether it is reinforced or unreinforced, will participate in carrying the load. The wall-beam system is much stronger and stiffer than accounted for when just considering the lintel.

This leaves the issue of deflections of lintels and beams during construction of the masonry. Sufficient stiffness is needed to support the masonry while it is being laid. Excessive deflections that are “locked” into the wall during construction will be aesthetically displeasing. In extreme cases, excessive deflection could cause the mortar to masonry bond to break before the mortar is fully hardened. Thus, it is recommended that short term flexural deflections under the weight of the masonry be checked and limited. The purpose is simply to provide sufficient stiffness during construction while the masonry is being laid.

There is little available literature to suggest what an appropriate deflection limit should be. Galambos and Ellingwood [7] state that beam deflections have to be greater than $l/300$ for these deflections to be visible. The rule of thumb in cabinetry construction is that deflections greater than $1/32$ in. (0.79 m) per foot (0.305 m) length will be visible, which corresponds to $l/384$. The $l/600$ limit currently in the MSJC code should prevent visible deflections and provide sufficient stiffness during construction. Given the historical nature of this value, it is suggested that it be retained. However, the purpose of the limit is different than stated in the code commentary. The limit would not be to control cracking, but rather to provide sufficient stiffness during construction to limit visible and aesthetically displeasing deflections. The lintel or beam does not need to be checked for deflections under additional superimposed loads or for long term deflections, just under the load produced by the weight of the masonry.

The implication of this proposed criteria is that if a beam or lintel has a calculated deflection in excess of $l/600$, it simply needs to be shored during construction. The size of the member does not necessarily have to be increased. The shoring is only necessary for a short period of time. In the lintel examined by McGinley et al. [6], the masonry veneer was laid in about 1.5 h, and the shores were removed immediately after the construction of the veneer. The deflection was still only 35 % of the computed flexural lintel deflection, indicating that the masonry achieves significant strength and stiffness very early in the curing process.

Calculation of Deflection of Reinforced Masonry Lintels

Since unreinforced masonry is often supported by reinforced masonry lintels, there is a need to be able to predict the deformations of reinforced masonry. This section examines various methods for determining the effective moment of inertia for calculating the deflections of reinforced masonry beams and lintels. Since there is very little experimental data on the deflections of masonry beams and lintels, researchers have examined the out-of-plane deflections of walls, assuming that the behavior of this “vertical” beam is similar to that of a lintel. Six methods of computing deflections will first be compared. Three of these methods are then applied to the limited test data on masonry beams, and to trial designs found in the literature.

Horton and Tadros [8] examined six methods for calculating the out-of-plane deflection of reinforced masonry walls. These methods are summarized in Table 4, along with a summary of their comments. The basis for this evaluation was wall tests they had performed, along with earlier slender wall tests conducted by others. The ACI 318-02 [9] method is the method referred to in commentary Section 3.1.5.3 of the MSJC code. The SEAOSC [10] method is used by the MSJC code in Section 3.3.5 for the out-of-plane strength design of walls. There appears, though, to be an inconsistent use of notation in the MSJC code. The term I_g is used in the SEAOSC equations in the MSJC code, whereas it seems that I_n , as used in Eq 1, would be more appropriate. Based on the results of Horton and Tadros’s investigation, designer’s

TABLE 4—Methods for calculation of deflection.

Method	Calculation	Advantages	Disadvantages
ACI 318	$I_{\text{eff}} = I_n \left(\frac{M_{\text{cr}}}{M_a} \right)^3 + I_{\text{cr}} \left[1 - \left(\frac{M_{\text{cr}}}{M_a} \right)^3 \right] \leq I_n$	Designer's familiarity	Tends to underestimate deflections
CEB Method	$\phi = \phi_n \left(\frac{f_{\text{cr}}}{f_a} \right)^2 + \phi_{\text{cr}} \left[1 - \left(\frac{f_{\text{cr}}}{f_a} \right)^2 \right]$	Most refined method; can incorporate axial load; good performance	Very difficult to use. Requires a computer program that can use M - ϕ relationships
Trost Method	$\Delta = \Delta_n \left(\frac{M_n - M_a}{M_n - M_{\text{cr}}} \right)^2 + \Delta_{\text{cr}} \left[1 - \left(\frac{M_n - M_a}{M_n - M_{\text{cr}}} \right)^2 \right]$	Deflection basis allows for a wide variety of support conditions and loadings. Can check Δ_{cr} and only need to further refine if that exceeds allowable.	Tends to overestimate deflections
SEAOSC Slender Wall	$\Delta = \frac{5M_{\text{cr}}I^2}{48E_nI_n} + \frac{5(M_a - M_{\text{cr}})I^2}{48E_{\text{m}}I_{\text{cr}}}$	Simple; used in strength design for walls.	Tends to underestimate deflections with low reinforcement ratios; at limit does not converge to fully cracked I
Abbound	$I_{\text{eff}} = (I_n - 2I_{\text{cr}}) \left(\frac{M_{\text{cr}}}{M_a} \right)^4$		No lower limit to moment of inertia; not very accurate
Horton	$\Delta = \Delta_{\text{cr}} \left[1 - \left(\frac{M_{\text{cr}}}{M_a} \right)^2 \left(2 - \frac{M_{\text{cr}}}{M_a} \right) \left(1 - \frac{I_{\text{cr}}}{I_g} \right) \right]$	Good agreement with tests; can check Δ_{cr} and only need to further refine if that exceeds allowable.	

familiarity, ease of use, and accuracy, the ACI 318, SEAOSC, and Horton's methods would be reasonable candidates for further consideration.

Abbound et al. [11] compared three methods of deflection calculation: theirs, SEAOSC (slender wall), and Horton's method to six reinforced masonry wall tests under out-of-plane loading. They observed that the SEAOSC and Horton method gave similar results, with the Horton method generally giving slightly higher deflections. Their method tended to initially underestimate deflections, and then to overestimate deflections at higher loads. Three experimental walls had significant additional gain in moment after cracking, walls 2, 3, and 4. Although it tended to consistently underpredict the deflections by about 20 %, Horton's method seems to work the best since it is slightly more accurate than the SEAOSC method, and significantly more accurate than Abbound's method.

Examining the equations used for the masonry deformation calculations, it is possible to show that Horton's method will always give higher deflections than the SEAOSC method. Multiply the SEAOSC method by (M_a/I_{cr}) (I_{cr}/M_a), or 1.0:

$$\begin{aligned} \Delta &= \frac{5M_{\text{cr}}I^2}{48EI_n} + \frac{5(M_a - M_{\text{cr}})I^2}{48EI_{\text{cr}}} \\ &= \frac{5I^2}{48E} \left(\frac{M_a}{I_{\text{cr}}} \right) \left(\frac{M_{\text{cr}}}{I_n} + \frac{M_a - M_{\text{cr}}}{I_{\text{cr}}} \right) \left(\frac{I_{\text{cr}}}{M_a} \right) = \frac{5L^2M_a}{48EI_{\text{cr}}} \left(\frac{M_{\text{cr}}}{I_n} \frac{I_{\text{cr}}}{M_a} + \frac{M_a - M_{\text{cr}}}{M_a} \right) = \Delta_{\text{cr}} \left[1 - \frac{M_{\text{cr}}}{M_a} \left(1 - \frac{I_{\text{cr}}}{I_n} \right) \right] \quad (2) \end{aligned}$$

where Δ_{cr} is the deflection using the cracked moment of inertia. Note that this gives a conceptual method for extending the SEAOSC method to other than simply supported conditions. The deflection is found based on the appropriate boundary conditions using the cracked moment of inertia, and then modified by the term in square brackets. The ratio of Horton's method to the SEAOSC method can now be determined as:

TABLE 5—Comparison of measured and calculated deflection from masonry lintel tests of Lee et al. [12].

Height (course)	Measured deflection, in. (mm)	Calc deflection, in. (mm)			Measured/calculated			Length/calc deflection		
		ACI	SEAOSC	Horton	ACI	SEAOSC	Horton	ACI	SEAOSC	Horton
2	0.866 (22.0)	0.665 (16.9)	0.601 (15.3)	0.645 (16.4)	1.30	1.44	1.34	213	236	220
3	0.579 (14.7)	0.341 (8.7)	0.301 (7.6)	0.327 (8.3)	1.70	1.92	1.77	416	471	434
4	0.315 (8.0)	0.238 (6.0)	0.207 (5.2)	0.227 (5.8)	1.32	1.52	1.39	596	684	625
		Average			1.44	1.63	1.50			

$$\frac{\Delta_{Horton}}{\Delta_{SEAOSC}} = \frac{1 - \frac{M_{cr}}{M_a} \left(1 - \frac{I_{cr}}{I_n} \right) \left[\frac{M_{cr}}{M_a} \left(2 - \frac{M_{cr}}{M_a} \right) \right]}{1 - \frac{M_{cr}}{M_a} \left(1 - \frac{I_{cr}}{I_n} \right)} \quad (3)$$

The term in the square bracket is always less than 1.0. Since it is part of the term that is subtracted from 1.0, the numerator is always greater than the denominator.

One of the few sources of data on masonry beams are the fourteen full-scale tests of Lee et al. [12]. Four of the beams were simply supported, four were restrained at the ends with large concrete blocks prestressed to the laboratory floor, and six were supported at the ends by varying lengths of wall (simulating actual construction). The beams were 11.8 ft (3.60 m) long and either 2, 3, or 4 courses high. There were 2–20M reinforcing bars in each beam. The tests showed that the end restraint reduced the deflections anywhere from 20 to 45 % of those of the simply supported specimens.

Table 5 gives the deflection results at yielding of the steel. The deflection from the three-course-high beam is the average from two beams. The deflections were calculated using the ACI 318, SEAOSC, and Horton’s method. Although both a modulus parallel and perpendicular to the bed joints was reported, the modulus perpendicular to the bed joint was used in the calculations as this is the modulus that would be used in a code calculation check. It is clear for the results listed in Table 5 that all these calculation methods underpredicted the measured deflection. One of the reasons for this inaccuracy is that all these methods only considered flexural deformations, and not shear deformations. For the deepest beam, length/height=4.6, shear deformations would have contributed about 10 % to the overall deformation. Furthermore, during testing, the deflections were measured relative to the laboratory floor so that any bearing deformations at the supports would be included in the measured deflections. There was no information on the bearings given in the article other than the beams being simply supported. This too would likely contribute to the inaccuracy of prediction but there does appear to be a systematic deficiency in the analytical model.

The deflections given in Table 5 were at yield. Calculations would actually be made at service levels, which would be well below yield. Using current MSJC criteria, the two-course high beam specimen would have likely been the only one that could have been controlled by serviceability, while the others probably would not.

To further evaluate the proposed deflection methods, three trial lintel designs were conducted using examples from three texts on masonry design and are summarized in Table 6. The given geometry and loadings of the examples were used and the reinforcement was determined using MSJC strength design criteria. Strength design produced smaller reinforcing steel areas but larger deformations than allowable stress design. None of these lintels have deflections close to approaching the deflection limit of $l/600$.

In summary, it appears that no one method for predicting the deformation of reinforced masonry, particularly lintels, is clearly the best. All the methods examined in detail appear to underestimate the deformation of reinforced masonry lintels by themselves if the effects of any unreinforced masonry is neglected. Since the ACI 318 method works reasonably well, designers are familiar with it, and it is currently in the MSJC commentary, it is recommended that this method (Eq 1) be used to obtain the

TABLE 6—Trial designs taken from the literature.

Description	Deflection, in. (mm)			Length/deflection		
	ACI	SEAOSC	Horton	ACI	SEAOSC	Horton
Drysdale et al. [13], Ex 6.5, 6.9. 2-wythe clay lintel; use $F_r=75$ psi (517 kPa), solid units	0.0609 (1.55)	0.0517 (1.31)	0.0585 (1.49)	2360	2780	2460
Masonry Designers Guide [14] TMS 12 Lintel. Use 1-#6 (strength design), $F_r=75$ psi (517 kPa)	0.0175 (0.44)	0.0161 (0.41)	0.0190 (0.48)	7340	7960	6750
Schneider and Dickey [15], Ex 9-1, Use 1-#4 (strength design), $F_r=75$ psi (517 kPa)	0.0419 (1.06)	0.0484 (1.23)	0.0570 (1.45)	3440	2980	2530

effective moment of inertia of reinforced masonry beams and lintels and subsequently the deformation of reinforced masonry lintels and beams.

Span Length Limit for Deflection Calculations

Lintels with a range of parameters, such as depth, steel ratio, f'_m , and type of masonry, were analyzed for different l/d ratios, where l is the span length and d is depth from the extreme compression fiber to the tension reinforcement. The results for $l/d=8$ are summarized in Table 7. The uniform load capacity was determined using the strength design provisions of the MSJC code [1]. The load capacity was divided by 1.4 to obtain a service load, where 1.4 is the average of the dead load factor of 1.2 and the live load factor of 1.6. The service load was used to calculate deflections. The cracking moment was calculated using a modulus of rupture of 75 psi (517 kPa), which is the lowest value in the MSJC code for fully grouted construction and tension parallel to the bed joints.

Based on these analyses, it appears that a value of $l/d=8$ is an appropriate limit for which deflections do not have to be checked, rather than the clear span being less than $15d$ as in the Canadian code [2]. This l/d ratio results in deflections of simply supported lintels near the current deflection limit of $l/600$.

Although some of the deflections exceed $l/600$ by as much as 23 %, the value of $l/d=8$ is recommended for several reasons. A modulus of rupture of 75 psi (517 kPa) was used in the analysis, which is the smallest value in the code for grouted masonry. With mortar types other than Type N masonry cement, the modulus of rupture would be higher, decreasing the deflections. Typically there will be some restraint, which should cause at least a 20 % decrease in deflections [12]. Finally, the worst case was examined, in which the applied load was the capacity of the member and the effects of any composite action with supported masonry is ignored. Due to the discrete nature of reinforcing bars, the capacity will often be greater than the applied load. For these reasons, most members will have actual deflections less than those shown in Table 7, and therefore $l/d=8$ seems to be an appropriate limit.

Conclusions

Issues related to beam deflection criteria for masonry were examined. Unreinforced masonry supported by beams and lintels act compositely with the beam. As the height of the masonry wall increases, the behavior of the assembly becomes more like that of a tied arch, with the masonry in compression and the beam acting as the tension tie. Cracking should not be a problem since the masonry is in compression. Deflection limits are only needed so that sufficient stiffness is provided during construction (and under construction loading) to prevent serviceability problems. The suggested limit deflection limit for these conditions is $l/600$. Beams and lintels that exceed this deflection do not necessarily have to be increased in size, but rather shores could be used during construction.

The purpose of the $l/600$ limit is different than stated in the current code commentary. The limit would not be to control cracking, but rather to provide sufficient stiffness during construction to limit visible and aesthetically displeasing deflections. Although in many cases this limit will control cracking, there are

TABLE 7—Properties of lintels with $l/d = 8$.

l , ft (m)	h , in. (mm)	b , in. (mm)	d , in. (mm)	Rebar	A_s/A_{bal}	f'_m , psi (MPa)	Masonry	ACI 318		Horton	
								Δ , in. (mm)	l/Δ	Δ in. (mm)	l/Δ
3.67 (1.12)	8 (203)	7.625 (194)	5.5 (140)	#4	0.605	1350 (9.31)	CMU	0.079 (2.01)	557	0.077 (1.96)	571
9.00 (2.74)	16 (406)	7.625 (194)	13.5 (343)	#4	0.246	1350 (9.31)	CMU	0.162 (4.11)	667	0.156 (3.96)	692
9.00 (2.74)	16 (406)	7.625 (194)	13.5 (343)	#5	0.382	1350 (9.31)	CMU	0.180 (4.57)	599	0.176 (4.47)	614
9.00 (2.74)	16 (406)	7.625 (194)	13.5 (343)	#6	0.542	1350 (9.31)	CMU	0.192 (4.88)	562	0.190 (4.83)	567
9.00 (2.74)	16 (406)	7.625 (194)	13.5 (343)	#6	0.488	1500 (10.34)	CMU	0.189 (4.80)	572	0.186 (4.72)	579
9.00 (2.74)	16 (406)	7.625 (194)	13.5 (343)	#7	0.499	2000 (13.79)	CMU	0.190 (4.83)	569	0.188 (4.78)	573
9.00 (2.74)	16 (406)	11.625 (295)	13.5 (343)	#7	0.485	1350 (9.31)	CMU	0.189 (4.80)	573	0.185 (4.70)	582
14.33 (4.37)	24 (610)	7.625 (194)	21.5 (546)	#6	0.341	1350 (9.31)	CMU	0.282 (7.16)	610	0.276 (7.01)	624
14.33 (4.37)	24 (610)	7.625 (194)	21.5 (546)	#7	0.465	1350 (9.31)	CMU	0.298 (7.57)	576	0.294 (7.47)	584
14.33 (4.37)	24 (610)	7.625 (194)	21.5 (546)	2-#5	0.480	1350 (9.31)	CMU	0.300 (7.62)	573	0.296 (7.52)	580
2.67 (0.81)	6.4 (162)	4.625 (117)	4.0 (102)	#4	0.661	2440 (16.83)	Clay	0.066 (1.68)	488	0.065 (1.65)	492
4.73 (1.44)	9.6 (244)	4.625 (117)	7.1 (180)	#4	0.372	2440 (16.83)	Clay	0.104 (2.64)	548	0.102 (2.59)	554
4.73 (1.44)	9.6 (244)	4.625 (117)	7.1 (180)	#5	0.577	2440 (16.83)	Clay	0.113 (2.87)	501	0.113 (2.87)	503
6.87 (2.09)	12.8 (325)	4.625 (117)	10.3 (263)	#5	0.398	2440 (16.83)	Clay	0.153 (3.89)	540	0.152 (3.86)	544
6.87 (2.09)	12.8 (325)	4.625 (117)	10.3 (263)	#6	0.565	2440 (16.83)	Clay	0.164 (4.16)	503	0.163 (4.14)	505

situations in which cracking could occur even when these deflection limits are met. Cracking can only be completely controlled by checking stresses.

The deformation of reinforced masonry beams and lintels was also examined and it was concluded that the equation currently used for reinforced concrete beams was as accurate as any method for finding an effective moment of inertia of cracked reinforced masonry flexural elements. This formula can be used to calculate the deflection of masonry elements to check deflection limits when these elements support unreinforced masonry. Masonry beams and lintels with span/depth ratio less than or equal to 8 should not be controlled by deflections and are more than stiff enough to limit cracking and unacceptable deformations. It is therefore recommended that members with span/depth ratios less than or equal to 8 be exempted from deflection checks.

References

- [1] MSJC, The Masonry Standards Joint Committee, "Building Code Requirements for Masonry Structures" (*ACI 530/ASCE 5/TMS 402*), 2005.
- [2] Canadian Standards Association, "Masonry Design for Buildings" (Limit States Design), *S304.1-94*, 1994.
- [3] Rosenhaupt, S., "Experimental Study of Masonry Walls on Beams," *ASCE J. Struct. Div.*, Vol. 88, No. ST3, 1962, pp. 137–166.
- [4] Burhouse, P., "Composite Action Between Brick Panel Walls and Their Supporting Beams," *Proc.-Inst. Civ. Eng.*, Vol. 43, 1969, pp. 175–194.
- [5] Stafford Smith, B., Pradolin, L., and Riddington, J. R., "Composite Design Method for Masonry Walls on Steel Beams," *Can. J. Civ. Eng.*, Vol. 9, No. 1, 1982, pp. 96–106.
- [6] McGinley, W. M., Johnson, E. N., and Bennett, R. M., "Considerations in the Design of Lintels for Masonry Veneers," Ninth North American Masonry Conference, The Masonry Society, Boulder, CO, 2003, pp. 346–357.
- [7] Galambos, T. V. and Ellingwood, B., "Serviceability Limit States: Deflection," *J. Struct. Eng.*, Vol. 112, No. 1, 1986, pp. 67–84.
- [8] Horton, R. T. and Tadros, M. K., "Deflection of Reinforced Masonry Members," *ACI Struct. J.*, Vol. 87, No. 4, 1990, 453–463.
- [9] American Concrete Institute (ACI), ACI Committee 318–02, "The Building Code Requirements for Reinforced Concrete," Publication of the American Concrete Institute, Detroit, 2002.
- [10] Structural Engineers Association of Southern California, Test Report on Slender Walls, 1982.
- [11] Abboud, B. E., Lu, S., and Schmitt, F. C., "An Evaluation of Three Current Deflection Methods for Predicting the Lateral Deflection of Masonry Walls," Sixth North American Masonry Conference, 1993, pp. 73–85.
- [12] Lee, R., Longworth, J., and Warwaruk, J., "Behavior of Restrained Masonry Beams," Third Canadian Masonry Symposium, Edmonton, Alberta, 1983, 37/1-16.
- [13] Drysdale, R. G., Hamid, A. A., and Baker, L. R., *Masonry Structures: Behavior and Design*, 2nd ed., The Masonry Society, Boulder, CO, 1999.
- [14] *Masonry Designers Guide*, 4th ed., The Masonry Society, Boulder, CO, 2003.
- [15] Schneider, R. R. and Dickey, W. L., *Reinforced Masonry Design*, 3rd ed., Prentice Hall, Englewood Cliffs, NJ, 1994.

Herb Nordmeyer¹ and Pam Hall¹

Variations in the Activity of Dry-Powder Water-Repellent Mortar Admixtures with Different Mortar Formulae

ABSTRACT: A number of water repellents are added to masonry mixes and masonry units. To be classified as a water-repellent mortar admixture, ASTM C 1384 Specification for Admixtures for Masonry Mortars, requires that the 24-h rate of water absorption needs to be reduced by at least 50 % when compared to a control mortar without the admixture. While testing two well-known water-repellent admixtures, a substantial difference in activity was noted with the mortar that was being tested. Testing was expanded to include other water-repellent admixtures and several additional mortar formulae. This paper discusses the findings of that study.

KEYWORDS: water absorption, water repellent, mortars, ASTM C 1384

Introduction

The senior author's laboratory, operated by a materials supplier, is charged with

- Oversight of a company-wide QA/QC program for manufactured products, including cements and stuccos;
- Bringing emerging technologies to commercial reality; and
- Improving products to make them more marketable.

This paper deals with one example of an offshoot of attempting to improve a product.

Since architects regularly specify water-repellent admixtures in mortars based on Standard Specification for Admixtures for Masonry Mortars (ASTM C 1384) [1], tests were run with two commercially-available, dry-powder water repellents to determine which would be most appropriate to introduce into our bagged mortar and masonry cements. Initial results were inconsistent with information in the product literature. A study was designed and implemented to bring about a better understanding of which water-repellent admixtures worked in which situations. While the study was undertaken for internal purposes, and specific ASTM techniques were not always used, the results mandated that they be disseminated to the industry so others could address the apparent problems we observed. Where there has been a deviation from the ASTM specifications, it is noted in this paper.

Design of the Study

A study was designed to answer the following questions:

- How effective are the different dry-powder water-repellent admixtures?
- Does the mortar formula impact the effectiveness of the dry-powder water-repellent admixtures?

A web search was done to identify as many different dry-powder water-repellent admixtures as possible. As each was identified, contact was made with the manufacturer or a manufacturer's technical sales agent. A sample, MSDS, and current product literature were requested, and the purposes of our study were discussed, including the need to comply with ASTM C 1384. Those manufacturers which requested that we sign a nondisclosure agreement or other document before receiving a sample were eliminated from the study.

Manuscript received November 18, 2005; accepted for publication June 18, 2007; published online July 2007. Presented at ASTM Symposium on Masonry on 13 June 2006 in Toronto, Canada; B. Trimble and J. Brisch, Guest Editors.

¹ Project & Technology Manager and Senior Lab Technician, respectively, San Antonio Lab, Headwaters Construction Materials, 5014 Callaghan Road, San Antonio, Texas 78228.

TABLE 1—Integral water-repellent admixtures tested.

ID	Form	Dosage Rate (%)	Active Ingredients
A	Control	0.00	...
B	Powder	1.50	Ethylene/Vinyl Acetate Copolymer
C	Powder	1.32	Hydrous Magnesium Aluminum Silicate
D	Powder	1.31	Stearate Water Repellents and Other Chemicals
E	Powder	1.31	Ca Stearate and Ca Lignosulfonate

Dry-powder water-repellent admixtures listed in Table 1 were selected for the study. They are identified by a letter rather than by product name. Active ingredients are identified, based on information found in MSDS and product literature.

There is considerable data available that are in conflict as to what constitutes a good mortar [2,3]. This paper does not attempt to resolve such conflict but is limited to addressing how four water-repellent admixtures impacted five mortar formulae.

Five Type S mortars were selected for testing. Besides a portland/lime blend and a traditional masonry cement, three formulae were included in the testing that utilized pozzolanic technology. These were included because it is known that pozzolans contribute to lowering the porosity of cured cementitious mixes [4,5]. A blend of 20-30 sand and graded standard sand was used for producing the mortars.

The portland cement and the hydrated lime are commercially-available products. The hydrated lime used was a Type S dolomitic hydrated lime. The pozzolanic cements are commercially available. The mortar types are listed in Table 2.

Dampproofing or waterproofing technology falls into several categories. They include:

- Water-repelling materials (soaps and fatty acids) which react with cement hydrates and line pore space (Water Repellents D and E);
- Finely-divided solids which are inert pore-filling materials (Water Repellent B);
- Chemically-reactive, finely-divided solids (Water Repellent C and Pozzolans such as fly ash found in Mortar Formulae II, III, and IV);
- Conventional water-reducing, air-entraining, and accelerating admixtures (Water Repellent E); and
- Miscellaneous, example—methyl siliconates [6].

Section 8.1 of ASTM C 1384 requires that the samples for absorption testing be mixed according to Standard Specification for Mortar for Unit Masonry (ASTM C 270) [7], except that the aggregate ratio shall be fixed at three times the volume of cementitious materials, and Section 5.3.1 specifies that the sand used for the absorption testing shall be an equal blend of ASTM C 778 (Standard Specification for Standard Sand) [8] graded standard sand and 20-30 sand. Formulae III, IV, and V arrived in bags that stated that they contained 75 pounds. An assumption was made that the bags contained one cubic foot of material. Calculations for the portland-lime mortar used a ratio of one cubic foot of portland cement to 1/2 cubic foot of hydrated lime. Calculations based on the density of each component resulted in a density of the portland/lime of 76 pounds per cubic foot. The Blended Hydraulic Cement was in a bag that was marked 94 pounds per cubic foot. Assuming that it contained one cubic foot, the density would have been 76 pounds per cubic foot. Actual density measurements were not taken. Based on 75 pounds per cubic foot cement, and three times the aggregate volume to the cement volume, the correct ratio between cement and aggregate would have been 506.25 grams cement to 1620 grams of aggregate. Based on 76 pounds per cubic foot cement, and three times the aggregate volume to the cement volume, the correct ratio between

TABLE 2—Mortars tested.

ID	Type	Hydrated Lime ^a	Fly Ash in Formula
I	Portland/Lime	17.5 %	No
II	Blended Cement/Lime	17.5 %	Yes
III	Pozzolanic Mortar Cement	~15.0 %	Yes
IV	Pozzolanic Mortar Cement	0.0 %	Yes
V	Traditional Masonry Cement ^b	0.0 %	No

^aPercent by weight.

^bThe cement that is referred to as a traditional masonry cement (ID V) is produced by a portland cement company and is a milled blend of portland clinker, limestone, and other ingredients.

the cement and aggregate would have been 513 grams of cement to 1620 grams of aggregate.

Batch sizes actually utilized for all of the batches were as follows:

- 510 grams of paste-making components;
- Each manufacturer's recommended dosage of water-repellent admixture (see Table 1);
- 810 grams of 20-30 sand; and
- 810 grams of graded standard sand.

Mortar was mixed according to the Standard Specification for Masonry Cement (ASTM C 91) [9] procedures.

ASTM C 1384 specifies that when testing for compressive strength, water retention, or determination of air content of plastic mortar, that the aggregate used should meet the requirements to Standard Specification for Aggregate for Masonry Mortar (ASTM C 144) [10]. ASTM C 144 sand was not used in running these tests. All testing was done based on the ASTM C 778 aggregate. The ratios and the aggregate used comply with the requirements under ASTM C 91 for testing Type S masonry cement.

The manufacturers' recommended dosage rates were in several cases unclear. If the recommendation was related to portland cement, then the assumption was made that the recommended dosage rate was for one cubic foot of paste-making materials rather than for 94 pounds of material.

The following parameters were measured or calculated during sample preparation:

- mixing water used,
- flow,
- flow after suction,
- water retention,
- weight of 400 mL cup, and
- air content—Section 5.3 of ASTM C 1384.

In each case at least five cubes were made with the mortar material. In some cases the volume of the mix allowed a sixth cube to be made. For this study three of the cubes were tested. Due to scheduling concerns in the lab, the initial tests were run after the samples had cured 21 days which is less than the 28 days specified in C 1384. The remaining cubes were stored for testing after 90 days of cure to determine whether the absorption rate changed during the additional cure.

Samples were cured in a moist cabinet over water rather than in a sealed bag as specified in C 1384. After samples had cured for 21 days (samples A, B, and C), they were placed in a vented drying oven at between 110°C and 115°C and dried to a constant weight. They were then allowed to cool for two hours in a low-humidity chamber to lab temperature prior to testing.

The following tests were run on the cured samples:

- Rate of water absorption
 - 15 min
 - 1 h
 - 4 h
 - 24 h

The rate of water absorption test was run according to ASTM Standard Test Method for Rate of Water Absorption for Masonry Mortars (ASTM C 1403) [11]. The dried samples were measured for length, width, and mass and then placed in an immersion tank. The samples were supported off the floor of the tank with glass rods so water could get to the bottom of the cubes. Water in the immersion tank was adjusted so each cube was sitting in 3.0 ± 0.5 mm of water. Test was initiated at 10 a.m., and the water level was adjusted to 3.0 ± 0.5 mm after 15 min and each hour until 5 p.m. when the lab was not manned until 8 a.m. the following morning. After 24 hours individual cubes were removed from the immersion tank and wiped dry, and the mass was determined. The results were converted to grams of water absorbed per 100 cm^2 in a 24-h period.

Cubes that were tested for rate of water absorption were then placed in the compressive strength machine and a nonspec compressive strength was determined. The values determined can be compared with other values within this paper but should not be compared with ASTM C 91, ASTM C 270 [7], or ASTM C 1384 compressive strength tests.

TABLE 3—Water/cement ratio.

Admixture	Mortar Formula				
	I	II	III	IV	V
Control	0.60	0.56	0.58	0.52	0.49
B	0.56	0.52	0.53	0.50	0.49
C	0.60	0.53	0.54	0.52	0.47
D	0.59	0.58	0.56	0.51	0.49
E	0.59	0.56	0.58	0.51	0.47

Table 3 lists the water/cement ratios for each formula to develop a flow of 110 % \pm 5 %. Addendum 1 lists supporting data for Table 3. Most of the integral water-repellent admixtures reduced the amount of water used, as compared to the control. There was more variation between the different mortar formulae than there was between the different water-repellent admixtures.

Table 4 lists the results of water retention tests. Addendum 1 lists supporting data for Table 4. Data is presented in the same order as in Table 3. In most cases the water retention remained constant, or was depressed. These tests were run with standard sand rather than with the ASTM C 144 sand as specified in ASTM C 1384.

Table 5 lists the results of testing air content. The method used was with a 400 mL cup as described in ASTM C 1384. Addendum 2 lists supporting data for Table 5. The portland/lime and the blended cement/lime did not contain air-entraining agents, so their air content was relatively low. Water Repellent B appeared to act as an air-entraining agent for those two formulae. The other dry-powder water repellents did not substantially impact the air content. None of the water-repellent admixtures had a substantial impact on Formulae III and IV. Water Repellent B appeared to act as a strong air-entraining agent on Formula V. Standard sand was used for the test, rather than the ASTM C 144 sand listed in ASTM C 1384.

Table 6 lists the compressive strength of the different mixes. These compressive strength results were produced from cubes that had been dried and then subjected to the water absorption test. Additionally they were made with standard sand rather than with ASTM C 144 sand. Supporting data are listed in Addendum 3. The result for Water Repellent B and Formula V is marked with an asterisk (*). Individual cubes broke at the following forces: 4200 lb, 4250 lb, and 6000 lb. As a result, a reasonable estimate of compressive strength could not be made. The cube that broke at the highest strength had a mass that was 4.2 % greater than the other two cubes.

TABLE 4—Water retention (%).

Admixture	Mortar Formula				
	I	II	III	IV	V
Control	90	85	83	93	88
B	89	85	86	77	85
C	87	78	93	87	62
D	84	85	86	91	71
E	83	87	87	88	76

TABLE 5—Percent air content.

Admixture	Mortar Formula				
	I	II	III	IV	V
Control	5.2	3.8	12.6	15.8	11.5
B	15.8	15.0	13.7	15.0	23.0
C	5.6	3.8	12.3	11.3	12.0
D	5.5	3.2	11.7	14.4	10.9
E	5.2	3.6	9.9	11.8	11.4

TABLE 6—Twenty-one-day compressive strength (psi).

Admixture	Mortar Formula				
	I	II	III	IV	V
Control	2560	2580	3030	2340	2230
B	2770	2730	2200	2300	*
C	2630	2570	2270	2400	2830
D	2860	2030	1800	2350	2130
E	2850	2220	1960	2680	2550

TABLE 7—Twenty-four-hour rate of water absorption—(grams/100 cm²).

Admixture	Mortar Formula				
	I	II	III	IV	V
Control	105	101	72	53	82
B	64	32	38	30	35
C	103	91	83	50	70
D	98	92	84	56	81
E	98	91	90	53	79

TABLE 8—Twenty-four-hour rate of water absorption—(as a percentage of control).

Admixture	Mortar Formula				
	I	II	III	IV	V
Control	100	100	100	100	100
B	61	32	53	57	43
C	98	90	115	94	85
D	93	91	117	106	99
E	93	90	125	100	96

Table 7 lists the results of the 24-h rate of water absorption tests for the dry-powder water-repellent admixtures. Tests were run on 2-in. cubes, and the results were extrapolated to grams per one hundred square centimetres as per ASTM C 1403. The same data are presented in Table 8, but as a percentage of the control, rather than absolute values. Supporting data for the 24-h tests and data concerning 15-min, 1-h, and 4-h testing are presented in Addendum 4.

Discussion

W/C Ratio, Water Retention, and Air Content

A review of the impact of the different water-repellent admixtures on the water/cement ratio varied with different mortar formulae; however, a pattern was not established. Increases of up to 0.02, to a decrease of 0.07, were observed.

The water retention was more heavily impacted than the water/cement ratio. Maximum variation from the control was with Formula V (traditional masonry cement—see note on Table 2). With Water Repellent C, the water retention dropped from 88 to 62 %. Since this drop did not appear to be reasonable when compared with other data found in the study, the test was repeated, and similar results were obtained. An explanation for this phenomenon has not been developed. In general, the water-repellent admixtures appeared to lower the water retention more with Formula V (traditional masonry cement) than with the other mortar formulae.

Water Repellent B, which the MSDS stated contained ethylene/vinyl acetate copolymer, increased the air content with all mortar formulae except Formula IV (low lime pozzolanic mortar cement). It was the only water-repellent admixture that appeared to have an impact on air content.

Impact on Compressive Strength

As mentioned earlier, samples were removed from the cure chamber at 21 days of age, dried, and then subjected to the 24-h rate of water absorption test before being tested for compressive strength. Admixtures can impact compressive strength in several ways, including, but not limited to:

- Water/cement ratio,
- Air content,
- Retarding effect, and
- Accelerating effect.

The impact of water/cement ratio and the entrained air content can be calculated for concrete based on Feret's law [12]. The well known Abram's Law, upon which water/cement ratios for concrete are based is a simplification of Feret's Law, in that it fixes the air content as a constant. In general, Feret's law states that increases in the absolute volume of air and in the absolute volume of water in a concrete will lower the compressive strength a calculable amount. No reference was found that stated that Feret's law could be applied to mortars.

The manufacturer of the high-lime mortar cement (Formula III) uses different additives than the manufacturer of the low-lime mortar cement (Formula IV) or the traditional masonry cement (Formula V).

All admixtures added to Formula III resulted in lowered compressive strength results. A determination was not made as to why these results were generated, but they should be studied in greater depth. MSDS and literature were consulted to determine whether any of the water-repellent admixtures contained calcium chloride. Those documents did not so indicate.

Impact on 24-h Rate of Water Absorption

The mortar formulae without water-repelling admixtures demonstrated a wide range of absorption. The portland/lime blend had the highest absorption (105 grams per 100 square centimetres of area in 24 hours). The low-lime pozzolanic mortar cement had the lowest absorption (52 grams per 100 square centimetres).

A majority of the water-repellent admixtures did not appear to meet the requirements of ASTM C 1384 for water-repellent admixtures (reducing the 24-h rate of water absorption by at least 50 %). Water Repellent B performed the best and met the requirement for Mortar Formulae II and V with relative values compared to the control mortars of 32 and 43 %, respectively. Water Repellent B also reduced water absorption significantly with relative values ranging from 53 to 61 % for Mortar Formulae I, III, and IV, but failed to meet the required 50 % maximum value specified in ASTM C 1384. Water Repellents C, D, and E actually increased the 24-h rate of water absorption for several of the mortar formulae and had relative values from 85 to 125 %, when compared to the control mortar.

Conclusions

There was a major difference in the rate of absorption of different mortars in the control group (i.e., without any admixture).

Mortar Formula IV (no-lime pozzolanic mortar cement) in the control group appears to have a rate of water absorption of about 50 % that of Mortar Formula I (Type S portland/lime blend) in the control group.

One dry-powder water-repellent mortar admixture, B, reduced the 24-h rate of water absorption significantly with all mortars but met the required 50 % maximum relative absorption compared to the control for only two of the five mortar formulae. For the other three formulae, it had relative values ranging from 53 to 61 % of the control mortar.

Three of the four dry-powder water-repellent mortar admixtures, C, D, and E, had relatively little effect on water repellency as measured by the 24-h rate of water absorption for all the mortar formulae tested. The admixtures had relative 24-h rate of water absorption values ranging from 85 to 125 % of the control mortars.

Recommendations

ASTM Committee C12 should include a statement in ASTM C 270 which addresses the apparent variation an admixture can exhibit when used with different mortar formulae.

Manufacturers of water-repellent mortar admixtures should voluntarily provide information concerning the mortar formulae that were tested when they are requested to certify that their water repellent

complies with ASTM C 1384, as this information is already required by the reporting section (11) of C 1384. If information is available that the masonry cement or mortar cement used was made with a technology that is different than that used traditionally by the portland cement companies, that information would be helpful to the user. Such technologies include, but are not limited to, pozzolanic technology, ground granulated blast furnace slag technology, mortar plasticizer technology, etc.

ASTM Committee C12 should encourage further study of this subject.

Addendum 1—Water requirements and water retention data.

Mortar Formula	Admixture	Cement (grams)	Water (mL)	Water/Cement Ratio	Flow (%)	Flow After Vacuum (%)	Water Retention (%)
I	Control	510	308	0.60	111	100	90
I	B	510	284	0.56	106	95	89
I	C	510	306	0.60	111	97	87
I	D	510	300	0.59	107	90	84
I	E	510	302	0.59	106	88	83
II	Control	510	287	0.56	108	92	85
II	B	510	264	0.52	112	95	85
II	C	510	272	0.53	106	83	78
II	D	510	295	0.58	114	97	85
II	E	510	285	0.56	110	95	87
III	Control	510	297	0.58	105	88	83
III	B	510	269	0.53	107	92	86
III	C	510	273	0.54	105	98	93
III	D	510	285	0.56	112	96	86
III	E	510	294	0.58	113	98	87
IV	Control	510	267	0.52	108	100	93
IV	B	510	253	0.50	105	81	77
IV	C	510	263	0.52	106	92	87
IV	D	510	260	0.51	115	105	91
IV	E	510	260	0.51	115	102	88
V	Control	510	251	0.49	112	98	88
V	B	510	249	0.49	112	93	83
V	C	510	240	0.47	106	66	62
V	D	510	250	0.49	109	77	71
V	E	510	240	0.47	110	83	76

^aSum of mass of portland cement, blended cement, masonry cement, mortar cement, fly ash, and hydrated lime.

Addendum 2—Air content calculations.

Mortar Formula	Admixture	Water (mL)	Cement (grams)	Density Cement gms/cm ³	Hydrated Lime (grams)	Density Lime gms/cm ³	Admixture (grams)	Density Admixture gms/cm ³	Aggregate (grams)	Density Aggregate gms/cm ³	Mass of 400 cm ³ Mortar (grams)	Density of Mortar gms/cm ³	Air Content (%)
I	Control	308	421	3.15	89	2.34	0.00	1	1,620	2.65	847.8	2.23	5.2
I	B	284	421	3.15	89	2.34	7.65	1	1,620	2.65	758.7	2.25	15.8
I	C	306	421	3.15	89	2.34	6.73	2.5	1,620	2.65	844.7	2.24	5.6
I	D	300	421	3.15	89	2.34	6.66	0.99	1,620	2.65	845.1	2.24	5.5
I	E	302	421	3.15	89	2.34	6.66	2.5	1,620	2.65	850.2	2.24	5.2
II	Control	287	421	2.772	89	2.34	0	1	1,620	2.65	854.5	2.22	3.8
II	B	264	421	2.772	89	2.34	7.65	1	1,620	2.65	760.9	2.24	15.0
II	C	272	421	2.772	89	2.34	6.73	2.5	1,620	2.65	861.7	2.24	3.8
II	D	295	421	2.772	89	2.34	6.66	0.99	1,620	2.65	853.9	2.20	3.2
II	E	285	421	2.772	89	2.34	6.66	2.5	1,620	2.65	857.5	2.22	3.6
III	Control	297	510	2.7			0	1	1,620	2.65	772.9	2.22	12.6
III	B	269	510	2.7			7.65	1	1,620	2.65	771.4	2.26	13.7
III	C	273	510	2.7			6.73	2.5	1,620	2.65	786.0	2.25	12.3
III	D	285	510	2.7			6.66	0.99	1,620	2.65	783.2	2.23	11.7
III	E	285	510	2.7			6.66	2.5	1,620	2.65	802.5	2.22	9.9
IV	Control	267	510	2.81			0	1	1,620	2.65	761.9	2.26	15.8
IV	B	253	510	2.81			7.65	1	1,620	2.65	771.4	2.23	15.0
IV	C	263	510	2.81			6.73	2.5	1,620	2.65	804.5	2.23	11.3
IV	D	260	510	2.81			6.66	0.99	1,620	2.65	773.4	2.22	14.4
IV	E	260	510	2.81			6.66	2.5	1,620	2.65	801.0	2.24	11.8
V	Control	251.2	510	3			0	1	1,620	2.65	816.5	2.31	11.5
V	B	249	510	3			7.125	1	1,620	2.65	694.6	2.30	23.0
V	C	240	510	3			6.73	2.5	1,620	2.65	817.5	2.32	12.0
V	D	250	510	3			1.43	0.99	1,620	2.65	822.4	2.31	10.9
V	E	240	510	3			1.43	2.5	1,620	2.65	822.1	2.32	11.4

Addendum 3—21 day compressive strength data.

Cube Number	Cube Designation	Formula	Admixture	Mass Dry (gms)	Force (lb)	Comp. Strength 21-day (psi)	Comp. Strength Average (psi)
E-1327	A	I	Control	255.58	10 050	2513	
E-1327	B	I	Control	255.70	10 150	2538	
E-1327	C	I	Control	255.73	10 500	2625	2558
E-1328	A	I	B	243.56	9800	2450	
E-1328	B	I	B	244.64	10 800	2700	
E-1328	C	I	B	245.43	10 250	2563	2571
E-1335	A	I	C	254.90	10 600	2650	
E-1335	B	I	C	254.73	10 150	2538	
E-1335	C	I	C	253.67	10 800	2700	2629
E-1331	A	I	D	254.35	11 500	2875	
E-1331	B	I	D	256.96	12 000	3000	
E-1331	C	I	D	254.71	10 850	2713	2863
E-1332	A	I	E	257.79	11 300	2825	
E-1332	B	I	E	254.09	11 350	2838	
E-1332	C	I	E	257.00	11 600	2900	2854
E-1337	A	II	Control	258.52	10 450	2613	
E-1337	B	II	Control	258.03	10 250	2563	
E-1337	C	II	Control	258.62	10 200	2550	2575
E-1338	A	II	B	246.16	10 500	2625	
E-1338	B	II	B	248.19	10 700	2675	
E-1338	C	II	B	250.60	11 600	2900	2733
E-1346	A	II	C	260.53	10 700	2675	
E-1346	B	II	C	261.75	9050	2263	
E-1346	C	II	C	263.12	11 050	2763	2567
E-1341	A	II	D	254.73	8000	2000	
E-1341	B	II	D	254.08	8250	2063	
E-1341	C	II	D	253.90	8100	2025	2029
E-1342	A	II	E	257.66	8900	2225	
E-1342	B	II	E	258.06	9200	2300	
E-1342	C	II	E	257.86	8550	2138	2221
E-1347	A	III	Control	242.69	11 900	2975	
E-1347	B	III	Control	245.03	12 650	3163	
E-1347	C	III	Control	244.38	11 850	2963	3033
E-1348	A	III	B	235.00	9200	2300	
E-1348	B	III	B	233.47	8300	2075	
E-1348	C	III	B	232.87	8850	2213	2196
E-1356	A	III	C	247.16	8650	2163	
E-1356	B	III	C	247.92	9250	2313	
E-1356	C	III	C	246.58	9350	2338	2271
E-1351	A	III	D	240.46	7450	1863	
E-1351	B	III	D	236.81	7000	1750	
E-1351	C	III	D	241.06	7100	1775	1796
E-1352	A	III	E	250.23	8850	2213	
E-1352	B	III	E	242.59	7500	1875	

58 MASONRY

Cube Number	Cube Designation	Formula	Admixture	Mass Dry (gms)	Force (lb)	Comp. Strength 21-day (psi)	Comp. Strength Average (psi)
E-1352	C	III	E	242.29	7150	1788	1958
E-1357	A	IV	Control	245.10	11 250	2813	
E-1357	B	IV	Control	236.15	8400	2100	
E-1357	C	IV	Control	236.11	8400	2100	2337
E-1358	A	IV	B	243.08	11 800	2950	
E-1358	B	IV	B	240.84	11 500	2875	
E-1358	C	IV	B	243.26	12 600	3150	2992
E-1366	A	IV	C	246.83	9500	2375	
E-1366	B	IV	C	244.35	9350	2338	
E-1366	C	IV	C	245.95	10 000	2500	2404
E-1361	A	IV	D	235.71	10 000	2500	
E-1361	B	IV	D	234.07	9500	2375	
E-1361	C	IV	D	234.91	8700	2175	2350
E-1362	A	IV	E	244.39	10 900	2725	
E-1362	B	IV	E	245.50	11 000	2750	
E-1362	C	IV	E	242.99	10 300	2575	2683
E-1367	A	V	Control	247.85	8900	2225	
E-1367	B	V	Control	249.77	9200	2300	
E-1367	C	V	Control	247.62	8700	2175	2233
E-1368	A	V	B	217.22	4200	1050	
E-1368	B	V	B	217.33	4250	1063	
E-1368	C	V	B	226.63	6000	1500	1204
E-1376	A	V	C	257.87	11 350	2838	
E-1376	B	V	C	259.94	11 000	2750	
E-1376	C	V	C	257.88	11 550	2888	2825
E-1371	A	V	D	251.61	8700	2175	
E-1371	B	V	D	252.38	8300	2075	
E-1371	C	V	D	250.47	8550	2138	2129
E-1372	A	V	E	250.94	10 050	2513	
E-1372	B	V	E	251.30	10 200	2550	
E-1372	C	V	E	251.97	10 400	2600	2554

Addendum 4—Water absorption data.

Cube Number	Cube Designation	Formula	Admixture	Dry Mass (gms)	Mass 15-min (gms)	Mass 1-hour (gms)	Mass 4-hour (gms)	Mass 24-hour (gms)
E-1327	A	I	Control	255.58	263.24	268.34	277.10	282.79
E-1327	B	I	Control	255.70	262.70	267.06	274.68	282.80
E-1327	C	I	Control	255.73	263.25	268.16	276.02	283.02
E-1328	A	I	B	243.56	247.42	250.00	253.70	261.14
E-1328	B	I	B	244.64	247.88	250.15	253.82	261.28
E-1328	C	I	B	245.43	248.12	250.09	253.58	261.11
E-1335	A	I	C	254.90	262.75	266.31	273.47	281.43
E-1335	B	I	C	254.73	262.02	265.67	272.56	281.16

Cube Number	Cube Designation	Formula	Admixture	Dry Mass (gms)	Mass 15-min (gms)	Mass 1-hour (gms)	Mass 4-hour (gms)	Mass 24-hour (gms)
E-1335	C	I	C	253.67	261.63	265.32	272.49	280.23
E-1331	A	I	D	254.35	260.56	263.99	270.00	275.41
E-1331	B	I	D	256.96	263.16	266.70	272.81	282.45
E-1331	C	I	D	254.71	260.51	263.84	269.72	279.72
E-1332	A	I	E	257.79	263.67	267.17	272.89	282.44
E-1332	B	I	E	254.09	261.05	264.46	271.00	280.01
E-1332	C	I	E	257.00	263.07	266.48	272.46	281.97
E-1337	A	II	Control	258.52	263.76	267.79	275.43	284.21
E-1337	B	II	Control	258.03	263.42	267.02	274.41	284.09
E-1337	C	II	Control	258.62	263.77	267.30	274.85	284.77
E-1338	A	II	B	246.16	247.54	248.31	250.20	254.20
E-1338	B	II	B	248.19	249.72	251.61	252.47	256.95
E-1338	C	II	B	250.60	259.08	252.93	254.66	258.82
E-1346	A	II	C	260.53	264.24	266.64	273.29	283.82
E-1346	B	II	C	261.75	267.19	270.04	277.32	286.74
E-1346	C	II	C	263.12	265.30	267.60	274.02	285.03
E-1341	A	II	D	254.73	259.42	262.21	267.78	278.28
E-1341	B	II	D	254.08	258.59	261.50	267.41	277.82
E-1341	C	II	D	253.90	258.45	261.27	267.55	277.81
E-1342	A	II	E	257.66	262.06	264.65	270.48	280.92
E-1342	B	II	E	258.06	262.42	264.96	270.71	281.44
E-1342	C	II	E	257.86	262.39	265.06	270.92	281.49
E-1347	A	III	Control	242.69	244.73	246.56	250.73	260.88
E-1347	B	III	Control	245.03	247.20	249.09	253.46	264.11
E-1347	C	III	Control	244.38	247.02	248.72	252.75	262.47
E-1348	A	III	B	235.00	235.90	236.75	239.97	245.88
E-1348	B	III	B	233.47	234.47	235.35	237.92	243.54
E-1348	C	III	B	232.87	233.78	234.59	236.22	241.41
E-1356	A	III	C	247.16	251.14	253.54	258.59	268.50
E-1356	B	III	C	247.92	251.99	254.45	259.70	269.54
E-1356	C	III	C	246.58	250.39	252.83	252.99	268.15
E-1351	A	III	D	240.46	243.54	245.85	250.94	261.99
E-1351	B	III	D	236.81	240.39	242.92	248.03	252.98
E-1351	C	III	D	241.06	244.98	242.68	253.02	263.04
E-1352	A	III	E	250.23	254.46	257.25	263.12	273.81
E-1352	B	III	E	242.59	246.87	249.95	255.22	265.58
E-1352	C	III	E	242.29	246.57	249.30	255.29	265.31
E-1357	A	IV	Control	245.10	247.16	248.34	250.24	256.81
E-1357	B	IV	Control	236.15	238.55	239.89	243.08	250.12
E-1357	C	IV	Control	236.11	238.48	239.91	243.31	251.18
E-1358	A	IV	B	243.08	244.21	244.96	246.89	251.52
E-1358	B	IV	B	240.84	241.83	242.51	244.12	248.46
E-1358	C	IV	B	243.26	244.10	244.77	246.42	250.52
E-1366	A	IV	C	246.83	249.17	250.79	255.29	264.63
E-1366	B	IV	C	244.35	246.36	247.74	251.36	260.55
E-1366	C	IV	C	245.95	247.62	248.80	252.05	259.82

Cube Number	Cube Designation	Formula	Admixture	Dry Mass (gms)	Mass 15-min (gms)	Mass 1-hour (gms)	Mass 4-hour (gms)	Mass 24-hour (gms)
E-1361	A	IV	D	235.71	237.29	238.41	241.00	247.13
E-1361	B	IV	D	234.07	236.27	237.88	241.24	248.39
E-1361	C	IV	D	234.91	237.07	238.65	242.09	252.42
E-1362	A	IV	E	244.39	246.19	247.62	250.76	259.45
E-1362	B	IV	E	245.50	247.42	248.77	251.93	259.45
E-1362	C	IV	E	242.99	244.44	245.62	248.48	255.52
E-1367	A	V	Control	247.85	253.14	255.25	262.53	268.96
E-1367	B	V	Control	249.77	255.85	258.36	266.17	270.88
E-1367	C	V	Control	247.62	253.05	256.65	263.29	268.59
E-1368	A	V	B	217.22	218.69	219.34	221.24	225.72
E-1368	B	V	B	217.33	218.83	219.56	221.56	226.36
E-1368	C	V	B	226.63	228.19	228.94	220.99	236.01
E-1376	A	V	C	257.87	260.91	262.93	266.82	275.11
E-1376	B	V	C	259.94	263.25	265.34	269.73	278.48
E-1376	C	V	C	257.88	260.75	262.57	266.81	276.15
E-1371	A	V	D	251.61	255.52	258.04	265.97	272.26
E-1371	B	V	D	252.38	256.68	259.57	265.94	273.34
E-1371	C	V	D	250.47	255.10	258.95	265.60	271.19
E-1372	A	V	E	250.94	254.77	257.24	262.79	271.21
E-1372	B	V	E	251.30	255.44	258.01	263.42	271.62
E-1372	C	V	E	251.97	256.74	259.52	265.50	272.52

References

- [1] ASTM C 1384, "Standard Specification for Admixtures for Masonry Mortar," ASTM International. For referenced ASTM standards, visit the ASTM website, www.astm.org. For *Annual Book of ASTM Standards* volume information, refer to the Standard's Document Summary page on the ASTM website.
- [2] Thompson, M., "Can Lime Be Replaced? Saying It Replaces Lime Doesn't Make it Lime," *Masonry Construction*, ISSN 0898-6088, Vol. 13, No. 3, 2000, pp. 29–32.
- [3] Meadowcroft, C. D., "Can Lime be Replaced? Lime Alternates Are Not And Do Not Want To Be Lime!," *Masonry Construction*, ISSN 0898-6088, Vol. 13, No. 3, 2000, pp. 29–33.
- [4] Nordmeyer, D. H., "High Pozzolan Mortars and Stuccos," *Masonry: Opportunities for the 21st Century*, ASTM STP 1432, D. Throop and R. E. Klingner, Eds., ASTM International, West Conshohocken, PA, 2003.
- [5] Helmuth, R., *Fly Ash in Cement and Concrete*, Portland Cement Association, 1987, pp. 117–120.
- [6] Ramachandran, V. S., Ed., *Concrete Admixtures Handbook, Properties, Science, and Technology, Second Edition*, Noyes Publications, Mill Road, Park Ridge, NJ, 1995, pp. 985–994.
- [7] ASTM C 270, "Standard Specification for Mortar for Unit Masonry," *Annual Book of ASTM Standards*, ASTM International, West Conshohocken, PA.
- [8] ASTM C 788, "Standard Specification for Standard Sand," *Annual Book of ASTM Standards*, ASTM International, West Conshohocken, PA.
- [9] ASTM C 91, "Standard Specification for Masonry Cement," *Annual Book of ASTM Standards*, ASTM International, West Conshohocken, PA.
- [10] ASTM C 144, "Standard Specification for Aggregate for Masonry Mortar," *Annual Book of ASTM Standards*, ASTM International, West Conshohocken, PA.

- [11] ASTM C 1403, "Standard Test Method for Rate of Water Absorption of Masonry Mortars," *Annual Book of ASTM Standards*, ASTM International, West Conshohocken, PA.
- [12] Lea, F. M., *The Chemistry of Cement and Concrete*, Chemical Publishing Company, Inc., 3rd ed., 1971, pp. 391–392.

Cody K. Parker,¹ Jennifer E. Tanner,² and Jorge L. Varela³

Evaluation of ASTM Methods to Determine Splitting Tensile Strength in Concrete, Masonry, and Autoclaved Aerated Concrete

ABSTRACT: Tensile strength of concrete or masonry is a fundamental material characteristic used to predict crack formation. ASTM C 496 and C 1006 are specifically designed to determine the splitting tensile strength of concrete cylinders and masonry units, respectively. Finite element studies for the above tests were completed with the maximum tensile strength compared to the theoretical value in the corresponding ASTM equations. The objectives of this paper are as follows: (1) evaluate current ASTM test methods to determine splitting tensile strength using finite element analysis; (2) evaluate the splitting tensile strength of masonry assemblages through modifying an existing ASTM test; (3) evaluate the application of ASTM test methods to determine the splitting tensile strength of autoclaved aerated concrete; and (4) evaluate a proposed ASTM test to evaluate the splitting tensile strength of thin-bed mortar used in AAC construction. A case study of the splitting tensile strength of autoclaved aerated concrete is used to propose a single test method for this new material.

KEYWORDS: splitting tensile strength, diagonal tension, autoclaved aerated concrete, AAC, masonry, masonry units

Introduction and Background on ASTM Tests to Evaluate Splitting Tensile Strength

Tensile strength of concrete or masonry is a fundamental material characteristic used to predict crack formation. This property is generally expressed as a function of the compressive strength of a material. The splitting tensile strength of concrete is typically determined by a split cylinder test in accordance with ASTM C 496 [1]. In this procedure, a cylinder is turned on its side to apply a distributed load along the top and bottom of the cylinder as shown in Fig. 1. This standard is correlated to the splitting tensile strength by evaluating the maximum horizontal stress between the applied loads using Eq 1, where P is the maximum applied load, D is the cylinder diameter, and l is the cylinder length ([1,2]). The same cylinder test is used in masonry mortars in Annex 8 of ASTM 780 [3]. ASTM C 1006 [4] measures splitting tensile strength of a masonry unit by applying compressive forces to the top and bottom of each specimen through

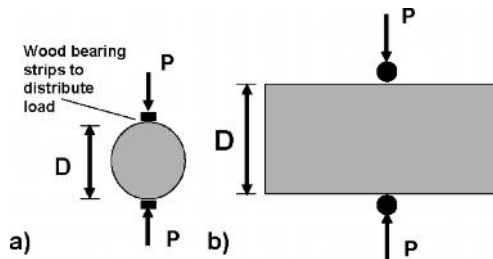


FIG. 1—ASTM test methods to determine splitting tensile strength (a) C 496 (b) C 1006.

Manuscript received December 22, 2005; accepted for publication November 20, 2006; published online February 2007. Presented at ASTM Symposium on Masonry on 13 June 2006 in Toronto, Canada; B. Trimble and J. Brisch, Guest Editors.

¹ Graduate Student, Civil and Architectural Engineering, University of Wyoming.

² Assistant Professor, Civil and Architectural Engineering, University of Wyoming.

³ Assistant Professor, Civil Engineering, Autonomous University of Yucatán, Mérida, Yucatán, México.

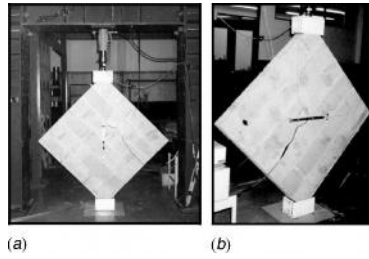


FIG. 2—ASTM E 519 test setup (a) with reaction frame (b) with instrumentation and loading shoes.

two rods (Fig. 1). The resulting stress distribution obtained using a finite element analysis is similar to that obtained for ASTM C 496, with high compressive stress under the load and uniform tensile stress along the line of action of loads. The ASTM C 496 formula is similar to that used in the ASTM C 1006, the difference is that in the former the diameter and the length of the cylinder are replaced with the height and width of the unit, respectively.

$$\sigma = \frac{2P}{\pi D l} \tag{1}$$

ASTM E 519 [5] was developed to determine the shear strength of masonry assemblages. In this test a vertical load is applied to a 4 ft by 4 ft (1.2 m) masonry assemblage placed at 45° from the horizontal as shown in Figs. 2 and 3(a). The shear strength is evaluated by dividing the components of force parallel to the specimen edges by the net area of a section (product of length *L* and thickness *t*) as indicated in Fig. 3(b).

$$f_v = \frac{0.707P}{Lt} \tag{2}$$

For fully grouted or solid autoclaved aerated concrete (AAC) units, the typical failure mode in this test is the formation of a crack along the specimen diagonal between the applied loads rather than on a plane parallel to a bed joint (Fig. 4). In the case of failure governed by splitting along the diagonal, Eq 1 may be used to evaluate the splitting tensile strength, replacing *l*, with the specimen thickness *t*. This equation is evaluated in the following section. For this failure mode, the ASTM E 519 formula is a conservative estimate of the average shear stresses acting along a bed joint because failure did not occur along the bed joint.

Analytical Models

Each of the above ASTM formulas was evaluated using a finite element model using the commercial program ANSYS. Plane-stress theory was used to evaluate each test procedure using a unit thickness for each model with a modulus of elasticity of 340 ksi (2.3 GPa). The load was selected to produce a

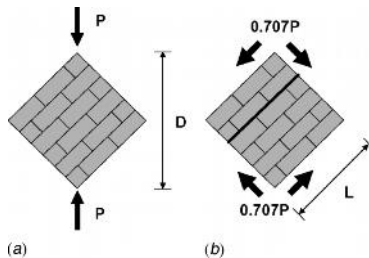


FIG. 3—(a) ASTM E 519 test of a masonry assemblage (b) potential failure plane across a bed joint.

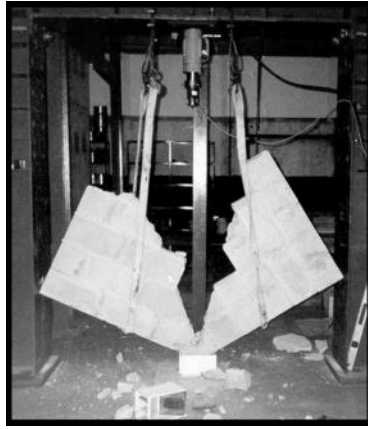


FIG. 4—Results of ASTM E 519 test failing in diagonal tension.

maximum tensile stress of 100 psi (0.7 MPa) in each test method. The finite element models evaluated the horizontal tensile stress distribution along the length D , as shown in Figs. 1 and 3. The first objective of the analytical models was to validate Eq 1 through agreement between this ASTM formula and finite element results for ASTM C 496. The second objective was to validate Eq 1 as a method for determining splitting tensile strength from ASTM C 1006 and ASTM E 519 test results.

The profile of the horizontal stress distribution for this loading condition based on the theory of elasticity is predicted by Eq 3. This equation considers the width of the applied load a , the cylinder radius, R , the cylinder length l , and the distance from the center of the cylinder r [6]:

$$\sigma = \frac{2P}{\pi al} \left[\frac{\left(1 - \frac{r^2}{R^2}\right) \sin 2\alpha}{\left(1 - \frac{2r^2}{R^2} \cos \alpha + \frac{r^4}{R^4}\right)} - \tan^{-1} \left(\frac{1 + \frac{r^2}{R^2} \tan \alpha}{1 - \frac{r^2}{R^2}} \right) \right]$$

$$\alpha = a/R \quad (3)$$

A finite element analysis of a 4-in. (100-mm) diameter by 8-in. (200-mm) tall cylinder was performed using ANSYS. The model used six-node, triangular elements taking advantage of symmetry by modeling half of a circle and restraining horizontal displacement along the centerline of the cylinder (Fig. 5). The load was applied over a 0.25-in. (8-mm) width of the model. The corresponding stress contour indicates maximum tensile stresses between the applied loads. The resulting horizontal stress distribution is in close agreement with the equation based on the theory of elasticity indicating reliability of the finite element analysis (Fig. 6). Both predict high compressive stresses under the points of load application and nearly uniform tensile stresses over the member depth with a maximum horizontal stress from the finite element model less than 0.1 % different from the stress predicted using Eq 1.

The effect of the distributed load width a in Eq 3 was evaluated to compare the stress distribution to that using a concentrated point load applied to a cross section of the specimen, or a line load. Both the finite element model and theoretical model identify a more rectangular tensile stress distribution with increased compressive stresses under the concentrated load (Fig. 7). Although the theoretical equation results are similar to the finite element results, it is not a practical test since local crushing would occur under the concentrated point load resulting in a load distributed over the zone of crushing. A point load corresponds to a line load on the specimen and a distributed load corresponds to an area load applied over the zone of crushing. This correlation between the theory of elasticity and proposed finite element validates the proposed model, which is applied to other ASTM tests.

ASTM C 1006 measures splitting tensile strength of a masonry unit by applying compressive forces to the top and bottom of each specimen through two rods. The resulting stress distribution obtained using a

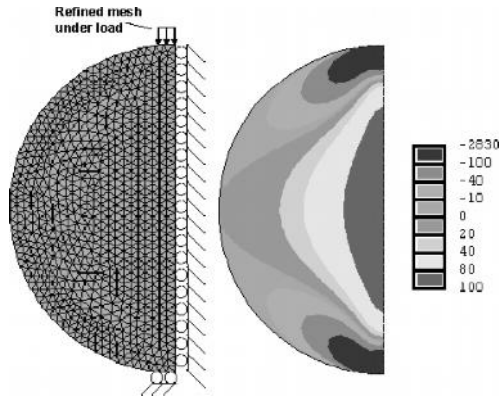


FIG. 5—Finite element model of ASTM C 496 and horizontal stress distribution in psi.

finite element analysis is similar to ASTM C 496 with high compressive stress under the load and uniform tensile stress along the line of action of loads. The same formula to predict maximum tensile stress in the specimen is applied, although in this case the diameter of the cylinder is replaced with the specimen height and the length is replaced with the specimen width. A second finite element analysis study was performed using eight-node quadrilateral elements with the load, boundary conditions and stress contours shown in Fig. 8. The resulting horizontal stress distribution is nearly uniform along the height of the solid unit used

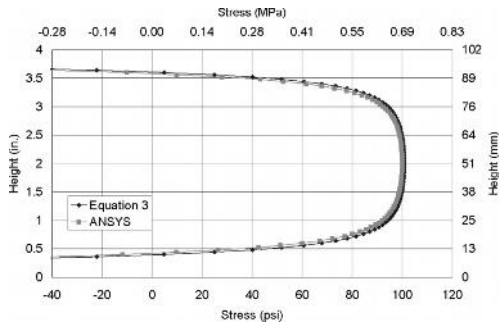


FIG. 6—Theoretical prediction of stresses and results of finite element study to predict horizontal stresses.

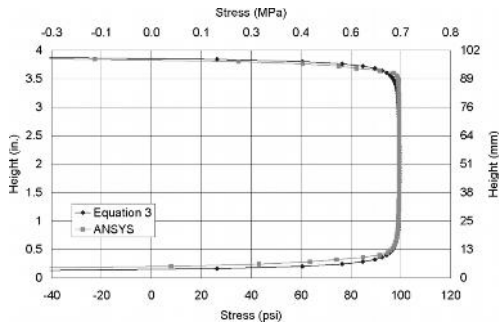


FIG. 7—Resulting horizontal stress distribution for a cylinder subject to a point load on a cross section of the specimen.

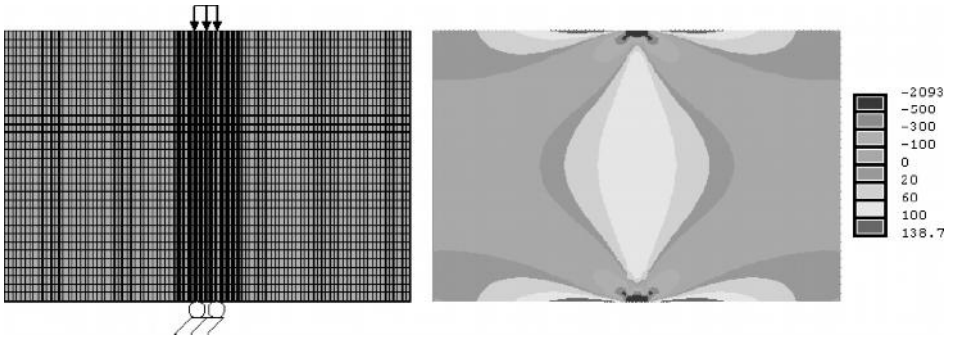


FIG. 8—Finite element model and resulting tensile stress in psi between loads for ASTM C 1006.

in this analysis (Fig. 9). The ratio of maximum calculated horizontal stresses using the finite element analysis to the calculated tensile stress using Eq 4 is 0.95. The finite element analysis stresses are lower due to additional material beyond that of a cylinder. A small decrease in tensile stress is observed at midheight of the specimen.

$$\sigma = \frac{2P}{\pi D l} \tag{4}$$

A third finite element study was performed on an ASTM E 519 test to determine the resulting tensile stresses over the member depth (Fig. 10). Eight-node quadrilateral elements were used with the load applied over 1 in. (25 mm) on each face. Maximum tensile stresses are located at the center of the specimen with high compressive stresses under the applied load (Fig. 11). A failure along a diagonal indicates a splitting tensile failure prior to a shear failure with the splitting tensile stress predicted by Eq 1 used in ASTM C 496 and C 1006. The ratio of calculated tensile stresses using the finite element analysis to stresses predicted using the modified equations for splitting tensile strength based on ASTM C 496 and C 1006 defined by Eq 1 is 1.07. Larger stresses in the finite element study are attributed to an area less than a cylinder of equivalent diameter.

In a case of failure governed by splitting along the diagonal, the ASTM formula used to predict shear strength is a conservative estimate of the average shear stresses acting along a bed joint because the failure does not occur on a plane parallel to the shear load as shown in Fig. 3(b). This ASTM test could be expanded to evaluate the splitting tensile strength of masonry assemblages as well as the average shear stress.

A summary of test analyses is presented in Table 1. The ratio of stresses determined using the finite

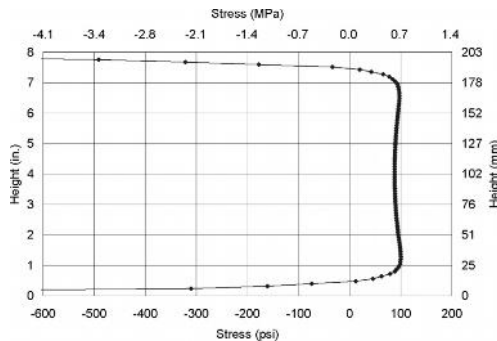


FIG. 9—Resulting horizontal stress distribution in ASTM C 1006 finite element analysis.

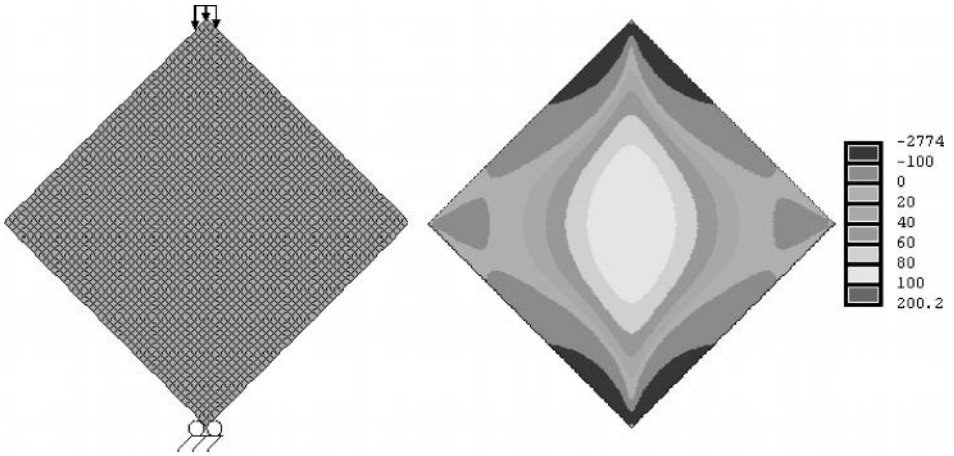


FIG. 10—Finite element model and resulting tensile stress in psi between loads for ASTM E 519.

element study to the calculated results using Eq 1 is shown in Row 2. All cases have ratios of stresses close to unity indicating that Eq 1 is validated by the finite element models.

An optimal splitting tensile strength test method results in a uniform tensile stress over a large depth. The shape of the tensile stress zone in each analysis was evaluated based on a uniformity ratio. The uniformity ratio is the area of tensile stress divided by a rectangular area defined as the product of the tensile strength depth and maximum tensile stress (Fig. 12). For a perfectly rectangular stress distribution, the uniformity coefficient is 1. For a distributed load, ASTM C 496 and ASTM C 1006 are equally close to a rectangular area, while ASTM E 519 is farther from rectangular, indicating maximum stresses in the center section only.

In the following sections, test results for ASTM C 496, ASTM C 1006, and ASTM E 519 are compared for autoclaved aerated concrete, an innovative material. Based on these results a single test method is proposed for evaluating the tensile strength of AAC.

Background on AAC

Autoclaved aerated concrete (AAC) is an innovative building material in the US that is intriguing due to its low unit weight, high fire rating, high energy efficiency, and sound damping properties. AAC is factory produced by mixing finely ground sand, cement, water, and possible lime. An expansive agent is added to create a cellular structure. The raw mass is cut into units and cured in an autoclave at temperatures of

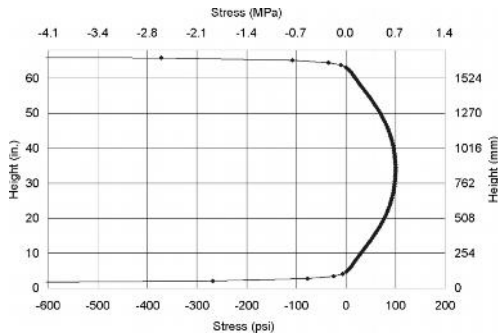


FIG. 11—Resulting horizontal stress distribution in ASTM E 519 finite element analysis.

TABLE 1—Summary of results from finite element analyses.

ASTM Method	C 496 Point load on cross- section	C 496 Distributed load on cross- section	C 1006	E 519
Figure (not to scale)				
Ratio of maximum stress from finite element solution to maximum stress using Equation 1	1.0	0.95	0.95	1.07
Uniformity coefficient	0.95	0.87	0.88	0.65

400 °F (205 °C) and pressures of 150 psi (1 MPa). Standard units in AAC structural systems are AAC shear walls and floor diaphragms. Shear walls may be constructed of modular blocks or panels oriented horizontally or vertically. Modular blocks are 8 in. (200 mm) in height and are 24 in. (610 mm) long. Wall panels are 24 inches (610 mm) in height and may have lengths up to 240 in. (6.10 m). The thickness of blocks and panels is variable, with a common thickness of 8 in. (200 mm) to 10 in. (250 mm). Floor panels have a width of 24 in. (610 mm) and are produced in lengths up to 240 in. (6.10 m). Individual AAC units are bonded together by thin-bed mortar joints approximately 1/16 in. (1.6 mm) thick.

AAC is receiving renowned attention as a building material in the US because it has a low unit weight. A comprehensive research program was carried out to propose design equations and develop the technical justification for autoclaved aerated concrete [7,8,15,16]. Although AAC has been used in Europe for 70 years, little data exist on the tensile strength and the authors know of no published ASTM tests applicable to AAC beyond the references included here. The published information includes an equation to predict the splitting tensile strength of AAC in the Masonry Standards Joint Committee Building Code Requirements for Masonry Standards and corresponding commentary [9] and is further validated through the experimental results.

Experimental Results

A series of tests was carried out to determine the splitting tensile strength in accordance with ASTM C 1006 (Fig. 13). The specimens were oriented so that splitting tensile stresses acted parallel to the direction of rise. Each data point in Table 2 represents the average for a group of four to nine specimens to comprise 50 specimens tested at the University Texas at Austin and an additional 20 specimens tested at the University of Wyoming. The moisture contents of those specimens fall within the 5 % to 15 % range permitted by ASTM C 1386 test results[10].

The results of the ASTM C 1006 splitting tensile strength are plotted with respect to the tested compressive strength in Fig. 14 with a linear regression having a good correlation coefficient of $R^2 = 0.86$ (Eq. 5). Equation 6 was proposed for the splitting tensile strength and the square root of the compressive strength and provides a good fit for data with compressive strengths above 500 psi (3.4 MPa). This expression is included in the 2005 MSJC Building Code and is also consistent in form with the ACI 318-05 expression for tensile strength [9,11].

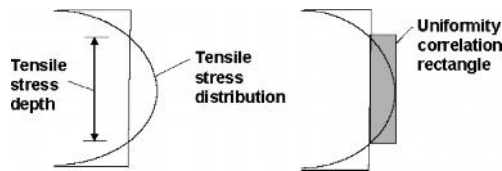


FIG. 12—Graphical representation of uniformity coefficient.



FIG. 13—C 1006 test setup.

$$f_t = 0.05f_{AAC} + 23.8, \quad f_t \text{ and } f_{AAC} \text{ in psi} \tag{5}$$

$$f_t = 2.4\sqrt{f_{AAC}}, \quad f_t \text{ and } f_{AAC} \text{ in psi.} \tag{6}$$

Additional tests were performed at the University of Wyoming to evaluate the splitting tensile strength using ASTM C 496 (Fig. 15). Each data point represents the average of four specimens for each class of AAC. Test reports of the shear strength according to ASTM E 519 were used to evaluate splitting tensile

TABLE 2—Results of C 1006 splitting tensile strength tests performed at UT Austin and UWyo.

Manufacturer	Average f_t psi (MPa)	Number of specimens	COV (%)	Average f_{AAC} psi (MPa)
Contec 1	71.2 (0.49)	6	10.5	781 (5.4)
Ytong 1	55.3 (0.38)	5	14.2	517 (3.6)
Ytong 2	62.7 (0.43)	8	4	650 (4.5)
Hebel 2	88.4 (0.61)	6	5.2	1330 (9.2)
Contec 2b	74.6 (0.51)	4	1.8	1040 (7.2)
Babb 1	84.7 (0.58)	5	10.1	1140 (7.9)
Babb 2a	52.5 (0.36)	5	12.7	495 (3.4)
Babb 2b	45.0 (0.31)	5	14.9	495 (3.4)
Contec 2a	54.0 (0.37)	9	6.8	1040 (7.2)
E-Crete C3	40.3 (0.27)	5	7.2	451 (3.1)
Aercon C2	48.7 (0.33)	5	16.6	582 (4.0)
Aercon C 4	67.1 (0.46)	5	8.5	791 (5.5)
Aercon C6	84.8 (0.58)	5	4	915 (6.3)

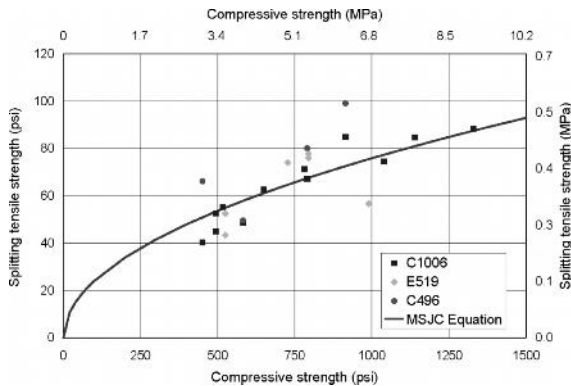


FIG. 14—Splitting tensile strength versus compressive strength.

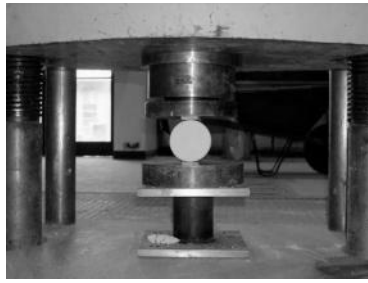


FIG. 15—ASTM C 496 test performed at University of Wyoming.

strength of AAC[12–14]. Data sets without a minimum of three specimens or reported compressive strength tests are not considered in this evaluation. These results and corresponding compressive strengths are compared to the ASTM C 1006 tests in Fig. 16. Data is presented in Tables 3 and 4. A clear trend exists between the compressive strength and tensile strength despite some lower data for ASTM E 519. In general, the splitting tensile strength based on cylinder tests is greater than that based on block tests. ASTM E 519 tests on AAC assemblages modified to evaluate splitting tensile strength showed the lowest

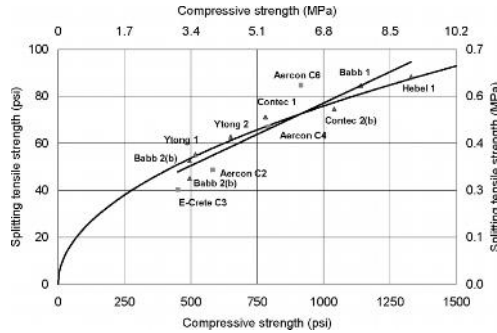


FIG. 16—Additional AAC splitting tensile strength data compared to ASTM C 1006 results.

TABLE 3—Results of splitting tensile strength based on E 519 data reported elsewhere.

Report	Average f'_s , psi (MPa)	Number of specimens	COV, %	Average f_{AAC} , psi (MPa)
UNAM	43.4 (0.30)	9–12	25	525 (3.6)
UNAM	52.5 (0.36)	9–12	9	525 (3.6)
UNAM	76.0 (0.52)	9–12	11	795 (5.5)
UNAM	77.8 (0.54)	9–12	14	795 (5.5)
Chile	74.0 (0.51)	5	11	730 (5.0)
AACOA	56.7 (0.39)	3	9.6	990 (6.8)

TABLE 4—Results of C 496 splitting tensile strength tests performed at UWyo.

Manufacturer	Average f'_s , psi (MPa)	COV, %	Average f_{AAC} , psi (MPa)
E-Crete C3	66.1 (0.46)	14.3	451 (3.1)
Aercon C2	49.6 (0.34)	15.1	582 (4.0)
Aercon C 4	80.1 (0.55)	14.9	791 (5.5)
Aercon C6	99.1 (0.68)	4.98	915 (6.3)

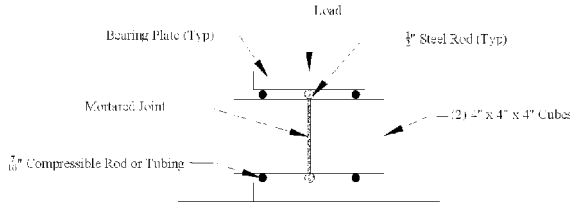


FIG. 17—Proposed test method to evaluate splitting tensile strength of thin-bed mortar.

test results. Although the differences in strength are small, a trend for increasing tensile strength is observed with decreasing specimen size. Because ASTM C 1006 provides the simplest and most consistent of the three methods, it is recommended as a single test method to determine the splitting tensile strength of AAC. Furthermore, finite element analysis results identify a relatively uniform tensile stress distribution along the height as indicated by the normalized area under the tensile stress diagram of 0.87. Although ASTM C 496 and ASTM C 1006 have the same normalized area, ASTM C 1006 also eliminates possible damage to specimens through coring cylinders.

Evaluation of Splitting Tensile Strength of Thin-Bed Mortar for AAC

ASTM Task Group C12.03.07 is evaluating a test to determine if there is a statistically significant difference between the splitting tensile strength of a solid piece of AAC and two pieces of AAC jointed with thin-bed mortar. According to this draft test method, two 4-in. AAC cubes are joined with thin-bed mortar. Load is applied through two 1/2-in. diameter (13 mm) rods at the location of and parallel to the thin-bed mortar joint. To initially stabilize the specimen and prevent rotation, compressible tubes are placed at ends of each specimen on the top and bottom (Fig. 17). During testing it is possible to remove the compressible rods or tubing indicating they do not affect the load path.

Another finite element analysis was performed on this proposed specimen to consider the tensile strength of thin-bed mortar. Eight-node quadrilateral elements were used for the AAC and thin-bed mortar elements using a 1/16-in. (1.6-mm) wide joint. The modulus of elasticity of AAC is 340 ksi (2.3 GPa) and the thin-bed mortar modulus of elasticity was 620 ksi (4.3 GPa). The final results were not sensitive to increasing or decreasing the modulus of elasticity of the thin-bed mortar by a factor of two. The resulting horizontal stress distribution was similar to that of ASTM C 1006 with a ratio of maximum calculated tensile stress using finite element and Eq. 4 of 0.94. Furthermore, the normalized area under the tensile stress zone is the same for both finite element analyses (Fig. 18). These factors indicate the proposed test produces a relatively uniform tensile stress distribution.

Experimental results of this test procedure were performed at the University of Wyoming to evaluate the tensile strength of thin-bed mortar. The average of three tests for four different classes of AAC is

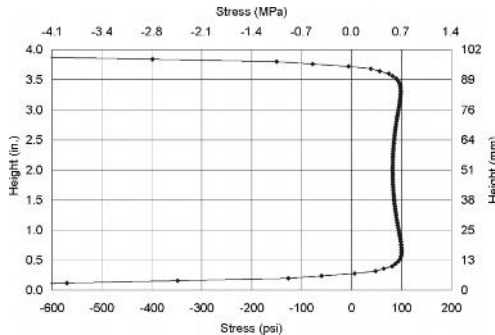


FIG. 18—Resulting horizontal stress distribution for proposed thin-bed mortar splitting tensile strength.

TABLE 5—Results of splitting tensile strength tests performed on thin-bed mortar joints at UWyo.

Manufacturer	Average thin-bed mortar f_t , psi (MPa)	COV, %	Average f_{AAC} , psi (MPa)	Average AAC f_t , psi (MPa)	Ratio of thin-bed mortar f_t to AAC f_t
E-Crete C3	35.1 (0.24)	13.4	451 (3.1)	40.3 (0.27)	0.72
Aercon C2	24.5 (0.17)	2.6	582 (4.0)	48.7 (0.33)	0.61
Aercon C 4	28.3 (0.20)	4.8	791 (5.5)	67.1 (0.46)	0.42
Aercon C6	22.7 (0.16)	27.5	915 (6.3)	84.8 (0.58)	0.27

shown in Table 5. The failure surface was in the thin-bed mortar joint as evidenced by thin-bed mortar on both sides of the failure area. The experimental tensile strength of the combined AAC and thin-bed mortar is relatively constant, ranging from 22.7 psi (0.16 MPa) to 35.1 psi (0.24 MPa). Because the splitting-tensile strength of AAC increases with increasing compressive strength the ratios of splitting tensile strength of thin-bed mortar and AAC specimens to solid AAC specimens range from 0.72 to 0.27. For this particular mortar, the tensile strength of the material alone is stronger than AAC and thin-bed mortar. This test is a good indicator of how well the thin-bed mortar and AAC work together.

Conclusions

A series of ASTM tests were evaluated experimentally and analytically to determine the splitting tensile strength of AAC. Experimental results of the splitting tensile strength of AAC were evaluated using three ASTM methods. There exists a clear trend of increasing tensile strength with increasing compressive strength for ASTM C 496, ASTM C 1006, and ASTM E 519. ASTM C 1006 is recommended as the primary method to determine splitting tensile strength based on uniformity of tensile stress distribution, reduced coefficient of variation and simplicity of testing method. The finite element analysis was verified through a comparison with results obtained from the theory of elasticity. Finite element extrapolations were applied to additional ASTM tests to explore additional ASTM testing methods.

A proposed ASTM standard under consideration by ASTM C 12.03.7 is evaluated using finite element method and the ASTM formula is validated through the similarity between the analytical results of this proposed test and the ASTM C 1006 test. Experimental results indicate the tensile strength of this particular combination of thin-bed mortar and AAC was lower than the tensile strength of the AAC alone. The proposed method to evaluate the splitting tensile strength of thin-bed mortar and AAC with respect to the splitting tensile strength of the AAC material is a good indicator of the combined performance of thin-bed mortar and AAC.

Acknowledgments

This work was begun under a comprehensive research program to evaluate the structural behavior of AAC masonry and reinforced panels under the supervision of Prof. Richard E. Klingner at the University of Texas at Austin. The authors appreciate his support as well as the financial and technical support of the Autoclaved Aerated Concrete Product Association AACPA to further develop this research.

References

- [1] ASTM, Standard C 496 "Standard Test Method for Splitting Tensile Strength of Cylindrical Concrete Specimens", *Annual Book of ASTM Standards* ASTM International, West Conshohocken, PA, 2002.
- [2] Timoshenko, S. P., and Goodier, J. N., *Theory of Elasticity*, McGraw-Hill, New York, 1970.
- [3] ASTM, Standard C 780 "Standard Test Method for Preconstruction and Construction Evaluation of Mortars for Plain and Reinforced Masonry," *Annual Book of ASTM Standards*, ASTM International, West Conshohocken, PA, 2002.
- [4] ASTM, Standard C 1006 "Standard Specification for Splitting Tensile Strength of Masonry Units," *Annual Book of ASTM Standards*, ASTM International, West Conshohocken, PA, 2001.

- [5] ASTM, Standard E 519 "Standard Test Method for Diagonal Tension (Shear) in Masonry Assemblages," *Annual Book of ASTM Standards*, ASTM International, West Conshohocken, PA, 2002.
- [6] Boresi, A. P., and Chong, K. P., *Elasticity in Engineering Mechanics*, Wiley-Interscience, John Wiley and Sons, New York, 2000.
- [7] Klingner, R. E., Tanner, J. E., Varela, J. L., Brightman, M. J., Argudo, and J., Cancino, U., "Technical Justification for Proposed Design Provisions for AAC Structures: Introduction and Shear Wall Tests," *American Concrete Institute (ACI) Special Publication 226*, 2005.
- [8] Klingner, R. E., Tanner, J. E., and Varela, J. L., "Technical Justification for Proposed Design Provisions for AAC Structures: Assemblage Test and Development of R and C_D Factors," *American Concrete Institute (ACI) Special Publication 226*, 2005.
- [9] MSJC (2005), *Building Code Requirements for Masonry Structures (ACI 530.1-05/ASCE 5-05/TMS 402-05)*, Masonry Standards Joint Committee, 2005.
- [10] ASTM, Standard C 1386, "Standard Specification for Precast Autoclaved Aerated Concrete (PAAC) Wall Construction Units," *Annual Book of ASTM Standards*, ASTM International, West Conshohocken, PA, 1998.
- [11] ACI 318-05, *Building Code Requirements for Structural Concrete and Commentary*, American Concrete Institute, Farmington Hills, MI, 2005.
- [12] Martínez, I. A., "Uso de Hormigón Celular en Chile como Albanilería y Otros," Universidad de Chile, Facultad de Ciencias Físicas y Matemáticas, Departamento de Ingeniería Civil, (University of Chile, Department of Civil Engineering), 1998.
- [13] Zepeda, J. A., Otalora, A. M., and Alcocer, S. M., "Estudio de Evaluación de las Propiedades Mecánicas del Sistema Hebel," Centro Nacional de Prevención de Desastres CENAPRED (National Center for Prevention of Disasters in Mexico), 2005.
- [14] CTL Testing and Materials Technology, Internal report, "Material Tests of ACCOA Autoclaved Aerated Concrete (AAC) Masonry Blocks and Assemblies," 1999.
- [15] Tanner, J. E., Varela, J. L., Brightman, M. J., Cancino, U., and Klingner, R. E., "Seismic Testing of Autoclaved Aerated Concrete (ACC) Shear Walls: A Complete Review," *ACI Structures Journal*, January/February 2005.
- [16] Tanner, J. E., Varela, J. L., and Klingner, R. E., "Design and Testing of a Two-Story, Full-Scale Autoclaved Aerated Concrete (AAC) Assemblage Specimen," *ACI Structures Journal*, May/June 2005.

David T. Biggs, P.E.¹ and Margaret L. Thomson, Ph.D.²

Type S Portland Cement-Lime Mortar as a Low-Lift Grout

ABSTRACT: Specification for Grout for Masonry, ASTM C 476, allows grouts to be specified by a proportion method using the cementitious materials of portland cement, blended cement, hydrated or putty lime (with a 1/10 by volume limit), and aggregate. There is no limitation on slump values in ASTM but industry standards recommend a slump of 8 to 11 in. (203 to 279 mm). A second method of specifying grout is by its properties with a minimum 28-day compressive strength value of 2000 psi (13 790 kPa). It is not an uncommon practice, however, for masonry contractors to use portland cement-lime mortars in low-lift (less than 5 ft [1.52 m] height) applications at a consistency of bedding mortar or a pourable consistency. According to ASTM C 476, this application would neither meet the proportion specification because of too much lime nor the property specification because of too low a slump. This study, investigating the comparative compressive strength properties and reinforcement pull-out strength of Type S and Type N ASTM C 270 proportioned cement-lime mortars, ASTM C 476 grout, and grout with comparable hydrated lime proportions to a Type S mortar, supports the following conclusions: • Type S portland cement-lime mortar at a bedding mortar consistency will perform as grout in specific low-lift grouting applications. • Type S portland cement-lime mortar at a pourable consistency will perform as grout in specific low-lift grouting applications. • Type M portland cement-lime mortar at a bedding mortar consistency or pourable consistency could also be used as grout in specific low-lift grouting applications.

KEYWORDS: low-lift grout, Type S portland cement-lime mortar, compressive strength, pull-out test

Introduction

Grouted, reinforced masonry began in the United States after the 1933 Long Beach, CA, earthquake [1]. The earthquake with an estimated magnitude 6.25 Ms occurred March 10, 1933. Unreinforced masonry walls often failed catastrophically. However, it was documented that buildings that were engineered and reinforced sustained little or no structural damage. As a result, the state passed two laws in 1933: the Field Bill and the State Earthquake Protection Law (Riley Act). The Field Bill was in response to public outcry over the vulnerability of school buildings to earthquake-related damage since approximately 70 school buildings were destroyed. Both legislative acts began the development of regulations to mandate earthquake-resistant structures. These acts signaled the end of unreinforced masonry in California.

ASTM began to develop C 476 in 1931. However, the first document was issued in 1961 under temporary designation ASTM C 476-61T Standard Specifications for Mortar and Grout for Reinforced Masonry. The scope states the specification covers both mortar and grout for use in construction of reinforced masonry structures. Prior to this, reinforced masonry was constructed using provisions within the building codes.

History

The development of grouting standards is intertwined with the advancement of building codes. The following summary outlines some of the highlights of grout development.

1927 The first Uniform Building Code (UBC) was issued. It primarily addressed fire safety.
1933 Long Beach, CA, earthquake.

Manuscript received November 30, 2005; accepted for publication November 20, 2006; published online January 2007. Presented at ASTM Symposium on Masonry on 13 June 2006 in Toronto, Canada; B. Trimble and J. Brisch, Guest Editors.

¹ Principal, Ryan-Biggs Associates, P.C., USA, e-mail: dbiggs@ryanbiggs.com

² Technical Manager, Type S Hydrated Lime Sales, Chemical Lime Company, USA, e-mail: margaret.thomson@chemicallime.com

- 1933 Riley Act and Field Bill improved earthquake-resistant construction in California.
- 1935 UBC required reinforcement of masonry foundations.
- 1937 UBC required "Cement grout shall be comprised of not less than one part portland cement and four and one-half parts of sand by volume. Sufficient water shall be added to produce a proper consistency for pouring without segregation of constituents."
- 1946 UBC required "Grout shall be Type A mortar to which is added water to produce consistency for pouring without segregation of constituents of the mortar." By proportions, Type A mortar was defined as 1 part portland cement, $\frac{1}{4}$ -part hydrated lime or lime putty, and 2 to 3 parts aggregates. By strength, Type A mortar cube strength was 2500 psi (17 237 kPa).
- 1950 Research in northern California was performed to develop high-lift grouting techniques.
- 1960 ANSI A41.2-1960 American National Standard "Building Code Requirements for Reinforced Masonry" [2] requires that the mortar proportions used consist of 1 part portland cement, $\frac{1}{4}$ to $\frac{1}{2}$ -part lime or lime putty, and fine aggregate consisting of $2\frac{1}{4}$ to 3 times the sum of the separate volumes of the cement and lime used (a Type S cement-lime proportion mortar). The grout was to be of type MG (mortar grout) or PG (pea gravel grout) consisting of common volumes of 1 part portland cement, $\frac{1}{4}$ -part hydrated lime or lime putty, and differing by fine aggregate consisting of $2\frac{1}{4}$ to 3 times the separate volumes of sand and lime used (MG) and fine aggregate consisting of 2 to 3 parts and 1 to 2 parts of coarse aggregate (PG). Mixing for both mortar and grout types are described as using the amount of water required to produce the desired workability.
- 1961 UBC requires all structural members to resist earthquake forces.
- 1961 ASTM C 476 first released Standard Specifications for Mortar and Grout for Reinforced Masonry. The grout was specified by proportion with 1 part portland cement or portland blast furnace slag cement, to $\frac{1}{10}$ part hydrated lime or lime putty, and aggregate $2\frac{1}{4}$ to 3 times the sums of the cementitious materials. The aggregate distinguished between fine and coarse of ASTM C 404-61 Standard Specification for Aggregates for Masonry Grout. No specific slump was required; it was only necessary to add sufficient water to obtain the desired consistency. These grout proportions were within the proportions specified in ASTM C 270-63 (68) for a Type M proportion cement-masonry cement mortar. The aggregate was to meet the requirements of ASTM C 144 Standard Specification for Aggregate for Masonry Mortar.
- 1980 ASTM C 476 Standard Specification for Grout for Reinforced and Nonreinforced Masonry eliminated mortar from its title, and allowed for the cementitious components to be specified by proportion, with fine and coarse aggregate, and only allowing up to $\frac{1}{10}$ volume of hydrated or putty lime. ASTM C 595-80 Standard Specification for Blended Hydraulic Cements, Type 1P cements and pumping aids are added to the materials section. Mixing instructions are for the grout to be mixed to a desired consistency.
- 1982 UBC included low-lift/high-lift. In UBC 1982, 1985, 1994, and 1997 [3], mortar continued to be acceptable as a grout in non-structural elements not exceeding 8 ft (2.4 m) in height above lateral support, including fireplaces and residential chimneys. Mortar of pouring consistency could be substituted for grout when the masonry is constructed and the pours are 12 in. or less in height.
- 1983 Residential codes from the Council of American Building Officials (CABO) allowed Type S or Type M mortar, with water added, to be used as grout. CABO became part of the International Code Council in 2000. The International Residential Code [4] also allowed Type S or Type M mortar.
- 1984 ASTM C 1019 Method for Sampling and Testing Grout was first published.
- 1985 UBC indicates that grout shall consist of part portland cement, part hydrated lime or lime putty, and either coarse or fine aggregate. It also revised its grouting requirements so that, "In non-structural elements, mortar of pouring consistency may be substituted for grout when the masonry is constructed and grouted in pours of 12 inches (305 mm) or less."
- 1989 ASTM C 1019 required the measurement of slump as measured for concrete (slump cone), with no specified value.
- 1991 ASTM C 476 still indicates that sufficient water is added to bring the mixture to the desired consistency.
- 1995 ASTM C 476 had a significant change. The grout can be specified by compressive strength, with

a minimum value of 2000 psi (13 790 kPa) at 28 days and shall be sampled according to ASTM C 1019. The construction mixing requirements remains as before, that sufficient water is added to bring the mixture to the desired consistency.

- 1998 ASTM C 476 indicated a slump requirement of 8 to 11 in. (203 to 279 mm) is required when the grout is specified to compressive strength. Construction mixing instruction remains as before, that sufficient water is added to bring the mixture to the desired consistency.
- 2000 The International Residential Code (R6091.1) allows Type S and Type M mortar with water added to be used as grout in reinforced masonry.
- 2000 The International Building Code does not allow mortar as grout.
- 2001 ASTM C 476 reorganizes the specification by defining grout by aggregate type and by proportion and compressive strength, with requirements for a minimum compressive strength of 2000 psi and a slump of 8 to 11 in. (203 to 279 mm) when tested using ASTM C 1019. Note 3, although not mandatory, indicates that building code provisions should be reviewed when selecting the specified compressive strength. Grout was also defined by the production and delivery methods. These include job site mixes using sacks of cementitious materials, aggregate delivery systems with separate compartments, a method for dispensing to the specified volumetric proportions and augers for wet mixing, factory dry-blended materials transported in a silo or super sacks, and wet mixed grout arriving in a ready-mixed consistency. Only the wet-mix grout indicates that the slump can be adjusted as necessary, with the remaining production types referring to obtaining desired consistency.

Low-Lift and High-Lift Grouting

Grouting techniques are continually evolving. Early standards after the 1933 Long Beach earthquake simply required that sufficient water shall be added to produce a proper consistency for pouring without segregation of constituents. No limits were given for the amount of grout that was placed at any one time. Often the grouting progressed course by course with the wall units. Six-ft (1.83 m) lengths of reinforcement were used; 4 ft (1.22 m) were grouted each day and 2 ft (0.61 m) were left for the lap splice. This was the genesis of low-lift grouting.

In northern California, masonry contractors wanted to speed up construction and proposed constructing the masonry full height and then grouting the wall full height. With limitations, the method was accepted by the state of California and has become known as high-lift grouting. Person [5] describes his role in the development of high-lift grouting through the completion of the 1955-1960 Testing Project No 922 *New Method of Reinforced Concrete and Masonry Construction Using High Lift Grouting System*. He states, "I recommend that only full height pours be used, and that the four-foot lift be used in only special circumstances; slump should be the maximum without separation—approximately 10 to 11 inches (254 to 279 mm)" [20 pp. 62–68]. Amrhein [6] points out that slump of 8 to 10 in. (203 to 254 mm) became the grout standard for both low-lift and high-lift grout. These characteristics were developed with brick masonry.

Current industry standards allow either low-lift or high-lift grouting techniques [[7], pp. 221–240]. It is important to understand the concept of grout pours and grout lifts. Grout is placed in increments called lifts. A grout lift is the height of the grout placed in a single continuous operation prior to consolidation and reconsolidation [[8], p. 25]. One or more lifts are placed in a day to create a pour. The pour height is limited by the size of the cell or cavity to be filled as well as the type of grout used (fine or coarse).

Low-lift grouting is used when masonry walls are built in less than 5 ft (1.53 m) increments, allowing for inspection and negating the need for cleanout openings in the first course. High-lift grouting procedure is used where the walls are built over 5 ft (1.54 m) up to a maximum of 24 ft (7.33 m) with cleanouts in the bottom course of each pour at the location of the reinforcing steel or in an even distribution as required by code.

Previous Reports

Isberner [9] states that "Grout for reinforced masonry as a material of construction has not been extensively researched. Consequently, construction practices heavily influence existing, codes, specification and

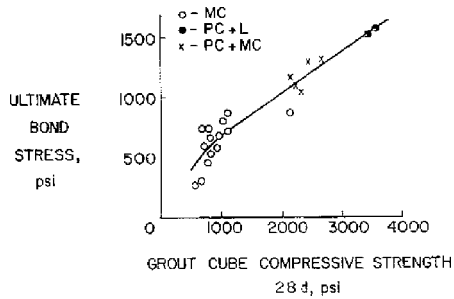


FIG. 1—Graph taken from Isberner [16] summarizing data produced by the Portland Cement Association in the early 1960s.

standards. It is fortunate we have as much as we do; it is unfortunate that we disallow certain practices and materials on little or no evidence.” He adds, “Although many grouted reinforced masonry structures are now in existence, the specifics of grout design and use are relatively unfounded.” He refers to work by the Portland Cement Association (PCA) in the early 1960s, which showed that grouts made with portland cement and lime produced the highest ultimate bond stress and grout cube compressive strength when compared to masonry cement and portland cement and masonry cement combined (Fig. 1). (Recall that ANSI A41.2-1960 recognized these material combinations.)

Randall and Panarese [10] give an excellent example of how practice disallows certain materials. They write, “All the materials included in ASTM C 476 are satisfactory for use in grout. Most projects using large volumes of grout obtain the grout from a ready mixed concrete producer; the use of lime then becomes uneconomic because of the expense of handling.” (p. 39). It is not, therefore, the technical appropriateness of lime in the grout that eliminates its use, but rather the delivery system.

ANSI A41.2-1960 [2] indirectly recognized low-lift and high-lift grouting. For reinforced grouted masonry where all interior joints, cores, or spaces had to be solidly filled, the maximum pour height for a clear dimension of least 2 in. (51 mm) or more using PG grout pour was not to exceed 48 times the clear dimension (approximately 8 ft (2.44 m), and using MG grout was not to exceed 64 times the clear dimension and not exceed 12 ft (3.66 m). For reinforced hollow masonry, the grout pour was not to exceed 4 ft in height unless cleanouts were left open at the bottom masonry course of each core to be reinforced.

The UBC provisions used the same philosophy of defining the grout type by the clear dimension within the grout spaces and in the same manner did not directly distinguish this as either low-lift or high-lift grouting method. The 2005 “Building Code Requirements for Masonry Structures” (ACI530-05/ASCE 5-05/TMS 402-05) [11] changed its criteria so that the maximum lift heights could increase from 5 ft (1.53 m) to as much as 12 ft-8 in. (3.87 m).

Mortar Used as Grout Remains a Practice in the Masonry Industry

The standards and the codes for reinforced masonry, and to a great degree the practice of grouting, has clearly developed toward almost exclusively high-lift grouting. This has effectively eliminated the use of mortar for grout in the masonry industry. However, high-lift grouting is not the common practice in every region of the country, and in spite of codes and standards, masonry contractors in some regions of the United States commonly substitute mortar for grout. These masonry contractors prefer to use mortar for grout for the following reasons:

1. Reduces installation costs in low-lift applications when the masonry is to be partially grouted. (Cost is contractor-dependent; some may find full grouting to be more economical.)
2. Reduces the number of mixers used since industry standards generally require separate mixing of mortar and grout.

Little research has been completed in the area of mortar used as grout since the elimination of it from the ASTM C 476. Biggs [12] summarizes the research available to support the use of mortars as grout in masonry construction.

TABLE 1—Grout mixes and strengths.

	Portland cement	Type S Hydrated Lime	Aggregate	Slump, inc.	Compressive Strength at 28 days ^c , psi ± st.dev., (kPa ± st.dev)
Bedding Mortar	1	0.5	4.5	Determined by mason	
Mix N (mortar fill)	1	1.0	6.0	Determined by mason	1433 ± 185 (9880 ± 1275)
Mix S ^a (mortar fill)	1	0.5	4.5	Determined by mason	2547 ± 110 (17561 ± 758)
Mix NSL (pourable mortar)	1	1.0	6.1	6.00	1537 ± 163 (10597 ± 1124)
Mix SSL (pourable mortar)	1	0.5	4.5	6.25	1800 ± 101 (12411 ± 696)
Mix G (grout)	1	0.1	3.0	10.25	4010 ± 60.2 (27646 ± 415)
Mix Mod G ^b (modified grout)	1	0.4	4.2	9.5	2795 ± 52.5 (19271 ± 362)

^aSame as bedding mortar.

^bSimilar to bedding mortar with a high slump.

^cTested in accordance with ASTM C 1019.

In 1991, Hedstrom and Thomas [13] evaluated mortar used in lieu of fine grout with concrete masonry units (CMUs). Types M, S, and N proportioned cement-lime mortars were mixed to a pourable consistency with a slump of 7 to 9 in. (178 to 229 mm) and were compared to three grout mixes with a similar slump range. The three grout mixes contained cement and sand but no lime. The aggregate ratios were varied to achieve compressive strengths similar to the mortars. A No. 5 (M16) reinforcing bar was pulled in tension from test specimens. The report concluded that further research was necessary but that pourable mortars “could become an effective substitute for grout.” No specific limitations were placed upon unit types or absorption.

A report by Brown [14] on the use of Type S masonry cement mortar in lieu of grout in reinforced hollow-clay walls compared bond strengths developed from three methods of filling the cell space around reinforcement in hollow clay units. The three methods included grouting with standard grout, slushing with mortar, and “souping” with mortar that had been tempered to a slump of about 10 in. Slushing involved filling the cells of the masonry units with mortar as the walls were laid without adding water to the mortar to increase its slump. The compressive strengths from mortar cubes were between 1076 and 1802 psi (7419 to 12 424 kPa). The souped mortar tested as grout at over 4500 psi (31 026 kPa) compressive strength. The grout compressive strengths were unrealistically high at over 11 000 psi (75 842 kPa).

Specimens were tested in pullout; some were tested in direct tension and others were tested to evaluate lap splices. Pull-out test results for the slushed mortar samples were similar to those for the souped mortar. The grouted specimen tests resulted in the highest pull-out results. However, the ratio of the compressive strength of the grout to the souped mortar was approximately 2.44, whereas the ratio of the pull-out strengths was 1.45. These authors’ interpretation of these results is that the mortars performed very well in comparison to the grout if higher compressive strengths are assumed to translate into proportionately higher pull-out capacities.

Biggs [12] reports on his most recent research on using ASTM C 270 volume proportion Type S and Type N mortars as grouts in reinforced masonry. The research came out of a need to validate the practice of several major masonry contractors in New York who commonly used mortar as grout in low-lift grout applications. The details of the source of the materials, all the methods used, the laboratories that completed the testing and other results of testing are reported in Biggs [12]. This paper will report the details of the mix designs, plastic properties, compressive strength, and pull-out test data of that research.

Materials and Grout Mix Designs

Several mixes were developed as shown in Table 1. Mix G is an ASTM C 476 grout. Mix Mod G is a grout

TABLE 2—Compressive strength of masonry.

Mix	Compressive strength, psi (kPa) from prism tests	Assumed f'_m , psi (kPa) (Compressive strength of masonry)
Mortar fill (N)	1433 (9880)	1433 (9880)
Mortar fill (S)	2547 (17 561)	2178 (15 017)
Pourable mortar (NSL)	1537 (10 597)	1537 (10 597)
Pourable mortar (SSL)	1800 (12 411)	1800 (12 411)
Grout (G)	4010 (27 648)	2178 (15 017)
Grout (Mod G)	2795 (19 271)	2178 (15 017)

created by adding lime to reduce the strength of Mix G to approximately 2500 psi. Mixes N and S are mortar mixes placed as mortar fill with no additional water. Mixes NSL and SSL are mortar mixes with sufficient water added to make them pourable. Proportions are provided for the bedding mortar that was the basis for Mix S.

Grout prisms (for Mixes G and Mod G) were made in accordance with ASTM C 1019 to determine compressive strength except that they were not sealed in a plastic bag. The curing temperature was approximately 70°F (21°C) with a relative humidity of approximately 55%. Prisms were kept moist with damp paper towels until block molds were removed. They were then hand-delivered to a testing laboratory and cured in a water tank, consistent with ASTM C 1019.

Three samples of each mix were tested at 7, 14, 28, and 90 days. Both mixes, G and Mod G, easily surpassed the minimum 2000 psi (13 790 kPa) compressive strength recommended in the Masonry Standards Joint Committee (MSJC).

Mortar fill prisms for Mixes N and S) and pourable mortar prisms for Mixes NSL and SSL, were also made in accordance with ASTM C 1019 except they were not sealed in a plastic bag. ASTM C 1019 was intended for grout and is not the traditional method for testing mortars. The temperature was approximately 70°F (21°C) with a relative humidity of approximately 55%. Prisms were kept moist with damp paper towels until the block molds were removed.

Three samples of each mix were tested at 7, 14, 28, and 90 days. Mix S met the MSJC minimum compressive strength of 2000 psi (13 790 kPa); Mix N, Mix NSL, and Mix SSL did not. None of the mixes met the minimum slump requirements of ASTM C 476.

The normal-weight concrete masonry units that were used were fabricated in accordance with ASTM C 90. Manufacturer's data indicates that the unit compressive strength is approximately 3138 psi (21 636 kPa) based upon testing in accordance with ASTM C 140 Standard Methods of Sampling and Testing Concrete Masonry Units. Some units had an integral water repellent to reduce the absorption of the units. Unlike clay masonry, there is no ASTM test for rate of absorption in CMUs.

Twenty-four-inch (0.61 m) lengths of No. 5 reinforcement meeting ASTM A 996 Standard Specification for Rail-Steel and Axle-Steel Deformed Bars for Concrete Reinforcement were used for the pull-out tests. The specified yield strength was 60 000 psi (413.7 mPa), and the specified tensile strength was 90 000 psi 620.5 mPa. Tested values were slightly higher for each. The specified yield capacity was 18.6 kips (82.7 kN), and the specified tensile capacity was 27.9 kips (124.1 kN).

Compressive Strength of Masonry

Using the Unit Strength Method, Section 1.4B.2.b, Table 2 of the 2002 Specifications for Masonry Structures (ACI530.1/ASCE 6-5/TMS 602-05) [15], the compressive strength of the masonry was determined based upon Type S mortar in combination with the CMU strength of 3138 psi (21 636 kPa). This gives a calculated compressive strength of the masonry equal to 2178 psi (15 017 kPa). While the grout strength is not included in the development of this value, the MSJC specification requires that the grout meets either ASTM C 476 or the grout compressive strength equals or exceeds f'_m but not less than 2000 psi (13 790 kPa).

For the study, the compressive strength of the masonry (f'_m) was taken conservatively as 2178 psi (15 017 kPa) or the mortar fill strength, whichever was less, as shown in Table 2.

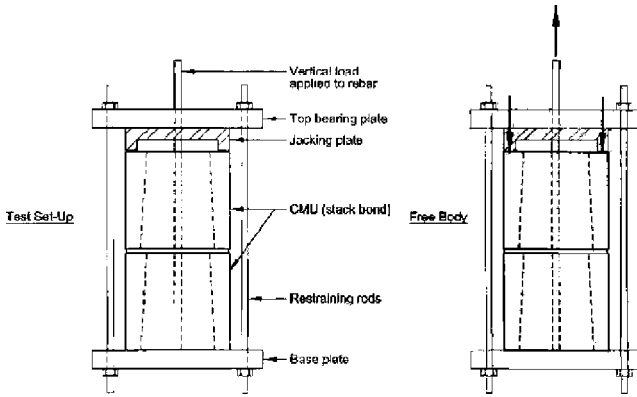


FIG. 2—Testing setup and free-body diagram. CMUs are 8 in. (203 mm) in height and 4 in. (101 mm) wide.

Pull-out Tests

Small-scale tests were developed to compare the performance of mortar fill to grout when prism-type samples containing a reinforcing bar are exposed to pull-out of the reinforcement after the method of Richart [16]. The tests were intended to force a failure in the mortar fill and the grout under pull-out. From these tests, it would be possible to compare the performance of the mortar fill and pourable mortar with the grout. The testing determined the performance of the mortar fill based on its

- capacity to develop tension in the reinforcement
- capacity to develop tension in the reinforcement relative to code requirements
- capacity to develop tension in the reinforcement relative to the grout

Specimens were tested in a tensile testing machine as shown in Fig. 2.

Figure 3 shows the results of the pull-out tests in kips that it took to cause pull-out failure. The plot has a horizontal line that is the calculated ultimate load using Allowable Stress methods for the No. 5 (M16) bar embedded 15.6 in. in 2000 psi (13 790 kPa) grout. The value was determined by using a development

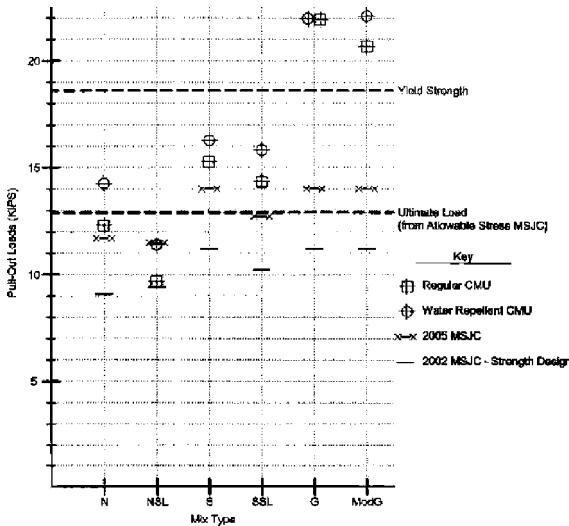


FIG. 3—Pull-out test results plotted against values expected in the 2002, 2005 MSJC.

length of 22.5 in. and factoring it by 2.5 to give an ultimate value. Since allowable stress design is based upon $0.4f_y$ for the reinforcement, this ultimate load effectively produces a bar stress equal to the yield stress ($0.4f_y \times 2.5 = f_y$). The load is calculated by 0.31 in.^2 (No. 5 bar) \times 60 ksi (yield stress) \times 15.6/22.5 (reduction factor based upon the embedded length) = 12.9 kips.

The 2002 MSJC Strength Design method and the 2005 MSJC yielded different results for pull-out capacity, which are also plotted. Strength design for both the 2002 MSJC and 2005 MSJC is based upon developing $1.25f_y$ for the reinforcement.

The 2002 capacity is based upon the development length from 2002 MSJC Eq 3-15: $I_d = 0.13d_b^2 f_y \gamma / \phi K \sqrt{f'_m}$. Using the actual embedded length of 15.6 in. for l_d , $d_b = 0.625$ in., $\gamma = 1.0$, $K = 3.13$ in., and f'_m , a reduced steel stress was determined (f_s) in place of f_y . From this, the pull-out capacity was calculated as A_b (area of the No. 5 bar) \times f_s .

The 2005 capacity is based upon 2005 MSJC Eq. 3-15: $I_d = 0.13d_b^2 f_y \gamma / K \sqrt{f'_m}$. The formulas are essentially the same except that the capacity reduction factor, $\phi = 0.80$, in the 2002 edition was eliminated in 2005. Effectively the pull-out capacities increased by $1/0.80 = 1.25$ from 2002 to 2005.

Finally for reference, the yield strength of the reinforcement is provided.

Mortar fill mix S and grout mixes G and Mod G all exceeded the 2000 psi (13 790 kPa) minimum strength required by MSJC, and the pull-out test results exceeded the required strengths by all three design procedures. Mixes G and Mod G actually exceeded the ultimate strength of the reinforcement. This was much stronger than required by the strength design methods.

Pourable mortar mix SSL did not meet the 2000 psi (13 790 kPa) minimum strength required by MSJC, but the pull-out test results exceeded the required strengths by all three design procedures.

Mortar fill mix N and pourable mortar mix NSL did not meet the 2000 psi (13 790 kPa) minimum strength required by MSJC, and the pull-out test results generally did not meet the required strengths by all three design procedures.

Pull-out load values from testing increased with lower absorption CMUs.

Conclusions

It has been shown that mortar mixes and pourable mortar mixes were used as grout in reinforced masonry for decades and are still allowed in residential applications. This is not a new concept.

It appears that after the 1955–1960 testing on high-lift specimens, the trend was to use grout with an 8 to 11-in. (203 to 279 mm) slump. There is no documentation that the mortar mixes were unacceptable, only that the grout mix gave greater flowability for high-lift grouting. Somehow this has continued until today for commercial construction.

Residential construction (2000 IRC) still allows Type M and Type S mortar as grout for reinforced masonry that is traditionally constructed using low-lift grouting techniques.

The research indicates that while grout (mixes G and Mod G) provides the highest strength results, Type S and Type M mortar fill and pourable fill provide acceptable strength. Therefore, the use of Type S mortar fill made from portland cement and lime is justified for reinforced masonry constructed with low-lift techniques provided certain criteria are met. Conservatively, the criteria include:

- The construction should be limited to concrete masonry construction until further testing is completed on clay masonry units.
- The grout mix (mortar fill or pourable mortar) should achieve a compressive strength of at least 2000 psi (13 790 kPa) or f'_m , whichever is greater, when tested in accordance with ASTM C 1019.
- These mixes should be only be used in a modified low-lift grouting application where pour heights do not exceed 4 f and lift heights do not exceed 12 in. (0.30 m).
- All lifts should be rodded or tamped in place; mechanical vibration is not required.
- Grouting is subject to continuous special inspection.

Recommendations

- ASTM C 476 should be revised to include a discussion on grouting techniques. The selection of a grout type should be dependent upon the type of masonry (CM or clay masonry), the size of the clear cavity or cell to be grouted and the type of grout.

2. Grout types should be expanded to include mortar fill and pourable mortar using Type S and Type M mortars. This could be accomplished by creating two types of fine grout; coarse grout would remain unchanged. Type F-1 Fine Grout would be the current fine grout. Type F-2 Fine Grout would be proportioned as 1 part portland cement, $\frac{1}{4}$ to $\frac{1}{2}$ -part hydrated lime or lime putty, and 2 $\frac{1}{4}$ to 3 parts fine aggregates.
3. Type F-2 grout shall be mixed with a water content that provides a workable plastic consistency to a pourable consistency and ensures proper placement, without segregation. The water content must provide a minimum grout strength of 2000 psi (13 790 kPa) or f'_m , which is greater.
4. A section on grouting techniques should be added:
 - (a) Type F-1 Fine Grout is suitable for either low-lift or high-lift grouting methods consistent with current industry standards.
 - (b) Type F-2 Fine Grout is suitable for low-lift grouting with the following limitations:
 - i. This only applies to CM construction since testing has not been completed on clay masonry.
 - ii. Maximum pour height is 48 in. (1.22 m).
 - iii. Maximum lift height is 12 in. (305 mm).
 - iv. Each lift shall be rodded or tamped; no mechanical vibration is required.
 - (c) Coarse Grout is suitable for either low-lift or high-lift grouting methods consistent with current industry standards.
 - (d) Continuous special inspection is required.

Acknowledgments

Major funding for this research was provided by the International Masonry Institute, National Lime Association, and Bricklayers and Allied Craftworkers, Local No. 1, New York, New York, and the National Concrete Masonry Association.

References

- [1] Harrington, R. W., "Construction of Quality Control of High Lift Grouted Reinforced Masonry," *Proceedings of the North American Masonry Conference*, The Masonry Society, J. L. Noland and J. E. Amrhein, Eds., Boulder Colorado, 1978, 61 pp.
- [2] ANSI A41.2-1960, "American National Standard Building Code Requirements for Reinforced Masonry," American National Standards Institute, Inc. New York, New York, 10018.
- [3] Uniform Building Code, International Code Council, Falls Church, VA.
- [4] International Residential Code, International Code Council, Falls Church, VA.
- [5] Person, O. F., "How the High Lift Grout System was Developed," 1978.
- [6] Amrhein, J. E., "Grout—The Third Ingredient," *Masonry Industry Magazine*, Vol. 19, 1980, pp. 19–22.
- [7] Chrysler, J., *Reinforced Concrete Masonry Construction Inspector's Handbook*, 4th edition, Masonry Institute of America, Torrance, CA, 2002, 537 pp.
- [8] Amrhein, J. E., *Reinforced Masonry Engineering Handbook Clay and Concrete Masonry*, Fifth Edition, Masonry Institute of America, Los Angeles, CA, 1992, 468 pp.
- [9] Isberner, A. W. Jr., "Grout for Reinforced Masonry," *Masonry: Materials, Properties and Performance, ASTM STP 778*, J. G. Borchelt, Ed., ASTM International, West Conshohocken, PA, 1980, pp. 38–56.
- [10] Randall, F. A. and Panarese, W. C., *Concrete Masonry Handbook for Architects, Engineers, Builders*, Portland Cement Association, Skokie, IL, 1976, 211 pp.
- [11] Masonry Standards Joint Committee, "Building Code Requirements for Masonry Structures," The Masonry Society, Boulder, CO, 2005.
- [12] Biggs, D. T., "Grouting Masonry Using Portland Cement-Lime Mortars," *International Building Lime Symposium*, National Lime Association, R. Jaffe, Ed., Arlington, VA, 2005, (CD). 15 pp.

- [13] Hedstrom, E. G., and Thomas, R. A., *Reinforcement Bond Strengths in Portland Cement-Lime Mortars, Masonry Cement Mortars, and Fine Grout*, NCMA Research and Development Laboratory.
- [14] Brown, *Feasibility of Using Mortar in Lieu of Grout for Reinforced Hollow Clay Wall Construction*, Russell Brown, Clemson University, 1998. Unpublished, but cited with permission of the Wall Committee of the National Brick Research Center, 1998.
- [15] Masonry Standards Joint Committee (MSJC), "Building Code Requirements for Masonry Structures," The Masonry Society, Boulder, CO, 2002.
- [16] Richart, F. E., "Bond Test Between Steel and Mortar in Reinforced Brick Masonry," *Structural Clay Products*, Vol. 32, 1949, pp. 271.

John P. Sanders¹ and Denis A. Brosnan¹

The Effect of Void Area on Brick Masonry Performance

ABSTRACT: Higher void (hollow) brick offer the potential for energy savings, decreased raw material usage and reduced environmental impact. These advantages are related to the movement toward “green” building materials. The National Brick Research Center has performed an extensive study comparing the wall system performance of hollow and solid brick. Hollow masonry units are defined by ASTM C 652 while solid masonry units are specified in ASTM C 216. The key differences between these two specifications are related to the permissible void area and face shell thickness. The objective of this work was to determine what effect, if any, increasing void area might have on important aspects of the performance of brick masonry. The effect of decreasing face shell thickness was also evaluated. For this study, the performance of several sets of comparison extruded brick was measured. These sets of comparison brick represent a range of manufacturers and, thus, a range of physical properties. Water penetration, flexural bond strength, and compressive strength were measured on each type of brick and used as indicators of potential performance in a wall. Additionally, mortar usage as a function of void area was studied. Based on the results of testing from these sets of comparison brick, increasing void area or decreasing face shell thickness did not result in increased water penetration or decreased flexural bond strength.

KEYWORDS: brick, brick masonry, wall system performance, ASTM C 216, ASTM C 652, void area, face shell, water penetration, flexural bond strength

Introduction

This study was undertaken to determine if increasing void area or decreasing face shell thickness had an effect on the performance of brick masonry. ASTM C 216 [1], Standard Specification for Facing Brick (Solid Masonry Units Made from Clay or Shale), specifies a maximum void area of 25 % and a minimum face shell thickness of 0.75 in. (19 mm), while ASTM C 652 [2], Standard Specification for Hollow Brick (Hollow Masonry Units Made from Clay or Shale), allows for higher levels of void area with a minimum face shell thickness of 0.625 in. (16 mm).

Four comparison sets will be discussed in this paper. For each comparison set, bricks were produced with a range of void area and face shell thicknesses. Each set of comparison brick was produced from the same raw materials and the same process in an effort to isolate the effect of face shell thickness and void area on performance in the wall. Water penetration, flexural bond strength and compressive strength were

TABLE 1—Description of test brick.

Designation	Description	Size	Void Area Range, %	Face Shell Range, in. (mm)
Comparison 1	Alluvial Clay Body	Modular	26.0–35.4	0.81–0.97 (21–25)
Comparison 2	Shale Body	Modular	25.3–31.5	0.75–0.76 (19)
Comparison 3	Clay Body	Modular	23.9–31.5	0.55–0.75 (14–19)
Comparison 4	Shale Body	Modular	21.7–34.2	0.56–0.75 (14–19)

Manuscript received April 10, 2006; accepted for publication December 11, 2006; published online January 2007. Presented at ASTM Symposium on Masonry on 13 June 2006 in Toronto, Canada; B. Trimble and J. Brisch, Guest Editors.

¹Research Associate/Assistant Professor and Professor and Director, respectively, The National Brick Research Center, Clemson University, 100 Clemson Research Blvd, Anderson, SC 29625.

measured on each type of brick and used as indicators of potential performance in a masonry system. A list of the test brick used in this study is given in Table 1.

The resistance to water penetration of masonry test panels was measured using ASTM E 514-04 Standard Test Method for Water Penetration and Leakage through Masonry laboratory procedure [3]. Flexural bond strength was measured using ASTM C 1072-00 Standard Test Method for the Measurement of Masonry Flexural Bond Strength [4]. Compressive strength measurements were determined by the procedure described in ASTM C 67-03 Standard Test Methods for Sampling and Testing Brick and Structural Clay Tile [5].

The performance of a masonry system is a function of several factors which includes the brick and mortar, brick and mortar interactions, and workmanship [6–9]. Grimm, in his definitive review of water penetration studies, stated, “Workmanship affects water permeance of masonry more than any other factor” [7]. Grimm also states that leakage is most likely to take place at the brick and mortar interface [7].

As stated, the objective of this work was to study how changes in the void area and face shell thickness of the brick impact the performance of a wall system. Since workmanship plays such an important role in masonry construction, construction variables were controlled as much as possible. Type N masonry mortar was used for all experiments. The effect of mortar type and brick and mortar interactions on flexural bond strength and water penetration, which are beyond the scope of this study, have been reported by Borchelt et al. [10] and Borchelt and Tann [11]. The void area and face shell thickness of each type of brick was determined by the configuration of the core tips used in extrusion. Other than the core configuration, all other production variables were held constant for each set of comparison brick in an effort to isolate the effect of void area and face shell thickness.

Test Methods

The physical properties of the brick, including compressive strength, were measured using the methods described in ASTM C 67 [5]. For each type of brick, 15 brick were randomly selected for testing during construction of the E 514 test panels. Physical dimensions, unit weight, face shell thickness, void area, initial rate of absorption, cold water absorption, boiling water absorption, and compressive strength were measured for each type of brick. The absorption and strength properties were measured to determine how similar the individual types of brick within each comparison set were in an effort to clarify the effect of void area and face shell thickness on masonry performance. Digital calipers were used in face shell measurements as a modification of the prescribed procedure in ASTM C 67 [5]. Extraneous material was removed from the core holes prior to these measurements.

For the ASTM E 514 measurements, three test panels were built for each type of brick. Type N masonry cement was used to construct all of the panels. The test panels were constructed using standard masonry practices by a skilled mason. Full mortar bedding and full head joints were specified for the E 514 test panels. Concave, tooled joints were used for all test panels. The water content of the mortar was adjusted to the mason’s preference. Brick with initial rates of absorption (IRA) values greater than 30 g/min/30 in.² (1.55 kg/min/m²) were pre-wet by the mason prior to laying as recommended in Note 5 of ASTM C 216-04 and Note 2 of ASTM C 652-04 [1,2]. A number of papers have been published which discuss the relationship between IRA and wall system performance [7,10,11]. The goal of this project was not to test construction practices or brick and mortar interactions, but to compare the performance of brick with varying face shell thicknesses and void areas using equivalent masonry practices.

The test panels were wrapped after construction, and after seven days the wrapping was removed. The walls were allowed to cure for seven more days before testing commenced. Essentially, the walls were tested after curing for at least 14 days. The test panels were tested in the order of construction. When constructed with modular brick, each test panel consisted of approximately 195 brick.

Prior to the water penetration test, a chamber was attached to the face of each panel. This test chamber covered an area of approximately 12 ft² (1.1 m²) of the masonry panel. The areas not covered by the test panel were sealed with a cement-based coating for waterproofing masonry to prevent water leakage on the untested face of the wall. Finally, a trough was attached to the bottom of the backside of the wall to collect water that penetrated through the masonry during the test. Section 7.3 of the E 514-04 test procedure states, “... attach to, or build flashing into masonry forming a trough to collect water that may pass through to the back side of the wall.”



FIG. 1—*E 514-04 test chamber.*

Water and air pressure were applied to the face of the test panel covered by the test chamber. An air pressure of two inches of water (5 cm of H₂O) and a flow rate of 40 gallons per hour (151 litres per hour) were applied to each wall. Each panel was tested for four hours as prescribed in ASTM E 514-04 [3]. A picture of the E 514 test chamber attached to a panel is given in Fig. 1. The trough used to collect water that penetrated through the test panels is shown in Fig. 2. An average water penetration rate (grams per hour) was calculated for each type of brick. While the average water penetration rate is a measured value, ASTM E 514-04 also specifies several subjective measurements which include: the time to the first appearance of dampness, the time to the first visible moisture, and the area of dampness on back of the test panel. The time to the first appearance of dampness and the area of dampness on the back of the test panel have been reported. The time to first moisture was not reported as no water was collected on some of the test panels.

The flexural bond strength of masonry prisms was measured according to ASTM C 1072-00. Five prisms were constructed for each type of test brick using Type N masonry cement. The test prisms were built by a skilled mason with 3/8 in. struck joints. The prisms were constructed using a line to achieve the proper mortar joint thickness. Each prism contained five joints for testing. A total of 25 measurements were made on each type of brick. The masonry prisms were aged for 28 days prior to testing. McGinly and Greenwald have reported on various aspects of flexural bond strength with hollow units [12].



FIG. 2—*Collection trough on back side of the test panel.*

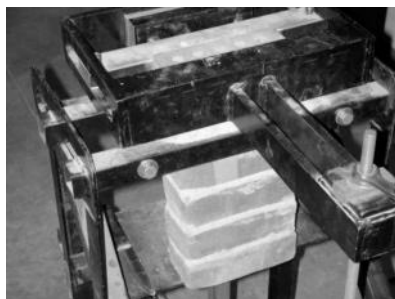


FIG. 3—C 1072-00 flexural bond strength measurement.

To determine the flexural bond strength, the masonry prisms were loaded in the testing jig shown in Fig. 3. An eccentric load was uniformly applied to the top brick of the prism, and the peak load at failure was recorded. After a joint had been tested, the prism was raised so that the next joint could be tested.

Finally, the physical property data such as void area, face shell thickness, IRA, water absorptions, and compressive strength are the result of 15 measurements for each type of brick. The water penetration data are the average of the measurements taken from three test panels while the flexural bond strength data were derived from measurements taken of five prisms which each had five joints for a total of 25 measurements.

All of the performance data are reported as a function of void area and face shell thickness. In most cases, void area and face shell thickness did not vary independently. In other words, most of the brick in this study with higher void areas typically had thinner face shell thicknesses. It is important to note that higher void area brick do not necessarily have thinner face shells. The brick size and coring configuration has also been reported for each type of brick. The amount of scatter in the performance data are indicated by the standard deviation in the data tables.

Results

Comparison 1

Three sets of modular brick made from an alluvial clay were studied in Comparison 1. These test brick were all three-hole brick made from an alluvial clay. The core holes were round with square sides for these brick. Void areas of 26.0, 32.3, and 35.4 % with face shells of 0.97, 0.81 and 0.81 in. (25, 21, and 21 mm), respectively, were tested. By increasing the void area from 26.0 to 35.4 %, the unit weight of the brick was reduced by approximately 14 %. A summary of the physical dimensions of the test brick is reported in Table 2, and physical properties of all three sets of brick in this comparison set are given in Table 3. IRA and water absorption levels were similar for all three types of brick in this comparison.

A summary of performance data for this set of comparison is given in Table 4. No significant change in water penetration was observed with increasing void area. A very small volume of water was collected for the 26.0 % void brick, but only a trace of water was collected for the 32.3 and 35.4 % void brick. The 26.0 % void brick had the lowest time to the first appearance of dampness and a larger wet area behind the test panel. The test panels constructed with equivalent mortar and masonry practice showed that decreasing the face shell from 0.97 to 0.81 in. (25 to 21 mm) did not increase the water penetration rate.

There does appear to be a slight trend of increasing flexural bond strength with increasing void area, but due to the scatter in the data, as reflected in the standard deviation, this trend is not significant. No change in compressive strength was observed as the void area was increased from 26.0 to 32.3 %, but a slight decrease was observed as the void area was increased to 35.4 %. Again, due to the overlap in the data, this trend may not be significant. No trend in compressive strength was observed due to decreasing face shell thickness.

The Comparison 1 test brick had a range of void area from 26.0 to 35.0 %, but no significant water penetration was observed for any of the brick. Reducing the face shell from 0.97 to 0.81 in. (25 to 21 mm)

TABLE 2—Physical dimensions—Comparison 1.

Size		Modular	Modular	Modular
Coring		3 Hole	3 Hole	3 Hole
		Round w/Square Sides	Round w/Square Sides	Round w/Square Sides
Void Area	Average of 15 (%)	26.0	32.3	35.4
	Standard Deviation (%)	0.7	0.5	0.4
	Coefficient of Variation (%)	2.7	1.5	1.2
Face Shell Thickness	Average of 15, in. (mm)	0.97 (25)	0.81 (21)	0.81 (21)
	Standard Deviation in. (mm)	0.04 (1.1)	0.04 (1.0)	0.04 (0.9)
	Coefficient of Variation (%)	4.6	4.9	4.5
Minimum Web Thickness	Average of 15, in. (mm)	0.71 (18)	0.55 (14)	0.56 (14)
	Standard Deviation in. (mm)	0.05 (1.4)	0.02 (0.5)	0.03 (0.7)
	Coefficient of Variation (%)	7.7	3.9	4.8
End Shell Thickness	Average of 15, in. (mm)	1.08 (28)	1.03 (26)	0.94 (24)
	Standard Deviation in. (mm)	0.04 (1.1)	0.03 (0.6)	0.02 (0.5)
	Coefficient of Variation (%)	4.0	2.5	2.1
Unit Weight	Average of 15, g	1572.1	1429.5	1348.1
	Standard Deviation, g	15.8	6.7	7.4
	Coefficient of Variation (%)	1.0	0.5	0.5
Bed Depth (Width)	Average of 15, in. (mm)	3.55 (90)	3.55 (90)	3.55 (90)
	Standard Deviation in. (mm)	0.02 (0.6)	0.01 (0.3)	0.01 (0.3)
	Coefficient of Variation (%)	0.7	0.3	0.3
Height	Average of 15, in. (mm)	2.25 (57)	2.23 (57)	2.26 (57)
	Standard Deviation in. (mm)	0.01 (0.2)	0.01 (0.32)	0.02 (0.5)
	Coefficient of Variation (%)	0.4	0.6	0.8
Length	Average of 15, in. (mm)	7.76 (197)	7.67 (195)	7.68 (195)
	Standard Deviation in. (mm)	0.03 (0.8)	0.03 (0.8)	0.02 (0.45)
	Coefficient of Variation (%)	0.4	0.4	0.2

TABLE 3—Physical properties—Comparison 1.

Size		Modular	Modular	Modular
Coring		3 Hole	3 Hole	3 Hole
		Round w/Square Sides	Round w/Square Sides	Round w/Square Sides
Void Area	Average of 15 (%)	26.0	32.3	35.4
	Standard Deviation (%)	0.7	0.5	0.4
	Coefficient of Variation (%)	2.7	1.5	1.2
Face Shell Thickness	Average of 15, in. (mm)	0.97 (25)	0.81 (21)	0.81 (21)
	Standard Deviation in. (mm)	0.04 (1.1)	0.04 (1.0)	0.04 (0.9)
	Coefficient of Variation (%)	4.6	4.9	4.5
Initial Rate of Absorption	Average of 15, g/min/30 in ² (kg/min/m ²)	17.0 (0.88)	14.5 (0.75)	16.7 (0.86)
	Standard Deviation, g/min/30 in ² (kg/min/m ²)	2.1 (0.11)	1.8 (0.09)	1.4 (0.07)
	Coefficient of Variation (%)	12.5	12.5	8.1
Cold Water Absorption	Average of 15 (%)	6.4	5.8	6.0
	Standard Deviation (%)	0.4	0.4	0.4
	Coefficient of Variation (%)	7.0	6.2	6.6
Boiling Water Absorption	Average of 15 (%)	9.1	8.4	8.7
	Standard Deviation (%)	0.6	0.7	0.4
	Coefficient of Variation (%)	6.2	8.3	4.3
C/B	Average of 15 (%)	0.70	0.69	0.68
	Standard Deviation (%)	0.01	0.00	0.02
	Coefficient of Variation (%)	1.7	0.2	2.5

TABLE 4—Performance data—Comparison 1.

Size		Modular	Modular	Modular
Coring		3 Hole	3 Hole	3 Hole
		Round w/Square	Round w/Square	Round w/Square
		Size	Size	Size
Void Area	Average of 15 (%)	26.0	32.3	35.4
	Standard Deviation (%)	0.7	0.5	0.4
	Coefficient of Variation (%)	2.7	1.5	1.2
Face Shell Thickness	Average of 15, in. (mm)	0.97 (25)	0.81 (21)	0.81 (21)
	Standard Deviation in. (mm)	0.04 (1.1)	0.04 (1.0)	0.04 (0.9)
	Coefficient of Variation (%)	4.6	4.9	4.5
Water Penetration	Average of 3, gal/h (l/h)	0.10 (0.39)	0.00 (0.00)	0.00 (0.00)
	Standard Deviation, gal/h (l/h)	0.17 (0.64)	0.00 (0.01)	0.00 (0.00)
	Coefficient of Variation (%)			
Time to Appearance of Dampness	Average of 3, min	15	42	19
	Standard Deviation, min	13	15	23
	Coefficient of Variation (%)	82.6	36.7	120.4
Damp Area after 4 h (Back of Test Panel)	Average of 3, %	47	13	27
	Standard Deviation, %	45	12	10
	Coefficient of Variation (%)	94.8	94.8	39.0
Flexural Bond Strength	Average of 25, psi (kPa)	104 (715)	109 (750)	119 (822)
	Standard Deviation, psi (kPa)	38 (260)	24 (165)	25 (170)
	Coefficient of Variation (%)	36.3	21.9	20.6
Compressive Strength	Average of 15, psi (MPa)	10183 (70)	10172 (70)	8024 (55)
	Standard Deviation, psi (MPa)	1773 (12)	1312 (9)	1908 (13)
	Coefficient of Variation (%)	17.4	12.9	23.8

did not increase water penetration. Likewise, there was no negative effect on flexural bond strength from increasing void area and decreasing face shell thickness. A slight decrease in compressive strength was observed at the highest void area, but due to the scatter in the data, this may not have been a significant effect.

Comparison 2

Comparison 2 consisted of three sets of modular all-shale brick. The void areas of these brick were 25.3, 27.7, and 31.5 % with face shell thickness of 0.76, 0.76, and 0.75 in. (19 mm), respectively. Increasing the void area from 25.3 to 31.5 % resulted in roughly 6 % reduction in the unit weight. The coring configuration, as noted in Table 5, was not consistent between the sets of brick in this comparison which added an extra factor into the consideration of performance test results. These brick in this comparison group also had a very narrow range of face shell thicknesses. A summary of the physical dimensions of the test brick is reported in Table 5, and the physical properties or the test brick for this comparison set are reported in Table 6. There was a general decrease in water absorption levels with increasing void area. In addition to changes to the coring configuration, differences in water absorption levels should be considered when comparing performance data.

A comparison of performance data for this comparison set of test brick is listed in Table 7. The 27.7 % void area test brick had the longest time to the appearance of dampness and had the lowest area of dampness on the back of the test panel. The time to the appearance of dampness and the area of dampness were very similar between the 25.3 and 31.5 % void area brick. Despite a large amount of scatter in the data, it does appear that the 31.5 % void had a higher leakage rate than either the 25.3 or 27.7 % brick. It is important to note that 25.3 and 27.7 % void area brick had nearly identical leakage rates. It is difficult to determine if the apparent increase in leakage rate was due to increased void, coring configuration, decreased water absorption, or possibly an interaction of all of these factors.

While there was significant overlap in the flexural bond strength data reported in Table 7, it does appear that the 28 % void brick had higher flexural bond strength than either the 25.3 or 31.5 % void brick. It is possible that coring configuration, which varied between the sets of test brick, could also have an

TABLE 5—Physical dimensions—Comparison 2.

Size		Modular	Modular	Modular
Coring		3 Hole	3 Hole	3 Hole
		Round w/ Square Sides	Round w/ Square Sides	Round w/ Square Sides
Void Area	Average of 15 (%)	25.3	27.7	31.5
	Standard Deviation (%)	0.5	0.5	0.7
	Coefficient of Variation (%)	2.0	1.6	2.2
Face Shell Thickness	Average of 15, in. (mm)	0.76 (19)	0.76 (19)	0.75 (19)
	Standard Deviation in. (mm)	0.01 (0.3)	0.02 (0.4)	0.02 (0.4)
	Coefficient of Variation (%)	1.7	2.0	2.1
Minimum Web Thickness	Average of 15, in. (mm)	0.30 (8)	0.39 (10)	0.51 (13)
	Standard Deviation in. (mm)	0.03 (0.8)	0.07 (1.7)	0.02 (0.5)
	Coefficient of Variation (%)	10.2	17.3	3.5
End Shell Thickness	Average of 15, in. (mm)	0.85 (22)	0.98 (25)	0.92 (23)
	Standard Deviation in. (mm)	0.04 (0.9)	0.05 (1.2)	0.03 (0.9)
	Coefficient of Variation (%)	4.1	4.7	3.7
Unit Weight	Average of 15, g	1626.5	1624.2	1531.4
	Standard Deviation, g	7.6	16.1	9.4
	Coefficient of Variation (%)	0.5	1.0	0.6
Bed Depth (Width)	Average of 15, in. (mm)	3.49 (89)	3.49 (89)	3.48 (88)
	Standard Deviation in. (mm)	0.02 (0.6)	0.03 (0.7)	0.03 (0.8)
	Coefficient of Variation (%)	0.7	0.8	0.9
Height	Average of 15, in. (mm)	2.28 (58)	2.26 (57)	2.27 (58)
	Standard Deviation in. (mm)	0.02 (0.5)	0.02 (0.46)	0.02 (0.6)
	Coefficient of Variation (%)	0.9	0.8	1.0
Length	Average of 15, in. (mm)	7.53 (191)	7.57 (192)	7.59 (193)
	Standard Deviation in. (mm)	0.03 (0.8)	0.02 (0.4)	0.03 (0.74)
	Coefficient of Variation (%)	0.4	0.2	0.4

TABLE 6—Physical properties—Comparison 2.

Size		Modular	Modular	Modular
Coring		3 Hole	3 Hole	3 Hole
		Round w/ Square Sides	Round w/ Square Sides	Round w/ Square Sides
Void Area	Average of 15 (%)	25.3	27.7	31.5
	Standard Deviation (%)	0.5	0.5	0.7
	Coefficient of Variation (%)	2.0	1.6	2.2
Face Shell Thickness	Average of 15, in. (mm)	0.76 (19)	0.76 (19)	0.75 (19)
	Standard Deviation in. (mm)	0.01 (0.3)	0.02 (0.4)	0.02 (0.4)
	Coefficient of Variation (%)	1.7	2.0	2.1
Initial Rate of Absorption	Average of 15, g/min/30 in ² (kg/min/m ²)	29.3 (1.52)	19.4 (1.00)	22.1 (1.14)
	Standard Deviation, g/min/30 in ² (kg/min/m ²)	6.6 (0.34)	4.8 (0.25)	4.5 (0.23)
	Coefficient of Variation (%)	22.5	24.6	20.2
Cold Water Absorption	Average of 15 (%)	4.9	3.5	2.9
	Standard Deviation (%)	0.8	0.6	0.7
	Coefficient of Variation (%)	16.4	16.1	24.6
Boiling Water Absorption	Average of 15 (%)	6.2	5.6	5.1
	Standard Deviation (%)	1.1	0.6	1.0
	Coefficient of Variation (%)	17.4	11.1	19.5
C/B	Average of 15 (%)	0.80	0.63	0.56
	Standard Deviation (%)	0.03	0.01	0.04
	Coefficient of Variation (%)	4.3	1.6	7.2

TABLE 7—Performance data—Comparison 2.

Size		Modular	Modular	Modular
Coring		3 Hole	3 Hole	3 Hole
		Round w/ Square	Round w/ Square	Round w/ Square
		Sides	Sides	Sides
Void Area	Average of 15 (%)	25.3	27.7	31.5
	Standard Deviation (%)	0.5	0.5	0.7
	Coefficient of Variation (%)	2.0	1.6	2.2
Face Shell Thickness	Average of 15, in. (mm)	0.76 (19)	0.76 (19)	0.75 (19)
	Standard Deviation in. (mm)	0.01 (0.3)	0.02 (0.4)	0.02 (0.4)
	Coefficient of Variation (%)	1.7	2.0	2.1
Water Penetration	Average of 3, gal/h (l/h)	0.06 (0.23)	0.01 (0.04)	0.31 (1.17)
	Standard Deviation, gal/h (l/h)	0.05 (0.20)	0.02 (0.06)	0.26 (0.98)
	Coefficient of Variation (%)	89.0	163.6	83.9
Time to Appearance of Dampness	Average of 3, min	7	40	18
	Standard Deviation, min	7	28	10
	Coefficient of Variation (%)	92.8	70.7	56.8
Damp Area after 4 h (Back of Test Panel)	Average of 3, %	92	42	93
	Standard Deviation, %	6	33	12
	Coefficient of Variation (%)	6.3	79.9	12.4
Flexural Bond Strength	Average of 25, psi (kPa)	98 (673)	141 (970)	91 (628)
	Standard Deviation, psi (kPa)	27 (184)	38 (261)	30 (210)
	Coefficient of Variation (%)	27.4	26.9	33.5
Compressive Strength	Average of 15, psi (MPa)	8058 (56)	10391 (72)	10611 (73)
	Standard Deviation, psi (MPa)	2743 (19)	3353 (23)	2167 (15)
	Coefficient of Variation (%)	34.0	32.3	20.4

effect on flexural bond strength. This set of comparison test brick had a small range of face shell thicknesses. Further, the high degree of overlap in the compressive strength data, as reflected in the standard deviation, indicate that any trend related to increasing the void area are probably not significant. The observed differences in compressive strength appear to mirror the previously noted differences in water absorption.

This set of comparison brick had different coring configurations for each level of void area while the face shell thickness was nearly identical for all the test brick. A very small increase in the water penetration rate was observed with the 31.5 % void brick. It was not possible to determine if this minor increase was due to increased void area, decreased water absorption, coring configuration, or a combination of these properties. Flexural bond strength and compressive strength data did not reveal any negative trends related to the void area or face shell thickness.

Comparison 3

The third set of comparison brick were all three-hole modular clay brick. This set of brick also had a wide range in face shell thicknesses. These brick had void areas of 23.9, 28.5, and 31.5 % with face shell thicknesses of 0.75, 0.60, and 0.55 in. (19, 15, and 14 mm) respectively. A reduction of unit weight of approximately 7 % was realized by increasing the void area to 31.5 %. The physical dimensions for this set of comparison test brick are reported in Table 8 while the physical properties for this set of comparison brick is given in Table 9. There was a general trend of increasing water absorption and IRA with increasing void area for this set of comparison brick.

A summary of the performance data for this set of comparison brick is given in Table 10. This set of test brick, as a whole, had the highest level of water penetration of any of the sets of comparison brick tested. Interestingly, this set of comparison brick also had the highest flexural bond strengths. These effects are likely related to the unique pore structure of these brick which is a function of particle size of the raw material, and particle packing which is related to manufacturing variables such as extrusion pressure, and moisture for extrusion, to name a few. Most importantly, no trend in water penetration rates was found

TABLE 8—Physical dimensions—Comparison 3.

Size		Modular	Modular	Modular
Coring		3 Hole	3 Hole	3 Hole
		Round w/ Square Sides	Round w/ Square Sides	Round w/ Square Sides
Void Area	Average of 15 (%)	23.9	28.5	31.5
	Standard Deviation (%)	0.3	0.5	0.4
	Coefficient of Variation (%)	1.5	1.6	1.4
Face Shell Thickness	Average of 15, in. (mm)	0.75 (19)	0.60 (15)	0.55 (14)
	Standard Deviation in. (mm)	0.01 (0.3)	0.01 (0.2)	0.01 (0.3)
	Coefficient of Variation (%)	1.6	1.5	1.8
Minimum Web Thickness	Average of 15, in. (mm)	0.96 (24)	0.95 (24)	0.98 (25)
	Standard Deviation in. (mm)	0.04 (0.9)	0.03 (0.9)	0.03 (0.9)
	Coefficient of Variation (%)	3.7	3.7	3.6
End Shell Thickness	Average of 15, in. (mm)	0.79 (20)	0.81 (21)	0.81 (21)
	Standard Deviation in. (mm)	0.03 (0.8)	0.02 (0.6)	0.03 (0.8)
	Coefficient of Variation (%)	4.0	2.9	4.0
Unit Weight	Average of 15, g	1411.4	1335.0	1313.4
	Standard Deviation, g	7.3	9.7	10.9
	Coefficient of Variation (%)	0.5	0.7	0.8
Bed Depth (Width)	Average of 15, in. (mm)	3.37 (86)	3.43 (87)	3.45 (88)
	Standard Deviation in. (mm)	0.03 (0.7)	0.02 (0.5)	0.02 (0.6)
	Coefficient of Variation (%)	0.8	0.6	0.7
Height	Average of 15, in. (mm)	2.19 (56)	2.19 (56)	2.20 (56)
	Standard Deviation in. (mm)	0.01 (0.3)	0.01 (0.26)	0.01 (0.3)
	Coefficient of Variation (%)	0.6	0.5	0.5
Length	Average of 15, in. (mm)	7.38 (188)	7.42 (188)	7.50 (190)
	Standard Deviation in. (mm)	0.03 (0.7)	0.04 (1.1)	0.03 (0.75)
	Coefficient of Variation (%)	0.4	0.6	0.4

TABLE 9—Physical Properties—Comparison 3.

Size		Modular	Modular	Modular
Coring		3 Hole	3 Hole	3 Hole
		Round w/ Square Sides	Round w/ Square Sides	Round w/ Square Sides
Void Area	Average of 15 (%)	23.9	28.5	31.5
	Standard Deviation (%)	0.3	0.5	0.4
	Coefficient of Variation (%)	1.5	1.6	1.4
Face Shell Thickness	Average of 15, in. (mm)	0.75 (19)	0.60 (15)	0.55 (14)
	Standard Deviation in. (mm)	0.01 (0.3)	0.01 (0.2)	0.01 (0.3)
	Coefficient of Variation (%)	1.6	1.5	1.8
Initial Rate of Absorption	Average of 15, g/min/30 in. ² (kg/min/m ²)	27.9 (1.44)	32.1 (1.66)	35.7 (1.84)
	Standard Deviation, g/min/30 in. ² (kg/min/m ²)	2.2 (0.12)	4.0 (0.21)	2.9 (0.15)
	Coefficient of Variation (%)	8.0	12.4	8.2
Cold Water Absorption	Average of 15 (%)	7.7	8.1	8.3
	Standard Deviation (%)	0.4	0.6	0.3
	Coefficient of Variation (%)	4.7	7.1	3.6
Boiling Water Absorption	Average of 15 (%)	10.2	10.7	11.0
	Standard Deviation (%)	0.3	0.8	0.3
	Coefficient of Variation (%)	2.9	7.0	2.9
C/B	Average of 15 (%)	0.75	0.75	0.76
	Standard Deviation (%)	0.02	0.86	0.01
	Coefficient of Variation (%)	2.3	114.0	1.4

TABLE 10—Performance Data—Comparison 3.

Size		Modular	Modular	Modular
Coring		3 Hole	3 Hole	3 Hole
		Round w/ Square Sides	Round w/ Square Sides	Round w/ Square Sides
Void Area	Average of 15 (%)	23.9	28.5	31.5
	Standard Deviation (%)	0.3	0.5	0.4
	Coefficient of Variation (%)	1.5	1.6	1.4
Face Shell Thickness	Average of 15, in. (mm)	0.75 (19)	0.60 (15)	0.55 (14)
	Standard Deviation in. (mm)	0.01 (0.3)	0.01 (0.2)	0.01 (0.3)
	Coefficient of Variation (%)	1.6	1.5	1.8
Water Penetration	Average of 3, gal/h (L/h)	1.20 (4.54)	0.86 (3.26)	0.90 (3.41)
	Standard Deviation, gal/h (L/h)	0.32 (1.22)	0.80 (3.03)	0.63 (2.39)
	Coefficient of Variation (%)	26.9	93.1	70.2
Time to Appearance of Dampness	Average of 3, min	6	10	7
	Standard Deviation, min	8	13	5
	Coefficient of Variation (%)	136.7	124.4	63.0
Damp Area after 4 h (Back of Test Panel)	Average of 3, %	98	92	98
	Standard Deviation, %	3	3	3
	Coefficient of Variation (%)	2.9	3.1	2.9
Flexural Bond Strength	Average of 25, psi (kPa)	163 (1125)	153 (1058)	225 (1551)
	Standard Deviation, psi (kPa)	49 (339)	44 (305)	87 (597)
	Coefficient of Variation (%)	30.1	28.8	38.5
Compressive Strength	Average of 15, psi (MPa)	7649 (53)	6474 (45)	6867 (47)
	Standard Deviation, psi (MPa)	3044 (21)	1952 (13)	2184 (15)
	Coefficient of Variation (%)	39.8	30.1	31.8

with either increasing void area or decreasing face shell thickness. There was very little difference in the time to the first appearance of dampness and damp area on the back of the test panel for this set of comparison brick.

There appears to be an increase in flexural bond strength for the highest void area brick in this comparison. Due to the overlap in the data, as reflected in the standard deviation, it is not clear if this difference is actually significant. There was no apparent difference in the flexural bond strength between the 23.9 and 28.5 % void brick. Since increasing void area and decreasing face shell thickness are linked, there also appeared to be a slight increase in flexural bond strength at the 0.55 in. (14 mm) face shell thickness. The 23.9 void brick which also had the lowest water absorption had the highest compressive strength. There was very little difference in the compressive strength between the 28.5 and 31.5 % void brick which had similar water absorption values. There does not appear to be any trend in compressive strength related to increasing the void area or decreasing the face shell thickness.

This set of comparison brick had a wide range of face shell thicknesses in addition to a range in void area. While no trends were observed in the water penetration data with respect to void area or face shell thickness, these brick did display the highest rate of moisture penetration of any set of comparison brick tested for this report. Since neither void area nor face shell appeared to influence water penetration, it appears that these higher values are related to the unique pore structure of these brick which is related to raw material and manufacturing variables. These brick also had high flexural bond strengths, but no clear trend was observed with respect to void area or face shell thickness for the 23.9 and 28.5 % void area test brick. The 31.5 % test brick had significantly higher flexural bond strengths. Finally, increasing void and decreasing face shell thickness did not appear to have any significant effect on compressive strength.

Comparison 4

The fourth set of comparison brick were modular shale brick with a ten-hole coring configuration. The physical dimensions and physical properties of these test brick are reported in Table 11 and Table 12,

TABLE 11—Physical Dimensions—Comparison 4.

Size		Modular	Modular	Modular
Coring		3 Hole	3 Hole	3 Hole
		Round w/ Square Sides	Round w/ Square Sides	Round w/ Square Sides
Void Area	Average of 15 (%)	21.7	29.8	34.2
	Standard Deviation (%)	0.3	0.9	0.6
	Coefficient of Variation (%)	1.4	3.1	1.6
Face Shell Thickness	Average of 15, in. (mm)	0.75 (19)	0.69 (18)	0.56 (14)
	Standard Deviation in. (mm)	0.01 (0.2)	0.01 (0.3)	0.01 (0.2)
	Coefficient of Variation (%)	1.3	1.7	1.1
Minimum Web Thickness	Average of 15, in. (mm)	0.41 (10)	0.34 (9)	0.32 (8)
	Standard Deviation in. (mm)	0.06 (1.5)	0.05 (1.2)	0.03 (0.8)
	Coefficient of Variation (%)	14.5	13.7	10.1
End Shell Thickness	Average of 15, in. (mm)	0.75 (19)	0.76 (19)	0.59 (15)
	Standard Deviation in. (mm)	0.02 (0.5)	0.01 (0.3)	0.03 (0.9)
	Coefficient of Variation (%)	2.8	1.4	5.7
Unit Weight	Average of 15, g	1695.3	1461.3	1430.9
	Standard Deviation, g	7.7	7.0	8.9
	Coefficient of Variation (%)	0.5	0.5	0.6
Bed Depth (Width)	Average of 15, in. (mm)	3.43 (87)	3.39 (86)	3.46 (88)
	Standard Deviation in. (mm)	0.03 (0.8)	0.10 (2.6)	0.03 (0.7)
	Coefficient of Variation (%)	0.9	3.0	0.8
Height	Average of 15, in. (mm)	2.21 (56)	2.22 (56)	2.20 (56)
	Standard Deviation in. (mm)	0.02 (0.4)	0.02 (0.42)	0.02 (0.6)
	Coefficient of Variation (%)	0.7	0.7	1.0
Length	Average of 15, in. (mm)	7.55 (192)	7.57 (192)	7.50 (191)
	Standard Deviation in. (mm)	0.03 (0.8)	0.04 (1.0)	0.03 (0.85)
	Coefficient of Variation (%)	0.4	0.5	0.4

TABLE 12—Physical Properties—Comparison 4.

Size		Modular	Modular	Modular
Coring		3 Hole	3 Hole	3 Hole
		Round w/ Square Sides	Round w/ Square Sides	Round w/ Square Sides
Void Area	Average of 15 (%)	21.7	29.8	34.2
	Standard Deviation (%)	0.3	0.9	0.6
	Coefficient of Variation (%)	1.4	3.1	1.6
Face Shell Thickness	Average of 15, in. (mm)	0.75 (19)	0.69 (18)	0.56 (14)
	Standard Deviation in. (mm)	0.01 (0.2)	0.01 (0.3)	0.01 (0.2)
	Coefficient of Variation (%)	1.3	1.7	1.1
Initial Rate of Absorption	Average of 15, g/min/30 in. ² (kg/min/m ²)	7.3 (0.38)	11.6 (0.60)	8.3 (0.43)
	Standard Deviation, g/min/30 in. ² (kg/min/m ²)	1.0 (0.05)	2.0 (0.10)	0.9 (0.05)
	Coefficient of Variation (%)	14.3	17.2	11.1
Cold Water Absorption	Average of 15 (%)	2.1	4.1	2.4
	Standard Deviation (%)	0.5	0.6	0.2
	Coefficient of Variation (%)	22.0	14.8	8.2
Boiling Water Absorption	Average of 15 (%)	3.3	5.8	3.4
	Standard Deviation (%)	0.7	0.7	0.3
	Coefficient of Variation (%)	21.6	12.1	8.3
C/B	Average of 15 (%)	0.65	0.70	0.72
	Standard Deviation (%)	0.03	0.00	0.02
	Coefficient of Variation (%)	4.4	0.0	3.3

TABLE 13—Performance Data—Comparison 4.

Size		Modular		Modular		Modular	
Coring		3 Hole		3 Hole		3 Hole	
		Round w/ Square Sides		Round w/ Square Sides		Round w/ Square Sides	
Void Area	Average of 15 (%)	21.7		29.8		34.2	
	Standard Deviation (%)	0.3		0.9		0.6	
	Coefficient of Variation (%)	1.4		3.1		1.6	
Face Shell Thickness	Average of 15, in. (mm)	0.75	(19)	0.69	(18)	0.56	(14)
	Standard Deviation in. (mm)	0.01	(0.2)	0.01	(0.3)	0.01	(0.2)
	Coefficient of Variation (%)	1.3		1.7		1.1	
Water Penetration	Average of 3, gal/h (L/h)	0.00	0.00	0.00	0.00	0.00	0.00
	Standard Deviation, gal/h (L/h)	0.00	0.00	0.00	0.00	0.00	0.00
	Coefficient of Variation (%)						
Time to Appearance of Dampness	Average of 3, min	10		12		12	
	Standard Deviation, min	9		16		8	
	Coefficient of Variation (%)	86.6		131.0		65.5	
Damp Area after 4 h (Back of Test Panel)	Average of 3, %	13		25		8	
	Standard Deviation, %	13		22		3	
	Coefficient of Variation (%)	94.4		87.2		34.6	
Flexural Bond Strength	Average of 25, psi (kPa)	113	(780)	213	(1471)	223	(1536)
	Standard Deviation, psi (kPa)	37	(253)	79	(548)	45.8	(316)
	Coefficient of Variation (%)	32.4		37.2		20.5	
Compressive Strength	Average of 15, psi (MPa)	13359	(92)	9317	(64)	10436	(72)
	Standard Deviation, psi (MPa)	2819	(19)	2303	(16)	1418	(10)
	Coefficient of Variation (%)	21.1		24.7		13.6	

respectively. This set of comparison brick had void areas of 21.7, 29.8, and 34.2 % with face shell thicknesses of 0.75, 0.69, and 0.56 in. (19, 18, and 14 mm), respectively. The unit weight of the test bricks was decreased by approximately 16 % for the highest level of void area. The 21.7 and 34.2 % void area brick had nearly identical absorptions and IRAs while the 29.8 % void area brick had higher absorptions and IRAs.

The performance data for this set of comparison brick are reported in Table 13. No water was collected on any of the E 514-04 test panels for these comparison brick. Similarly, the time to the appearance of dampness and the damp area on the back of the test panel were very similar for each set of test brick in this comparison. Additionally, decreasing face shell thickness does not appear to play any role in the water penetration.

The 29.8 % void area test brick, which had the lowest compressive strength in this set of comparison brick, also had a higher water adsorption than the other brick in this comparison set. The higher level of water absorption appears to have more effect on these test brick than increased void and decreased face shell thickness. There was a general increase in flexural bond strength with increasing void area for this set of comparison brick as has been observed in several of the other comparison sets reported in this study.

This set of comparison brick had a wide range of both void area and face shell thickness. Test panels constructed with equivalent mortar and workmanship, illustrate that void area and face shell thickness do not affect water penetration. Similarly, an increase in flexural bond strength was observed with increasing void area. Further, decreasing face shell thickness had no apparent effect on flexural bond strength.

Mortar Consumption Data

During the course of this work, it was decided to measure mortar consumption during the construction of the E 514-04 panels. To determine how increasing void influences mortar consumption, the amount of mortar used to construct each of the test panels for the Comparison 2, 3, and 4 brick was carefully measured. The usage data were calculated in terms of the number of brick laid per bag of mortar cement and bags of mortar per 1000 brick. It is important to note that for each type of brick, three E 514-04 panels

TABLE 14—Mortar consumption data for comparison 2 brick.

Coring Configuration	Void Area, %	Bricks/Bag of Masonry Cement	Bags of Masonry Cement/1000 Bricks
10 Hole	25.3	178	5.6
5 Hole	27.7	168	6.0
3 Hole	31.5	148	6.8

were constructed. With modular brick, each E 514-04 panel contained approximately 195 brick. Again, the panels were constructed by an experienced mason using standard construction practices. Mortar consumption data for the Comparison 2 brick are reported in Table 14, data for Comparison 3 are reported in Table 15 and finally, data for Comparison 4 are reported in Table 16.

For the Comparison 2 brick there was a small decline in the number of brick laid per bag of cement with increasing void for these brick. By increasing the void area from 25 to 31 %, the mortar consumption increased by approximately 17 %. For the Comparison 3 brick the trend in increasing mortar consumption was not as clear. This set of comparison brick had a different coring pattern for each void level. For the Comparison 3 brick, increasing the void area from 24 to 28 % resulted in an increase in mortar consumption of approximately 10 %. There was very little difference in the actual mortar consumption between the 28 % void and 31 % void brick. For the fourth set of comparison brick, there was also a slight increase in mortar consumption with increasing void. In short, increasing void area only resulted in a moderate increase in mortar consumption. It is possible that the increased flexural bond strengths observed for the higher void area brick might be related to these small increases in mortar consumption. The observed increase was below the industry standard estimate of seven bags of mortar per 1000 brick.

Conclusions

In conclusion, seven sets of comparison brick were evaluated to determine what effects, if any, increasing void area and decreasing face shell thickness might have on some important aspects of wall system performance. Four sets of comparison test brick were studied. Each set of comparison brick contained individual brick with varying void areas and face shell thicknesses. Each set of comparison brick was produced using a single raw material and production line. The differences in void area and face shell thickness for each comparison set were produced by changing the coring configuration of the extruder during production. All test panels and test prisms were built by a skilled mason using Type N masonry cement. By limiting the performance variables relating to brick and mortar interaction and workmanship, the effect of void area and face shell thickness could be isolated for study. Analysis of the test data yielded the following conclusions:

1. Water penetration rates, and flexural bond strengths were not significantly affected by increasing void area for any of the sets of comparison brick.
2. Increasing the void area of a particular group of brick did not contribute to increased rates of water penetration or decreased flexural bond strength.

TABLE 15—Mortar consumption data for comparison 3 brick.

Coring Configuration	Void Area, %	Bricks/Bag of Masonry Cement	Bags of Masonry Cement/1000 Bricks
3 Hole	23.9	172	5.8
3 Hole	28.5	155	6.4
3 Hole	31.5	158	6.3

TABLE 16—Mortar consumption data for comparison 4 brick.

Coring Configuration	Void Area, %	Bricks/Bag of Masonry Cement	Bags of Masonry Cement/1000 Bricks
10 Hole	21.7	178	5.6
10 Hole	29.8	168	6.0
10 Hole	34.2	148	6.8

3. Similarly, decreasing face shell thickness did not appear to negatively impact water penetration or flexural bond strength.
4. A wide range of brick were tested in this study and, in general, increasing void area and decreasing face shell thickness, did not have a significant impact on compressive strengths.
5. Finally, the quantity of mortar required to build the E 514-04 test panels for several sets of comparison brick was measured during construction and a slight increase in mortar usage was observed with increasing void area. The small increase in mortar consumption with higher void area brick did not exceed the industry standard measurement of seven bags of mortar mix per 1000 brick.

References

- [1] ASTM Standard C 216-04, "Standard Specification for Facing Brick (Solid Masonry Units Made from Clay or Shale)," *Annual Book of ASTM Standards*, Vol. 4(5), ASTM International, West Conshohocken, PA.
- [2] ASTM Standard C 652-04, "Standard Specification for Hollow Brick (Hollow Masonry Units Made from Clay or Shale)," *Annual Book of ASTM Standards*, Vol. 4(5), ASTM International, West Conshohocken, PA.
- [3] ASTM Standard E 514-04, "Standard Test Method for Water Penetration and Leakage Through Masonry," *Annual Book of ASTM Standards*, Vol. 4(5), ASTM International, West Conshohocken, PA.
- [4] ASTM Standard C 1072-00a, "Standard Test Method for Measurement of Masonry Flexural Bond Strength," *Annual Book of ASTM Standards*, Vol. 4(5), ASTM International, West Conshohocken, PA.
- [5] ASTM Standard C 67-03a, "Standard Test Methods for Sampling and Testing Brick and Structural Clay Tile," *Annual Book of ASTM Standards*, Vol. 4(5), ASTM International, West Conshohocken, PA.
- [6] Ramamurthy, K. and Anand, K. B., "Classification of Water Permeation Studies on Masonry," *Masonry International*, Vol. 14, No. 3, 2001, pp. 74–79.
- [7] Grimm, C. T., "Water Permeance of Masonry Walls: A Review of the Literature," *Masonry: Materials, Properties, and Performance*, ASTM STP 778, J. G. Borchelt, Ed., 1982, pp. 178–199.
- [8] Ribar, J. W., "Water Permeance of Masonry: A Laboratory Study," *Masonry: Materials, Properties, and Performance*, ASTM STP 778, J. G. Borchelt, Ed., ASTM International, West Conshohocken, PA, 1982, pp. 200–220.
- [9] Groot, C. J. and Gunneweg, J., "Water Permeance Problems With Single Wythe Masonry Walls: The Case of Wind Mills," *Constr. Build. Mater.*, Vol. 18, 2004, pp. 325–329.
- [10] Borchelt, J. G., Melander, J. M., and Nelson, R. L., "Bond Strength and Water Penetration of High IRA Brick and Mortar," *8th North American Masonry Conference*, Austin, TX, June 1999.
- [11] Borchelt, J. G. and Tann, J. A., "Bond Strength and Water Penetration of Low IRA Brick and Mortar," *7th North American Masonry Conference*, South Bend, IN, June 1996.
- [12] McGinley, W. M. and Greenwald, J., "Hollow Unit Bond Wrench Test Trials," *10th Canadian Masonry Symposium*, Banff, Alberta, June 8–12, 2005.

Jeffrey H. Greenwald¹ and Thomas C. Young²

Evaluation of the Effectiveness of Clear Water Repellent Coatings on Partially Grouted Single-Wythe Concrete Masonry Walls

ABSTRACT: The use of architectural concrete masonry to construct commercial and institutional buildings is common in the northwestern United States. By combining different block sizes, shapes, colors, and surface treatments, architects have designed many striking structures. This test program focused on the evaluation of clear water repellent coatings because they are an important component of a water resistant wall system. The number of repellents produced has grown and their chemical composition has changed during recent years. The test results will provide guidance in updating the industry recommendation used by design professionals and building owners. A total of 14 walls were constructed and tested in accordance with ASTM E 514, "Standard Test Method for Water Penetration and Leakage Through Masonry." The walls were all constructed with materials shipped from northwest block producers and represent construction techniques used in the Pacific Northwest. Each wall was initially tested uncoated to establish a baseline performance. Afterwards, a clear water repellent was applied and each wall was retested. The walls were then tested a third time after aging outside for approximately one year. The test results will establish comparative behavior between wall assemblies.

KEYWORDS: concrete block, damp-proofing, water permeance, water repellent, masonry testing

Introduction

This describes the results of water penetration testing of concrete masonry walls by the National Concrete Masonry Association Research and Development Laboratory [1]. The testing was performed for the Northwest Concrete Masonry Association (NWCMA).

Purpose

The primary objective of the test program was to evaluate the effectiveness of clear water repellent coatings on single-wythe concrete masonry walls. Repellent performance was tested after initial curing and retested to determine environmental aging effects.

A secondary objective was to investigate the effects of wall design. Walls were constructed with a grouted bond beam at mid-height to represent typical northwest design practice. The impact of concrete masonry unit density was also evaluated.

Background

The use of architectural concrete masonry to construct commercial and institutional buildings is common in the northwestern United States. By combining different block sizes, shapes, colors, and surface treatments, architects have designed many striking structures. The interest in architectural block has led to the development of industry recommendations for rain resistant construction in the wet western portions of Oregon and Washington. These recommendations have been based upon laboratory research and field experience.

The test program was a continuation of previous research on this subject and focused on the evaluation of clear water repellent coatings because they are an important component of a water resistant wall system.

Manuscript received May 1, 2006; accepted for publication June 18, 2007; published online September 2007. Presented at ASTM Symposium on Masonry on 13 June 2006 in Toronto, Canada; B. Trimble and J. Brisch, Guest Editors.

¹ Executive Director, North American Steel Sheet Piling Association, Alexandria, VA 22314.

² Executive Director, Northwest Concrete Masonry Association, Lynnwood, WA 98036.

TABLE 1—*Scope of research (construction variations for each test wall).*

Wall No.	Wall Designation	IWR Present	Unit Weight (pcf)
1	LW-1	Yes	101.4
2	LW-2	Yes	101.4
3	LW-3	Yes	101.4
4	LW-4	Yes	101.4
5	LW-5	Yes	101.4
6	LW-6	Yes	101.4
7	LW-7	Yes	101.4
8	LW-8	Yes	101.4
9	LW-9	Yes	101.4
10	LW-10	Yes	101.4
11	MW-11	No	110.2
12	MW-12	No	110.2
13	MWIR-13	Yes	110.2
14	MWIR-14	Yes	110.2

The number of repellents produced has grown and their chemical composition has changed during recent years. The test results will provide guidance in updating the industry recommendation used by design professionals and building owners.

Scope

A total of 14 walls were constructed and tested in accordance with ASTM E 514, "Standard Test Method for Water Penetration and Leakage Through Masonry." A summary of the scope is shown Table 1. The wall designation indicates that the wall assemblies were constructed with lightweight (LW) or medium-weight (MW) concrete masonry units (CMU). Furthermore, all the LW CMU contained an integral water repellent (IWR) as did two walls constructed with MW CMU. The other two MW CMU walls were constructed with units with an efflorescence control additive, which is common in the drier areas of the Pacific Northwest.

The walls were all constructed at the NCMA Laboratory with materials shipped from two northwest block producers. They were representative of northwest construction assemblies. Each wall was initially tested uncoated to establish a baseline performance. Afterwards, a clear water repellent was applied and each wall was retested. The walls were then tested a third time after aging outside for approximately one year. The walls were aged at the NCMA Laboratory in Herndon, Virginia. The test results will establish comparative behavior between wall assemblies.

Ten different water repellents to be tested were applied to the ten partial grouted, lightweight CMU wall assemblies (a repellent numbering system was used for manufacturer confidentiality). Additionally, two good performing repellents and two other lesser performers from the first ten tests were selectively applied to the partial grouted, medium-weight CMU wall assemblies.

Materials

Concrete Masonry Units

Split-face concrete masonry units were delivered to the laboratory in ready-to-build condition. Delivery of the CMU was arranged by NWCMA. All unit types were tested for compressive strength and absorption in accordance with ASTM C 140 "Standard Test Method for Sampling and Testing Concrete Masonry Unit and Related Units." Three units types, designated as CMU LW, MW, MWIR, used in this study, are listed in Table 2.

TABLE 2—Properties of concrete masonry units.

Physical Property (Average of 3 Units)	CMU LW— With IWR	CMU MW— Without IWR ^a	CMU MWIR— With IWR
Classification	Light Weight	Medium Weight	Medium Weight
Width (in.)	7.84	7.66	7.87
Height (in.)	7.65	7.62	7.59
Length (in.)	15.60	15.64	15.61
Minimum faceshell thickness (in.)	1.28	1.30	1.33
Minimum web thickness	1.20	1.30	1.20
Percent solid (%)	52.2	60.1	54.3
Density (pcf)	101.4	110.2	110.2
Absorption (pcf)	11.7	11.1	8.9
Net compressive strength of unit (psi)	2400	3360	3030

^aEfflorescence control CMU.

Mortar

Type S portland cement-lime (PCL) mortar was supplied by the client and batched according to ASTM C 270 with or without an IWR. The mortars were tested in accordance with ASTM C 780, “Standard Test Method for Preconstruction and Construction Evaluation of Mortars for Plain and Reinforced Masonry.”

The 28-day compressive strength of 2-in. mortar cubes was determined in accordance with ASTM C 780. Results of the mortar tests are summarized in Table 3.

Grout

All walls were constructed with a bond beam at mid-height and the bond beam was grouted with grout conforming to the proportion specification of ASTM C 476, “Standard Specification for Grout for Masonry.”

Water Repellent Coatings

A total of ten clear water repellent coatings were tested. Table 4 provides the chemical composition and carrier for each coating.

TABLE 3—Mortar test results.

Mortar/Use	Average 28-day Compressive Strength (psi)
Type S PCL with IWR—wall LW-1 through LW-10	2020
Type S PCL without IWR—wall panels MW-11 and MW-12	2480
Type S PCL with IWR—wall panels MWIR-13, MWIR-14	Not tested

TABLE 4—Water repellent types.

Water Repellent	Chemical Composition	Carrier
1	Silicone Elastomer	Solvent
2	Silane/Siloxane	Water
3	Silane/Siloxane	Water
4	Siloxane	Solvent
5	Silane/Siloxane	Water
6	Siloxane	Solvent
7	Modified Vinyl	Alcohol
8	Silane/Siloxane	Solvent
9	Siloxane	Solvent
10	Silane/Siloxane	Water

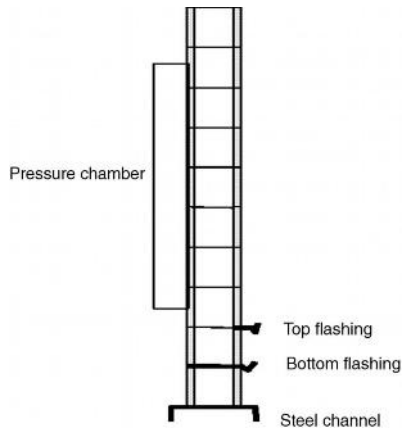


FIG. 1—Wall panel cross section.

Construction and Curing of Wall Panels

Workmanship

All panels were constructed using good construction techniques in accordance with ACI 530.1/ASCE 6/TMS 602, "Specification for Masonry Structures." Wall assemblies were constructed at the NCMA Research and Development Laboratory during May 2003.

Construction of Wall Panels

The overall nominal dimensions of all the finished wall panels were 72 in. in height, 56 in. in length, and 8 in. in thickness. Figure 1 shows a sketch of the wall panel cross section.

Each panel was constructed using a running bond pattern. The concrete masonry units were laid using face shell bedding, except at the ends of each panel where mortar was also placed on the end webs of the units. Mortar joints were concave-tooled when the mortar in the joint became thumb print hard. The pressure chamber is mounted on the split-face side of the wall assemblies.

The wall panels were constructed on an inverted steel channel to provide a level base. The steel channel also facilitated any necessary movement of the specimens within the laboratory. The base course was placed in a bed of mortar onto the steel channel. A piece of steel through-panel flashing was placed directly on top of the base course without the use of mortar. Weep ropes were placed on the bottom flashing every eight inches beginning four inches from the end of the panel, so there was a weep rope in the middle of each core of the units of the second course. The second course in the panel was placed in a bed of mortar directly on top of the bottom flashing and weep ropes. At this point, approximately two inches of pea gravel was poured into each core of the units. Directly on top of the second course, the top flashing was installed without the use of mortar. The third course was laid into a bed of mortar (including mortar on the top surface of the top flashing). The remaining units were laid for the wall panel and each one had a bond beam constructed at wall mid-height. Bond beam units were made for the CMU by knocking out a portion of the CMU web to form a horizontal channel allowing grout to fill in behind the mortar head joints. The CMU course below the bond beam was lined with plastic mesh to form a grout stop. Joint reinforcement or bond beam steel was not used in any of the wall sections.

Curing Test Panels

All of the panel specimens were wrapped in plastic and cured in this condition for seven days. Thereafter, the wall specimens were cured in ambient laboratory conditions for at least seven days prior to testing.

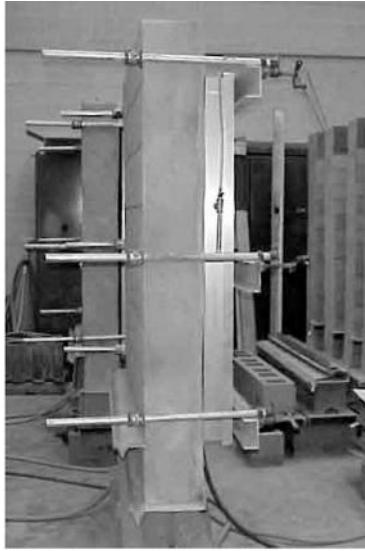


FIG. 2—Side view of wall assembly with test chamber.

Laboratory schedule and testing equipment availability required that the baseline water repellency testing be conducted approximately one month after wall assembly grouting. The laboratory temperature ranged from 60 to 80°F.

Test Procedures

All wall panels were tested in accordance with ASTM E 514, with modifications described in this section of the report. Three rounds of ASTM E 514 tests were conducted. Round one tested the walls with no modifications to the exterior surface (water applied surface) of the wall panel. Round two tested the walls after the application and curing of a surface water repellent to the exterior surface. Round three tested the walls after exposure to outside conditions for approximately one year. Below is a general description of the testing procedures as well as a presentation of the results of each testing round. Thereafter, the observations between rounds one, two, and three are given.

Water Penetration Testing

Three days prior to testing, the front of each specimen (except for the test area) and the panel sides were parged with mortar in accordance with ASTM E 514. The top of the wall was not parged in order to be able to observe water migration by looking in at the top CMU cores. The parging on the front of the panels formed a smooth “frame” around the test area that facilitated the watertight seal between the test chamber and the panel. Twenty-four hours prior to the onset of testing, a 12 ft² test chamber (36-in. wide by 48-in. high) was clamped to the exterior front face of the panel test specimen. The edges of the chamber were lined with 2-in. thick foam rubber and silicone caulk to provide a watertight and airtight seal. Figure 2 provides a side view of the wall assembly with the test chamber.

Water was applied to the front face of the panel through a spray pipe within the test chamber at a rate of 40.8 gallons per hour (measured as approximately 0.68 gallons per minute), which is equal to 3.4 gal/ft² of panel per hour and is equivalent to a rainfall of approximately 5-1/2 in. per hour. Simultaneously, a 10 psf (measured as approximately 1.92 in. of water column on a water manometer) positive air pressure was applied to the front surface of the panel through the test chamber. This 10 psf applied pressure is equivalent to the positive pressure created by a 62.5 mph sustained wind. ASTM E 514 requires that these test

TABLE 5—Round 1 results.

Wall Designation	Total Water Accumulation (gal)		
	4 hours	8 hours	24 hours
LW-1	1.05	5.34	47.51
LW-2	1.98	4.67	22.19
LW-3	1.22	4.67	26.41
LW-4	4.49	9.87	31.15
LW-5	1.39	4.51	24.38
LW-6	0.04	0.38	8.96
LW-7	3.70	12.81	52.82
LW-8	0.09	2.48	44.59
LW-9	1.45	5.78	36.69
LW-10	2.01	7.70	36.59
MW-11	2.10	5.25	17.60
MW-12	0.16	1.22	11.24
MWIR-13	1.30	3.29	23.29
MWIR-14	1.92	4.84	26.85

conditions be maintained for a period of four hours. However, the test was continued for a period of 24 hours.

During the testing, the water that collected in the top and through the weep holes onto bottom flashings was measured and recorded every 30 minutes for the first four hours, every hour up to 8 hours, and again at 24 hours. The bottom flashing measures the total amount of water penetrating through the face shell under pressure. The top flashing measures the total amount of water that migrates along the webs and mortar fins under ambient pressure and penetrates the back wall face. Also, at each recording interval, a photograph was taken of the back wall face.

Test Results and Observations

A discussion of the results of the tests and observations is included in this section. The measure of performance used in this research was determined to be the total water collected onto both bottom and top flashing pans. This was used to evaluate the performance of the repellents as to their ability to stop water from entering into the wall assembly. A secondary measure of performance was dampness on the back wall face.

Round 1 Water Repellency Testing

Wall assemblies without a water repellent coating were tested in Round 1. These walls were tested according to ASTM E 514 for a period of 24 hours. This test phase established the baseline panel performance. Table 5 lists the total water penetrating the wall assembly (addition of top and bottom pan accumulation).

Round 2 Water Repellency Testing

Wall assemblies were allowed to dry in laboratory air for approximately two weeks before applying the water repellent coating. The coating was then spray applied in a saturating “flood coat” with a rundown below the contact point of the spray pattern, per the manufacturer’s instruction. This visually controlled application technique provided even coverage and uniform application.

The wall assemblies were then allowed to cure in the laboratory for seven to nine days prior to retesting in accordance with the procedures of ASTM E 514. Table 6 lists the total water penetrating the wall assembly (addition of top and bottom pan accumulation).

Walls LW-1 through LW-10 were tested in Round 2 prior to selecting the coatings to apply to the

TABLE 6—Round 2 results.

Wall Designation	Coating Number	Total Water Accumulation (gal)		
		4 hours	8 hours	24 hours
LW-1	1	0.00	0.00	0.00
LW-2	2	0.06	1.70	51.55
LW-3	3	0.69	2.50	15.68
LW-4	4	0.00	0.03	1.84
LW-5	5	0.06	0.52	11.90
LW-6	6	0.00	0.00	0.23
LW-7	7	5.47	17.46	73.08
LW-8	8	0.00	0.00	0.00
LW-9	9	0.00	0.00	0.00
LW-10	10	1.23	5.26	38.26
MW-11	1	0.16	0.90	3.52
MW-12	8	0.00	0.10	0.60
MWIR-13	3	1.14	3.20	13.22
MWIR-14	2	0.47	2.30	15.69

medium-weight unit walls. Coatings No. 1 and 8, which were two of the best performers on the lightweight IWR CMU, were applied to the non-IWR MW CMU. Two lesser performers, coatings No. 2 and 3, were applied to the medium weight IWR CMU.

Round 3 Water Repellency Testing

Wall assemblies were placed outside for 12 to 15 months to age them and to evaluate environmental effects on the applied water repellent coatings. The wall assemblies were oriented to a southern exposure for the aging duration. Table 7 lists the total water penetrating the wall assembly (addition of top and bottom pan accumulation).

Observations on Lightweight CMU Walls

This section presents observations on the data collected for all three rounds of water repellency testing. ASTM E 514 requires that a wall assembly be subject to water exposure for a minimum of four hours. These tests were run for 24 hours to provide additional data and to confirm that the water exposure was sheeting onto the wall assemblies.

TABLE 7—Round 3 results.

Wall Designation	Coating Number	Total Water Accumulation (gal)		
		4 hours	8 hours	24 hours
LW-1	1	0.00	0.00	0.05
LW-2	2	0.09	0.62	1.91
LW-3	3	0.00	0.00	1.08
LW-4	4		Wall damaged	
LW-5	5	0.00	0.00	0.00
LW-6	6	0.00	0.00	0.05
LW-7	7	1.97	6.22	32.36
LW-8	8	0.00	0.00	0.00
LW-9	9	0.00	0.00	0.00
LW-10	10	0.00	0.00	0.28
MW-11	1	0.44	1.24	4.97
MW-12	8	0.00	0.00	0.00
MWIR-13	3	0.00	0.00	0.16
MWIR-14	2	0.00	0.00	0.14

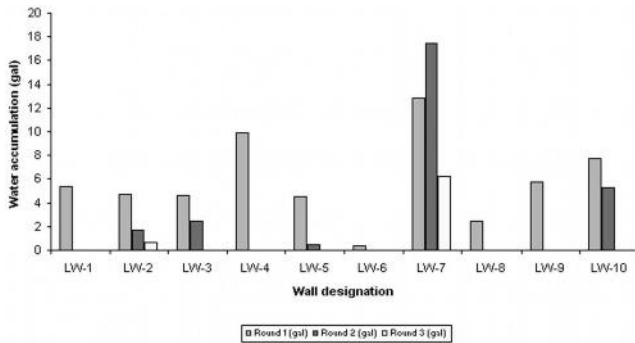


FIG. 3—Eight-hour water penetration results.

The data observations that follow are based on eight-hour water exposure, which was sufficient to evaluate the repellent performance. Furthermore, the walls were continuously monitored for air pressure and water flow throughout the eight-hour time period, but were left unattended from 8 hours to 24 hours. During this time, the lab could not continuously monitor air pressure and water flow.

Figure 3 presents the water penetration results after eight hours for the wall assemblies constructed with LW CMU—walls LW-1 through LW-10. The figure shows the water penetration for all three rounds for the ten different water repellent coatings. For example, wall assembly LW-2 shows approximately 4.5 gallons of water penetrating during round one after eight hours. For Round 2, 1.7 gallons of water penetrated, and for Round 3 about 0.5 gallons penetrated the wall assembly.

The test results in the figure show that some repellents performed better than others. For nine of the ten walls shown in the figure, water penetration was reduced by the presence of a water repellent coating. For example, the water penetrating LW-1 was reduced to zero in the second round of testing. In all cases for these ten walls, exposing them to the weather had no negative effect upon the water repellent coating's performance. All ten walls performed better in Round 3.

Figure 4 shows the calculated percentage reduction of water penetrating the wall assemblies for each water repellent coating. This was determined by subtracting the total water collected in Round 2 from that collected in Round 1. Therefore, 100 % indicates that the repellent completely stopped any water from penetrating the wall assemblies. From these data, five repellents reduced the water penetration to zero. In all these cases, the best performers were solvent-based water repellents.

The condition of the back wall faces at eight hours are shown in Table 8. The presence of the bond beam in the wall assemblies blocks water from draining down the cores onto the bottom flashing pan. The effect of this can be seen as water streaks emanating from the bed joint at the top of the bond beam. Dampness on the wall interior should be considered along with accumulated water in evaluating overall wall water penetration resistance.

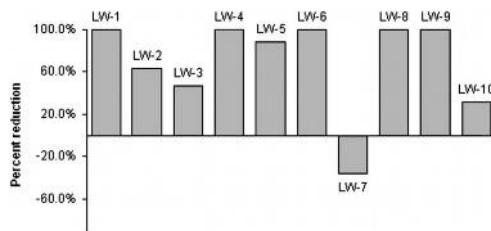
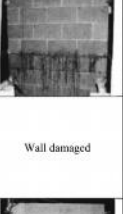
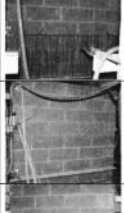
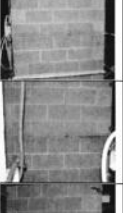
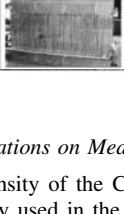
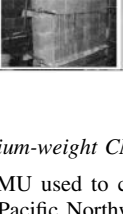
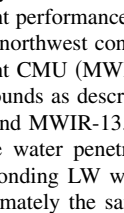
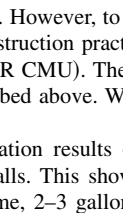
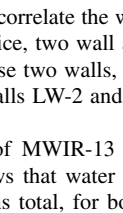
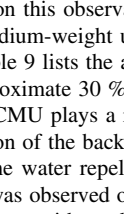
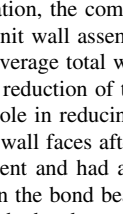
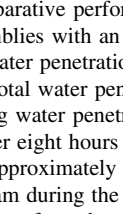
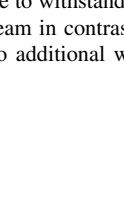
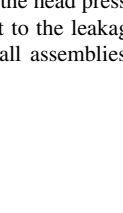
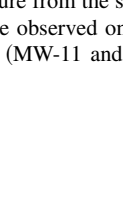
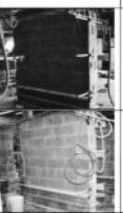
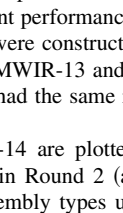
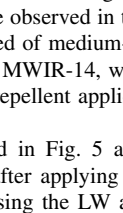
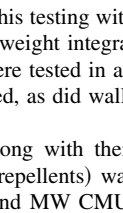
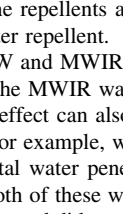
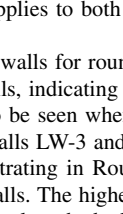
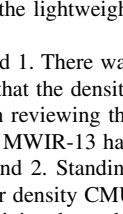
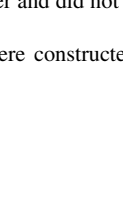
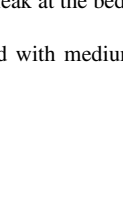
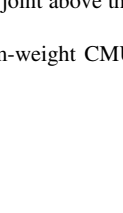


FIG. 4—Reduction of water penetration.

TABLE 8—Wall back faces at eight-hour testing.

Wall Designation	Round One	Round Two	Round Three
LW-1			
LW-2			
LW-3			
LW-4			Wall damaged
LW-5			
LW-6			
LW-7			
Wall Designation	Round One	Round Two	Round Three
LW-8			
LW-9			
LW-10			
MW-11			
MW-12			
MWIR-13			
MWIR-14			

Observations on Medium-weight CMU Walls

The density of the CMU used to construct the first ten wall assemblies was a lighter unit weight than typically used in the Pacific Northwest. This was deemed acceptable and a more stringent test of water repellent performance. However, to correlate the water repellent performance observed in this testing with typical northwest construction practice, two wall assemblies were constructed of medium-weight integral repellent CMU (MWIR CMU). These two walls, designated MWIR-13 and MWIR-14, were tested in all three rounds as described above. Walls LW-2 and MWIR-14 had the same repellent applied, as did walls LW-3 and MWIR-13.

The water penetration results of MWIR-13 and MWIR-14 are plotted in Fig. 5 along with their corresponding LW walls. This shows that water penetration in Round 2 (after applying repellents) was approximately the same, 2–3 gallons total, for both wall assembly types using the LW and MW CMU. Based on this observation, the comparative performance of the repellents applies to both the lightweight and medium-weight unit wall assemblies with an integral water repellent.

Table 9 lists the average total water penetration for the LW and MWIR walls for round 1. There was an approximate 30 % reduction of total water penetrated for the MWIR walls, indicating that the density of the CMU plays a role in reducing water penetration. This effect can also be seen when reviewing the condition of the back wall faces after eight hours (Table 8). For example, walls LW-3 and MWIR-13 had the same water repellent and had approximately the same total water penetrating in Round 2. Standing water was observed on the bond beam during the testing of both of these walls. The higher density CMU was able to withstand the head pressure from the standing water and did not leak at the bed joint above the bond beam in contrast to the leakage observed on LW-3.

Two additional wall assemblies (MW-11 and MW-12) were constructed with medium-weight CMU

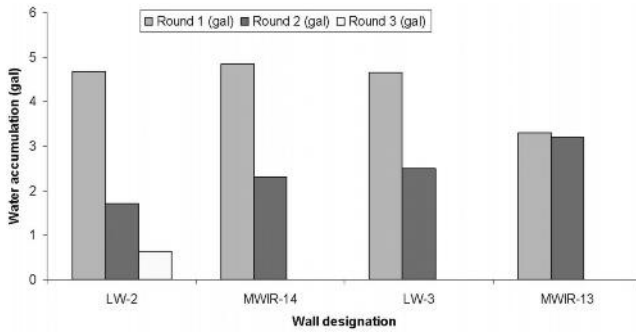


FIG. 5—*CMU density effects on water repellent performance.*

that contained a water repellent admixture, but not a full dosage integral water repellent. These blocks are common in the eastern portions of Oregon and Washington, which have a more arid climate as compared to the coastal areas of these states. Two of the better performing water repellents were applied to these walls for Round 2 testing and Table 10 shows the percent reduction of water penetration between Rounds 1 and 2. Both repellents showed good performance reducing the water penetrating these walls by over 80 %. Observing the state of the wall faces between Rounds 1 and 2 also shows this performance. Round 1 showed a bond beam leak for both walls, while no leaking was observed in Round 2.

Conclusions

This paper documents the water penetration performance of single-wythe concrete masonry wall assemblies that were coated with post-applied water repellents. Fourteen walls were constructed and tested in accordance with ASTM E 514. Walls were constructed with one horizontal grouted bond beam to simulate typical practices employed in the Pacific Northwest area of the United States. Walls were tested in three rounds: Round 1—no post-applied water repellent, Round 2—with a post-applied water repellent cured for approximately one week, and Round 3—after exposure to outside weather conditions for 12–15 months.

Conclusions are made based upon the total water quantity penetrating the wall assemblies and the condition of the interior (back) wall face after eight hours of ASTM E 514 test exposure.

1. Post-applied water repellents generally improve the water penetration resistance. The amount of water that penetrated the wall assemblies was reduced after application of the repellents in all cases but one.
2. Exposure to outside conditions further reduced the amount of water penetrating the wall assemblies. There were no detrimental aging effects.
3. Round 2 testing showed that solvent-based repellents performed better than water-based repellents. In every case solvent-based repellents reduced the water penetration to zero. After Round 3

TABLE 9—*CMU density effects on water penetration.*

Wall Type (number of walls)	Density (pcf)	Average Water Penetration (gal)
LW (10)	101.4	5.8
MWIR (2)	110.2	4.1

TABLE 10—*Water Penetration Reduction.*

Wall Designation	Coating Number	Percent Decrease
MW-11	1	83.0
MW-12	8	92.0

testing, most of the water-based repellents exhibited similar performance to the solvent-based products.

4. Quality post-applied water repellents were effective in reducing water penetration through walls constructed with medium-weight CMU that were manufactured without a full dosage of integral water repellent. This may be a consideration for the more arid areas of the Pacific Northwest.
5. The bond beams obstructed water in the top half of the wall assemblies such that it could not drain down the CMU cores. This caused standing water within the wall which eventually leaked out the bed joint above the bond beam. Consideration should be given to the design of a vertical water path within horizontal wall obstructions.
6. The wall panels did not effloresce or show any other deposits on the face after exposure to outside conditions.

Acknowledgments

The authors would like to acknowledge the following companies for their generous contributions to this project: Northwest Concrete Masonry Association, Masonry Industry Promotion Group and the Masonry Institute of Oregon. Further, the authors would like to thank the following companies who donated materials that were used in the construction of research test specimens: Eastside Masonry Products and Central Pre-Mix Concrete Products, Co.

References

- [1] "Evaluation of the Effectiveness of Clear Water Repellent Coatings on Partially Grouted Single-Wythe Concrete Masonry Walls," NCMA Project No. 03-292, September 2005.

Gregory L. Cohen,¹ Richard E. Klingner,² John R. Hayes, Jr.,³ and Steven C. Sweeney⁴

Seismic Evaluation of Low-Rise Reinforced Masonry Buildings with Flexible Diaphragms

ABSTRACT: This paper provides an integrated approach to the seismic evaluation of low-rise reinforced masonry buildings with flexible roof diaphragms. The paper is divided into four phases. In Phase 1 (Behavior), results from shaking-table testing, quasi-static testing, and analytical predictions are integrated to provide a coherent description of the seismic response of low-rise reinforced masonry buildings with flexible roof diaphragms. Two half-scale, low-rise reinforced masonry buildings with flexible roof diaphragms are subjected to earthquake ground motions on the Tri-axial Earthquake and Shock Simulator at the United States Army Construction Engineering Research Laboratory, Engineer Research and Development Center. Following the shaking-table tests, diaphragms and top four courses of attached masonry walls are salvaged from the half-scale structures and tested quasi-statically in their own plane. A new index, the diaphragm drift ratio, is introduced to describe the potential for diaphragm damage. In Phase 2 (Analysis), coordinated analytical modeling is developed and implemented to corroborate and extend the results of that experimental work, and to examine the efficacy and accuracy of different analytical modeling approaches. Linear elastic finite-element models, simplified two-degree-of-freedom models, and nonlinear lumped-parameter models are developed; all agree well with measured responses. In Phase 3 (Seismic Evaluation), the first two phases are used to develop and verify a simple extension to FEMA 310, the predominant seismic evaluation methodology for low-rise reinforced masonry buildings with flexible diaphragms. In Phase 4 (Application and Verification), the proposed extension, applied to four existing buildings, is shown to be simple, useful, and necessary.

KEYWORDS: low-rise, masonry, flexible diaphragm, seismic response, seismic evaluation

Introduction

Changes in the United States military, combined with recent destructive earthquakes in the United States and around the world, have made the United States Department of Defense aware of the potential seismic vulnerability of the military's building inventory. For this reason, the United States Army Construction Engineering Research Laboratory, Engineer Research and Development Center (CERL) allocated funds for a research effort to assess and mitigate the seismic vulnerability of military facilities. This study, part of that effort, comprises four phases. Details are given in Cohen [1], and in Cohen et al. [2-4].

- Phase 1: Behavior. The earthquake response of low-rise reinforced masonry buildings with flexible roof diaphragms is evaluated through a coordinated study of shaking-table testing and quasi-static testing, and observations from that testing are related to the Diaphragm Drift Ratio, a new index describing the potential for roof diaphragm damage.
- Phase 2: Analysis. The results of the experimental program are corroborated and complemented by analytical modeling.
- Phase 3: Seismic Evaluation. Observations from experimental testing and analytical modeling are synthesized into a simple tool for seismic evaluation.
- Phase 4: Application and Verification. The proposed evaluation tool is applied to sample existing low-rise reinforced masonry buildings with flexible roof diaphragms.

Manuscript received November 21, 2005; accepted for publication April 26, 2006; published online June 2006. Presented at ASTM Symposium on Masonry on 13 June 2006 in Toronto, Ontario, Canada; B. Trimble and J. Brisch, Guest Editors.

¹ Ph.D. in Civil Engineering, The University of Texas, Austin, TX 78712.

² L.P. Gilvin Professor in Civil Engineering, The University of Texas, Austin, TX 78712.

³ Director, National Earthquake Hazards Reduction Program, National Institute of Standards and Technology, Gaithersburg, MD 20899. Formerly %US Army Engineer Research and Development Center.

⁴ US Army Engineer Research and Development Center, Champaign, IL, 61826.

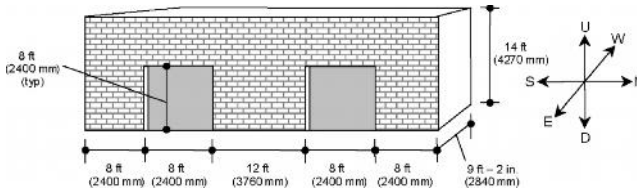


FIG. 1—Schematic of full-scale prototype building.

Phase 1: Behavior

From September 1999 to March 2001 two, half-scale low-rise masonry buildings with flexible roof diaphragms were constructed based on identified prototypical configurations. One specimen was constructed with a diagonally sheathed lumber diaphragm, the other with a welded metal-deck diaphragm. The specimens were subjected to a coordinated testing program on the US Army Tri-axial Earthquake and Shock Simulator (TESS). Those tests qualitatively and quantitatively substantiated the generally accepted premise (by the earthquake engineering technical community) that diaphragm flexibility can significantly affect the seismic response of these types of buildings; they demonstrated that low-rise reinforced masonry buildings with flexible roof diaphragms behave at least as two-degree-of-freedom (2DOF) system, with one degree of freedom associated with the in-plane response of the shear walls and another with the roof diaphragm, and essentially as single-degree-of-freedom (SDOF) systems, with a single degree of freedom associated with the in-plane response of the roof diaphragm.

Following shaking-table testing, from March 2001 to August 2001, roof diaphragms and top four courses of reinforced masonry from the two building specimens were removed and subjected to reversed cyclic quasi-static displacements. That testing characterized the hysteretic behavior of those types of diaphragms, and the relationships between diaphragm deformations and diaphragm damage. It helped place this study in the context of performance-based engineering.

Development of Half-scale Test Specimens

This research was directed at the seismic vulnerability of United States Army structures designed and built before 1960 in the central United States. For that reason, the prototype masonry structures were designed to be typical of that time period. The structures represent warehouse or storage facilities with large length-to-width ratios in plan and openings on one long side. Such structures are common in the United States Army building inventory, and typically have flexible roof diaphragms of lumber sheathing, corrugated metal decking, or precast concrete planks.

A survey of the existing United States Army building inventory provided typical construction details for low-rise reinforced masonry buildings with flexible diaphragms designed and built before 1960. Based on that survey, two prototypical building specimens were configured (Fig. 1), geometrically scaled by one-half (Fig. 2), and then constructed (Figs. 3 and 4. Half-scale specimen walls used 4-in. (100 mm) CMU grouted vertically at 24 in. (600 mm) with one #3 (10 M) reinforcing bar per grouted cell and grouted horizontally at bond beams with two #3 (10 M) reinforcing bars per bond beam (Fig. 2).

Based on that survey, two roof diaphragms were also configured. The first half-scale test specimen, Specimen #1, had a diagonally sheathed spruce-pine-fir lumber roof diaphragm. The second half-scale test

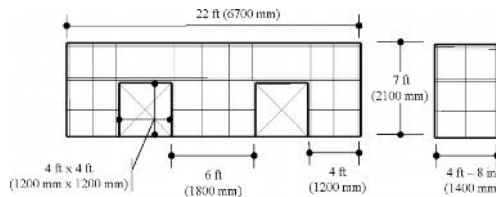


FIG. 2—Schematic of half-scale specimen reinforcement for longitudinal and transverse walls.

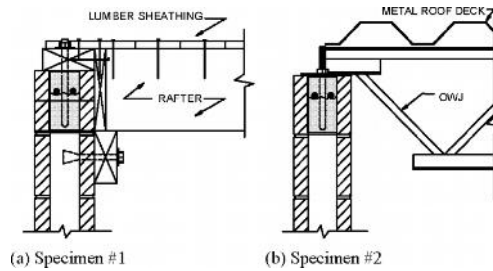


FIG. 3—Typical details of rafter-to-wall connections for half-scale specimens. (a) Specimen #1. (b) Specimen #2.

specimen, Specimen #2, had a roof diaphragm of metal deck on open-web joist (OWJ). Table 1 provides the specimen designs, and Figs. 3(a) and 3(b) show typical roof details for Specimens #1 and #2, respectively. Figure 4 shows an overall photo of Specimen #1.

Remarks on Structural Scaling and Input Ground Motions

To arrive at meaningful conclusions and recommendations regarding the behavior, analysis, and design of low-rise reinforced masonry buildings with flexible roof diaphragms, the implications of geometric scaling need to be examined [5]. In this study, however, practical and technological constraints prevented complete similitude between the half-scale specimens and the full-scale prototype structures. No supplementary mass was affixed to the half-scale specimens. Attaching supplementary mass in a manner that would permit complete, unrestrained, and compatible response between the specimens and masses was judged to be quite difficult, time-consuming, and probably not cost effective. TESS can provide large input accelerations, however, permitting the specimens to be driven to levels of damage comparable to what they might sustain if fitted with supplementary masses.

Similitude between scaled and prototype material mechanical properties generally imposes severe theoretical and practical restrictions on the possible selection of specimen materials. At small scales, a lack of similitude can result in significant distortions between scale and prototype responses. For this study, however, the relatively large scaling factor of one-half did not change the essential behavioral characteristics discussed here, such as the tendency of the roof diaphragm to respond independently of the transverse shear walls.

True similitude between scale specimen and prototype building would have required scaling the time dimension of the ground motions by the square root of the geometric scaling factor. The relaxed similitude constraints discussed here (no supplementary masses, the use of prototype materials, and the fact that gravity response was not important) were met by scaling the time dimension by the geometric scaling

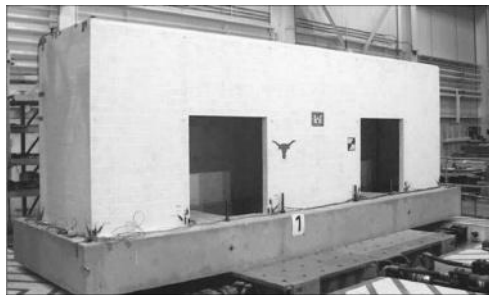


FIG. 4—Overall photo of Specimen #1.

TABLE 1—Roof diaphragm design of half-scale specimens.

Specimen	Prototypical Element	Half-Scale Element
#1 (lumber)	SPF 1-1/2 in. by 11-1/2 in. (38 mm by 290 mm) joists	SPF 3/4 in. by 5-1/2 in. (19 mm × 140 mm) joists
	SPF 3/4 in. by 5-1/2 in. (19 mm by 140 mm) sheathing 8d or 10d nails	SPF 3/8 in. by 3-1/4 in. (10 mm by 83 mm) sheathing 4d nails
#2 (metal deck)	12 to 24 in. (300 to 600 mm) deep OWJ	Vulcraft-8K1, 8 in. (200 mm) deep OWJ
	18 to 22 gauge, wide-rib decking One to three #10 side-lap screws per span	Vulcraft-1.5B22, wide-rib deck One #10 side-lap screw per span
	36/3 to 36/4 puddle welding	36/3 puddle welding

factor—in this case, 1/2. This preserved the relationship between spectral peaks of the input records and the lower natural frequencies of the half-scale specimens, thus allowing the responses of the half-scale specimens to be consistently related to those of the prototypes.

Shaking-table testing used artificial ground motions developed by Wen and Wu [6] for Carbondale, IL. In the nomenclature of that study, the motions selected for transverse and longitudinal excitation were, respectively, C02_09s and C02_03s (prototype peak ground accelerations (PGAs) of 0.67g and 0.55g, respectively). For the reasons discussed above, the input time steps of those motions were changed from 0.010 to 0.005 s. The scaled input record had ordinates (acceleration values) identical to those of the prototype record.

Dimensional analyses show that the prototype structures would have sustained higher levels of damage, as discussed later in the paper, than the half-scale specimens under the same levels of excitation. Specifically, for a given ground motion in the appropriate time scale, stresses in the prototype structures would have been twice as large as those in the half-scale specimens. The additional damage would have likely manifested itself as additional cracking along yield lines, and increased damage to the roof diaphragms. This relaxed similitude between scale and prototype mass and scale and prototype material mechanical properties did not adversely affect the results of the study; the conclusions regarding the response of the half-scale specimens are therefore valid for the full-scale prototype structures as well.

Concept of Diaphragm Drift Ratio

Potential damage sustained by the half-scale specimens can be characterized using drift ratios. Drift ratios are typically calculated by dividing the interstory drift between two floor levels by the corresponding interstory height. The structural engineering community generally accepts that ratio as an index of potential structural damage for framed structures with rigid floor diaphragms. Potential seismic damage in walled structures with flexible horizontal diaphragms, however, cannot be completely characterized by interstory drift. It must also be characterized by a measure of the in-plane deformation of the horizontal diaphragms themselves. The diaphragm drift ratio (DDR) is one such measure:

TABLE 2—Dynamic properties of half-scale specimens before seismic testing.

Specimen	Direction	Lowest Natural Frequency, Hz (s)	Equivalent Viscous Damping, %
#1 (lumber)	Transverse	14 (0.071)	3
	Longitudinal	20 (0.050)	7
	Vertical	38 (0.026)	3
#2 (metal deck)	Transverse	12 (0.083)	5
	Longitudinal	20 (0.050)	5
	Vertical	25 (0.025)	N/A (data lost)

TABLE 3—Eleven seismic test motions for Specimen #1 (*L* = Longitudinal, *T* = Transverse).

Test	Direction	Input PGA, <i>g</i>		Measured PGA, <i>g</i>	
		Longitudinal	Transverse	Longitudinal	Transverse
1	T	—	0.10	—	0.10
2	L	0.08	—	0.10	—
3	T	—	0.50	—	0.48
4	L	0.41	—	0.41	—
5	T	—	0.67	—	0.67
6	L	0.55	—	0.55	—
7	L+T	0.28	0.33	0.29	0.33
8	L+T	0.55	0.67	0.57	0.67
9	T	—	1.00	—	1.05
10	T	—	1.34	—	1.49
11	L+T	1.10	1.34	0.99	1.54

$$DDR = \frac{\Delta_{\text{diaph}}}{L/2} \quad (1)$$

where Δ_{diaph} is the in-plane deflection of the diaphragm at a given floor level relative to the supporting shear walls at that level and L is the plan length of the diaphragm. In the case of Specimens #1 and #2, L is 264 in. (6700 mm), and the characteristic deflection Δ_{diaph} is taken from test data.

Seismic Testing of Half-Scale Specimens

The half-scale specimens were initially subjected to low-level ($PGA < 0.1g$) dynamic tests intended to evaluate their natural frequencies and equivalent viscous damping ratios (Table 2). White-noise and sine-sweep or resonant-search excitations, performed prior to seismic testing, provided the natural frequencies of the half-scale specimens. Sine-decay testing, performed prior to seismic testing, provided their equivalent viscous damping ratios. White-noise tests, following each seismic test, were used to detect test-to-test changes in natural their frequencies.

Seismic Testing of Specimen #1 (Lumber Sheathing)—Specimen #1 was subjected to a sequence of 11 seismic tests at increasing levels of maximum input acceleration (PGA). The 11 input records were the modified Motions C02_09s and C02_03s, scaled to predetermined and generally increasing maximum input accelerations. From each uniaxial test to the next, the direction of excitation was alternated between longitudinal and transverse, so that the structure would sustain similar deterioration in both principal plan directions as the test sequence progressed (Table 3). Visible and audible damage to Specimen #1 occurred first during Test 5, at a maximum input acceleration of 0.67*g*, and increased with increasing maximum excitations. At maximum input accelerations greater than 1.00*g* (Tests 9, 10, and 11), cracking propagated throughout the structure along what became evident out-of-plane yield lines (Fig. 5). Also, one of the transverse walls developed bed-joint cracks that were characteristic of wall rocking. Visible damage to the roof diaphragm finally occurred at a maximum input acceleration of 1.05*g* in the transverse direction (Test 9). Inspection revealed splitting at nailing points; the end of one piece of sheathing lumber pulled loose; and some sheathing split parallel to the grain. The diaphragm sustained no other visible damage.

Seismic Testing of Specimen #2 (Metal Deck)—Specimen #2 was subjected to a sequence of 12 seismic tests at increasing levels of maximum input acceleration. As with Specimen #1, the 12 input

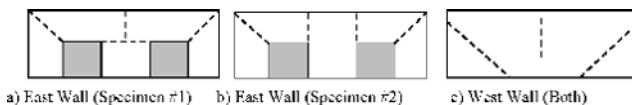


FIG. 5—Observed yield lines in longitudinal walls. (a) East Wall (Specimen #1). (b) East Wall (Specimen #2). (c) West Wall (both).

TABLE 4—Twelve seismic test motions for Specimen #2 (*L* = Longitudinal, *T* = Transverse).

Test	Direction	Input PGA, <i>g</i>		Measured PGA, <i>g</i>	
		Longitudinal	Transverse	Longitudinal	Transverse
0	L	0.05	—	0.03	—
1	L	0.17	—	0.11	—
2	T	—	0.20	—	0.16
3	L+T	0.12	0.20	0.07	0.16
4	L	0.33	—	0.23	—
5	T	—	0.40	—	0.34
6	L+T	0.23	0.40	0.15	0.35
7	L	0.83	—	0.55	—
8a	L	1.25	—	0.91	—
8b	L	2.20	—	1.56	—
9	T	—	1.00	—	0.86
10	T	—	1.34	—	1.13

records were the modified Motions C02_09s and C02_03s, scaled to predetermined and generally increasing maximum input accelerations. In contrast to Specimen #1, the testing sequence was coordinated to minimize the possible influence of prior damage in each of the two principal plan directions of the structure. Several longitudinal tests at increasing levels of maximum input acceleration preceded high-level transverse testing (Table 4). At a peak longitudinal input acceleration of 0.91*g* (Test 8a), visible and audible damage occurred when two puddle welds connecting the metal deck to the OWJ failed. At a maximum longitudinal input acceleration of 1.56*g* (Test 8b) diaphragm damage increased when an additional puddle weld fractured and a shear crack formed above the north opening in the east perforated longitudinal wall, though the longitudinal walls were otherwise undamaged. Damage spread quickly and extensively throughout the structure during strong transverse excitation. As with Specimen #1, cracking propagated through the walls along what became evident out-of-plane yield lines (Test 9, Fig. 5). At a maximum input acceleration of 1.13*g* (Test 10) in the transverse direction, additional damage occurred to the roof diaphragm; side-lap screws at the north and south ends of the diaphragm pulled out.

Results and Implications of Seismic Testing

Results of seismic tests are summarized in Tables 5 and 6. Instrumentation of the half-scale specimens measured deformations, displacements and accelerations. The data presented here are typical, and were selected to convey significant concepts. For instance, Fig. 6 shows the deformed shape of Specimen #1's roof diaphragm during peak response, during the ninth seismic test only. Similar figures are not provided for the other ten seismic tests, although identical conclusions could have been drawn from any of those. Mechanical properties of the masonry used in the half-scale specimens were also measured.

The approximate deformed shape of the diaphragms at any time during a test could be determined by analyzing the diaphragm response data as illustrated in Fig. 7. Figure 6 shows an example of this with the approximate shape of the diaphragms of Specimen #1 and #2, during peak response of Test 9. The figure shows, as expected, that shearing deformations dominated the overall in-plane response of the diaphragms.

TABLE 5—Observed diaphragm drift ratio and related damage (Specimen #1).

Element	Test	PGA, <i>g</i>	DDR, %	Damage
Longitudinal Walls	5	0.67	0.2	Hairline cracking of out-of-plane walls
Longitudinal Walls	9	1.05	0.35	Extensive cracking of out-of-plane walls, distinct cracking patterns emerge, yield lines begin to emerge
Longitudinal Walls	10	1.49	0.7	Extensive cracking, hinging about distinct out-of-plane yield lines, slight spalling at crack edges
Diaphragm	10	1.49	0.7	Splitting of sheathing at nailing points, nail withdrawal

TABLE 6—Observed drift and related damage (Specimen #2).

Element	Test	PGA, <i>g</i>	DDR, %	Damage
Longitudinal Walls	5	0.34	0.09	Hairline cracking of out-of-plane walls
Longitudinal Walls	9	0.86	0.40	Extensive cracking of out-of-plane walls, distinct cracking patterns emerge, yield lines begin to emerge
Longitudinal Walls	10	1.13	1.00	Extensive cracking, hinging about distinct out-of-plane yield lines, slight spalling at crack edges
Diaphragm	10	1.13	1.00	Side-lap screw withdrawal and bearing failure

Analytical studies, discussed subsequently, calculated a fundamental mode of response controlled by the in-phase, in-plane, and single-curvature response of the roof diaphragm and the transverse shear walls. Figure 6 corroborates this, and shows that the roof diaphragms of both specimens responded in-plane and approximately in single curvature. Figure 8 shows that the plan center of the diaphragm of Specimen #1 and the tops of that specimen’s transverse shear walls responded primarily in phase during transverse response. That observation implies that the transverse response of the diaphragm was dominated by the fundamental mode of the specimen. The arrows in Fig. 9, however, mark several typical regions of amplitude cancellation (“beating”) in the acceleration response of Specimen #1, during Test 5. Figure 9 therefore suggests that a higher mode participated in the acceleration response of the specimen at a detectable but small level. Specimen #2 exhibited behavior very similar to that shown in Figs. 8 and 9.

The transverse shear walls of the specimens remained elastic during low levels of excitation, with no visible cracking or permanent deformation. This observation is substantiated by the fact that even at high input accelerations, wall drift ratios are less than 0.1 %. During very strong seismic tests ($PGA > 0.67g$), however, a continuous bed-joint crack developed along the entire plan length of the south shear wall in Specimen #1. This crack was characteristic of rigid-body rotation of the shear wall about that crack (wall rocking). Shear walls of Specimen #2 remained elastic throughout the seismic testing.

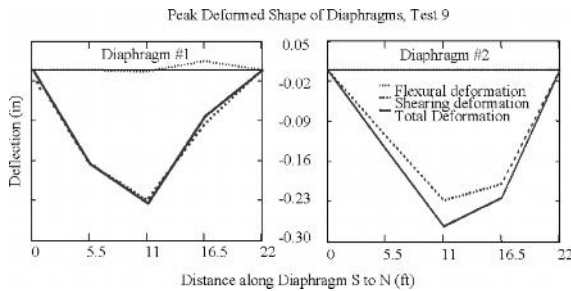


FIG. 6—Deformed shape of diaphragms during peak response (Test 9).

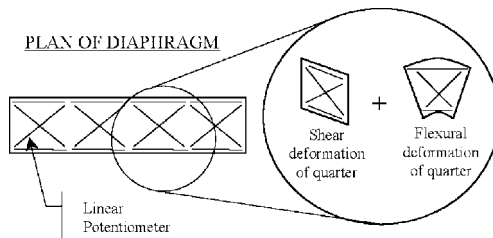


FIG. 7—Characteristic deformations of instrumented diaphragm quarters.

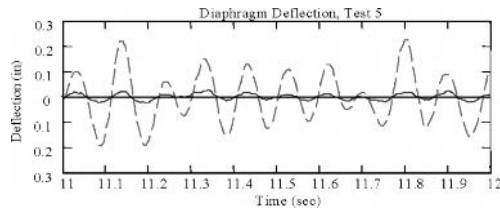


FIG. 8—Transverse displacement response of center of diaphragm and tops of transverse shear walls as measured relative to base of specimen (Test 5, Specimen #1).

Quasi-Static Testing of Roof Diaphragms

Following the shaking-table tests, the diaphragms and the top four courses of the attached masonry walls were removed from the half-scale specimens, and tested quasi-statically. The diaphragm-masonry chord assembly from Specimen #1 is called Diaphragm #1; the diaphragm-masonry chord assembly from Specimen #2 is called Diaphragm #2. Visibly damaged components of the diaphragms were removed, replicated, and replaced in their original configuration. Specifically, five pieces of damaged sheathing lumber were replaced in Diaphragm #1 and the metal deck was replaced in Diaphragm #2.

During the quasi-static testing, the diaphragms were tested in a horizontal orientation, supported by a steel test frame bolted to the CERL strong floor (Fig. 10). Four, 12-in. (300 mm), built-up, box columns supported the diaphragms at their corners, and structural channels supported the diaphragms at their third points. Greased tetrafluoroethylene (Teflon®) pads were placed between the supporting channels and their contact points on the diaphragms to reduce frictional forces between the channels and the diaphragm assembly.

The diaphragms were loaded at their two outer quarter points using 50-kip (222,400-N) actuators, each with a maximum stroke of ± 3.0 in. (76 mm). The actuators maintained equal displacements throughout the testing. To distribute the applied load between the two longitudinal masonry chords, two loading struts made of structural tubing connected the east and west masonry chords at the points of load application.

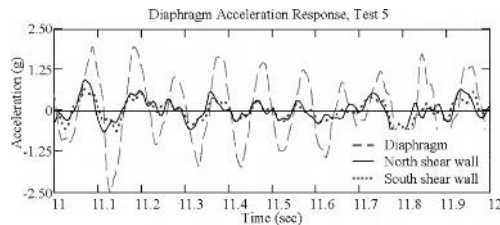


FIG. 9—Transverse acceleration response of center of diaphragm and tops of transverse shear walls (Test 5, Specimen #1).

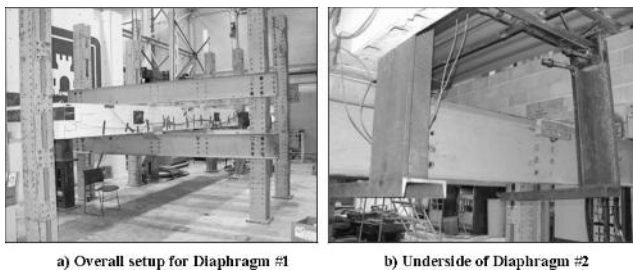


FIG. 10—Test setups for quasi-static testing of diaphragms. (a) Overall setup for Diaphragm #1. (b) Underside of Diaphragm #2.

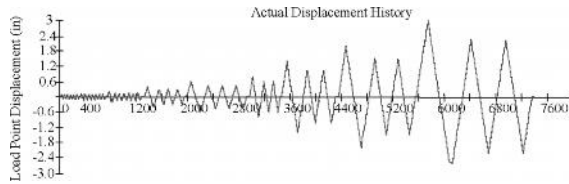


FIG. 11—Displacement history of actuators for quasi-static testing of Diaphragm #1, similar for Diaphragm #2.

The diaphragms were probably subjected to twisting moments in a vertical plane about their longitudinal axes as a result of vertical eccentricity between the shear centers of the diaphragms and the lines of action of the actuators. The test setup for Diaphragm #1 used channels above and below the diaphragm, resting on Teflon® pads, to restrain possible out-of-plane rotations resulting from those moments (Fig. 10(a)). Similarly, the test set up for Diaphragm #2 used L-shaped members extending from the connection between the load strut and the masonry wall, below the supporting channels, and resting on low-friction bearings attached to those channels (Fig. 10(b)). The diaphragms were loaded using a protocol [7] that required that displacement histories comprise a sequence of large cycles to monotonically increasing maximum displacement, each followed by several smaller-amplitude cycles (Fig. 11).

Quasi-Static Testing of Diaphragm #1 (Lumber Sheathing)—Diaphragm #1 sustained slight visible damage at diaphragm drift ratios (DDRs) less than 0.6 % (load-point deflections less than 0.8 in. (20 mm)). Damage occurred in the form of longitudinal splitting at nail holes, some nail withdrawal, and some nail tear-out at board ends. Damage increased with increasing diaphragm drift ratios. At a DDR of 1.1 % (load-point deflection of 1.4 in. (36 mm)) some nails connecting blocking elements and nailers partially withdrew in the corners of the diaphragm. Diaphragm #1 sustained significant damage at DDRs greater than 1.1 %: tension butt splices spread significantly; several nails withdrew from connecting joists; several nails tore through the ends of the connecting sheathing boards; and several sheathing boards sustained additional longitudinal splitting at points of nailing.

Quasi-Static Testing of Diaphragm #2 (Metal Deck)—Damage to metal-deck diaphragms generally manifests itself as failed deck-to-joist and deck-to-deck connections. To detect weld damage, puddle welds were coated with a thin layer of Hydrostone®. Diaphragm #2 sustained no visible damage at diaphragm drift ratios less than 0.45 % (load-point deflections less than 0.6 in. (15 mm)). At a DDR of 0.45 %, many of the Hydrostone® weld coatings in the south-end quarter and north-end quarter flaked slightly, suggesting yielding of the metal deck around the welds. At a DDR of 0.61 % (load-point deflection of 0.8 in. (20 mm)) decking panels in the south-end quarter and the north-end quarter buckled out of plane (Fig. 12), and one weld failed (Fig. 13(a)). Decking panels in the two outer quarters of the diaphragm consistently buckled out of plane at diaphragm drift ratios greater than about 0.6 %. Such buckling does not indicate failure, provided that sufficient connectivity is maintained between the panels and surrounding frame to mobilize diagonal tension fields in each direction when the diaphragm is subjected to reversed cyclic loading. Eventual failure of the panel welds at higher diaphragm drift ratios, however, ultimately destroyed

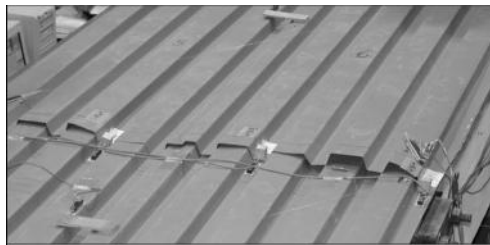


FIG. 12—Example of out-of-plane panel buckling in north-end quarter at high diaphragm drift ratio.

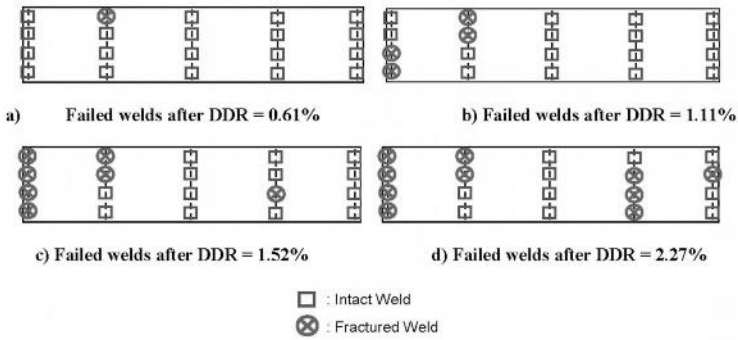


FIG. 13—Locations of failed puddle welds with increased diaphragm drift ratios. (a) Failed welds after $DDR = 0.61\%$. (b) Failed welds after $DDR = 1.11\%$. (c) Failed welds after $DDR = 1.52\%$. (d) Failed welds after $DDR = 2.27\%$.

the tension fields, thus precluding further panel buckling.

Damage increased with increasing diaphragm drift ratios. Figures 13(b)–13(d), summarize the weld failures observed at high diaphragm drift ratios. As the applied DDR was increased, damage increased in the form of weld failure and bearing deformation of side-lap screw into the metal deck. At a maximum DDR of 2.27 % (load-point deflection of 3.0 in. (76 mm)) a sufficient number of welds had failed such that the metal decking no longer significantly contributed to the shear strength or stiffness of the diaphragm.

All damage sustained by the diaphragms occurred in their outer two quarters. This is consistent with the hypothesis that since in-plane deformations of the diaphragm result almost entirely from shearing deformations of the two outer quarters, those should sustain much more damage than the two inner quarters under transverse loading.

Result and Implications of Quasi-Static Testing

Data from the instrumentation of Diaphragms #1 and #2 were evaluated for deflections, deformations, and, where appropriate, internal strains. Of particular interest were the hysteretic relationships between applied lateral load and diaphragm drift ratio.

Hysteretic Behavior of Diaphragm #1—The diaphragm was supported at its third points by structural channels. At those support points the diaphragm slid on greased tetrafluoroethylene (Teflon®) pads. Some frictional forces still resisted the applied lateral forces, however. This effect is especially pronounced in hysteresis of the diaphragm at very low levels of deformation ($DDR < 0.6\%$), when the diaphragm itself should respond in a linear-elastic manner (Fig. 14(a)). The loops in that figure have constant loading and unloading slopes but are open, implying frictional dissipation of energy. In the case of Diaphragm #1,

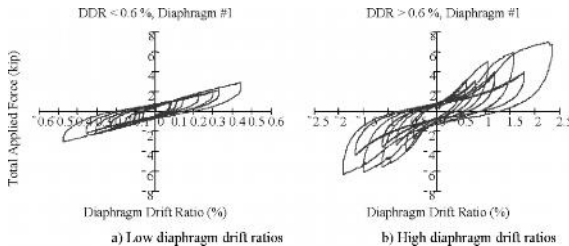


FIG. 14—Relationship between applied load and diaphragm drift ratio of Diaphragm #1. (a) Low diaphragm drift ratios. (b) High diaphragm drift ratios.

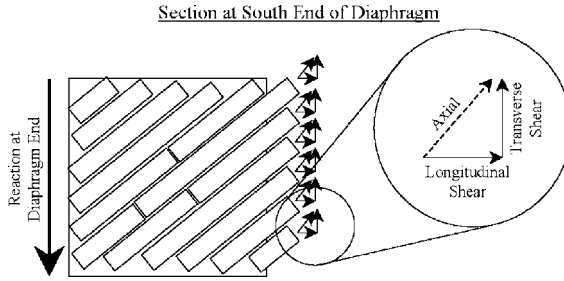


FIG. 15—Decomposition of measured axial forces in sheathing boards.

friction develops from two mechanisms: friction between the Teflon® pads and friction within the diaphragm itself. Those forces totaled about 0.50 kip (2224 N). Diaphragm #1 had an elastic stiffness (Force/DDR) of about 7 kips (31 100 N) for each increase of one percentage point in diaphragm drift ratio. In other words, Diaphragm #1 had an effective elastic shearing rigidity $A'G$ of about 175 kip (778 400 N), where

$$A'G = \frac{VL}{8\Delta} \quad (2)$$

and V is the total applied load to the diaphragm, L is the length of the diaphragm, and Δ is deflection of the diaphragm.

Although Figs. 14(a) and 14(b) have identical vertical axes, their horizontal axes differ. Figure 14(a) includes both major and minor cycles of applied lateral force and shows that Diaphragm #1 exhibited stable hysteretic behavior for diaphragm drift ratios less than 0.6 %. Figure 14(b) also includes both major and minor cycles of applied lateral load and shows that, for high diaphragm drift ratios (DDR > 0.6 %), Diaphragm #1 sustained considerable stiffness degradation and no strength degradation. Others have made a similar observation (for example, Medearis and Young [8]). Diaphragm #1 also exhibited considerable hysteretic pinching behavior at high levels of diaphragm drift ratio (Fig. 14(b)). In the case of a diagonally sheathed lumber diaphragm, pinching occurs as a result of bearing failure of the sheathing at nail holes, and plastic deformation of the nails themselves. These mechanisms were observed in these tests, and have been noted elsewhere (for example, Soltis and Mtenga [9]).

Instrumentation of Diaphragm #1 provided in-plane longitudinal strains in the diaphragm sheathing, in a transverse cross section, in the south-end quarter of the diaphragm. Sheathing board axial forces, derived from the measured strains, were decomposed into components aligned with the transverse and longitudinal axes of the diaphragm (Fig. 15). The components of force parallel to the transverse axis of the building thus represented the in-plane shear force in the sheathing. Figures 16(a) and 16(b), respectively, show the measured shear in the sheathing, at that particular cross section in the diaphragm, for cycling at a low diaphragm drift ratio and a high diaphragm drift ratio.

Figure 16(a) shows that the diaphragm sheathing resisted only a portion of the total applied shear in

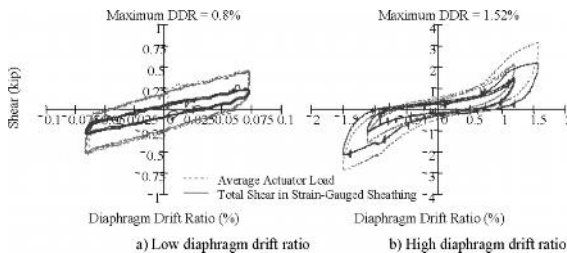


FIG. 16—Comparison of applied in-plane shear and that resisted by lumber sheathing. (a) Low diaphragm drift ratio. (b) High diaphragm drift ratio.

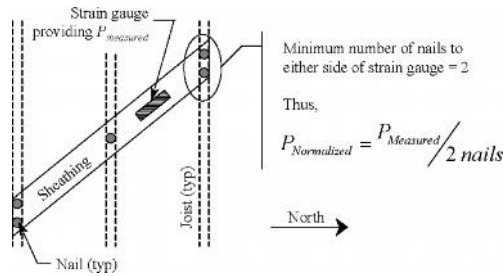


FIG. 17—Schematic process for normalizing axial forces in sheathing boards.

the diaphragm. Frictional forces between the test frame and the diaphragm assembly, as well as those within the sheathing, resisted a significant portion of the applied lateral load at low levels of diaphragm drift ratios. Masonry chords and lumber nailers also resisted in-plane shears by their own out-of-plane bending stiffnesses. This is detectable by the difference in slopes of the hysteretic loops for the instrumented sheathing and for the total applied shear (Fig. 16(a)).

Unlike material resistance, frictional resistance does not change with deformation. Comparison of Figs. 16(a) and 16(b) shows that the diaphragm sheathing and nails resisted a greater proportion of the applied shear at higher diaphragm drift ratios; the proportion of lateral force resisted by friction decreases with increasing deformations.

Strain data from the sheathing also permitted the determination of a force profile across the transverse cross-section of the diaphragm. Typically, the complex nature of a lumber diaphragm precludes a rational determination of such a force profile. Many researchers have shown, however, that the in-plane flexibility and strength of a lumber-sheathed diaphragm depends chiefly on the number and size of the sheathing nails [10–14]. For that reason, the measured axial force in each sheathing board was divided by the lesser number of nails, on either side of the strain gauge, over the length of that board. For instance, if a board had two nails connecting it to the diaphragm north of its strain gauge and three nails connecting it to the diaphragm south of its strain gauge, the axial force in the board was divided by 2 (Fig. 17). This process effectively normalized the force in each board by the smaller number of nails connecting that board and allowed comparison among sheathing boards in the same transverse cross-section of the diaphragm.

This normalization was justified only when each nail resisted approximately equal force. At low diaphragm drift ratios (in the elastic range of response for the diaphragm), the actual distribution of force to each nail, for a particular sheathing board, could not be determined by simple rational analysis. At high diaphragm drift ratios, near the lateral load capacity of the diaphragm, the nails of the strain-gauged sheathing boards were observed to behave well into their inelastic range. It is thus plausible that the nails of a given sheathing board resisted similar loads at high diaphragm drift ratios. For these reasons, the normalized force distribution is presented, as an example, at a high diaphragm drift ratio of $\pm 1.52\%$ (Figs. 18(a) and 18(b)).

That figure shows that the distribution of normalized axial forces across that particular transverse cross section of Diaphragm #1 was approximately uniform. The normalized axial forces are a measure of transverse force per nail, for the nails comprising the lesser group that lay to either side of the strain gauge. The LRFD Reference Lateral Resistance for the nails (4d) used in Diaphragm #1 is about 130 lb (578 N) [14]. Figures 18(a) and 18(b) show average nail forces, respectively, of about 100 lb (445 N) and about 130 lb (578 N), consistent with that value.

Normalized axial forces vary somewhat, however. Reasonable variation in the normalized axial force, as seen for instance in the middle nine boards, was expected due to the complex nature of a lumber diaphragm and the simplified techniques used here to evaluate it. The larger anomalous variations (for instance, second-to-last board in Fig. 18(a) and first and last boards in Fig. 18(b)) may result from one or more of the following: relatively high in-plane or out-of-plane bending of the board; erroneous strain data; erroneous or uncharacteristic elastic moduli; or other sources. Nevertheless, the conclusion of uniformly distributed normalized axial forces in that particular cross section of Diaphragm #1, is reasonably consistent and is thus justified.

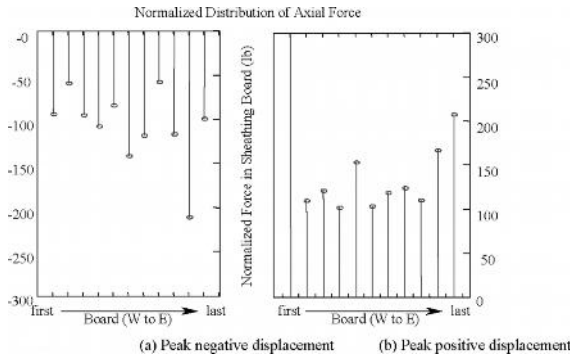


FIG. 18—Normalized axial force distribution in sheathing boards, for a transverse cross section in south-end quarter, at peak diaphragm drift ratios (Diaphragm #1, $DDR = \pm 1.52\%$). (a) Peak negative displacement. (b) Peak positive displacement.

Hysteretic Behavior of Diaphragm #2 (Metal Deck)—For similar reasons discussed for Diaphragm #1 of this report, frictional forces in the test setup for Diaphragm #2 resisted a portion of the applied lateral forces. This effect is especially pronounced in hysteresis of the diaphragm at low levels of diaphragm drift ratio, when the diaphragm should respond in a linear-elastic manner.

Figure 19(a) shows the hysteretic relationship between the applied load and the diaphragm drift ratio for Diaphragm #2, for low levels of diaphragm drift ratio ($DDR < 0.45\%$). That figure shows that frictional forces totaled about 0.42 kip (1870 N) and that Diaphragm #2 had an elastic stiffness (Force/DDR) of about 6.3 kips (28 000 N) for each increase of one percentage point in drift. Similarly, Diaphragm #2 had an effective elastic shearing rigidity, $A'G$ (2), of about 160 kips (711 700 N).

Figure 19(a) includes both major and minor cycles of applied lateral force, and shows that Diaphragm #2 exhibited stable hysteretic behavior for diaphragm drift ratios less than 0.45%. Figure 19(b) also includes both major and minor cycles of applied lateral load and shows that, for high diaphragm drift ratios ($DDR > 0.45\%$), the diaphragm sustained considerable stiffness and strength degradation. Furthermore, the figure shows that the diaphragm maintained a linear elastic relationship of load and diaphragm drift ratio between points of significant strength degradation.

Welded metal-deck diaphragms exhibit nonlinear behavior because of yielding and tearing of metal deck around welds and side-lap connectors, out-of-plane buckling of the metal-deck panels, and failure of welds and side-lap connectors. The first two are generally not significant, however. Yielding occurs only in regions very local to the welds and side-lap screws, and thus does not significantly affect the load-drift relationship of the diaphragm. Buckling is generally detectable but not significant because metal-deck panels preserve significant in-plane stiffness by maintaining diagonal tension fields. Weld failure, however, significantly decreased the strength and stiffness of Diaphragm #2 and can be seen by comparing the

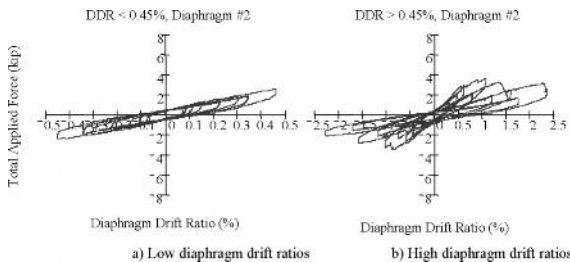


FIG. 19—Relationship between applied load and diaphragm drift ratio of Diaphragm #2. (a) Low diaphragm drift ratios. (b) High diaphragm drift ratios.

number of failed welds in the diaphragm during each test (Figs. 13(a)–13(d) with the corresponding apparent diaphragm stiffness and maximum load sustained during that cycle (Figs. 19(a) and 19(b)).

Summary and Conclusions from Phase 1 (Behavior)

The half-scale specimens were moderately damaged from shaking-table tests. Their masonry walls sustained damage in the form of yield lines and some slight shear cracking. The lumber diaphragm of Specimen #1 was lightly damaged, sustaining nailing-point splitting and some splitting parallel to the grain. The metal deck diaphragm of Specimen #2 was moderately damaged, sustaining fracture of puddle welds and pullout of side-lap screws. Both diaphragms deformed primarily in shear. Structural scaling theory implies that the prototype structures would have sustained higher levels of damage than the half-scale specimens under the same magnitude of excitation. The additional damage would probably have been in the form of additional cracking along yield lines, and increased damage to the roof diaphragms.

During quasi-static testing, diagonally sheathed Diaphragm #1 exhibited stable overall hysteretic behavior with significant degradation of lateral stiffness at diaphragm drift ratios greater than 0.6 %. Bearing deformation in the wood matrix around nail holes, in combination with plastic deformation of the nails themselves, caused pinching in the hysteretic loops. A uniform distribution of in-plane forces in the sheathing of Diaphragm #1 was identified at high diaphragm drift ratios. The magnitudes of those forces were consistent with the predicted strength of diaphragm nails, confirming the general belief that strength of the nails controlled the overall strength of the diaphragm. Welded metal deck Diaphragm #2 exhibited stable hysteretic behavior with little degradation of lateral stiffness at diaphragm drift ratios less than 0.45 %. The diaphragm exhibited unstable nonlinear-elastic hysteretic behavior with significant degradation of lateral strength and stiffness at diaphragm drift ratios greater than 0.45 %. Failure of welds caused abrupt degradations in strength and stiffness.

In contrast to what is usually assumed in design, low-rise reinforced masonry buildings with flexible roof diaphragms do not behave as systems with a single degree of freedom associated with the in-plane response of the shear walls. Rather, they behave at least as 2DOF systems (with one degree of freedom associated with the in-plane shear walls and one with the roof diaphragm), and essentially as SDOF systems with that degree of freedom associated with the in-plane response of the roof diaphragm.

The in-plane deformations of the diaphragm and consequent levels of damage can be characterized using the diaphragm drift ratio. That drift ratio could be useful for the seismic evaluation of these types of buildings.

Phase 2: Analysis

From August 2001 to August 2002, a simple analysis tool was developed, tested, and validated based on observations and conclusions from Phase 1 (Behavior). A 2DOF analysis tool was developed for the general case and then analytically bounded, through parameter studies, to the particular analysis of low-rise reinforced masonry buildings with flexible diaphragms. Parameter studies suggested that the 2DOF tool could be further simplified to a SDOF system, with that degree of freedom associated with the in-plane response of the diaphragm only. The 2DOF and SDOF tools were validated in the linear elastic and nonlinear ranges of response using data from shaking-table testing, finite-element modeling (FEM), and lumped-parameter modeling. Results of analytical modeling of masonry structures with flexible diaphragms are reported in Abrams and Paulson [15], Costley and Abrams [16], Tena-Colunga and Abrams [17], and Tena-Colunga [18]. Other previous studies include the seminal work of Agbabian, Barnes, and Karotis [19], which investigated the performance characteristics of wooden diaphragms and their effects on masonry buildings.

Linear Elastic Finite-Element Modeling

Linear elastic finite-element models representing the half-scale shaking-table specimens were created using SAP2000 [20] to validate low-level measured responses from shaking-table tests and test the accuracy and efficacy of the modeling approach. Since the models were linear and elastic, they were useful only to compare calculated and measured responses at low levels of input acceleration. Observations of cracking patterns during testing suggested that the specimens remained basically elastic during tests with

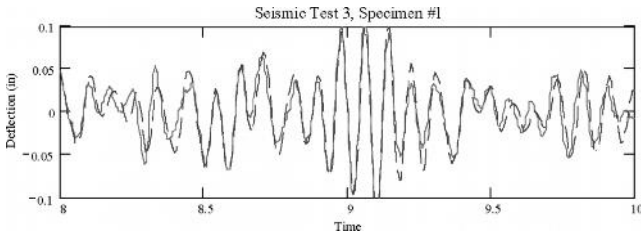


FIG. 20—2-*s* comparison of measured and calculated diaphragm deflection during peak response (Test 3, Specimen #1).

peak ground accelerations less than about 0.50g. In general, the third seismic test (Test 3) of Specimen #1 and the fifth seismic test (Test 5) of Specimen #2 provided the bases for this modeling. Modeling used measured table accelerations, in both the longitudinal and transverse directions, for model input accelerations to eliminate the possibility of spurious shaking-table accelerations causing disagreement between the calculated and measured responses. Clark [21] offers a complete discussion of the possible sources of such unintended table accelerations and the techniques used to reduce those accelerations.

Calibration of calculated to measured responses for Specimen #1 was somewhat iterative. To calibrate the shearing flexibility of the diaphragm, the thickness of the diaphragm shell elements was systematically decreased from the specified sheathing thickness, 3/8 in. (9.5 mm) to zero, in increments of 1/16 in. (1.6 mm). Similarly, the equivalent viscous damping ratio was systematically increased from 0 % to 5.0 %, in increments of 0.5 %. At each step in the calibration process, the finite-element model was run and calculated and measured responses were compared. Using a diaphragm shell-element thickness of 1/16 in. (1.6 mm), the measured modulus of the masonry (325 ksi, 2241 MPa), and an equivalent viscous damping ratio of 5.0 % led to a sufficient level of agreement between the measured and calculated responses of Specimen #1 (Fig. 20).

The difference between specified diaphragm thickness and that used in the final analysis was expected. Flexibility of complex lumber assemblages, such as a diaphragm, derives from several mechanisms, chief among which is the flexibility of the nails, rather than that of the lumber. Decreasing the element thickness, as done in this study, represents only one method of arriving at an effective shearing rigidity. An equally justifiable method would have been to systematically decrease the shear modulus of the diaphragm material until there was a sufficient agreement between calculated and measured responses.

Calibration of calculated to measured responses of Specimen #2 was more direct than that for Specimen #1. An effective shearing rigidity of 560 kip (2490 MN) for the diaphragm was calculated using the published procedures of the Steel Deck Institute [22,23]. Using that value, the measured modulus of the masonry (480 ksi, 3309 MPa), and the measured value for the equivalent viscous damping ratio in the transverse direction (5.0 %) led to consistent overall agreement in the time history (for example, Fig. 21).

The models also calculated elastic stress patterns, and thus expected cracking patterns, in the masonry walls for any given ground motion. Those predictions agreed well with the observed cracking patterns of Specimen #1 and Specimen #2. Modeling of the specimens offered two important conclusions: measured

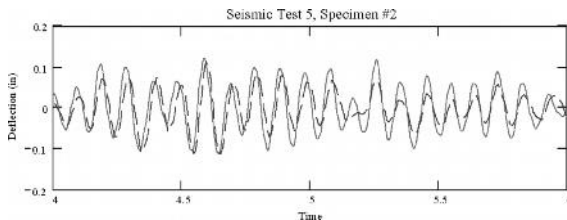


FIG. 21—2-*s* comparison of measured and calculated diaphragm deflection during peak response (Test 5, Specimen #2).

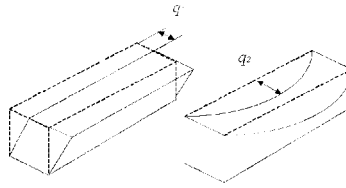


FIG. 22—Degrees of freedom for 2DOF idealizations.

responses of the shaking-table specimens are reliable; and relatively simple linear elastic finite-element models can accurately calculate linear elastic responses of these types of buildings.

Two-Degree-of-Freedom Idealization and Modeling

As discussed previously, low-rise reinforced masonry buildings with flexible roof diaphragms behave as 2DOF systems. Specifically, the roof diaphragm tends to respond independently of the transverse shear walls, and the transverse shear walls tend to respond together, in phase. To investigate the possibility of developing a simplified modeling approach based on these observations, these types of buildings were modeled as 2DOF systems. To do this, the generalized coordinates q_1 and q_2 , described in Fig. 22, were chosen. Because those generalized coordinates were selected so as to be kinematically independent, they are referred to here as degrees of freedom. The first (q_1) is associated with the in-plane deformation of the transverse shear walls. The second (q_2) is associated with the in-plane deformation of the diaphragm.

First Degree of Freedom, q_1 —Relative contribution of shearing and flexural deformations to the deflection of a cantilever shear wall depends on that wall’s vertical aspect ratio. This analysis considers both deformation mechanisms. Thus, the chosen shape function $\phi(y)$ has nonuniform first and second derivatives

$$\phi(y) = 1 - \cos\left(\frac{y\pi}{2H}\right) \tag{3}$$

where H is the height of building and y is the vertical coordinate. The generalized mass M_1^* associated with q_1 is

$$M_1^* = \int_0^H \mu(y)[\phi(y)]^2 dy = \frac{1}{5} \mu H + M_{diaph} \tag{4}$$

where $\mu(y)$, the mass of the building per unit height, is piecewise continuous because it must include the concentrated mass of the roof diaphragm M_{diaph} at $y=H$. The generalized stiffnesses, K_{s1}^* and K_{f1}^* , representing, respectively, the shearing stiffness and the flexural stiffness of one transverse shear wall associated with DOF q_1 are

$$K_{s1}^* = A'G \int_0^H [\phi'(y)]^2 dy = \frac{A'G \pi^2}{H} \frac{8}{8} \tag{5}$$

and

$$K_{f1}^* = EI \int_0^H [\phi''(y)]^2 dy = \frac{EI \pi^4}{H^3} \frac{4}{32} \tag{6}$$

where G =masonry shearing modulus, A' =effective shear area of transverse walls, E =masonry elastic modulus, and I =in-plane moment of inertia of transverse walls.

Thus, the total generalized stiffness for the two transverse shear walls is

$$K_1^* = 2 \cdot \frac{K_{s1}^* K_{f1}^*}{K_{s1}^* + K_{f1}^*} \tag{7}$$

Second Degree of Freedom, q_2 —The shape function approximating the deflected shape of the diaphragm during transverse excitation is

$$\phi(x) = \sin\left(\frac{\pi}{L}x\right) \quad (8)$$

where L is the longitudinal dimension of the building and x is the horizontal coordinate. The expression for the generalized mass M_2^* associated with the second degree of freedom q_2 is thus

$$M_2^* = \int_0^L \mu(x)[\phi(x)]^2 dx = \frac{1}{2}\mu L \quad (9)$$

where $\mu(x)$, the mass per unit length of the diaphragm plus one-half the mass per unit length of the longitudinal walls, is a constant μ . The in-plane responses of most flexible diaphragms are dominated by shearing deformations. Thus, the generalized stiffness K_2^* associated with the second degree of freedom q_2 is

$$K_2^* = A'G \int_0^L [\phi'(x)]^2 dx = A'G \frac{\pi^2}{2L} \quad (10)$$

For clarity, K_1^* is called k_{walls} , K_2^* is called k_{diaph} , M_1^* is called m_{walls} , and M_2^* is called m_{diaph} .

General Expressions for Modal Response—To arrive at general expressions describing the spectral response of a 2DOF system, it is useful to consider the ratios of the generalized stiffness and mass corresponding to degrees of freedom q_1 and q_1

$$\alpha \equiv \frac{K_2^*}{K_1^*} = \frac{k_{\text{diaph}}}{k_{\text{walls}}} \quad (11)$$

and

$$\beta \equiv \frac{M_2^*}{M_1^*} = \frac{m_{\text{diaph}}}{m_{\text{walls}}} \quad (12)$$

The equation of motion for an undamped MDOF system is

$$\mathbf{M}\ddot{\mathbf{u}} + \mathbf{K}\mathbf{u} = \mathbf{0} \quad (13)$$

For the generalized 2DOF system the stiffness matrix is

$$\mathbf{K} = \begin{Bmatrix} (k_{\text{walls}} + k_{\text{diaph}}) & -k_{\text{diaph}} \\ -k_{\text{diaph}} & k_{\text{diaph}} \end{Bmatrix} \quad \text{or} \quad \mathbf{K} = \begin{Bmatrix} (1/\alpha + 1) & -1 \\ -1 & 1 \end{Bmatrix} \alpha k_{\text{walls}} \quad (14)$$

and the mass matrix is

$$\mathbf{M} = \begin{Bmatrix} m_{\text{walls}} & 0 \\ 0 & m_{\text{diaph}} \end{Bmatrix} \quad \text{or} \quad \mathbf{M} = \begin{Bmatrix} 1 & 0 \\ 0 & \beta \end{Bmatrix} m_{\text{walls}} \quad (15)$$

The corresponding modal matrix of the system is

$$\Phi = \{\underline{\phi}_1 \ \underline{\phi}_2\} = \begin{Bmatrix} \phi_{11} & \phi_{12} \\ \phi_{21} & \phi_{22} \end{Bmatrix} \quad (16)$$

Dynamic response of these types of buildings is dominated by the fundamental mode (for example, Cohen et al. [2,3], Jain and Jennings [24], Tremblay and Steimer [25]). For that reason, this analysis considers only that mode. After arbitrarily assigning the diaphragm DOF a fundamental modal amplitude of $\phi_{21}=1$, the corresponding amplitude of the shear-wall DOF can be shown to be

$$\phi_{11} = \frac{\alpha - \gamma^2\beta}{\alpha} \quad (17)$$

The fundamental mode shape thus becomes

$$\underline{\phi}_1 = \begin{Bmatrix} \left(\frac{\alpha - \gamma^2 \beta}{\alpha} \right) \\ \alpha \\ 1 \end{Bmatrix} \quad (18)$$

Contribution of the fundamental mode to the total distribution of inertial mass is

$$\underline{s}_1 = \Gamma_1 \mathbf{M} \underline{\phi}_1 \quad (19)$$

where the scalar Γ_1 is

$$\Gamma_1 = \frac{\underline{\phi}_1^T \mathbf{M} \begin{Bmatrix} 1 \\ 1 \end{Bmatrix}}{\underline{\phi}_1^T \mathbf{M} \underline{\phi}_1} \quad (20)$$

Specific contributions of inertial mass to each DOF are

$$\underline{s}_1 = \begin{Bmatrix} s_1 \\ s_2 \end{Bmatrix} = \begin{Bmatrix} s_{\text{walls}} \\ s_{\text{diaph}} \end{Bmatrix} = m_{\text{walls}} \begin{Bmatrix} \phi_{11} \frac{\phi_{11} + \beta}{\phi_{11}^2 + \beta} \\ \beta \frac{\phi_{11} + \beta}{\phi_{11}^2 + \beta} \end{Bmatrix} \quad (21)$$

Similarly, inertial forces are

$$\underline{f}_1 = \begin{Bmatrix} f_1 \\ f_2 \end{Bmatrix} = \begin{Bmatrix} f_{\text{walls}} \\ f_{\text{diaph}} \end{Bmatrix} = S_a m_{\text{walls}} \begin{Bmatrix} \phi_{11} \frac{\phi_{11} + \beta}{\phi_{11}^2 + \beta} \\ \beta \frac{\phi_{11} + \beta}{\phi_{11}^2 + \beta} \end{Bmatrix} \quad (22)$$

where S_a is the spectral acceleration defined at the fundamental frequency ω_1 . Finally, the spectral displacements \underline{u}_1 are

$$\underline{u}_1 = \Gamma_1 \underline{\phi}_1 S_a = \Gamma_1 \underline{\phi}_1 \frac{S_a}{\omega_1^2} \quad (23)$$

or

$$\underline{u}_1 = \begin{Bmatrix} u_1 \\ u_2 \end{Bmatrix} = \begin{Bmatrix} u_{\text{walls}} \\ u_{\text{diaph}} \end{Bmatrix} = \frac{S_a}{\omega_1^2} \frac{\phi_{11} + \beta}{\phi_{11}^2 + \beta} \begin{Bmatrix} \phi_{11} \\ 1 \end{Bmatrix} \quad (24)$$

The fundamental frequency is

$$\omega_1 = \gamma \sqrt{\frac{k_{\text{walls}}}{m_{\text{walls}}}} \quad (25)$$

where γ can be shown to be

$$\gamma = \sqrt{\frac{1}{2\beta} [\beta + \alpha\beta + \alpha + (\beta^2 + 2\alpha\beta^2 - 2\alpha\beta + \alpha^2\beta^2 + 2\alpha^2\beta + \alpha^2)^{1/2}]}. \quad (26)$$

Implementation of 2DOF Idealization using Shaking-Table Specimens—To verify the accuracy of the 2DOF idealization, it was implemented using the two, half-scale shaking-table specimens. Most of the generalized mass and stiffness values described in Eqs. 4–10 were readily evaluated using measured quantities of the half-scale specimens. Equation 10, however, requires the shearing rigidity of the diaphragm ($A'G$). The in-plane stiffness of lumber sheathed diaphragms cannot be predicted by simple rational analysis (ATC 1981;²⁶ FEMA 1997a²⁷,b²⁸; WWPA 1973²⁹) [26–29]. Thus, in the case of Specimen #1, an effective shearing rigidity $A'G_{\text{eff}}$ of the diaphragm was derived empirically from experimental data.

The diaphragm shear $V(x,t)$ at any time t and at any distance x along the length of the diaphragm is

TABLE 7—Calculated and measured peak responses of Specimens #1 and #2.

Specimen	Model	Fundamental Frequency, Hz (s)	Diaphragm acceleration, g	Diaphragm displacement, in. (mm)
#1 (lumber)	Measured	14 (0.07)	1.6	0.120 (3.0)
	Finite-element model	12 (0.08)	1.8	0.128 (3.3)
	2DOF RSA	12 (0.08)	$S_a=1.5$	0.114 (2.9)
#2 (metal-deck)	Measured	12 (0.08)	1.2	0.120 (3.0)
	Finite-element model	10 (0.10)	1.2	0.115 (2.9)
	2DOF RSA	12 (0.08)	$S_a=1.2$	0.119 (3.0)

$$V(x,t) = \int_0^x \mu(\xi) \ddot{u}(\xi,t) d\xi \quad (27)$$

where $\mu(x)$ =mass associated with the response of the diaphragm, approximated here as the mass per unit length of the diaphragm plus one-half the mass per unit length of the longitudinal masonry walls; and $\ddot{u}(x,t)$ =lateral acceleration of the diaphragm.

In the case of Specimens #1 and #2, the transverse diaphragm acceleration is known at only three points: the two ends of the diaphragms and their plan centers. The transverse diaphragm acceleration can be estimated using a Ritz function $\Psi(x)$ such that

$$\ddot{u}(x,t) \approx \ddot{q}_1(t) + \Psi(x)\ddot{q}_2(t) \quad (28)$$

where $\Psi(x)=\sin(\pi/Lx)$; $\ddot{q}_1(t)$ =known acceleration history at the tops of the transverse walls; and $\ddot{q}_2(t)$ =known acceleration history at the plan center of the diaphragm relative to the tops of the transverse walls.

At the plan center of the diaphragm, the in-plane deflection due to shearing deformation is then

$$q_2(t) = \frac{1}{A'G_{\text{eff}}} \int_0^{L/2} \left[\int_0^x \mu(\xi) \ddot{u}(\xi,t) d\xi \right] dx \quad (29)$$

or

$$q_2(t) = \frac{1}{A'G_{\text{eff}}} \int_0^{L/2} \int_0^x \mu(\xi) \{ \ddot{q}_1(t) + \Psi(\xi) [\ddot{q}_2(t)] \} d\xi dx \quad (30)$$

Evaluation of this integral gives

$$q_2(t) = \frac{\mu L^2}{8A'G_{\text{eff}}} [\ddot{q}_1(t) + 0.463 \cdot \ddot{q}_2(t)] \quad (31)$$

Using measured peak values of displacement and acceleration at the plan center and at the ends of the diaphragm ($A'G_{\text{eff}}$) is

$$A'G_{\text{eff}} = \frac{\mu L^2 [\ddot{q}_{1,\text{Peak}} + 0.463(\ddot{q}_{2,\text{Peak}} - \ddot{q}_{1,\text{Peak}})]}{8 q_{2,\text{Peak}}} \quad (32)$$

For Test 3 of Specimen #1,

$$A'G_{\text{eff}} = 1300 \text{ kips} \quad (33)$$

and likewise for Test 5 of Specimen #2,

$$A'G_{\text{eff}} = 610 \text{ kips} \quad (34)$$

That value (Eq 34) is close to that used in the linear elastic finite-element modeling of Specimen #2, 560 kips. These values allowed for the evaluation of k_{diaph} (Eq 10). Results of the response spectrum analyses (RSA) in Table 7 show that the 2DOF idealizations accurately calculated responses of the specimens.

TABLE 8—Properties of finite-element models used for verification of 2DOF idealization.

General Property		VM1		VM2	
Plan Footprint		187.5 ft by 75 ft		100 ft by 100 ft	
Height ^a		18 ft		32 ft	
Plan Aspect Ratio		3.5		1	
Masonry Walls		CMU and brick cavity wall		CMU barrier wall	
Weight of Walls		100 psf		74 psf	
Openings		On three sides		On two sides	
Interior Columns		Steel tube shapes		Steel wide-flanges	
Diaphragm Surface Mass for Analysis		20 psf		20 psf	
Specific Property	VM1 Wood	VM1 Metal	VM2 Wood	VM2 Metal	
Diaphragm	Straight lumber sheathing with panel overlay	1.5B20 screw-connected	Diagonal lumber sheathing	1.5B22 welded	
Roof Framing	Glu-lam rafters and girders	Open-web steel joists and girders	Dimension rafters and Glu-lam girders	Open-web steel joists and girders	

^aIncludes 4-ft parapet

Implementation of 2DOF Idealization Using Hypothetical Prototypical Finite-Element Building Models—Linear elastic finite-element models of four low-rise reinforced masonry buildings (Table 8) were created using SAP2000 [19] to further verify the accuracy and usefulness of the 2DOF modeling approach. RSA of the finite-element models, and the 2DOF idealizations representing them, provided a direct measure of the accuracy of the 2DOF analysis tool. Analysis used a uniform 1g-acceleration response spectrum. In each case, the fundamental mode was characterized, as expected, by the in-plane, single-curvature response of the roof diaphragm. Table 9 compares results of these analyses and shows that, in general, the 2DOF idealizations predicted the calculated responses well.

Nonlinear Lumped-Parameter Modeling

Nonlinear lumped-parameter models were created and tested using the program CANNY [30] to verify that responses of these types of buildings could be reasonably approximated in the nonlinear range of response, using a 2DOF idealization. Nonlinear modeling used the same mass values as the 2DOF idealizations. The program CANNY has a suite of analysis elements and hysteresis models. From that suite, four-noded, eight-degree-of-freedom panel elements were selected for analysis. Those elements have four available deformation mechanisms (Fig. 23), each governed by an appropriate hysteresis model. The shaking-table specimens were idealized using two elements; one representing the wall degree of freedom, and one representing the diaphragm degree of freedom (Figs. 22 and 23).

Spring stiffnesses for the wall elements used the measured elastic moduli of the masonry in the specimens, and, to be consistent with experimental observations, linear elastic hysteresis models. Axial and flexural spring stiffnesses for the diaphragm elements were assigned artificially high values to specifically characterize the observation that flexible roof diaphragms deform primarily in shear. Hysteretic models

TABLE 9—Comparison of responses from finite-element modeling and 2DOF modeling.

Response	Units	Analysis	Equation	VM1		VM2	
				Wood	Metal	Wood	Metal
α	—	—	11	0.0009	0.0014	0.0130	0.0007
β	—	—	12	0.658	0.658	0.561	0.561
ω	Hz	FEM	—	6.41	7.31	20.27	8.85
ω	Hz	2DOF	25	6.04	7.31	29.30	6.98
u_{diaph}	in.	FEM	—	12.80	9.91	0.51	6.91
u_{diaph}	in.	2DOF	24	10.60	7.25	0.46	7.90

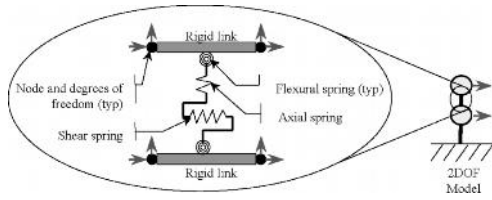


FIG. 23—Schematic of lumped-parameter panel element and 2DOF model.

governing the diaphragm shear springs were based on measured responses of the two shaking-table specimens. Those models, as well as evaluation of the test-to-test accumulation of damage, were different in the models representing Specimen #1 and Specimen #2, and are discussed next.

Nonlinear Modeling of Shaking-Table Specimen #1 (Lumber)—Damage in lumber assemblies increases only with increasing maximum levels of deformation; damage does not typically increase with cyclic deformations to constant maximum amplitude. Although visibly damaged pieces of sheathing and roof joist were removed, replicated, and replaced prior to quasi-static testing, the diaphragm still embodied some damage and therefore also a degraded stiffness. This explains why stiffness degradation was not observed during quasi-static testing until the diaphragm-masonry chord assembly was deformed to DDRs roughly equal to those sustained during seismic testing—in this case, 0.7 %.

Since the nonlinear modeling discussed in this paper was intended to investigate specimen behavior at deformation levels consistent with those observed during seismic tests, it was useful to evaluate the lateral stiffness of Specimen #1’s roof diaphragm during the seismic tests themselves.

That evaluation used measured acceleration and displacement values at the roof diaphragm level as well as the diaphragm degree-of-freedom mass (Eq 9), to arrive at hysteretic loops of diaphragm reaction shear versus DDR. Diaphragm reaction shear is defined, in this paper, as one-half the total effective inertial shear on the diaphragm (product of the diaphragm degree-of-freedom mass and diaphragm acceleration). Figure 24 shows hysteresis and backbone stiffnesses for transverse seismic testing of Specimen #1. The relative scale of abscissa to ordinate in Fig. 24 was deliberately maintained to clarify the degradation in

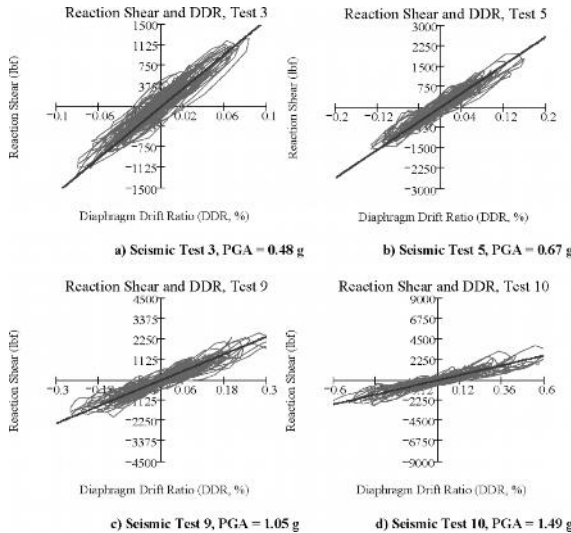


FIG. 24—Hysteresis and backbone stiffness of Specimen #1; seismic tests 3, 5, 9, and 10. (a) Seismic Test 3, PGA = 0.48g. (b) Seismic Test 5, PGA = 0.67g. (c) Seismic Test 9, PGA = 1.05g. (d) Seismic Test 10, PGA = 1.49g.

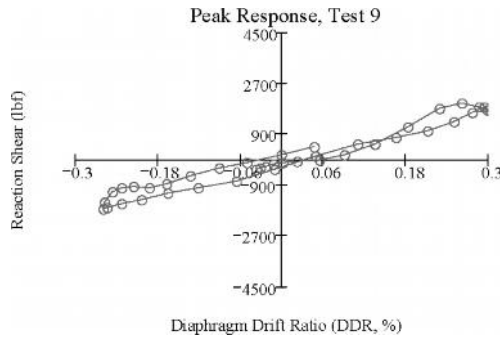


FIG. 25—Hysteresis of peak response of Specimen #1; Seismic Test 9.

lateral stiffness.

Those hysteresis plots show that the seismic behavior of Specimen #1 could be characterized as degrading, linear, and elastic with Coulomb damping (friction). Coulomb damping was observed during quasi-static testing of the lumber diaphragm as well as during seismic testing. The latter is particularly evident, for example, in the hysteresis of peak response for Seismic Test 9 (Fig. 25).

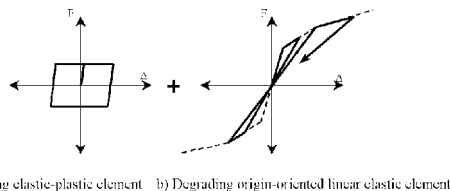
For these reasons, the diaphragm was modeled using two elements in parallel. Coulomb damping was modeled using an elastic-perfectly plastic element designed so that plasticity occurred at very small deformations. Thus, the additional stiffness contributed by this element did not alter the overall frequency response of the model (Fig. 26(a)). Lateral stiffness and stiffness degradation were modeled using an origin-oriented degrading linear elastic element designed so that the element's secant stiffness was defined by the previous point of maximum deformation on a tri-linear envelope curve (Fig. 26(b)).

Modeling also accounted for test-to-test accumulation of damage. At the beginning of each analysis, the model was subjected to an artificial pulse acceleration designed to deform the model to a level consistent with the peak deformation sustained during the prior seismic test. For example, if a seismic test, such as Test 1, deformed the specimen to a certain DDR, then a pulse acceleration, that would deform the specimen to that same DDR, was included at the beginning of the analysis simulating Test 2. Figures 27(a)–27(d) show results of the nonlinear modeling of Specimen #1. Note that the ordinate scales of those figures are different.

Figure 27(a) (Seismic Test 3) shows that calculated and measured displacements agree reasonably well over most of the time history but deviate somewhat during peak response (11 to 12.5 s). Figures 27(b) and 27(c) (Seismic Tests 5 and 9) show that calculated and measured displacements agree reasonably well. Figure 27(d), however, shows unsatisfactory agreement between calculated and measured displacements.

Although not shown in this paper, some additional refinement of calculated response was still possible. Increasing equivalent viscous damping and decreasing Coulomb damping in the model improved the agreement shown in Fig. 8(a) during peak response (11 to 12.5 s) of Seismic Test 3. Refinement of those two parameters generally bettered the agreements shown in Figs. 27(b) and 27(c) as well.

The transverse shear walls of Specimen #1 rocked during very high-level seismic testing. The modeling described here used linear elastic wall elements, and did not account for such behavior. For this



a) Coulomb damping elastic-plastic element b) Degrading origin-oriented linear elastic element

FIG. 26—Schematic of element hysteresis rules used to model lumber diaphragm. (a) Coulomb damping elastic-plastic element. (b) Degrading origin-oriented linear elastic element.

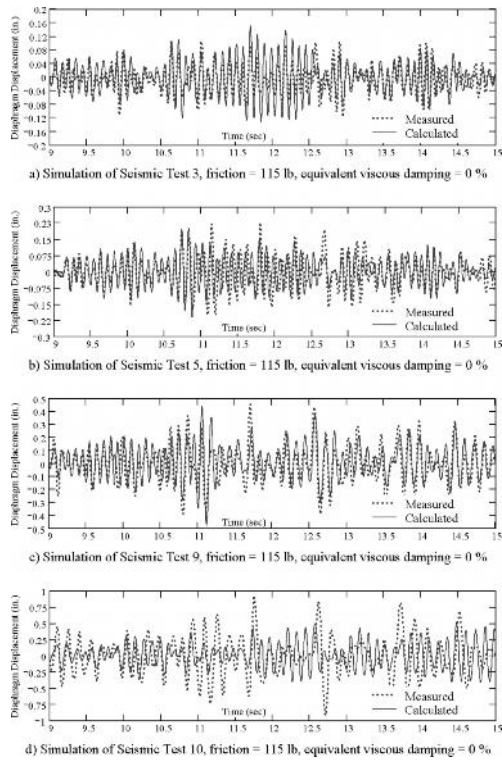


FIG. 27—Results of nonlinear modeling of Specimen #1; Seismic Tests 3, 5, 9, and 10. (a) Simulation of Seismic Test 3, friction = 115 lb, equivalent viscous damping = 0 %. (b) Simulation of Seismic Test 5, friction = 115 lb, equivalent viscous damping = 0 %. (c) Simulation of Seismic Test 9, friction = 115 lb, equivalent viscous damping = 0 %. (d) Simulation of Seismic Test 10, friction = 115 lb, equivalent viscous damping = 0 %.

reason, the observed wall rocking in Specimen #1 likely explains the disagreement between calculated and measured response during Seismic Test 10 (Fig. 27(d)). That wall rocking, however, was primarily an artifact of the vertical aspect ratios of transverse walls and would not characterize typical prototype building behavior.

Nonlinear Modeling of Shaking-Table Specimen #2—Damage in welded metal-deck assemblies generally manifests itself as sudden failure of puddle welds and associated abrupt decreases in in-plane stiffness and strength. It also manifests itself as bearing deformation of side-lap screws into metal deck, but this is generally not detectable in lightly connected metal-deck assemblies such as those discussed here.

Specimen #2, however, did not sustain puddle-weld fractures as a result of transverse seismic testing. The sequence of seismic tests for Specimen #2 comprised several low-level transverse tests; followed by several longitudinal tests of increasing excitation; followed by several transverse tests of increasing excitation. Rather surprisingly, the specimen sustained puddle-weld fractures as a result of strong longitudinal testing and therefore only degraded in lateral stiffness during that sequence of tests.

For that reason, modeling discussed here did not account for the strength degrading or stiffness degrading behavior observed during quasi-static testing. Modeling instead accounted for the observed stiffness degradation during seismic testing by using two different diaphragm stiffnesses: one before the sequence of longitudinal tests (not yet degraded in stiffness); and another after the sequence of longitudinal

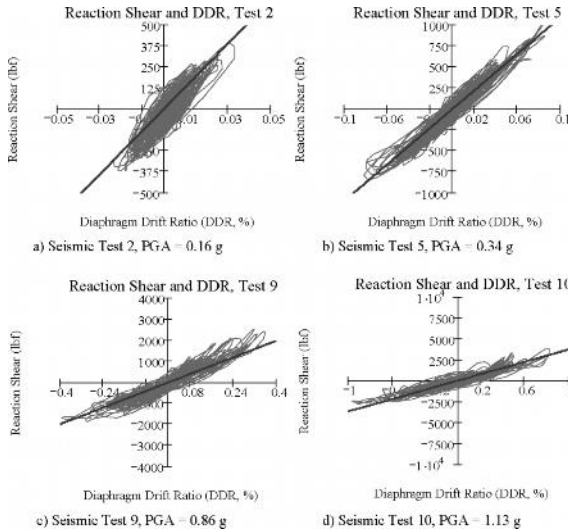


FIG. 28—Hysteresis and backbone stiffness of Specimen #2: Seismic Tests 2, 5, 9, and 10. (a) Seismic Test 2, $PGA = 0.16g$. (b) Seismic Test 5, $PGA = 0.34g$. (c) Seismic Test 9, $PGA = 0.86g$. (d) Seismic Test 10, $PGA = 1.13g$.

tests (degraded in stiffness).

As discussed for Specimen #1, Fig. 28 shows hysteresis and backbone stiffnesses for transverse seismic testing of Specimen #2. The relative scales of abscissa to ordinate in Fig. 28 were deliberately maintained to clarify the degradation in lateral stiffness.

The hysteresis of Figs. 28(a)–28(d) show that the seismic behavior of Specimen #2 could be characterized as linear and elastic and, unlike that of Specimen #1, without Coulomb damping. The latter is particularly evident in the individual hysteresis loop for peak response of Seismic Test 9 (Fig. 29). For these reasons, the diaphragm of Specimen #2 was modeled as linear and elastic. Figures 30(a)–30(e) show the results of modeling of Specimen #2. Note that the ordinate scales of those figures are different.

Figure 30(a) (Seismic Test 2) shows that calculated and measured displacements agree reasonably well over the majority of the time history, but deviate in certain regions. Figure 30(b) (Seismic Test 5) shows that calculated and measured displacements agree well over the entire time history. Figure 30(c) (Seismic Test 9) shows significant deviation between calculated and measured displacements for the majority of the time history but shows better agreement following peak response (time greater than about 7.5 s). Figure 30(d) shows that calculated and measured displacements agree reasonably well over the entire time history

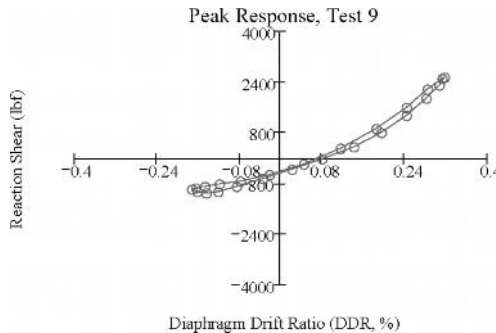


FIG. 29—Hysteresis for peak response of Specimen #2 during Seismic Test 9.

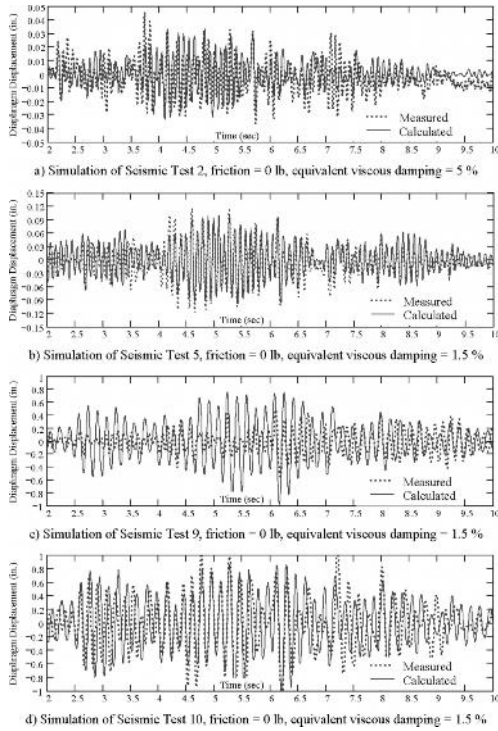


FIG. 30—Results of nonlinear modeling of Specimen #2; Seismic Tests 3, 5, 9, and 10. (a) Simulation of Seismic Test 2, friction = 0 lb, equivalent viscous damping = 5 %. (b) Simulation of Seismic Test 5, friction = 0 lb, equivalent viscous damping = 1.5 %. (c) Simulation of Seismic Test 9, friction = 0 lb, equivalent viscous damping = 1.5 %. (d) Simulation of Seismic Test 10, friction = 0 lb, equivalent viscous damping = 1.5 %.

with particularly good agreement during peak response (4 to 6 s).

Analyses shown in Figs. 30(b)–30(d) used 1.5 % equivalent viscous damping. The analysis shown in Fig. 30(a), however, used 5 % equivalent viscous damping. That figure represents very low-level responses of Specimen #2 (PGA=0.16g).

Figure 30(c) (Seismic Test 9) initially suggests that the analytical model did not accurately represent Specimen #2, at least for simulation of that seismic test. Recall, however, that during seismic testing of Specimen #2, however, the specimen was subjected to low-level transverse tests, then high-level longitudinal tests, and finally high-level transverse tests, the first of which was Seismic Test 9. Because of this, the longitudinal walls of Specimen #2 were essentially undamaged prior to Seismic Test 9. During that test, those walls sustained significant cracking consistent with their out-of-plane response and the effective lateral stiffness of the diaphragm was consequently decreased. This is not evident in Fig. 28(c) because that figure shows a backbone stiffness based only on peak responses.

Figure 31, however, shows hysteresis and backbone stiffnesses for two portions of the time history of Seismic Test 9: the first for 0 to 5 s and the second for 5 to 10 s. The difference in backbone stiffnesses of the two portions shows the effect of cracking in the longitudinal walls during the test. This plausibly explains the differences of calculated and measured responses shown in Fig. 30(c). Specifically, the analytical model used a diaphragm stiffness that was consistent only with the stiffness of the specimen after the longitudinal walls had cracked.

Implications of Nonlinear Analyses—The nonlinear analyses presented in the preceding paragraphs, in combination with the linear analyses presented earlier, have two important implications. First, the 2DOF

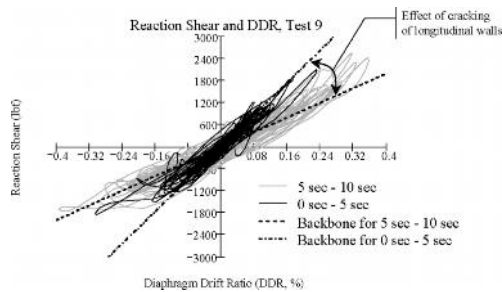


FIG. 31—Hysteresis for Seismic Test 9 of Specimen #2.

idealization presented in this paper is a justified, simple, and accurate tool for the analysis of low-rise reinforced masonry buildings with flexible diaphragms. Second, that idealization can predict the nonlinear response of such buildings with reasonable accuracy, if certain important parameters are modified appropriately.

The lumped-parameter analyses of shaking-table Specimen #1 and #2 were essentially linear elastic analyses with modified parameters. For example, although Coulomb damping introduced nonlinearity to the analysis of Specimen #1, the analysis stiffness parameter was defined by a degrading linear elastic element. That element was degraded before each analysis to a level of damage consistent with that of the previous seismic test. Similarly, analysis of Specimen #2 was linear and elastic throughout. That analysis accounted for the measured nonlinearity (weld fractures and attendant degradation in stiffness) by explicitly decreasing the diaphragm stiffness. These suggest, that nonlinear responses could be predicted with reasonable accuracy using linear analysis, a decreased approximate stiffness, and an equivalent viscous damping ratio.

Nonlinear modeling of the shaking-table specimens showed that reasonable agreement between responses of the specimens and those of the 2DOF model representing them, was possible, even at high levels of excitation (for example, Fig. 27(c), $PGA=1.05$ g). The fact that the same set of hysteretic parameters (stiffness models and damping) resulted in this reasonable agreement, suggests that the nonlinear 2DOF models were robust. That is, they did not require extensive refinement from test to test.

Summary and Conclusions from Phase 2 (Analysis)

First, linear elastic finite-element models were created and tested based on conclusions drawn from shaking-table testing. Next, observations from physical testing were distilled into a simplified two-degree-of-freedom analysis tool. That tool was implemented using two half-scale shaking-table specimens and two prototypical analytical building models, and was shown to accurately calculate their responses. Non-linear lumped-parameter modeling validated the accuracy of the 2DOF tool at high levels of excitation.

These studies demonstrated that the 2DOF analysis tool developed here is simple and justified for the seismic analysis of low-rise reinforced masonry buildings with flexible roof diaphragms. The tool is accurate in its calculation of response and robust with respect to required analysis parameters. The tool provides a logical method for the expedient calculation of global building response.

Phase 3: Seismic Evaluation

From August 2002 to September 2003, data and knowledge from Phase 1 (Behavior), additional data from other studies, and the analysis tool developed in Phase 2 (Analysis) are combined and integrated with the predominant existing seismic evaluation document, *Handbook for the Seismic Evaluation of Buildings—A Prestandard* (FEMA 310) [31], to develop a supplementary methodology to fill identified gaps in that document. As the research described here was in its final phases, the American Society of Civil Engineers (ASCE) completed and published *Seismic Evaluation of Existing Buildings* ASCE 31-03 [32]. That document is based on, and intended to replace, FEMA 310. In contrast to FEMA 310, however, that ASCE document is intended to serve as a nationally applicable seismic evaluation methodology, and to be

suitable for adoption into building codes. Because the general approach of ASCE 31-03 is similar to that of FEMA 310, the research described here remains applicable.

Critical Review of Existing Evaluation Methodology

Low-rise reinforced masonry buildings with flexible diaphragms may have many different seismic deficiencies. Seismic evaluation provisions of FEMA 310 designed to identify such deficiencies comprise tiered evaluation criteria of incrementally increasing rigor: the Screening phase (Tier 1); the Evaluation phase (Tier 2); and the Detailed Evaluation phase (Tier 3). The Screening phase uses limited analyses and checklists to quickly identify probable seismic deficiencies. The checklist items are chiefly based on correlations between observed seismic damage and specific building characteristics. If deficiencies are identified in the Screening phase, the evaluating engineer can choose to perform the Evaluation phase (Tier 2), or can directly recommend rehabilitation. The Evaluation phase (Tier 2) involves more rigorous evaluations on either a deficiency-specific or a building-wide basis. In the former, more common case, only deficiencies identified by the Screening phase are reevaluated; in the latter, the entire structure is reevaluated. If deficiencies are still identified by the Evaluation phase, the evaluating engineer can choose to perform the final Detailed Evaluation phase (Tier 3), or can directly recommend rehabilitation. The Detailed Evaluation phase basically comprises a rigorous analysis of the deficient structure or its deficient components, according to accepted methodologies for seismic rehabilitation or for new construction, such as *Prestandard and Commentary for the Seismic Rehabilitation of Buildings* (FEMA 356) [33], and the *International Building Code* [34], respectively.

In this study, FEMA 310 was revisited to identify and propose refinements for potential gaps in its methodology. In this process, potential deficiencies were critically compared with the existing evaluation criteria intended to identify them.

Checklists of the Screening phase do not explicitly require the comparison of diaphragm shear demand and capacity or of diaphragm deformation demand and capacity; as is shown later here, they do not sufficiently characterize the performance of flexible diaphragms. In some cases, possible limit states are checked qualitatively. For example, diaphragm shear forces are implicitly checked by the requirement that straight-sheathed lumber diaphragms have aspect ratios less than or equal to 2:1; diaphragm deflections are implicitly checked by the requirement that wood diaphragms with spans greater than 24 ft be constructed of diagonal sheathing or structural paneling; and other checklist items are similar. While these checklist items and others like them are effective for some buildings, they do not explicitly identify diaphragm force and deformation limit states.

Procedures of the Evaluation phase are more complete: they directly address diaphragm capacity, and indirectly address diaphragm deformation capacity (through the use of component-specific force-reduction factors). These procedures are activated, however, only if the diaphragm is first found to be deficient in the Screening phase. It is principally this gap in the Screening phase that the study intends to fill. Specifically, this study concerns the development of a supplementary evaluation methodology. If that supplementary methodology is implemented in the Screening phase, potential deficiencies will be identified, and are well addressed by the more rigorous procedures of the Evaluation phase.)

Development of Proposed Supplementary Evaluation Methodology

Fundamental to the supplementary evaluation methodology is the development of a basic index of probable diaphragm performance, and a method of including that index in the current evaluation procedures. To characterize diaphragm performance, test data from previous diaphragm tests, performed by others, were reevaluated in the context of performance-based engineering. Data from studies previously designed to identify strength and initial stiffness properties of lumber diaphragms [10],[35–38] and metal-deck diaphragms [39–41] were re-evaluated to correlate strength, deformation, and damage. Two key parameters were extracted from the test data: DDRs and the measure of initial diaphragm rigidity G' . The latter is related to shear rigidity $A'G$ as

$$G'B = A'G \quad (35)$$

where B is the diaphragm width in the direction of loading, A' is the effective shear area of the diaphragm, and G is the shear modulus of the diaphragm. The complex nature of most flexible diaphragms, whether

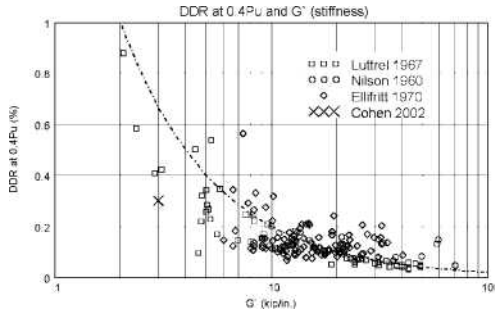


FIG. 32—Relationship between a measure of diaphragm shear stiffness G' and the diaphragm drift ratio, at onset of damage, for metal-deck diaphragms.

constructed of lumber or metal deck, greatly complicates the explicit definition of either a diaphragm shear modulus or an effective shear area. For that reason, G' is widely used and represents an effective quantity describing the shear rigidity of the diaphragm per unit width, in the direction of loading. In the case of metal-deck diaphragms, DDRs and stiffnesses were extracted at 40 % of the ultimate capacity of the diaphragm. That percentage is generally accepted as the load level at which metal-deck diaphragms begin to sustain measurable damage and exhibit nonlinearity in their load-displacement responses [40]. Diaphragm studies listed earlier suggest that lumber diaphragms exhibit similar incipient damage and nonlinearity at approximately 50 % of their ultimate capacity; stiffnesses and DDRs were therefore extracted at that load level.

Figure 32 shows that, for metal-deck diaphragms, there is an inverse relationship between G' and the diaphragm drift ratio at 40 % of the ultimate load. The dotted curve in that figure is,

$$DDR_{40\%Pu} = \frac{2}{G'} \tag{36}$$

where G' is in units of kips/in. and $DDR_{40\%Pu}$ is in units of percent. For lumber diaphragms, Figure 33 shows a similar relationship:

$$DDR_{50\%Pu} = \frac{1}{G'} \tag{37}$$

Equations 36 and 37 describe an important interrelationship between an intrinsic characteristic of a diaphragm (G') and its seismic performance (DDR at 40 % and 50 % of ultimate capacity). This implies

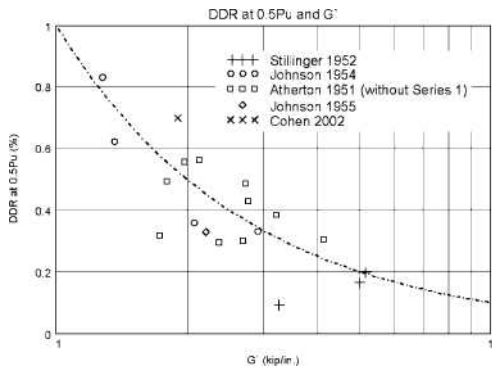


FIG. 33—Relationship between a measure of diaphragm shear stiffness G' and diaphragm drift ratio, at onset of damage, for lumber sheathed diaphragms.

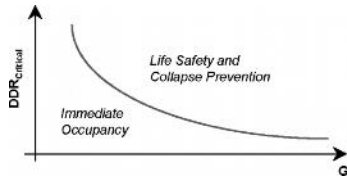


FIG. 34—Link between FEMA Performance Levels and proposed supplementary methodology.

that the level of deformation in a diaphragm at the onset of damage (yielding) is not purely kinematical, but it also depends on its stiffness. As a contrasting example, yielding (damage) in an elastic-plastic steel-plate diaphragm is purely kinematical, occurring at the same deformation (DDR) regardless of the stiffness.

The relationships of Eqs 36 and 37 make physical sense as well. The in-plane stiffness of these types of diaphragms depends on complex mechanisms that, for lumber diaphragms, chiefly derive from nailing patterns, nail sizes, and lumber sizes. For metal-deck diaphragms, they chiefly derive from welding patterns, weld sizes, deck thickness, side-lap fastener patterns, and deck profile. These same elements also contribute to diaphragm strength. For instance, the more nails in a lumber diaphragm or welds in a metal-deck diaphragm, the greater its strength. A stronger diaphragm would therefore be a stiffer diaphragm, would therefore deform less, and would therefore exhibit such an inverse relationship as Eqs 36 or 37.

FEMA 310 defines three seismic performance levels: Immediate Occupancy (IO), Life Safety (LS), and Collapse Prevention (CP). A design earthquake would cause little to no damage for IO; some damage but no immediate threat to human life for LS; and large amounts of damage but continued overall structural stability for CP. Inherent to their development, the relationships of Eqs 36 and 37 roughly define boundaries between the first and latter two performance levels (Fig. 34); deformation levels at or below those described by the equations are consistent with IO, and levels above them are consistent with LS and CP.

Summary and Recommendations from Phase 3 (Seismic Evaluation)

Observations made during Phase 1 (Behavior), the analysis tool developed in Phase 2 (Analysis), and the diaphragm performance indices (Eqs 36 and 37) and criterion (Fig. 34) developed in this phase were combined to form a supplementary evaluation methodology. The supplementary methodology was designed to fill a gap in the FEMA 310 Screening phase (Tier 1), and is intended to be implemented in that same phase. It is shown schematically in Fig. 35, and is presented step-wise below using the example building plan configuration of Fig. 36(a).

- (1) **Define diaphragm systems.** Buildings with multiple diaphragms are described as a set of indi-

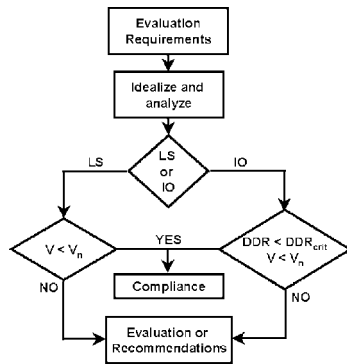


FIG. 35—Organization of proposed supplementary methodology for the Screening phase.

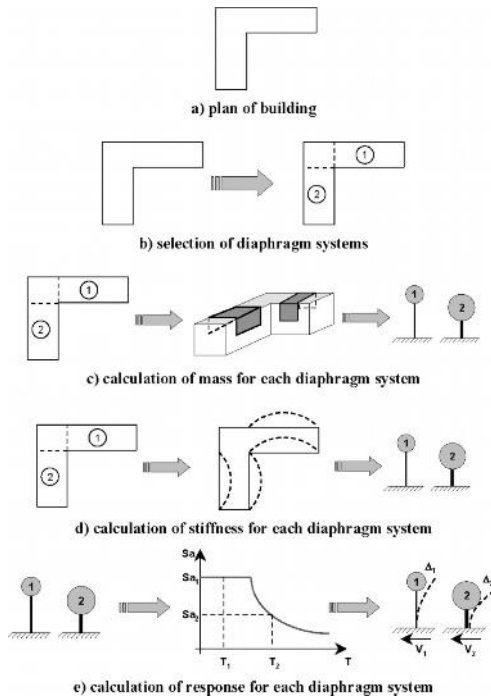


FIG. 36—Proposed supplementary methodology for FEMA 310, (a) Plan of building. (b) Selection of diaphragm systems. (c) Calculation of mass for each diaphragm system. (d) Calculation of stiffness for each diaphragm system. (e) Calculation of response for each diaphragm system.

vidual diaphragm systems. For example, a building with the plan of Fig. 36(a) is described as the collection of diaphragm systems in Fig. 36(b).

- (2) **Couple mass and assign stiffness to diaphragm systems.** Using the methods developed in Phase 2: Analysis, appropriate mass and stiffness values are assigned to each diaphragm system. The mass coupled with each diaphragm system is one-half the total mass of the diaphragm itself, plus one-half the mass of any out-of-plane walls associated with response of the diaphragm. This quantity is illustrated by the darkly shaded areas in Fig. 36(c). The deformed shapes of the diaphragm systems are approximated as sinusoids (Fig. 36(d)). The in-plane stiffness consistent with this is

$$k = \frac{BG' \pi^2}{L} \quad (38)$$

where B is the diaphragm width and L is the diaphragm length.

- (3) **Calculate period of each diaphragm system.** Treating each as a SDOF system, calculate a period for each diaphragm system (Fig. 36(e)).
- (4) **Calculate response of each diaphragm system.** Using appropriate loading criteria (for example, a response spectrum) calculate in-plane forces and DDRs for each diaphragm system (Fig. 36(e)).
- (5) **Compare calculated responses with capacities.** For each diaphragm system, compare applied loads to known capacities. For Immediate Occupancy performance levels, also compare calculated DDRs to critical values (Eqs 36 and 37).
- (6) **Recommend further evaluation or rehabilitation.** Based on results of Step 5, proceed with evaluation as outlined in FEMA 310.

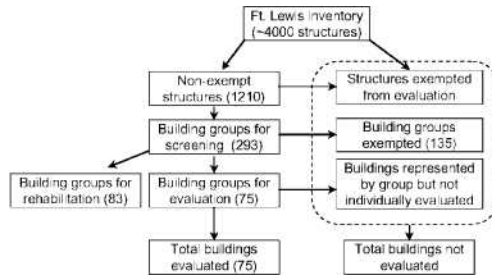


FIG. 37—Hierarchical building-classification system used by URS Greiner for Ft. Lewis, WA.

Phase 4: Application and Verification

As the final phase of this study, four, existing military-owned low-rise reinforced masonry buildings with flexible diaphragms were evaluated for seismic deficiencies. The buildings were evaluated using two methodologies: that of FEMA 310; and the supplementary methodology proposed here. Results of the evaluations were compared with each other, and with the results from existing seismic evaluations of the same buildings performed by URS Greiner Inc. (San Francisco, CA) in the mid-1990s.

Selection of Buildings for Evaluation

Structures with different building characteristics can, as a result, have drastically different seismic response and performance characteristics. It was therefore important to select a manageable number of buildings for evaluation, based on careful consideration of their applicability to the goals of this research. As described below, a large inventory was evaluated and distilled to four representative buildings that were very applicable to this research.

In the mid-1990s, the US Army contracted URS Greiner to screen their existing building inventory in Ft. Lewis, Washington, for seismic deficiencies [42]. They performed a facility-wide seismic screening of over 4000 structures [43]. To simplify the evaluation of such a large number of structures, URS Greiner and CERL developed the hierarchical building-classification system described in Fig. 37.

Ft. Lewis comprises an inventory of over 4000 structures, of which 1210 were classified as “nonexempt” and were considered for seismic evaluation. Based on criteria established by CERL, the remaining inventory of 1210 buildings was divided into 293 “building groups.” Each building group comprised a subset of the nonexempt inventory that shared key structural characteristics such as, among others, year of construction, primary structural system, and number of stories. One representative building from each building group was then selected for evaluation, and group-wide dispositions were based on that single evaluation. The number of buildings comprising each group ranged from only one to over 80.

Preliminary screening of the 293 building groups by URS Greiner determined that 135 building groups were exempted from further evaluation, 83 building groups were classified in need of rehabilitation without further evaluation, and 75 building groups were classified in need of further evaluation before assignment of disposition.

In this study, the entire nonexempt Ft. Lewis building inventory was examined to identify candidate buildings for evaluation. The inventory was filtered, using several simple criteria, for the subset of one-story reinforced masonry buildings with flexible diaphragms. Presented in the form of questions, those filters are:

- Is the building one-storied?
- Was the building built between the years 1950 and 1980?
- Was the building already evaluated by URS Greiner?
- Is the structure a low-rise masonry building with a flexible wood or metal-deck diaphragm (FEMA 310 Type RM1)?

Of the 1210 nonexempt buildings in Ft. Lewis, 186 buildings complied with Criterion 1; 97 buildings complied with Criteria 1 and 2; 17 buildings complied with Criteria 1, 2, and 3; and 7 buildings complied with all the criteria. A separate CERL selection process had previously identified an additional three

TABLE 10—Numerical assessment of candidate buildings.

Building	Criterion						Total Score
	A	B	C	D	E	F	
1	1	0	2	0	2	2	8
2	2	1	2	0	2	0	7
3	2	2	2	1	2	2	11
4	1	2	2	1	1	2	9
5	2	2	2	1	2	2	11
6	2	2	2	1	2	2	12
7	2	2	2	2	2	2	12
8	2	2	2	2	2	2	12
9	2	2	2	1	2	2	11

buildings, for a total of ten candidate buildings. Those 10 buildings were further compared with a set of six selection criteria to determine their applicability to this study. Presented in the form of questions, those criteria are identified as A through F below:

- (A) Are the diaphragms flexible?
- (B) Are the plan aspect ratios of diaphragms greater than 1?
- (C) Are the walls constructed of reinforced masonry?
- (D) Are the general plan and vertical layouts of the building regular?
- (E) Are structural drawings available?
- (F) Is the building located near other potential candidate buildings?

The compliance of each building with each criterion was assessed numerically, using numerical scores of zero, one, or two to represent increasing levels of compliance. Overall compliance scores were then calculated for each building. Table 10 summarizes results of that assessment; buildings are arbitrarily assigned numerical identifications.

Based on this, Buildings 3, 6, 8, and 9 (Fig. 38) were selected for possible further evaluation. All four buildings have reinforced CMU walls and welded metal-deck roof diaphragms. Of two sets of buildings with the same compliance scores and very similar construction, use, and configuration, Building 8 was selected rather than Building 7 because Building 8 has a larger diaphragm plan aspect ratio, and Building 9 was selected rather than Building 5 because Building 5 is two-storied.

Application of Existing and Proposed Supplementary Seismic Evaluation Methodologies

The four selected buildings were evaluated using two methodologies, FEMA 310 and the supplementary methodology developed in this study, three times each: once using seismicity consistent with Ft. Lewis, WA and a diaphragm stiffnesses consistent with as-built conditions; again using seismicity consistent with



FIG. 38—Buildings 3, 6, 8, and 9 (clockwise from upper left).

TABLE 11—Dispositions of selected buildings using FEMA 310 procedures.

Building	Screening (Tier 1)		Evaluation (Tier 2)
	Disposition	Deficiency	Disposition
Ft. Lewis, Washington ($S_s=1.2g, S_1=0.4g$) ^a			
8	Compliant	—	—
9	Noncompliant	Shear transfer from diaphragm to wall	Compliant
6	Noncompliant	Shear transfer from diaphragm to wall	Compliant
3	Noncompliant	Shear transfer from diaphragm to wall	Compliant
San Francisco, California ($S_s=2.0g, S_1=0.9g$)			
8	Compliant	—	—
9	Noncompliant	Shear transfer from diaphragm to wall	Compliant
6	Noncompliant	Shear transfer from diaphragm to wall	Noncompliant
3	Noncompliant	Shear transfer from diaphragm to wall	Compliant

^aIdentical results for cases of evaluations using reduced diaphragm stiffness

Ft. Lewis, WA but with a hypothetically reduced diaphragm stiffnesses (this is discussed next); and finally using a seismic design category consistent with San Francisco, CA and a diaphragm stiffnesses consistent with as-built conditions. The buildings were assumed to be founded on soil corresponding to Site Class D (stiff soil) and were evaluated at the Life Safety performance level. In addition to the evaluations performed as part of this study, URS Greiner evaluated the four selected buildings using the methodology of FEMA 178 [44] and site-specific seismicity consistent with Ft. Lewis, WA.

Diaphragms in the four selected buildings have unusually high in-plane stiffnesses compared to other typical metal-deck diaphragms. As an example, these diaphragms as-built (20 gage, 36/7 puddle welding, button-punched @ 18-in. o/c; $G'=60$ kip/in.) are more than 10 times stiffer in-plane than those constructed using another typical configuration (for example, 22 gage, 36/3 puddle welding, button-punched @ 18-in. o/c; $G'=5$ kip/in.). The evaluations presented here are intended to demonstrate gaps in the existing FEMA 310 methodology, rather than identify specific deficiencies in specific buildings. The four buildings were thus evaluated twice using seismicity consistent with Ft. Lewis, WA: once, using the nominal diaphragm stiffnesses ($G'=60$ kip/in.); and again using hypothetically decreased, but still typical, diaphragm stiffnesses ($G'=5$ kip/in.).

In the four evaluations performed by URS Greiner, only Building 9 was found deficient. Table 11 summarizes results of the 12 FEMA 310 evaluations performed as part of this study.

The goal of these evaluations was to verify suspected gaps in the Screening phase of the FEMA 310 methodology, and to provide a comparison to both the URS Greiner methodology and the supplementary methodology proposed in this study. For seismicity consistent with Ft. Lewis, WA and San Francisco, CA, Screening (Tier 1) indicated deficient diaphragm-to-wall shear-transfer mechanisms in three of the four buildings (Buildings 9, 6, and 3). In those cases, the metal-deck diaphragm itself was connected to the shear walls only through the joist-to-wall connections; that condition was considered deficient. Modern construction of metal-deck diaphragms requires that the metal deck itself be continuously connected to all shear walls along the diaphragm perimeter. This is generally accomplished using continuous structural angles anchored along the tops of perimeter shear walls, and intermittently welded or otherwise connected to the metal deck. Further deficiency-specific Evaluation (Tier 2) of the joist-to-wall connections, indicated that, for seismicity consistent with Ft. Lewis, WA, the connections were actually sufficient to transfer the diaphragm shear. For seismicity consistent with San Francisco, CA, Evaluation (Tier 2) indicated that connections in Building 6 were deficient due to insufficient shear capacities of anchor bolts connecting the roof framing to the masonry walls.

The four selected buildings were also evaluated for Life Safety using the supplementary methodology proposed in this study. These evaluations emphasized three items not currently addressed by the Screening

TABLE 12—Periods calculated using FEMA 310 Screening provisions and the proposed supplementary methodology.

Building	Period, s	
	FEMA	Supplementary Methodology
	Nominal Diaphragm Stiffness	
8	0.17	0.13
9	0.12	0.13
6	0.13	0.22
3	0.14	0.14
Reduced Diaphragm Stiffness		
8	0.17	0.47
9	0.12	0.47
6	0.13	0.77
3	0.14	0.50

phase of FEMA 310: accurate calculation of building period; comparison of diaphragm shear force demand and capacity; and in the case of Immediate Occupancy performance, comparison of diaphragm deformation demand and capacity.

Tables 12 and 13 summarize results of the supplementary evaluations. Table 12 shows that fundamental periods calculated by the FEMA 310 Screening Phase (Tier 1) provisions are generally significantly shorter than those calculated by the proposed supplementary methodology. The FEMA 310 Evaluation Phase (Tier 2), however, includes a period expression developed specifically for low-rise buildings with

TABLE 13—Dispositions of buildings using proposed supplementary methodology.

Building	Diaphragm Shear, plf (Demand/Capacity)	DDR, % (Demand/Capacity)	Disposition
Ft. Lewis, WA			
Nominal Diaphragm Stiffness			
8	915/780	0.05/0.03	Noncompliant
9	473/780	0.05/0.03	Compliant
6	769/780	0.09/0.03	Compliant
	528/780	0.06/0.03	
3	462/780	0.05/0.03	Compliant
	397/780	0.04/0.03	
Ft. Lewis, WA			
Reduced Diaphragm Stiffness			
8	915/391	0.66/0.40	Noncompliant
9	473/391	0.66/0.40	Noncompliant
6	486/391	0.68/0.40	Noncompliant
	478/391	0.67/0.40	
3	447/391	0.65/0.40	Compliant
	386/391	0.54/0.40	
San Francisco, CA			
Nominal Diaphragm Stiffness			
8	1386/780	0.08/0.03	Noncompliant
9	716/780	0.08/0.03	Compliant
6	1166/780	0.13/0.03	Noncompliant
	799/780	0.09/0.03	
3	699/780	0.08/0.03	Compliant
	601/780	0.07/0.03	

TABLE 14—Dispositions of selected buildings from evaluations.

Building	URS Greiner (FEMA 178)	FEMA 310			Proposed Supplementary Methodology		
		Ft. Lewis	Ft. Lewis (reduced stiffness)	San Francisco	Ft. Lewis	Ft. Lewis (reduced stiffness)	San Francisco
8	C	C	C	C	NC	NC	NC
9	NC	C	C	C	C	NC	C
6	C	C	C	NC	C	NC	NC
3	C	C	C	C	C	C	C

C: Compliant/Sufficient

NC: Noncompliant/Deficient

flexible diaphragms (FEMA 310 Eq 4-1). References listed in the beginning of this paper show that equation to be reasonably accurate for flexible diaphragm systems and would calculate periods similar to those calculated by the proposed supplementary methodology.

Table 13 shows that evaluations using the proposed supplementary methodology found 6 of the 12 evaluations to indicate noncompliance with a Life Safety performance level. Each pair of diaphragm demand and capacity values listed in the table (second and third columns) represents the response of one of the diaphragm systems used to idealize the building (Step 1 in the proposed supplementary methodology, Fig. 36). For instance, the table shows that Building 6 was idealized with three diaphragm systems. The table also shows that DDR demands were greater than DDR capacities in many cases. This requirement, according to the proposed supplementary methodology, applies to Immediate Occupancy performance levels only, and is hence not considered further.

In the deficient cases, shown in Table 13, diaphragm shear demands exceeded diaphragm shear capacities. As demonstrated in Phase 1 (Behavior) of this study and in other studies [39–41], metal-deck diaphragms exhibit stiffness degradation and sustain significant damage at load levels greater than about 40 % of ultimate capacity, and exhibit instability, as well as stiffness and strength degradation, at load levels greater than ultimate capacity. Responses calculated using the proposed supplementary methodology therefore imply that during an earthquake with spectral ordinates consistent with those used in these evaluations, diaphragms of the deficient buildings would at least sustain significant damage, would likely lose significant strength and stiffness, and would possibly lose overall diaphragm action.

Summary and Conclusions from Phase 4 (Application)

Table 14 compares results from all the evaluations, and shows that the proposed supplementary methodology found a significantly greater number of buildings to be deficient, at the Life Safety performance level, than either the FEMA 310 or URS Greiner (FEMA 178) methodologies.

The evaluation results from FEMA 310 and those from the supplementary methodology are fundamentally different, however. As described, those buildings determined to be potentially deficient (Table 11) by FEMA 310 Screening (Tier 1) were so classified because they had insufficient connectivity between diaphragms and supporting walls. Subsequent Evaluation (Tier 2) found that most of those conditions were, in fact, sufficient. The buildings were therefore found to be seismically sufficient without ever checking diaphragm capacities.

The proposed supplementary methodology, however, explicitly checks this important aspect of seismic performance, and shows (Table 13) that many of those buildings indeed have deficient diaphragms. Furthermore, because the proposed methodology is not comprehensive, but rather supplementary to the existing FEMA 310 methodology, a full Screening of the buildings would not only find that many of the diaphragms themselves are deficient (Table 13), but would also identify the same connectivity deficiencies listed in Table 11. This indicates that a small but critical gap exists in the FEMA 310 Screening Phase (Tier 1) for low-rise reinforced masonry buildings with flexible diaphragms. The supplementary methodology proposed here successfully fills that gap.

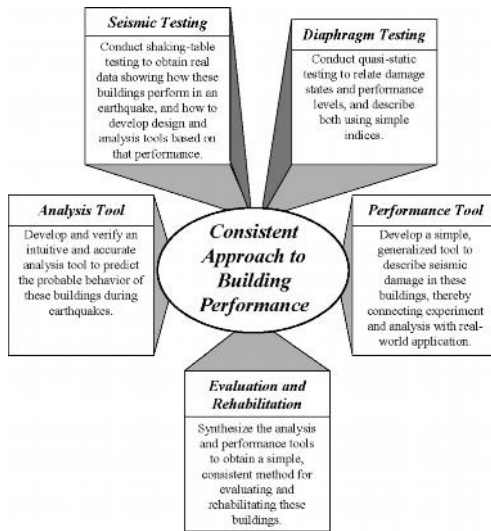


FIG. 39—Synthesis of study phases into a consistent approach to seismic performance of low-rise reinforced masonry buildings with flexible diaphragms.

Overall Summary, Results, and Conclusions

This study was completed in four inter-related phases: behavior, analysis, seismic evaluation, and application and verification (Fig. 39). Shaking-table and quasi-static testing demonstrated the affect of diaphragm flexibility on building behavior and also the need for an analysis tool to characterize that behavior (Phase 1: Behavior). To meet this need, simple 2DOF and SDOF idealizations of low-rise buildings with flexible diaphragms were developed and verified (Phase 2: Analysis). The analysis tool was enhanced with the reevaluation of existing data, and then integrated into the predominant seismic evaluation methodology, FEMA 310, to improve its assessment of low-rise reinforced masonry buildings with flexible diaphragms (Phase 3: Seismic Evaluation). Simple describable relationships exist between an intrinsic measure of diaphragm stiffness and critical levels of diaphragm deformation (diaphragm drift ratio). These relationships, in combination with the SDOF analysis tool, comprise the proposed supplementary methodology.

To assess and validate the usefulness of the proposed supplementary methodology, four military-owned low-rise reinforced masonry buildings with flexible diaphragms were evaluated for seismic deficiencies (Phase 4: Application and Verification). The evaluations substantiated the hypothesis that the existing FEMA 310 methodology, while complete in many ways, does not sufficiently identify potential diaphragm deficiencies in low-rise reinforced masonry buildings with flexible diaphragms. The proposed supplementary methodology was ultimately shown to be simple, effective, and necessary.

Acknowledgments

The United States Army Corps of Engineers, Research and Development Center provided project funding. Vulcraft Steel Joist and Deck Company donated the corrugated metal decking used in this project. Larry Herm and Mark Johanningsmeier, both of Vulcraft, provided expertise regarding metal-deck construction and detailing. Jim Gambill and Bill Gordon, both of CERL, provided expertise in operating the shaking table and providing other technical support.

References

- [1] Cohen, G. L., "Seismic Evaluation and Rehabilitation of Low-Rise Reinforced Masonry Buildings With Flexible Diaphragms," Ph.D. dissertation, The University of Texas at Austin, Austin, TX, 2004.
- [2] Cohen, G. L., Klingner, R. E., Hayes, J. R. Jr., and Sweeney, S. C., "Seismic Evaluation of Low-Rise Reinforced Masonry Buildings With Flexible Roof Diaphragms Part I: Seismic and Quasi-static Testing," *Earthquake Spectra*, Vol. 20, No. 3, 2004.
- [3] Cohen, G. L., Klingner, R. E., Hayes, J. R. Jr., and Sweeney, S. C., "Seismic Evaluation of Low-Rise Reinforced Masonry Buildings With Flexible Roof Diaphragms Part II: Analytical Modeling," *Earthquake Spectra*, Vol. 20, No. 3, 2004.
- [4] Cohen, G. L., Klingner, R. E., Hayes, J. R., Jr., and Sweeney, S. C., "Seismic Response of Low-Rise Masonry Buildings With Flexible Roof Diaphragms, Part III: Synthesis and Application," *EERI Spectra* (accepted for publication, August 2005).
- [5] Harris, H. G. and Sabnis, G. M., *Structural Modeling and Experimental Techniques*, 2nd ed., CRC Press, Boca Raton, FL, 1999.
- [6] Wen, Y. K. and Wu, C. L., *Generation of Ground Motions for Mid-America Cities*, Mid-America Earthquake Center, University of Illinois at Urbana-Champaign, 1999.
- [7] Krawinkler, H., Parisi, F., Ibarra, L., and Medina, R., "Development of a Testing Protocol for Wood Framed Structures," Draft Report, Department of Civil and Environmental Engineering, Stanford University, Stanford, CA, 2000.
- [8] Medearis, K. and Young, D. H., "Energy Absorption of Structures Under Cyclic Loading," *ASCE J. Struct. Div.*, Vol. 90, No. 1, 1964, pp. 61–91.
- [9] Soltis, L. A. and Mtenga, V. A., "Strength of Nailed Wood Joints Subjected to Dynamic Load," *For. Prod. J.*, Vol. 35, Nos. 11/12, 1985, pp. 14–18.
- [10] Atherton, G. H. and Johnson, J. W., "Diagonally Sheathed Wood Diaphragms", *Proceedings of the Annual Meeting of the Structural Engineer Association of California*, Yosemite, CA, 1951.
- [11] Stillinger, J. R. and Johnson, J. W., "Racking Test on Quarter-Scale Diagonally Sheathed Wall Panels," Report No. T-1, Oregon Forest Products Laboratory, 1954.
- [12] English, J. M. and Knowlton, C. F., "Load Test of a Diagonally Sheathed Timber Building, *Proceedings of the American Society of Civil Engineers Structural Division*, Vol. 81, 1955, p. 830.
- [13] Foschi, R. O., "Analysis of Wood Diaphragms and Trusses. Part I: Diaphragms," *Can. J. Civ. Eng.*, Vol. 4, 1977, pp. 345–352.
- [14] American Forest and Paper Association (AFPA), *Manual for Engineered Wood Construction, Load and Resistance Factor Design*, American Wood Council, Washington, D. C., 1996.
- [15] Abrams, D. and Paulson, T., "Modeling Earthquake Response of Concrete Masonry Building Structures," *ACI Struct. J.*, Vol. 88, No. 4, 1991, pp. 475–485.
- [16] Costley, A. C. and Abrams, D. P., "Dynamic Response of Unreinforced Masonry Structures With Flexible Diaphragms," Structural Research Series No. 605, Department of Civil Engineering, University of Illinois at Urbana-Champaign, October, 1995.
- [17] Tena-Colunga, A. and Abrams, D. P., "Seismic Behavior of Structures with Flexible Diaphragms," *J. Struct. Eng.*, Vol. 122, No. 4, 1996, pp. 439–445.
- [18] Tena-Colunga, A., "Displacement Ductility Demand Spectra for the Seismic Evaluation of Structures," *Eng. Struct.*, Vol. 23, No. 10, 2001, pp. 1319–1330.
- [19] Agbabian, Barnes, and Kariotis, "Methodology for Mitigation of Seismic Hazards in Existing Unreinforced Masonry Buildings: Diaphragm Testing," Topical Report ABK-TR-02, El Segundo, CA, 1981.
- [20] SAP2000 Non-Linear V7.10, Computers and Structures, Inc., Berkeley, CA, 1999.
- [21] Clark, A. J., "Dynamic Characteristics of Large Multiple Degree of Freedom Shaking Tables," *Proceedings of the Tenth World Conference on Earthquake Engineering*, Madrid, 1992, pp. 2823–2828.
- [22] Steel Deck Institute (SDI), *Diaphragm Design Manual*, 1st ed., St. Louis, MO, 1981.
- [23] Steel Deck Institute (SDI), *Diaphragm Design Manual*, 2nd ed., St. Louis, MO, 1995.
- [24] Jain, J. K. and Jennings, P. C., "Analytical Models of Low-Rise Buildings With Flexible Floor

- Diaphragms," *Earthquake Eng. Struct. Dyn.*, Vol. 13, 1984, pp. 225–241.
- [25] Tremblay, R. and Stiemer, S., "Seismic Behavior of Single-Story Steel Structures With Flexible Roof Diaphragm," *Can. J. Civ. Eng.*, Vol. 23, 1996, pp. 49–62.
- [26] Applied Technology Council (ATC), "Guidelines for the Design of Horizontal Wood Diaphragms," Publication ATC-7, Berkeley, CA, 1981.
- [27] Federal Emergency Management Agency (FEMA), *NEHRP Guidelines for the Seismic Rehabilitation of Buildings*, Publication 273, Washington D.C., 1997.
- [28] Federal Emergency Management Agency (FEMA), *NEHRP Commentary on the Guidelines for the Seismic Rehabilitation of Buildings*, Publication 274, Washington D.C., 1997.
- [29] Western Wood Products Association (WWPA), *Western Woods Use Book*, 4th ed., Portland, OR, 1996.
- [30] CANNY 99 V1.0, "CANNY Structural Analysis," Vancouver, BC, Canada, 1996.
- [31] Federal Emergency Management Agency (FEMA), *Handbook for the Seismic Evaluation of Buildings—a Prestandard*, Publication 310, Washington D.C., 1998.
- [32] ASCE 31-03, *Seismic Evaluation of Existing Buildings*, ASCE, New York, 2003.
- [33] Federal Emergency Management Agency (FEMA), *Prestandard and Commentary for the Seismic Rehabilitation of Buildings*, Publication 356, Washington D.C., 2000.
- [34] International Code Council (ICC), *International Building Code*, Los Angeles, CA, 2000.
- [35] Johnson, J. W., "Lateral Tests on Full-Scale Lumber-Sheathed Roof Diaphragms of Various Length-Width Ratios," Report No. T-9, Oregon Forest Products Laboratory, 1954.
- [36] Johnson, J. W., "Lateral Tests on a 12- by 60-foot Plywood-Sheathed Roof Diaphragm," Report No. T-11, Oregon Forest Products Laboratory, 1955.
- [37] Johnson, J. W., "Lateral Tests on a 12- by 60-foot and 20- by 80-foot Lumber-Sheathed Roof Diaphragms," Report No. T-12, Oregon Forest Products Laboratory, 1955.
- [38] Stillinger, J. R. and Johnson, J. W., "Lateral Tests on Full-Scale Lumber Sheathed Diaphragms," Report No. T-3, Oregon Forest Products Laboratory, 1952.
- [39] Nilson, A. H., "Shear Diaphragms of Light Gage Steel," *ASCE J. Struct. Div.*, Vol. 86, No. 11, 1960, pp. 111–139.
- [40] Luttrell, L. D., "Strength and Behavior of Light-Gage Steel Shear Diaphragms," *Engineering Research Bulletin 67-1*, Cornell University, Ithaca, NY, 1967.
- [41] Ellifritt, D. S. and Luttrell, L. D., "Strength and Stiffness of Steel Deck Subjected to In-plane Loading," Report No. 2011, West Virginia University Department of Civil Engineering, Morgantown, WV, 1970.
- [42] United States of America, *Executive Order 12941*, Washington, D.C., 1994.
- [43] URS Greiner, Inc., "Seismic Evaluation of Existing Buildings, Fort Lewis, Washington, Final Evaluation Report," Final Report to US Army Corps of Engineers, San Francisco, CA, 1997.
- [44] Federal Emergency Management Agency (FEMA), *Handbook for the Seismic Evaluation of Existing Buildings*, Publication 178, Washington D.C., 1992.

Keith Bargaheiser¹ and D. Herbert Nordmeyer²

Greening of Mortars with Pozzolans

ABSTRACT: Growing interest in sustainable building has created a strong interest in fly ash and other coal combustion products (CCPs). Emergence of agencies like the U.S. Green Building Council (USGBC) and the Coal Combustion Products Partnership (C2P2) of the USEPA has accelerated this trend. Their primary goal is sustainable development, focusing on environmental and social concerns. More than 30 % of the 100 million tons of coal combustion products produced in the U.S. annually are being beneficially used in such things as manufactured stone, ceramic tile, shingles, concrete, aerated cellular concrete blocks, concrete blocks, stuccos, and mortars. The use of CCPs positively impacts the environment. Specifiers, contractors, and industry need to recognize that environmental stewardship today affects our children tomorrow. The features and benefits recognized in pozzolanic mortars reach beyond the technical, environmental, social, and sustainable aspects of this mortar. They signal future generations to track, improve, and develop mortars beyond any of our current technology.

KEYWORDS: mortars, pozzolans, LEED, sustainable, masonry cement, green

Introduction

The United Nations World Commission on the Economy and the Environment in 1987 defined sustainable development as “the ability of humanity to ensure that it meets the needs of the present without compromising the ability of future generations to meet their needs” [1]. But sustainable design is not a new construction concept. Rather, it is a lost focus or art from our past. Our ancestors in ancient Greece and Rome had to focus on sustainable construction, for their structures took as long to build as our structures last today.

With the development of the United States Green Building Council (USGBC), the idea of “green” construction has been introduced to the public. To some, the words *sustainability* and *green* are interchangeable. However, sustainability encompasses much more than visions of recyclables or modifiers to make a product work better or last longer.

The concrete and masonry industry as a whole has recently been faced with issues either unanticipated or dismissed as speculation, including cement shortages and the depletion of our raw materials. The U.S. has always been recognized as a land of plenty with endless resources. For the first time, economic and societal issues are being discussed within the scope of their business/environmental relationships. This is being driven in part by the energy crunch felt by our nation at the gasoline pump. We are realizing that economics and social development must coexist with environmental concerns simultaneously for our future products. What we are reacting to and describing could be termed “The Fourth Wave of Development.”

Understanding the Societal Waves of Growth

Alvin Toffler, writer and futurist, describes in his book, *The Third Wave*, three types of societies within mankind’s social evolution as waves [2].

The first wave of societal transformation began when the first seed was planted and nurtured to grow. The Agricultural Age was born. As people ceased nomadic wandering and began to cluster in villages, new cultures developed. Wealth was defined by land. Land was owned by groups or individuals, and outsiders

Manuscript received November 21, 2005; accepted for publication June 9, 2006; published online October 2006. Presented at ASTM Symposium on Masonry on 13 June 2006 in Toronto, Ontario, Canada; B. Trimble and J. Brisch, Guest Editors.

¹ National Manager of CCP Utilization, Headwaters Resources, 7006 Regents Park Blvd., Toledo, OH 43617.

² Project & Technology Manager, Headwaters Construction Materials, San Antonio Laboratory, 5014 Callaghan Road, San Antonio, TX 78228.

were driven away. Limited education prevented any infrastructure to support or share new ideas.

The second wave began with the Industrial Revolution in the 18th century when people left the agrarian culture to work in factories. Wealth was diversified into three factors of production: land, labor, and capital. As with the land in the agrarian culture, each factor was discrete, allowing for only one owner at a time. The central theme of this culture was centralization and standardization. Mass production was of primary importance, linking everything to central control; however, mass production processes were not without drawbacks. To quote Henry Ford, "They can have a car of any color they like, as long as it is black" [3]. This was a period when selection referred only to the quantity needed. Individual differences were limited.

The third wave was driven by technology and called the Information Age or Knowledge Age. It would have co-drivers, worldwide social demands, and greater freedom and individualization. Wealth comprised the harnessing of knowledge, allowing those willing to learn to prosper, and not just one person at a time. As the intent of the Industrial Revolution was to bring everything under one roof, the Communication Age would be to decentralize. Technology and education revert towards individualization and diversity.

Today we are still experiencing a transition from the second to the third wave. That is why implications of both still exist, and transformation is not always obvious. As knowledge replaces material and manpower as the centerpiece of our economy, there is a blurring of meanings. Toffler used a cup of coffee to clarify this period. In early small towns across America, the coffee in each town had its own distinctive taste because each town had its own roaster. With mass production and the appearance of mass distribution outlets such as McDonalds, products became uniform. Every McDonalds' cup of coffee was exactly like every other McDonalds' cup of coffee. Now we see small specialty shops, such as Starbucks, popping up all over the country. They have the ability to produce to an individual's demand, whether it is coffee or some other product. Society is progressing towards economical and individual independence.

The fourth wave is transitioning into our society before elements of our second wave have been completed. It is being driven by the continued thrust for individual and economic freedom on a worldwide scale. Sustainability is changing an individual's mindset, by forcing him to look at the products he uses and question whether they are the best choice. Price is no longer the only factor (second wave item).

Evaluating the products for their differences (third wave item) and the impact each will have on the environment (fourth wave item) are now topping most individuals' decisions. The concept of economic and social development co-existing with our environment defines the fourth wave. A prime example is the USGBC's LEED™ program [4], offering designers and builders economic, social, and environmental choices for sustainable construction projects.

Mortars

Very few can see the relevance of economic, social, and environmental issues concerning mortars, since it is one small piece of the construction industry. The impact is not one that society or industry can see catastrophically affecting us, as gasoline has. In the past, who would have imagined gasoline prices influencing society to change the way their daily lives were conducted? We need to look into the future and ask ourselves, will our mortars today be available or even desired as currently manufactured? Will the materials or the processes even exist to make today's mortars part of the fourth wave?

Governmental Concerns of Sustainability

On October 20, 1993, the first version of section 6002 of the Resource Conservation and Recovery Act (RCRA) was developed under Executive Order 12873 [5]. Congress acknowledged the importance of recycling by mandating that government agencies increase their purchase of products containing recovered materials (i.e., waste materials and by-products that have been recovered or diverted from solid waste). To further that mandate, the RCRA specifies that the Environmental Protection Agency (EPA) develop and issue procurement guidelines designating specific items that are or can be made with recovered materials and to recommend practices with respect to the procurement of recovered materials and items containing such materials. Procuring agencies (federal, state, and political subdivisions of states that use appropriated federal funds) and their contractors are required to buy designated items with the highest recovered-material content practicable. CCPs were at the top of this list.

Even with the RCRA increasing the rate of recycling in the U.S. and increasing the use of recyclables in building products, there still is an uphill battle to be faced. Leading the list for nonacceptance of recyclables has been the undervaluing of energy and public perception regarding alternatives to virgin resources. We must consider the true societal costs of energy use, consumption, and pollution from manufacturing. Again, gasoline serves as a good example. To quote an article from *Environmental Building News* [6]: "Estimates of the 'societal costs' of petroleum consumption should range up to \$5.00 per gallon (\$1.32/L) of gasoline equivalent, or even higher. The American Lung Association calculated that just the healthcare costs of automobile-caused air pollution in the U.S. totaled about \$100 billion per year, or roughly \$1.00 per gallon (26 cents/L)." All energy sources have advantages and disadvantages. Fossil fuels and nuclear energy have long been known to be health and environmental hazards. Solar cells and hydrogen technologies, while promising cheap, renewable energy, are expensive and technically impractical for now. Choosing the best source for today's needs and balancing the economic and social costs to the environment are the challenges.

Sources of Energy

Oil Power

Oil prices, for example, have soared 90 % in the last 18 months. Drilling for new sources does not appear to be a good economic or social decision. In 2003 the oil industry spent \$8 billion on exploration but discovered only \$4 billion of commercially useful oil. Further exacerbating the problem of burning fossil fuels is the release of carbon dioxide, considered a major contributor to greenhouse gases, which may cause global climate changes. Sadly, most alternatives to conventional energy sources cannot provide the amount of energy we need without damaging our environment, jeopardizing our national security, or bankrupting us. [7]

Nuclear Power

Nuclear energy produces its own unique economic, social, and environmental problems. When used, there are no greenhouse gases emitted. However, disposal of waste products and security issues are major problems. To meet American's energy demands over the next 50 years using nuclear power, 1200 new nuclear power plants are needed in addition to the current 104. This means building one plant every two weeks until 2050. This alternative still presents formidable issues with regard to environment, national security, and economics [7].

Solar Power

Solar power has always been viewed as an environmentally friendly energy source. However, technology has not developed methods of capturing solar energy which would make it a logical alternative either environmentally or economically. Satisfying today's current electricity demand, using today's technology, would require 10 billion square metres of photovoltaic panels to store the energy, at a cost of \$5 trillion dollars or nearly half the U.S. annual gross domestic product. Other negatives would be the environmental issue of battery disposal and the lack of regionally adequate sunlight [7].

Hydrogen Power

Hydrogen power is an up and coming energy source that has also been viewed as an environmentally friendly energy source. If the number of cars and trucks in use today in the U.S. alone were powered by hydrogen, America would have to produce 230 000 tons of hydrogen gas each day. This would be enough gas to fill 13 000 Hindenburg-size dirigibles every day [7]. Theoretically, with current technology, water electrolysis could meet this capacity. However, scientists are estimating that 50 % of the world will face water shortages within 50 years, so electrolysis could be a huge societal issue restricting the outcome [8].

Carbon-Free Energy

For carbon-free renewable energy to be effective, America would have to double its electrical output. This would mean covering an area the size of Massachusetts with solar panels or New York State with wind-

mills. Although technologies are always improving, it will take one or a combination of these technologies to surpass fossil fuels economically, socially, and environmentally, while minimizing national security threats [7].

Energy Source of the Fourth Wave

Considering the economic, social, and environmental impact of our current options, fossil fuels, specifically coal, remain our best energy source. With no significant change expected for another two generations (our grandchildren), research on old and new technologies will continue to measure their significance in a fourth wave society. Bridge technologies incorporating fossil fuels and new technologies are leading the way to solving our economic, social, and environmental needs through coal gasification. Since this paper is directed towards mortars with pozzolans, we will be focusing on how CCPs, in particular fly ash, will benefit the fourth wave since they are a valuable by-product of coal-burning, electricity-generating power plants.

USGBC and Mortars

LEED™ is a credit-based program of the U.S. Green Building Council, allowing projects to earn points for environmentally friendly actions taken during the design and construction processes. A project with a minimum of 26 points qualifies for LEED™ certification. The advanced levels include silver with 33 points, gold at 39, and platinum at 52 points. The USGBC recognizes concrete masonry in the LEED™-NC Green Building Rating System, version 2.1. Points of credit for masonry materials include sustainable sites, energy and atmosphere, materials and resources, indoor environmental quality, and innovation in design processes. Pozzolanic mortars can further qualify for credits based on the following ways: decreased life cycle environmental impacts (due to mortar's low embodied energy and its longer life cycle), durability, and low maintenance. The LEED™ program goes far beyond any previous specification/requirement for construction or design by addressing fourth wave issues. The point system below demonstrates LEED™ influence over the economic, social, and environmental impact of a structure [4].

Sustainable Site Credit—Development Density (1 Point)

Redevelopment of brown fields can earn the project a point towards LEED™ certification. Since concrete masonry units are small and portable, they can be used in cramped and irregular-shaped lots. They also require less storage space and minimize transportation and handling issues.

Energy and Atmosphere Credit—Optimizing Energy Performance (1–10 Points)

The focus here is to increase the building's energy efficiency above the minimum level required by the LEED™ program. This is determined by ASHRAE/IESNA 90.1-999 or the local energy code, whichever is stricter. One to ten points can be awarded for energy cost savings of 15 to 60 % for new construction and 5 to 50 % for existing building. Thermal mass inherent in concrete masonry aids in accomplishing this goal. Simply, masonry units reduce the heating and cooling loads of a building by the inherent insulating properties of wall thickness.

Materials and Resources Credit—Building Reuse (1–2 Points)

Conserving resources and reducing waste, as well as extending usable building life, can mediate the adverse environmental impact normally caused by new construction. Up to two credits are earned when the majority of the building's structure and shell are maintained. One point is given for 75 % of the existing building and two points if 100 % is left in place.

Materials and Resources Credit—Recycled Content (1–2 Points)

One point can be given for 5 % and two points for 10 % total recycled content. This includes both post-consumer and one-half post-industrial content. As a partial replacement in mortar, fly ash aids in obtaining this goal.

Materials and Resources Credit—Local/Regional Materials (1–2 Points)

Up to two points can be gained by incorporating 20 % of materials that are manufactured or harvested, or both, within a 500-mile radius of the site. An additional point can be earned if the 50 % mark is obtained. Again, the availability of fly ash aids in obtaining this goal.

Innovation in Design (1–4 Points)

Up to four points can be gained with design innovations that exceed the LEED™ requirements. Previously awarded points have come from life cycle impacts, improved indoor air quality, efficient use of materials, increased acoustic performance, and increased fire safety.

Mortars for Fourth Wave

Type N masonry cement produced with pozzolanic technology or ground granulated blast furnace slag technology can contain over 60 % of post-industrial recycled materials. We refer to mortars produced using the Type N masonry cement as the fourth wave mortars. Compared with mortar that is most commonly specified by architects (portland cement/hydrated lime), fourth wave mortars can reduce the environmental load of a project by roughly 65 %. Only 27 lb of carbon dioxide (CO₂) is produced with a bag of fourth wave mortars, as compared to 76 lb for an equivalent amount of portland/lime mortar. (This number holds true for both Type N and Type S portland/lime mortars.) Only 84 000 BTUs of energy are required to produce a bag of fourth wave masonry cement, as compared to 244 000 BTUs of energy needed to produce an equivalent amount of portland/lime mortar.

Standard Specification for Masonry Cement (ASTM C 91) [9] is the international standard for masonry cement. It includes requirements for Types N, S, and M masonry cements. Within the past decade, there has been a gradual switch from Type N to Type S, which has become the most common masonry cement. The cause for this change has been twofold:

1. A belief among many masons that Type S will carry more sand.
2. A belief among specifiers that greater strength automatically means “better.”

We will discuss why fourth wave mortars are not only the best answer for today’s needs, but also important to our future.

ASTM C 91 Mandates

ASTM C 91 mandates that masonry cements must comply with specific physical requirements. These include fineness, autoclave expansion, time of setting, compressive strength at 7 and 28 days, air content, and water retention. Standards exist for Type N, Type S, and Type M masonry cements. The pozzolanic technology and the ground granulated blast furnace slag technology masonry cement that are commercially available today comply with the ASTM C 91 mandates. Beyond that, they have specific characteristics which will be discussed in the following paragraphs.

Required Strengths

ASTM C 91 mandates a compressive strength of 6.2 MPa (900 psi) after 28 days for Type N masonry cement, 14.5 MPa (2100 psi) for Type S, and 20.0 MPa (2900 psi) for Type M. From a perspective of compressive strength alone, the Type N products are adequate to support a masonry wall from 21 to 25 stories high. Many codes limit Type N masonry cement to not more than four stories by prescription or by calculations of stresses on the wall. This would indicate the commonly used argument that “higher compressive strengths are needed” is not valid in most situations.

ASTM C 91 does not include flexural bond strength requirements. Standard Specification for Mortar Cement (ASTM C 1329) [10] is the international standard for mortar cement. It is usually required for masonry within seismic zones. It mandates minimum flexural bond strengths for Type N at 0.5 MPa (70 psi), Type S at 0.7 MPa (100 psi) and 0.8 MPa (115 psi) for Type M. Many experts believe the parameter of flexural bond is more important than that of compressive strength [11].

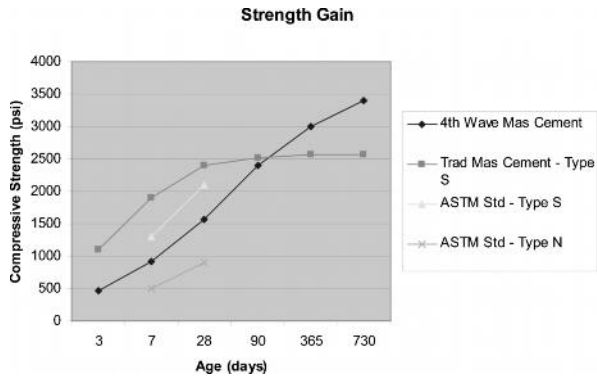


FIG. 1—Strength gain with fourth wave masonry cement mortar.

Strength Gain with Time

Figure 1 depicts the strength gain over time with Type S traditional masonry cement and with fourth wave masonry cement mortar. It also contains the minimum compressive strength requirements for Type N and Type S ASTM C 91 masonry cement. Fourth wave masonry cement mortars (hereafter termed “fourth wave mortars”) do not obtain the 28-day strength requirements of Type S masonry cement until around 56 days. However, they exceed the compressive strength found in traditional Type S masonry cements shortly after 100 days.

Traditional masonry cements are composed of a mixture of portland cement, ground limestone, and an air-entraining agent (usually Vinsol resin). As a result, strength gain is accomplished in the same manner as portland cement. At seven days, approximately 75 % of the ultimate strength is reached, and at 28 days approximately 90 to 95 % of the ultimate strength is reached. Several traditional masonry cements show little or no compressive strength gain after 28 days, and most show no strength gain after one year.

Fourth wave mortars utilize the chemical reaction between fly ash and cement mortar to enhance the end product. This technology makes beneficial use of the calcium ions (very small, chemically reactive, and mobile) that are produced when portland cement hydrates. The calcium ions are chemically reacted with an amorphous silica or alumina (pozzolans) to produce additional cement binder. Furthermore, the hydrated lime that is incorporated into the mix for workability has larger particles that are not as reactive and mobile as ionic calcium. It slowly reacts with the amorphous silica and alumina to produce additional cement binder over a period of several years. This results in autogenous healing in the event minor cracking occurs.

A side benefit of the designed slower strength gain of fourth wave mortars results in walls that are easier to clean over a longer period of time. This allows the mason to make better use of his time.

Flexural Bond Strength

Since ASTM C 91 does not mandate flexural bond strength, most traditional masonry cements are not designed based on this parameter. Tests of traditional masonry cements for flexural bond strength (both Type N and Type S) indicate a range from 5 to 70 psi after 28 days. In fairness to the producers of the traditional masonry cements, since ASTM C 1329 was adopted, there has been an increase in flexural bond strength. This growing acceptance is a direct result of the masonry cement industry’s experiences with veneer walls in modern buildings.

Fourth wave mortars are designed to comply with ASTM C 91, not ASTM C 1329; therefore, flexural bond strength testing is not required. However, testing over the years has found that the flexural bond strength usually will range from 75 to 97 psi at 28 days.

Efflorescence

Efflorescence describes water soluble salts that are carried to the surface of masonry cements through evaporation, leaving a white residue. Efflorescence can be caused by alkaline earth compounds or by

sodium and potassium salts in the mortar or masonry unit that migrate to the surface and are left on the surface when water evaporates. The only common alkaline earth compound found in masonry is calcium. Sodium and potassium salts normally can be brushed or washed off. When calcium ions move to the surface, they react with carbon dioxide in the air; the result is calcium carbonate or limestone deposits on the wall. Scrubbing with acid is required to remove the calcium carbonate efflorescence. Portland cement releases 20 to 30 % of available calcium (measured as calcium hydroxide) during the hydration process. Since traditional masonry cements contain from 50 to 65 % portland cement, from 7 to 12 lb of calcium hydroxide is released per bag of masonry cement into the mortar and may migrate to the surface as efflorescence. Portland/lime mortars release even more available calcium. Fourth wave masonry cements contain less than half of the portland cement found in traditional masonry cements. As a result, only 5 lb of calcium hydroxide are released per bag. Pozzolans in the fourth wave masonry cement chemically react with the calcium hydroxide and reduce the amount of calcium hydroxide that is available to effloresce.

Workability

Traditional masonry cements depend on ground limestone and entrained air to provide workability. Neither adds to the flexural or compressive strength of the product. Fourth wave mortars utilize hydrated lime and fly ash to provide workability. Both add to the long-term flexural and compressive strength of the product. The fly ash particles are spherical in shape and act as miniature ball bearings, or a natural lubricant, in the mix. Additionally, the fly ash particles do not absorb as much water as portland cement or ground limestone, so workability can be obtained with a lower water/cement ratio. The low water absorption of the fly ash also leads to a longer board life. The greater workability of the fourth wave mortar can allow masons to lay 5 to 10 % more brick in a day.

Extent of Bond

A by-product of the increased workability is greater extent of bond. Within a brand, as one moves to greater compressive strength, the mortar usually becomes harsher. With harsher mortars, greater skill is required for a mason to achieve full head and bed joints. Mortar that is not present in a wall does not contribute to the overall bond between the masonry units and the mortar. Low levels of bonding can often be observed by examining the brick/mortar interface with a magnifying glass. A hairline crack indicates areas where the bond does not exist. Other than through penetrations such as improperly installed doors and windows, most water penetration through masonry walls occurs

1. In walls built with moderate-to-low IRA (instantaneous rate of absorption) brick;
2. Through areas where mortar is lacking (failure to fully butter the head and bed joints); or
3. Where the bond is lacking.

Little water passes through the bricks themselves or the mortar. Fourth wave mortars' high workability allows a competent mason to lay brick with a high extent of bond.

Cement Shortages

When there is a shortage of cement, most portland cement companies prefer to continue making portland cement, rather than switch to producing masonry cement. The use of fourth wave mortars will actually help to extend the availability of the limited amounts of portland cement as well as the availability of other natural resources.

Green

Whether one believes in global warming or not, there is a groundswell of interest in green building. As stated, fourth wave mortars are some of the greenest mortars and underlying masonry cements can be manufactured without:

1. Paying extra manufacturing costs that will be passed on to the consumer;
2. Sacrificing workability; or
3. Sacrificing performance.

Cost

When one purchases a better product, one expects to pay more. Switching to fourth wave mortars from a portland/lime mortar or from a traditional masonry cement provides a better product usually at a lower cost. Additionally, users can advertise that the product is one of the “greenest” masonry cements on the market.

Standards Development

Pozzolanic masonry cements and mortar cements are currently being produced and are meeting the ASTM C 1329 and ASTM C 91 standards. An examination of Fig. 1 reveals that pozzolanic cements continue to gain strength after conventional masonry cements have ceased to gain strength. If the current 28 day compressive strength requirement for Type S masonry cement were selected as the optimum compressive strength for fourth wave mortar, and if the standard allowed 60 to 90 days to achieve that strength, rather than 28 days, a very green product could be produced and used. To allow such a usage, ASTM Committee C12 would need to examine the fourth wave mortar and make modifications to ASTM C 91, ASTM C 1329, or develop a separate standard. If standards under C12’s control were modified, it would provide strong support that would lead to the acceptance of fourth wave mortars and to greener building.

Conclusion

Changes are occurring today at a very rapid pace. What was good for business yesterday may not make sense today, or for future growth. We all search for ways to be on the cutting edge for ourselves and our companies. This paper addresses where we are, where we have been, and where we need to go, to succeed with mortars. Sustainability has impacted the cement masonry world like no other factor before it. The USGBC’s LEED™ program is demanding that all of us consider the economic, social, and environmental impact of our material decisions. The fourth wave of societal evolution mandates that products be selected not only by the cost alone, but also by weighing the issues of the times. The need for economic and social development to co-exist with environmental concerns weighs heavily on the product choices we make now and in the future.

Type N masonry cements, with 60 % or more post-industrial recycled materials, are used to produce fourth wave mortars. They aid in lowering CO₂ production, a greenhouse gas which has been implicated in discussions of global warming. Fourth wave mortars improve not only the physical and chemical properties of mortar, but also help to sustain our environment. Keeping true to the needs of our fourth wave society, fourth wave mortars encompass economic, social, and environmental needs by maintaining high quality without increased cost or adverse environmental impacts.

References

- [1] Pincetl, S. “Practice and Theory of Urban Sustainability in the Developed and Developing Nations,” *USC Center for Sustainable Cities*, Fall 2002, p. 2.
- [2] Toffler, A., *Third Wave*, William Marrow Co., Inc., New York, 1980.
- [3] “World of Words, Top 100 Quotes from the Oxford Dictionary of Quotations” #58 <http://www.askoxford.com/worldofwords/quotations/100quotes/>.
- [4] United States Green Building Council (USGBC). www.usgbc.org.
- [5] “Executive Order 12873, Federal Acquisition, Recycling and Waste Prevention,” Issued October 20, 1993, by President Bill Clinton.
- [6] *Environmental Building News*, Vol. 12, No. 4, 2005, Editorial.
- [7] Homer-Dixon, T. and Friedman, S. J., “Coal in a Nice Shade of Green,” *The New York Times*, March 25, 2005, p. 17.
- [8] Vergano, D. “Water Shortages Will Leave World in Dire Straits,” *USA Today*, January 26, 2003, http://usatoday.com/news/nation/2003-01-26-water-usat_x.htm.
- [9] ASTM C 91, “Standard Specification for Masonry Cement,” ASTM International, West Consho-

hochen PA, For referenced ASTM standards, visit the ASTM website, www.astm.org. For *Annual Book of ASTM Standards* volume information, refer to the Standard's Document Summary page on the ASTM website.

- [10] ASTM C 1329, "Standard Specification for Mortar Cement," ASTM International, West Conshohochen PA, For referenced ASTM standards, visit the ASTM website, www.astm.org. For *Annual Book of ASTM Standards* volume information, refer to the Standard's Document Summary page on the ASTM website.
- [11] Nordmeyer, D. H., "High Pozzolan Mortars and Stuccos," *Masonry: Opportunities for the 21st Century*, ASTM STP 1432, D. Throop and R. E. Klingner, Eds., ASTM International, West Conshohocken, PA, 2003.

John T. Conway¹

Replacement of the Final Time of Setting Maximum with an Initial Time of Setting Maximum as measured with the Gillmore Needles in ASTM C 91, C 1328, and C 1329

ABSTRACT: ASTM Subcommittee C01.11 on Masonry Cement, established a task group on methods of test which determined whether the final time of setting maximum limit could be replaced with an initial time of setting maximum limit. A review was conducted of 52 Cement and Concrete Reference Laboratory proficiency samples (spanning 26 years) and data from the *Portland Cement Association Masonry Cement Survey*. Findings indicate a very reliable and simple linear relationship exists between masonry cement initial and final Gillmore time of setting. Data is presented which resulted in a specification change to ASTM C 91, ASTM C 1328, and ASTM C 1329 in 2005.

KEYWORDS: Gillmore, time of setting

Introduction

ASTM Subcommittee C01.11 on Masonry Cement wanted to determine if an initial time of setting set maximum could replace the final time of setting set maximum as a specification limit. The purpose of considering a change was to save time in the laboratory, so personnel did not have to wait for a final set to occur. The action of the task group was to use existing data to make this determination. No actual change in the setting requirements for the cements was desired. In other words, the action was simply to translate the current requirements from final time of setting to initial time of setting.

Brief History of Masonry Cement and ASTM C 91

Masonry Cement was developed in 1917 [1] and patented in 1919 [2]. Mortars previous to that time were made with natural cement, portland cement, lime, or combinations of these materials. The patented product is described as follows: "The cement produced by the above described process is not only slow setting but has a remarkable degree of plasticity or fatness which renders it of special utility in brick and tile laying where mortar is required—for the mortar can be mixed in larger batches, be tempered more slowly, and enable the workmen to produce a more workmanlike and careful job [2]".

The first ASTM specification for masonry cement was designated ASTM C 91-32T. Initial time of setting was required to be measured with the Gillmore needles and to be not less than 60 min. The final time of setting was required to be within 48 h. These specification limits were continued until ASTM C 91-40 when the final time of setting was required to be within 24 h. Masonry cements were designated as Types I and II at that time. About 1983 the designations changed to the current Types N, S, and M, corresponding to the mortar types listed in ASTM C 270 [3]. The 24-h maximum limit on final time of setting continued until the change, which is the subject of this paper.

A Brief History of the Gillmore Time of Setting Test

The Gillmore test has apparently been used for nearly 200 years, as has the Vicat time of setting test. A report of the American Society of Civil Engineers (ASCE) in 1912 [4] states that the Gillmore wires

Manuscript received October 12, 2005; accepted for publication June 9, 2006; published online August 2006. Presented at ASTM Symposium on Masonry on 13 June 2006 in Toronto, Ontario, Canada; B. Trimble and J. Brisch, Guest Editors.

¹ Manager of Quality Assurance, Holcim (US) Inc., PO box 122, Dundee, MI 48131.

Copyright © 2006 by ASTM International, 100 Barr Harbor Drive, PO Box C700, West Conshohocken, PA 19428-2959.



FIG. 1—General Quincy Adams Gillmore 1825–1888 [6].

appear to have first been proposed by M. A. Racourt and were used prior to 1830. That report recommends the Vicat method, but mentions the Board of Army Engineers adopted the Gillmore needles. It also states that General Q. A. Gillmore recommends their use (Figs. 1 and 2). A report by General Gillmore mentions use of the Gillmore wires prior to 1830 by General Totten [5].

General Gillmore was probably most famous for his role in the civil war as the Union General in charge of the campaign against Charleston, SC. After the war, he became a Major of Engineers in the US Army. Some of his engineering expertise was probably applied to the use of cannons on masonry forts.

The Gillmore apparatus is comprised of two thin rods (needles) with weights on them. The final set needle weighs one pound (453.6 g) and has a tip diameter of 1/24th of an inch (1.06 mm), and the initial set needle weighs one-quarter pound (113.4 g) and has a tip diameter of 1/12th of an inch (2.12 mm).

Time of setting is defined in ASTM C 266-04 [8] as the stiffness at which the needle can be supported by the paste specimen without leaving an appreciable indentation.

The Relationship Between the Gillmore Initial and Final Times of Setting

Data was provided by the Cement and Concrete Reference Laboratory (CCRL) [9] from the last 52 masonry cement proficiency samples. This represents 26 years of tests on one pair of samples per year. In the CCRL proficiency sample program, commercially available cements are sent to many laboratories for testing and comparison of results. Current participation in the masonry cement testing program is about 78 laboratories. The averages of all the laboratories' results on the Gillmore tests were used in calculating the conversion from initial to final time of setting. The data is included in Table 1.

Figure 3 shows the simple, linear relationship between the initial and final times of setting in the data. From this it is easily estimated from the linear formula below that an initial time of setting of 996 min corresponds to a final time of setting of the ASTM C 91-04 specification limit of 1440 min. An initial time of setting maximum of 1000 was proposed. Note the relatively high R^2 value, indicating a good fit of the data.

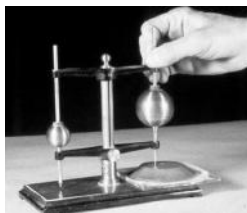


FIG. 2—The Gillmore Apparatus [7].

TABLE 1—CCRL Data [9].

Year	Sample	Initial Gillmore (min)	Final Gillmore (min)	Year	Sample	Initial Gillmore (min)	Final Gillmore (min)
1978	1	142	260	1991	27	169	300
	2	161	311	1991	28	256	477
1979	3	110	240	1992	29	174	293
	4	158	301	1992	30	140	252
1980	5	178	306	1993	31	128	239
	6	339	502	1993	32	165	271
1981	7	157	268	1994	33	143	249
	8	184	312	1994	34	160	283
1982	9	171	312	1995	35	158	287
	10	127	248	1995	36	205	323
1983	11	173	307	1996	37	145	260
	12	171	305	1996	38	195	309
1984	13	125	242	1997	39	260	385
	14	278	448	1997	40	173	287
1985	15	208	377	1998	41	244	378
	16	153	298	1998	42	182	336
1986	17	144	274	1999	43	145	260
	18	186	340	1999	44	188	321
1987	19	154	273	2000	45	152	267
	20	152	282	2000	46	183	316
1988	21	197	346	2001	47	288	432
	22	147	271	2001	48	208	343
1989	23	341	561	2002	49	210	332
	24	134	270	2002	50	302	440
1990	25	151	272	2003	51	147	254
	26	209	315	2003	52	158	265

Applying this formula to a subsequent CCRL sample pair (Nos. 53 and 54, for 2005), the calculated initial Gillmore times of setting were 225 and 199 versus actual results of 241 and 197, respectively. The validity of the calculation is illustrated in Figs. 4 and 5.

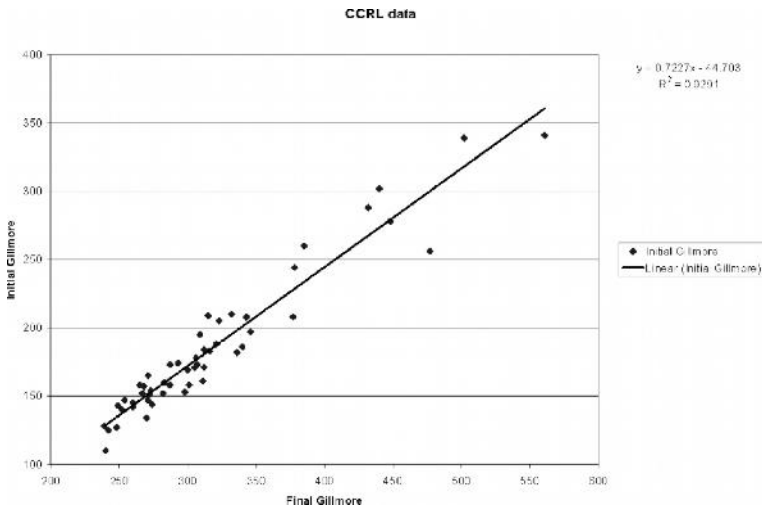


FIG. 3—Relationship between initial and final Gillmore setting time.

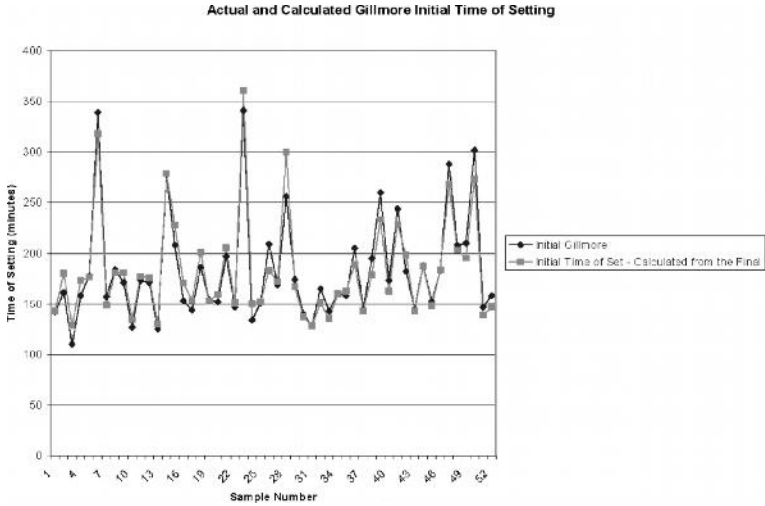


FIG. 4—Illustration of actual initial time of setting and initial time of setting calculated from the final time of setting.

A graphical perspective of the data and the specification limits is shown in Fig. 6.

An initial time of setting of 1000 min as well as a final time of setting of 1440 min is outside the range of the CCRL data. This could result in error when applying the equation to these higher numbers, so the Portland Cement Association Masonry Cement Survey of 1999 was consulted [10]. That data, reported by about 2/3 of the plants in North America producing masonry cement, showed no values of time of setting even close to the limits of 1000 min for initial or 1440 for final. The maximum value for initial time of setting for any type of masonry or mortar cement was 660 min, and the maximum final time of setting value was 720 min.

The new initial time of setting maximum limit of 1000 min should not cause any problems, since no reported cements approach that limit, nor did they approach the now-replaced final time of setting maxi-

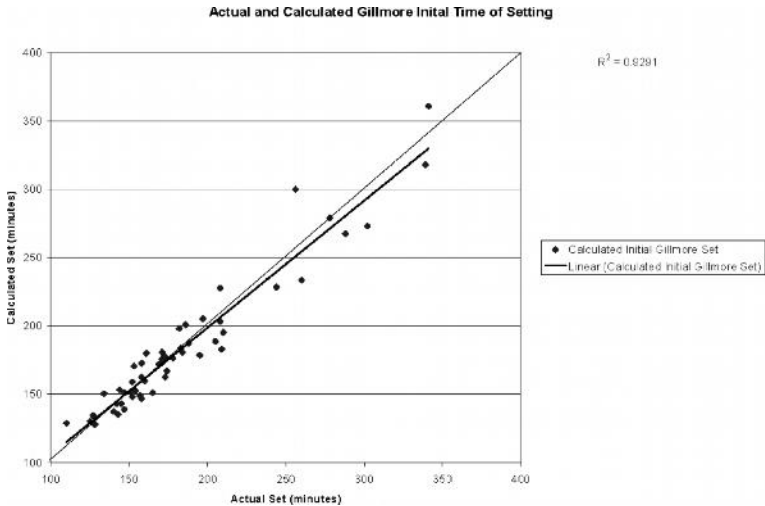


FIG. 5—Linear plot of actual and calculated Gillmore initial time of setting.

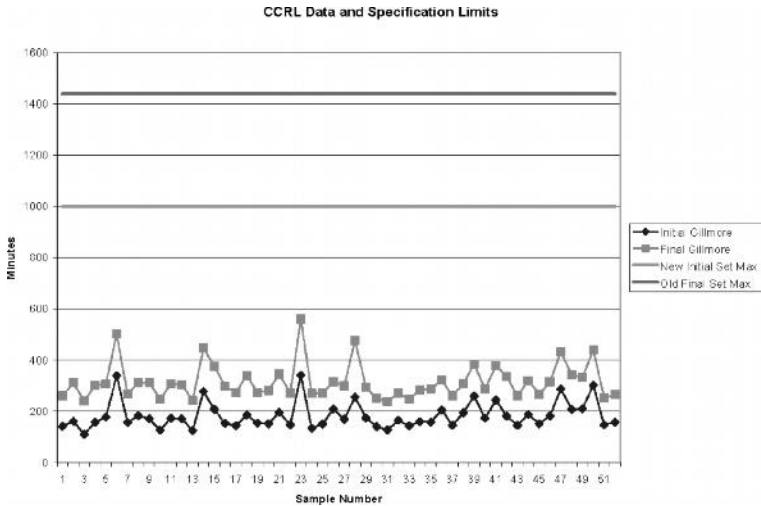


FIG. 6—Gillmore time of setting and specification limits.

num. The replacement of the final time of setting has passed the ASTM process and will appear in ASTM C 91 [11], ASTM C 1328 [12], and ASTM C 1329 [13]. The revision was not complete in time to make the 2005 printing.

Conclusions

- The time of setting tests have stood the test of time, since they have been used for a span approaching 200 years.
- Cements for masonry have been shown to have a very consistent and predictable relationship between their initial and final Gillmore times of setting.
- An equivalent maximum value for the initial time of setting (1000 min) has been incorporated into ASTM specifications to replace the maximum final time of setting specification (1440 min) to save time in the laboratory. This should not impact the performance of the material, but will save time in testing.
- CCRL data is a very useful database for studying this type of relationship and was instrumental in accomplishing this change.

References

- [1] Elliott, David P., "From Weighted Needles to the X-Ray Spectrometer," *Pit and Quarry*, 1980, pp 78–82.
- [2] *Patent No. 1323953*, United States Patent Office, December 2, 1919 (filed March 17, 1917).
- [3] Melander, John M., and Ghosh, Satyendra K., "Development of Specifications for Mortar Cement," *Masonry: Esthetics, Engineering, and Economy*, Donald H. Taubert and Tim Conway, eds., ASTM STP 1246, American Society for Testing and Materials, Philadelphia, PA, 1996.
- [4] "Final Report of the Special Committee on Uniform Tests of Cement," American Society of Engineers, 1912.
- [5] Gillmore, Q. A., "Practical Treatise on Limes Hydraulic Cements, and Mortars," *Professional Papers of the Corps of Engineers*, USA, No. 9, 11th ed., D. Van Nostrand Company, New York, 1896, p. 80.
- [6] www.generalsandbrevets.com
- [7] Portland Cement Association file photograph.

- [8] ASTM Standard C 266-04.
- [9] Personal correspondence from Mr. Robin K. Haupt, Cement and Concrete Reference Laboratory, National Institute of Standards and Technology, Gaithersburg, Maryland.
- [10] "Masonry Cement Survey," Portland Cement Association, May, 1999.
- [11] ASTM Standard C 91-03a, "Standard Specification for Masonry Cement," *Annual Book of ASTM Standards*, Vol. 4(1), ASTM International, West Conshohocken, PA.
- [12] ASTM Standard C 1328-03a, "Standard Specification for Plastic (Stucco) Cement," *Annual Book of ASTM Standards*, Vol. 4(1), ASTM International, West Conshohocken, PA.
- [13] ASTM Standard C 1329-04, "Standard Specification for Mortar Cement," *Annual Book of ASTM Standards*, Vol. 4(1), ASTM International, West Conshohocken, PA.



www.astm.org

ISBN: 978-0-8031-3492-8

STOCK #: STP1496